Mammalian and *Saccharomyces cerevisiae* ER-mitochondria contact site regulation by small Rab GTPases and ER folding assistants

by

Maria Sol Herrera

A thesis submitted in partial fulfillment of the requirements for the degree of

Doctor of Philosophy

Department of Cell Biology
University of Alberta

Abstract

Membrane-bound organelles allow eukaryotes to compartmentalize components and processes in a highly organized manner. Organelles can communicate with one another through membrane contact sites (MCS): membrane appositions 10-50nm apart. MCS were not widely accepted as *bona fide* sites of organelle communication until biochemical fractions of endoplasmic reticulum (ER) and mitochondria contacts were isolated and characterized. This biochemical fraction is now known as the mitochondria-associated membrane (MAM). We now know most organelles establish MCS. One of the most prominent MCS in mammalian cells is the MAM, which can occupy up to 20% of all mitochondrial surface in any one cell.

Mitochondria-ER contact sites (MERCs) are established by protein complexes that form physical links between the ER and mitochondrial membranes. Numerous essential cellular processes occur at the MAM, including apoptosis, Ca^{2+} flux, mitochondrial dynamics, and autophagy. Ca^{2+} release from the ER plays a key role in several processes at the MAM. For example, Ca^{2+} is required for several Krebs cycle enzymes, so Ca^{2+} flux regulates respiration. Mitochondrial Ca^{2+} overload instead triggers apoptosis. Therefore, a fine balance must be maintained between the pro-survival and pro-death functions of the MAM. The MAM is also highly dynamic, as it can assemble and disassemble to adapt to stress or energetic demands. These observations highlight the complexity and dynamic nature of this MCS.

In this work, we attempt to develop a better understanding of how MAM structure, tethering, and function, is regulated, and whether key mechanisms are conserved from mammals to the model organism *Saccharomyces cerevisiae.* We first focused on the MAM-enriched small guanosine triphosphatase (GTPase) Rab32, which regulates several aspects of the MAM, including ER-

mitochondria Ca^{2+} flux and activation of the mitochondrial fission GTPase Dynamin related protein 1 (Drp1). Here, we investigated its poorly understood role in autophagy, a process whereby double membraned vacuoles capture cellular components to degrade them via fusion with the lysosome. We demonstrate activation of Rab32 promotes selective autophagy of the MAM, causing a decrease in several MAM-localized proteins. This process also caused a significant decrease in MERCs as assayed by electron microscopy. Additionally, we identified a new Rab32 effector: the autophagy receptor long isoform of Reticulon-3 (RTN3L). Lastly, we report dominant-active Rab32 delayed apoptosis in breast cancer cells. Given almost 25% of breast cancers have high protein levels of Rab32, we investigated if Rab32 could affect breast cancer patient outcomes. We found patients with high levels of Rab32 mRNA had a significantly worse disease outcome, as did those with high RTN3L. However, patients with high mRNA for both Rab32 and RTN3L had even worse outcomes, suggesting these proteins act synergistically in this disease.

We also sought to investigate if mammalian mechanisms of MAM regulation are conserved in *S. cerevisiae,* a model organism that has been essential in furthering our understanding of MAMs. We first sought to identify a homolog for Rab32. Through phylogenetics, we identified Ypt7 as the closest homolog for Rab32 and show inactive Ypt7 increases the number of MERCs per cell. We also observed defects linked to respiration in Ypt7 mutants, suggesting Ypt7 also regulates MAM function.

Lastly, we investigated folding assistants in *S. cerevisiae* given these proteins can extensively regulate MAMs in mammals. We focused on Cne1 and Eps1, the yeast homologs of the chaperone Calnexin and the reductase thioredoxin-related transmembrane protein 1 (TMX1),

which regulate the activity of the sarco-endoplasmic reticulum Ca^{2+} ATPase 2b (SERCA2b) pump in mammals. Specifically, Calnexin is required to maintain SERCA2b activity while TMX1 inhibits it. Loss of these proteins therefore results in changes in Ca^{2+} flux, MAM tethering, and respiration. Here, we demonstrate Cne1 acts as a MAM regulator in *S. cerevisiae* since its loss significantly increases respiration and the number of MERCs per cells while Eps1 loss had no effect.

In brief, this work describes a novel type of autophagy that selectively degrades the MAM, which we have proposed to call "MAMphagy". We also demonstrate for the first time that Ypt7 and the chaperone Cne1 can regulate MAMs in *S. cerevisiae*. Together, these results help us better understand how MAM structure and function are regulated.

Preface

The data presented in Chapter 3 includes collaborative work with Dr. Roseline Godbout and Dr. Rongzong Liu, who contributed all the human breast cancer patient data analysis. This included generation of a gene expression microarray dataset from a human breast cancer cohort that included patient material and clinical information collected under Research Ethics Board Protocol ETH-02-86-17. Megan Yap performed the Annexin V staining flow cytometry experiment and analysis as well as the Reticulon-3 and Rab32 co-localization immunofluorescence and Mander's coefficient analysis. Dr. Nasser Tahbaz obtained all electron microscopy images. These specific contributions are also attributed in the figure legends. All other data and components of this chapter are my original work conducted under the supervision of Dr. Thomas Simmen.

The data and all other components presented in Chapter 4 are my original work obtained with the help of Dr. Nasser Tahbaz, who obtained all electron microscopy images, and Dr. Gary Eitzen, who contributed to experimental planning and design. Dr. Richard Rachubinski and Dr. Gary Eitzen provided the yeast strains.

The data presented in Chapter 5 was partially obtained with Alicia Wu. The spot assays, electron microscopy sample preparation and quantification and respirometry data collection were performed in conjunction with Alicia Wu. Dr. Nasser Tahbaz obtained all electron microscopy images and Dr. Hélène Lemieux analyzed the respirometry data collected by myself and Alicia Wu. These contributions are attributed in the figure legends. Dr. Richard Rachubinski also provided the yeast strains. All other components of this thesis are my original work completed under the supervision of Dr. Thomas Simmen.

Dedication

For my grandparents and for my mom and dad.

Acknowledgements

I would first like to sincerely thank my supervisor, Dr. Thomas Simmen, for his guidance throughout my degree. I could not have chosen a better supervisor. Your advice, kind words, and encouragement have been essential these past years. Thank you for giving me freedom to learn, explore, and grow at my pace.

I would also like to thank my committee members, Dr. Ing Swie Goping and Dr. Paul LaPointe, for providing constructive feedback and helping develop this work throughout the years. Thank you to Dr. Tom Hobman and Dr. Jean Vance for participating as examiners in my candidacy exam and to all members of my PhD defense committee. Additional thanks to my funding sources, including the national sciences engineering research chair (NSERC).

I also thank and recognize Dr. Roseline Godbout and Dr. Rongzong Liu for their collaboration as well as Dr. Nasser Tabahz for his contribution with the electron microscopy. Thank you to Megan Yap for her help and work on the Rab32 project. Thank you to Dr. Hélène Lemieux for allowing me to perform the respirometry experiments in her laboratory. I also extend my thanks to Dr. Gary Eitzen for his help and advice on the yeast projects as well as to Alicia Wu. I also want to thank members of the department and the Goping lab for always being willing to help and share reagents.

Thank you to all the past and current members of the Simmen lab for their camaraderie and support. I also want to thank all the amazing undergraduate and high school students I worked with. Your enthusiasm constantly renewed my passion for science.

Thank you to my dear friends, both inside and outside the department, for your love and friendship all these years. I am deeply, deeply grateful to have you in my life.

I would also like to sincerely thank my family. Thank you to my mom, dad, brothers, sister-in-law, aunts, cousins and grandparents. I am so unbelievably grateful to you all. Thank you for your unwavering belief in me, your unending support, encouragement, and love.

Above all, I want to thank my parents. I could not have done this without you. Words cannot express the admiration and gratitude I have for the sacrifices you have made, all the hard work you do, and the determination you had to move us to Canada. In other words: I am standing on the shoulders of giants. Thank you.

A final thank you goes to Luna, for existing, and to her parents, for sharing her with me.

Table of contents

List of tables

List of figures

List of abbreviations

Abbreviation	Definition
BAPTA-AM	1,2-Bis(2-aminophenoxy)ethane-N,N,N′,N′-tetraacetic acid tetrakis(acetoxymethyl ester)
2-DG	2-deoxyglucose
AKAP	A-kinase anchoring protein
AP	Adaptor protein
ATF6	Activating transcription factor 6
BLAST	Basic local alignment search tool
BLOC-3	Biogenesis of lysosome-related organelles complex 3
BSO	Buthionine sulfoximine
CaMKI	Ca^{2+}/calmodulin-dependent protein kinase I
CCPG1	Cell cycle progression 1
CCS	Calcium cell survival
CCV	Clathrin-coated vesicle
ChiMERA	Construct helping in mitochondria-ER association
CHOP	CCAAT/enhancer binding homologous protein
CL	Cardiolipin
CORVET	Complex class C core vacuole/endosome tethering
CPY*	Carboxypeptidase Y*
DHE	Dihyroethidium
Drp1	Dynamin related protein 1
eIF2α	Eukaryotic translation initiation factor 2 subunit-α
EMC	ER membrane protein complex
ER	Endoplasmic reticulum
ERAD	ER-associated protein degradation
ERdj5	ER-localized J protein 5
ERMES	ER-mitochondria encounter structure
ERp44	ER-resident protein 44
FACL4	Fatty acid-CoA ligase type 4
FCCP	Carbonyl cyanide 4-(trifluoromethoxy) phenylhydrazone
FUNDC1	FUN14 domain containing protein 1
GAP	GTPase activating protein
GD3	Ganglioside 3
GDF	GDI displacement factor
GDI	GDP-dissociation inhibitor
GDP	Guanosine diphosphate
GEF	Guanine nucleotide exchange factor
Grx6	Glutaredoxin 6
GTP	Guanosine triphosphate

GTPase	Guanosine triphosphatase
HACS	High affinity calcium system
HOPS	Homotypic vacuolar fusion and protein sorting
IMM	Inner mitochondrial membrane
IP_3R	Inositol-1,4,5-triphosphate (IP_3) receptor
IRE	Inositol-requiring enzyme 1
KD	Knockdown
KO	Knockout
L4	Loop 4
LACS	Low affinity calcium system
LD	Lipid droplet
LECA	Last eukaryotic common ancestor
LIR	LC3-interacting region
LRO	Lysosome-related organelle
MAM	Mitochondria-associated membrane
MCS	Membrane contact site
MCU	Mitochondrial calcium uniporter
MEF	Mouse embryonic fibroblast
MERC	Mitochondria-ER contact site
MOMP	Mitochondria outer membrane permeabilization
mPTP	Mitochondrial permeability transition pore
mRNA	Messenger ribonucleic acid
mTORC1	Mammalian target of rapamycin complex 1
NADPH	Nicotinamide-adenine dinucleotide phosphate
NCBI	National Centre for Biotechnology Information
NCLX	Na^+/ Ca^{2+}/Li^+ exchanger
NDP52	Nuclear dot protein 52 kDa
Nox4	Nicotinamide-adenine dinucleotide phosphate oxidase 4
NVJ	Nucleus-vacuole junction
OD	Optical density
OMM	Outer mitochondrial membrane
OPTN	Optineurin
OSBP	Oxysterol-binding protein
OST	Oligosaccharyltransferase
OXPHOS	Oxidative phosphorylation
PA	Phosphatidic acid
PACS-2	Phosphofurin acidic cluster sorting protein 2
PAS	Pre-autophagosomal structure
PC	Phosphatidylcholine
PCD	Programmed cell death

PE	Phosphatidylethanolamine
PEG	Polyethylene glycol
PEMT	PE methyltransferase
PERK	protein kinase R-like endoplasmic reticulum kinase
PI3K III	Phosphtatidyl-inositol-3-phosphate (PI3P) kinase class III
PI3P	Phosphtatidyl-inositol-3-phosphate
PINK1	Phosphatase and tensin homolog-induced kinase 1
PKA	Protein kinase A
PS	Phosphatidylserine
PSD1	PS decarboxylase-1
PSD2	PS decarboxylase-1
PSS1	Phosphatidyl synthase-1
PSS2	Phosphatidyl synthase-2
PTPIP51	Protein tyrosine phosphatase interacting protein 51
RBH	Reciprocal best BLAST hits
rER	Rough ER
RHD	Reticulon homology domains
RIP-ChIP	RNA chromatin immunoprecipitation
RNA	Ribonucleic acid
ROS	Reactive oxygen species
ROX	Residual oxygen consumption
RT-PCR	Reverse transcription polymerase chain reaction
RTC	Ribosome-translocon complex
RTN3L	Reticulon-3 long isoform
sER	Smooth ER
SERCA	Sarco-endoplasmic reticulum calcium ATPase
SIGMAR1	Sigma-1 receptor
SMP	Synaptotagmin-like mitochondrial lipid-binding protein
SNARE	N-ethylmaleimide-sensitive factor attachment protein receptor
SPCA	Secretory pathway Ca^{2+} ATPase
SPLICS	Split-green fluorescent protein-based contact site sensor
STIM1/2	Stromal interaction molecules 1 and 2
TBCD151	TBC1 domain family member 15
TCA	Tricarboxylic acid cycle
TGN	Trans-Golgi network
TMD	Transmembrane domain
TOM	Translocase of the outer membrane
TRAIL	TNF-related apoptosis inducing ligand
Trp1	Tyrosinase and tyrosinase-related protein 1
Trp2	Tyrosinase and tyrosinase-related protein 2

TRX	Thioredoxin
UGGT	UDP-glucose glycoprotein glucosyltransferase
ULK1	Unc-51 like autophagy activating kinase-1
UPR	Unfolded protein response
UPRE	UPR responsive element
VAPB	Vesicle-associated membrane protein-associated protein B
vCLAMP	Vacuole and mitochondria patch
VCP	Valosin-containing protein
VDAC1	Voltage-dependent anion channel 1
VGCC	Voltage gated Ca^{2+} channel
VPS34	Vacuolar protein sorting 34
WIPI	WD-repeat domain phosphoinositide-interacting protein
XBP1	X-box-binding protein 1
Yno1	Yeast NADPH oxidase 1
YPA	Yeast extract peptone acetate
YPD	Yeast extract peptone dextrose

Chapter 1: Introduction

1.1 The Mitochondria-associated membrane (MAM)

1.1.1 Membrane contact sites

Eukaryotic cells compartmentalize components into membrane-bound organelles to perform the vast number of complex processes required to sustain life. Early cell biologists hypothesized communication between organelles could occur via three non-exclusive mechanisms: vesicular transport, diffusion through the cytoplasm, or close membrane contacts [1]. Studies in the early 80's showed protein-coated vesicles carried cargo from the endoplasmic reticulum (ER) to the Golgi [2]. This vesicular model was predominantly favored for communication of the ER with other organelles, although electron micrograph studies in the 50's and 60's described close contacts between the ER and mitochondria [3,4]. These contacts were initially interpreted as artifacts rather than distinctive domains of close membrane contacts [5]. Similarly, biochemically isolated ER membranes that contained mitochondria were initially thought to be mere contaminations [6]. Nevertheless, several studies continued reporting biochemically distinct ER fractions containing mitochondria [7,8], including the identification of fraction X, now known as the mitochondria-associated membrane (MAM) [9]. These and subsequent studies in the 90's robustly confirmed lipid transfer between the ER and mitochondria does not occur via vesicles or cytosolic proteins, suggesting the membrane contacts described previously could mediate the process instead [9,10]. Indeed, biochemical isolation and analysis of the MAM demonstrated this is a distinct ER subtype that is particularly enriched in lipid biosynthesis enzymes [9,11,12]. This breakthrough allowed scientists to determine lipid exchange requires lipid-binding proteins that are found almost exclusively at close ER-mitochondria contact sites [10,13]. Since then, the study of membrane contact sites (MCS) has grown exponentially, as research continues to demonstrate MCS are an important form of communication between most organelles in the cell [14].

MCS, defined as appositions of 10-50nm between membrane-bound organelles, serve as platforms to allow efficient signaling and communication [14]. This includes protein-protein interactions, non-vesicular lipid transfer, and molecule exchange. The ER, usually the largest organelle in most cells, has MCS with most organelles, including mitochondria, Golgi, plasma membrane, endosomes, lipid droplets, lysosomes, and peroxisomes [14]. Since its biochemical isolation by Dr. Jean Vance in 1991, the MAM has become one of the most studied MCS.

Mitochondria-ER contact sites (MERCs) are maintained by physical links formed by proteinaceous tethering complexes [15,16]. MERCs are defined as the physical sites of contact formation between ER and mitochondrial membranes while MAM refers specifically to the biochemical fraction housing specific lipids and proteins that are particularly enriched here [17]. MERCs are mostly commonly visualized by electron microscopy and are formed by both rough ER (rER) and smooth ER (sER) [15]. rER MERCs are maintained at a distance between 20-50nm to accommodate ribosomes while sER MERCs average 10nm [15]. This early study suggested different types of MERCs exist based on the distance between the ER and mitochondrial membrane. Specifically, the authors showed sER and rER MERCs have different rates of ER Ca^{2+} release into mitochondria, one of the main functions of MAMs. Indeed, sER contacts released more Ca^{2+} from the ER, the cell's main Ca^{2+} reservoir, compared to rER MERCs. This was determined by fluorometric measurements of permeabilized cells loaded with fluorescent Ca^{2+} probes. When cells were serum starved to induce apoptosis, the massive Ca^{2+} flow of sER MERCs resulted in mitochondria outer membrane permeabilization (MOMP), cytochrome c release, and apoptosis. rER MERCs did not release nearly as much Ca^{2+} and did not undergo apoptosis under the same conditions. These early observations have contributed to the current model of MAMs existing in different functional units [17].

We also know MAMs are highly dynamic structures that can quickly adapt to a variety of stimuli and stressors [17]. This includes changes in its proteome and the formation or loss of tethering upon changing conditions [18]. Thus, although the average HeLa cell has roughly 5-20% of all mitochondrial surface engaged in MCS with the ER at any one time, this percentage can change significantly with stressors [15,19]. For example, ER stress can increase the number of MERCs by up to 25% [15]. Other factors influencing the number and type of MERCs include cell type, nutrient levels, and cytotoxic insults [18].

There are numerous processes that occur at the MAM [20]. These can be broadly classified into four main categories: i) molecule exchange, ii) organelle dynamics and movement, iii) lipid exchange and biosynthesis, and iv) signaling platform for complex formation. Some specific functions include Ca^{2+} signaling, reactive oxygen species (ROS) exchange, mitochondrial fission and metabolism regulation, autophagy, apoptosis, lipid biosynthesis and exchange, and ER stress and proteostasis regulation [20,21]. Clearly, the MAM must maintain a fine balance between its homeostatic and apoptotic roles. Understanding how the MAM does so to create an integrated

response while performing multiple functions simultaneously has become an important question which is slowly being answered. Another important black box in the field is understanding how tethering proteins respond to stressors and signaling pathways to form and disassemble MAMs. These tethering proteins and complexes will be discussed in the following section.

1.1.2 Composition and tethering

MERCs are highly dynamic structures regulated by various stressors and signals which promote or disassemble the contacts as needed [18]. MAMs perform numerous functions, a fact that is reflected by the large number of proteins found at these MCS. Indeed, a study investigating the MAM proteome in mice found over 1300 proteins [22]. From these hundreds of proteins, several studies, screens, and meta-analyses have helped determine a core group of proteins that consistently reside at this MCS [22–25]. They include Ca^{2+} channels, ER chaperones and oxidoreductases, tethers and tethering factors, and lipid biosynthesis and transport proteins [20].

The discovery that the MAM is maintained by proteinaceous tethers occurred after studies demonstrated limited proteolysis disrupted the contact sites while synthetic linkers artificially connecting the two organelles restored them [15]. One of the first tethering complexes identified at MAMs is composed of the mitochondrial voltage-dependent anion channel 1 (VDAC1), the cytosolic chaperone Grp75, and the ER Ca^{2+} channel inositol-1,4,5-triphosphate (IP_3) receptor (IP_3R) [26] (Figure 1.1). Apart from its tethering abilities, this complex also allows Ca^{2+} to be released from the ER via IP_3R and to immediately traverse the outer mitochondrial membrane (OMM) via VDAC1 [26].

The ER vesicle-associated membrane protein-associated protein B (VAPB) also forms a tethering complex with protein tyrosine phosphatase interacting protein 51 (PTPIP51), an OMM protein [27]. This tethering complex has been shown to recruit proteins that initiate autophagy, a process of degradation that can originate at the MAM [28]. Yet another complex is formed specifically during apoptosis, where it serves as a platform to recruit and activate pro-caspase 8 [29]. This complex is called the ARCosome and is formed by Bap31, an ER transmembrane chaperone, and the mitochondrial fission protein Fis1. The ARCosome serves to promote contact formation and increase ER-mitochondrial Ca^{2+} flux during apoptosis, eventually causing MOMP.

Another category of proteins regulating the distance between the ER and mitochondria are tethering regulators. These proteins do not form physical bridges between membranes, as opposed to tethers, but rather have an indirect effect on the distance between them [20]. One of them is phosphofurin acidic cluster sorting protein 2 (PACS-2), whose loss results in reduced contacts, as assayed by electron microscopy [30]. PACS-2 is a cytosolic sorting protein with multiple functions. One of its functions is to mediate localization of ER membrane proteins, including that of the ER chaperone Calnexin [31]. The mechanism for its tethering regulation has remained unclear, though one possibility is that PACS-2 helps maintain Bap31 stability [30], suggesting PACS-2 could regulate tethering by maintaining the ARCosome.

Arguably the most well-known tether is Mitofusin-2, a small guanosine triphosphatase (GTPase) that also mediates mitochondrial fusion [16]. Mitofusin-2 is found on both the ER and mitochondria, while the closely related Mitofusin-1 is only found on mitochondria. Mitofusin-2's tethering ability occurs through homo- and heteromeric complexes formed with Mitofusin-1. Mitofusin-2 disruption results in fewer ER-mitochondria contacts as assayed by electron tomography, and also impairs ER to mitochondria Ca^{2+} flux, one of the main functions of the MAM (see below). However, other studies have instead suggested Mitofusin-2 counteracts tethering. These studies showed Mitofusin-2 ablation increases Ca^{2+} flux into mitochondria [32] as well as ER-mitochondria contacts, particularly those formed by sER [32,33].

There are several possible explanations for these discrepancies. Firstly, there appear to be important differences between Mitofusin-2 knockout (KO) versus knockdown (KD) cells. For instance, KOs downregulate the mitochondrial Ca^{2+} uniporter (MCU), a channel on the inner mitochondrial membrane (IMM) that allows for ion transport into the mitochondrial matrix, while KD cells do not [32,33]. This could be a compensatory mechanism for the altered Ca^{2+} flux caused by Mitofusin-2 loss in KOs only. Secondly, culture conditions have also been shown to affect the number of contacts in Mitofusin-2 deficient cells [33]. Therefore, the discrepancy could simply be due to differences in culture conditions. Lastly, Mitofusin-2 KOs have high levels of ER stress, which is a well-known promoter of MAMs [33]. Thus, Mitofusin-2 KOs could compensate by increasing MAMs in an ER-stress dependent manner. In brief, it is likely these discrepancies are due to complex compensatory mechanisms involving Ca^{2+} channel levels, ER-stress dependent contact sites, and culture conditions. Thus, Mitofusin-2 is still largely regarded as a tether rather than tether antagonist [33,34].

Although these seemingly contradictory results seem to still point to Mitofusin-2 being a tether, these studies highlight an important reckoning in the field: are the effects caused by tether ablation a result of loss of function of a *bona fide* tether, or a result of compensatory mechanisms that mask the true function of the protein of interest? An avenue that could help us distinguish between these scenarios is returning to a model organism with a simpler system.

The ease and rapidity of genetic screening studies in *Saccharomyces cerevisiae* has made this model organism an important resource to identify tethers. One of the first tethers described using this methodology was the ER-mitochondria encounter structure (ERMES) complex [35]. ERMES is composed of two OMM proteins, Mdm10 and Mdm34, the ER membrane protein Mmm1, and the cytosolic protein Mdm12. The complex also interacts with the OMM GTPase Gem1, which inhibits the complex [36]. Apart from its tethering function, ERMES is also required for lipid transfer and mitochondrial protein import. Several ERMES subunits have synaptotagmin-like mitochondrial lipid-binding protein (SMP) domains, which grants them the ability to bind phospholipids, likely allowing them to act as lipid transfer proteins across these membranes [13]. Other studies have also shown the Mdm10 subunit participates in mitochondrial protein import via interaction with the sorting and assembly machinery (SAM), which is required for OMM protein localization following import via the translocase of the outer membrane (TOM) complex [37].

ERMES orthologs in mammals have been difficult to identify. One of them is Miro-2, thought to be the mammalian ortholog of Gem1, which is known to regulate mitochondrial motility in a Ca^{2+}-dependent manner [36]. The other is PDZD8, hypothesized to be an ortholog of Mmm1 [38]. PDZD8 loss decreases MERCs, and although it also contains a SMP domain, its effect on lipid transfer remains untested [38,39]. There is also no evidence of a complex or any interaction between these mammalian proteins, so it remains unknown if ERMES is truly conserved in mammals. It is also still unknown if the Mitofusin homolog Fzo1 mediates tethering in this organism [20].

Another complex postulated to tether the ER and mitochondria is the ER membrane protein complex (EMC). EMC is a heteromeric complex composed of ER proteins Emc1 through Emc7, as well as Emc10 [40,41]. Mammals have two additional proteins in the complex: Emc8, and Emc9 [41]. These ER proteins interact with Tom 5 on the mitochondrial side to form a tethering complex [40]. No enzymatic activity has been attributed to any individual Emc protein but EMC dysfunction

results in defects of membrane protein insertion [42,43]. Indeed, EMC was shown to promote the *in vitro* insertion of transmembrane domains (TMDs) into liposomes [42]. This activity allows EMC to promote the correct topology of proteins with multiple TMDs [42]. The complex also appears to participate in lipid transfer since deletion of multiple subunits causes significant phospholipid defects [40]. Unlike ERMES though, no known lipid-binding domains have been identified in EMC proteins [13,40]. One hypothesis for this effect is that its compromised activity in membrane protein assembly results in lipid transport proteins failing to insert into the membrane [41]. Thus, the lipid defect would be an indirect effect.

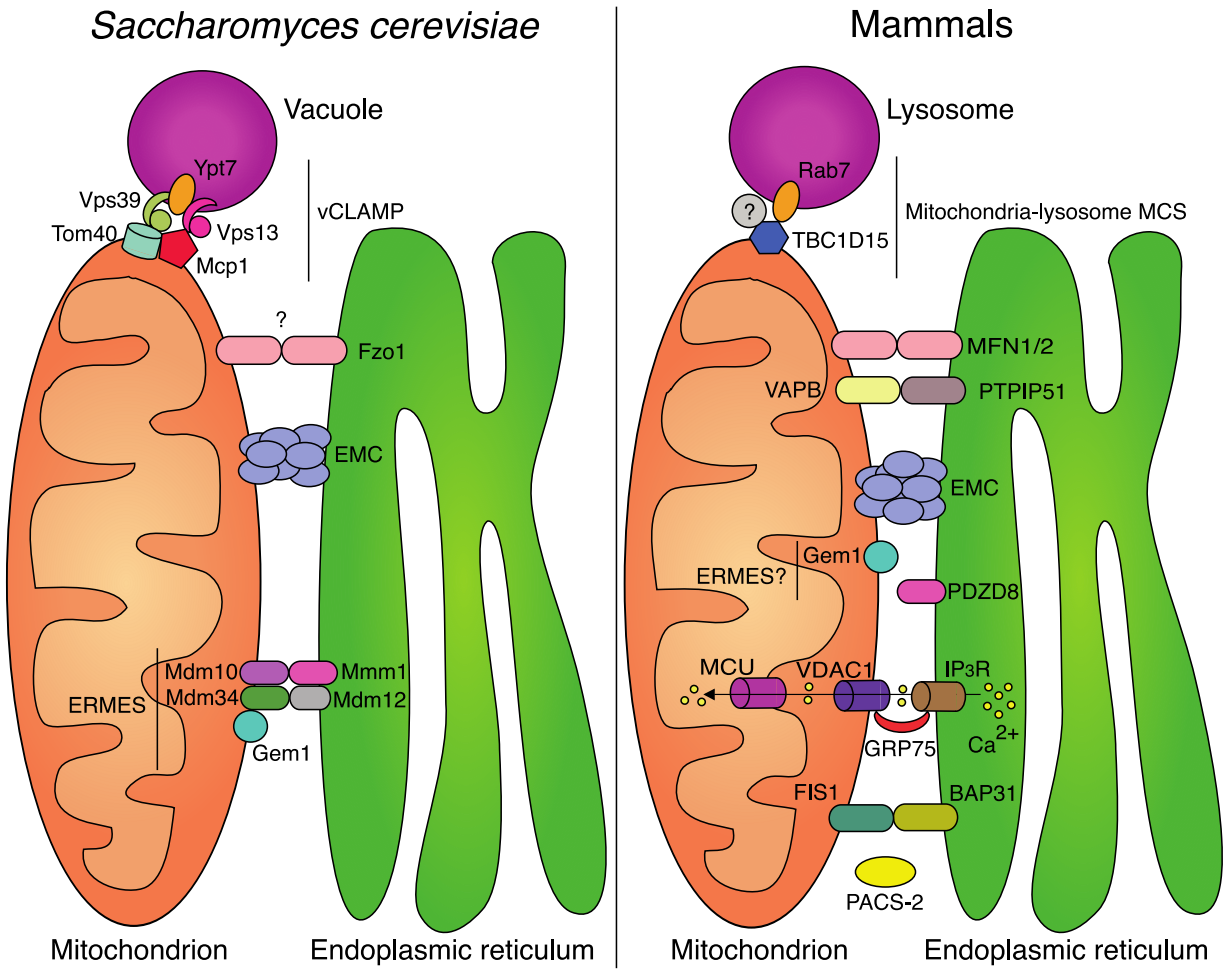

Figure 1.1 *Saccharomyces cerevisiae* and mammalian tethering proteins at membrane contact sites.

Schematic drawing of membrane contact sites (MCS) and their tethers and tethering regulators. In *S. cerevisiae,* the ER-mitochondria encounter structure (ERMES) tethers the ER and mitochondria. It is unknown if this complex is conserved in mammals though two homologs (Gem1 and PDZD8) have been described. The ER membrane proteins complex (EMC) in yeast is composed of 8 subunits while the mammalian complex has 10. It is unknown if Fzo1, the homolog of Mitofusins 1 and 2 (MFN1/2), acts as a tether in *S. cerevisiae*. The vacuole and mitochondria patch (vCLAMP) tethers the vacuole and mitochondria in yeast. In mammals, mitochondria-lysosome MCS have been identified and have been shown to contain Rab7 and its GAP TBC1 domain family member 15 (TBC1D15) though the full list of tethering components remains unknown. Other tethering complexes for ER-mitochondria contacts in mammals are shown. IP_3R-Grp75-VDAC1 allows Ca^{2+} transport from the ER lumen into mitochondria and the MCU into the mitochondrial matrix. The mechanism for the tethering regulator PACS-2 is still unknown.

1.1.3 Functions

1.1.3.1 Lipid biosynthesis

The MAM is enriched in enzymes required for cholesterol, triacylglycerol, and phospholipid synthesis and exchange [9,11,44,45]. The phospholipids synthesized at the MAM include phosphatidylserine (PS), phosphatidylethanolamine (PE), and phosphatidylcholine (PC) [10]. Briefly, PS synthesis at the ER by phosphatidyl synthase-1 (PSS1) and -2 (PSS2) is followed by its transport to mitochondria [45]. Here, PS decarboxylase-1 (PSD1) and -2 (PSD2) in the IMM catalyze its processing into PE [10,12]. PE can then be transported back to the ER and redistributed to other organelles of the endomembrane system or synthesized into PC by PE methyltransferase (PEMT) [10,11]. Phosphatidic acid (PA) is another phospholipid synthesized and shuttled at the MAM [10]. PA is a precursor for cardiolipin (CL), a critical lipid for mitochondrial metabolism and apoptosis [10,46,47]. Although mitochondria can synthesize their own PA, they are largely dependent on ER-imported PA to synthesize CL [10]. Its shuttling is mediated by proteins such as oxysterol-binding protein (OSBP) related protein (ORP) 5 and 8, which can also transport PS from the ER to mitochondria [48].

Another important lipid metabolism enzyme at the MAM is long-chain fatty acid-CoA ligase type 4 (FACL4), which ligates coenzyme A to fatty acids and participates in triacylglycerols synthesis [49]. Sterol homeostasis also depends on the MAM. For example, the cholesterol-binding protein caveolin-1 resides at the MAM, where it also serves as a scaffold for lipid-related enzymes [50]. Another lipid-binding protein at MAMs is Lam6, which is also found in the commonly used model organism *S. cerevisiae* [51]. Lam6 binds sterols and imports them to mitochondria [52]. Manipulation of Lam6 alters ER-mitochondria tethering [51], which also occurs with several other lipid and sterol binding proteins described above [20]. Thus, lipid composition is important for MAM maintenance and function.

Studies in mammalian cells have shown PS and PE synthesis is adenosine triphosphate (ATP)-dependent, as is PS transport to mitochondria [10,12]. However, lipid synthesis in *S. cerevisiae* does not require ATP [12,53]. Otherwise, the pathways described for mammals are largely conserved in yeast with some small differences, including the fact that PS is generated by a single enzyme, Cho1 [54]. Similarly, while PSD1 also resides in mitochondria, PSD2 is present in the Golgi in yeast [55,56].

1.1.3.2 Ca^{2+} flux

Ca^{2+} is a multifunctional ion that can act as a secondary messenger, enzymatic modulator, and structural component [57]. As the main storage site for Ca^{2+} in mammals, the ER must tightly regulate the uptake and release of this ion to maintain a concentration between 0.1-1 mM [58]. This is much higher than the cytosolic concentration, which is roughly 100nM, or the resting mitochondrial concentration of ~200nM [59,60]. Ca^{2+} can be released passively from the ER through Ca^{2+} leak, a slow release that occurs across channels on the ER membrane [61]. This occurs mainly at the ribosome-translocon complex (RTC), where proteins are translated and translocated through a channel on the ER membrane. The main mechanism of ER Ca^{2+} release in most mammalian cell types is through the IP_3R channels [57]. IP_3R opening results in large bursts of Ca^{2+} release that create a transient but massive increase in cytosolic Ca^{2+} concentration well into the tens of μM [62–64]. This concentration is several orders of magnitude larger than that of the majority of the cytosol [59]. These areas of high cytosolic Ca^{2+} are also known as Ca^{2+} hotspots or microdomains [62–64].

Three isoforms of this channel exist: IP_3R1, IP_3R2, and IP_3R3, all encoded by separate genes [65]. Although IP_3R3 was originally thought to be the main isoform enriched at the MAM [65], more recent studies suggest all isoforms can contribute to ER-mitochondria Ca^{2+} flux at these MCS [66]. IP_3R opening requires Ca^{2+} and IP_3, a secondary messenger synthesized upon activation of phospholipase C (PLC) [62,67]. Extracellular ligands such as ATP and histamine can trigger signaling cascades that activate PLC and trigger IP_3 generation, thereby opening IP_3R [68,69]. Conversely, cytosolic Ca^{2+} levels above 250nM induce its closure [70,71]. Although ATP is not required for IP_3R activity, it can act as an allosteric activator that increases IP_3R's Ca^{2+} affinity, potentiating Ca^{2+} release [72,73].

Mitochondria can take up roughly 15-50% of Ca^{2+} released from IP_3R at these microdomains [74]. This process begins at the OMM, where VDAC1 serves as a pore for multiple ions, including Ca^{2+} [26]. Once inside the mitochondrial intermembrane space, Ca^{2+} can enter the mitochondrial matrix through the MCU on the IMM [75]. MCU has a very low affinity for Ca^{2+}, so relatively large Ca^{2+} concentrations, usually above 3μM, are required for Ca^{2+} to enter the matrix [64,75]. Thus, only the short distances provided by the MAM allow the Ca^{2+} bursts from the ER to reach the necessary concentration for MCU activity [75]. This allows mitochondria to reach a maximal Ca^{2+} concentration of ~100μM [76]. Additional studies have shown microdomain Ca^{2+}

concentrations over 1μM promote MERC formation while those below 100nM oppose them [19,77]. Lastly, mitochondrial Ca^{2+} release occurs through an antiporter on the IMM: the Na^{+}/ Ca^{2+}/Li^{+} exchanger (NCLX) [78].

ER Ca^{2+} uptake is performed by the sarco-endoplasmic reticulum Ca^{2+} ATPase (SERCA) pump, which transports Ca^{2+} from the cytosol into the ER lumen through ATP hydrolysis [79]. Three different genes encode for SERCA pumps in humans: *SERCA1, SERCA2* and *SERCA3* [60]. Of these, SERCA2b is the most abundant, widely expressed, and MAM-enriched isoform [60,80]. SERCA2b is also regulated by Ca^{2+}, whereby high luminal Ca^{2+} inhibits its activity [81].

Another important factor that influences ER Ca^{2+} homeostasis is ER-plasma membrane contact sites. These contact sites allow Ca^{2+} from the extracellular medium to enter the ER when luminal Ca^{2+} levels drop, such as after incubation with SERCA inhibitor thapsigargin [82]. This drop in Ca^{2+} is sensed by stromal interaction molecules 1 and 2 (STIM1/2), which have Ca^{2+}-binding motifs [82,83]. Ca^{2+}-binding induces a change in STIM1/2 conformation, which in turn promotes oligomerization and allows STIM1/2 to relocate to ER closely associated to the plasma membrane, also known as cortical ER [83,84]. Here, STIM1/2 can interact with Orai1, a plasma membrane Ca^{2+}-release Ca^{2+} activated channel [83]. This binding triggers Orai1 oligomerization and activation, allowing Ca^{2+} to enter through the plasma membrane [84]. This process of Ca^{2+} entry in response to ER Ca^{2+} depletion is known as store-operated Ca^{2+} entry (SOCE) [83]. SOCE can also be activated by IP_3R, which binds STIM1 following activation by IP_3 [85]. This interaction enhances STIM1-Orai Ca^{2+} entry through a mechanism that is not yet fully understood [85].

Saccharomyces cerevisiae has also been successfully used as a model organism for Ca^{2+} studies despite its differences compared to mammalian cells [86,87]. One of the main differences in yeast is that the majority of Ca^{2+} is stored in the vacuole rather than the ER [88,89]. Vcx, a H^{+}/ Ca^{2+} exchanger, and Pmc1, an ATPase, introduce Ca^{2+} to the vacuole lumen [87] (Figure 1.2). Release from the vacuole occurs through the Yvc1 channel [90]. Most Ca^{2+} in the vacuole is found in a complex with inorganic phosphate [91]. Therefore, although the total vacuolar Ca^{2+} concentration is ~2mM, the free Ca^{2+} concentration is closer to 30μM [92]. This makes most of the pool of vacuolar Ca^{2+} unusable, which likely explains why the vacuole rarely releases Ca^{2+} in homeostasis [91]. The main role of the vacuole in terms of Ca^{2+} appears to be Ca^{2+} uptake to prevent cytotoxic cytosolic Ca^{2+} levels, rather than the more active role the ER plays in mammalian cells [89].

There are two known pathways for Ca^{2+} entry at the yeast plasma membrane. The first is the low affinity Ca^{2+} system (LACS), which is active when extracellular Ca^{2+} is high [93]. The second is a high affinity Ca^{2+} system (HACS), which is better characterized [94,95]. HACS is active in both high and low extracellular Ca^{2+} levels as well as in response to extracellular stressors such as oxidative stress [95,96]. HACS consists of two subunits, Cch1 and Mid1, which come together to form a channel [95,97]. Both proteins are homologous to mammalian voltage gated Ca^{2+} channel (VGCC) subunits [95].

The yeast ER has a free Ca^{2+} concentration of roughly 10μM, which is ~100 times higher than that of the cytosol [92]. Ca^{2+} entry into the ER is partly mediated by the ATPase Pmr1 [92,98] and the Ca^{2+}/H^{+} antiporter Gdt1/Grc1 [99]. Pmr1 is mostly found in the Golgi, where the Ca^{2+} concentration is ~300μM [98,100]. Although only a small pool of it is found on the ER, Pmr1 is considered the main mechanism of Ca^{2+} import into the ER since Δ*pmr1* cells have only half the ER Ca^{2+} content of WT cells [92,98,101,102]. Moreover, Pmr1 has a very high affinity for Ca^{2+} [98,101]. The ER-localized ATPase Spf1/Cod1 is also thought to transport Ca^{2+} into the ER lumen since Δ*spf1/cod1* cells largely phenocopy Δ*pmr1* Ca^{2+}-associated defects [102–104]. Firstly, indirect evidence suggests Δ*spf1/cod1* also have lower ER Ca^{2+} [102]. This is because Δ*spf1/cod1* cells, like Δ*pmr1* cells, have impaired degradation of the same mutant misfolded protein [98,102]. This degradation defect has been previously attributed to impaired action of a Ca^{2+}-dependent glycosylation enzyme, suggesting both mutant strains have low ER Ca^{2+} [98,102]. Both mutants also upregulate Ca^{2+}-related genes such as the vacuolar pump Pmc1 [104]. However, several studies have failed to demonstrate Ca^{2+} is a substrate [102,104,105], so the Ca^{2+} pumping function of Spf1/Cod1 remains speculative.

No SERCA-related Ca^{2+} channel has been identified in the ER or Golgi of *Saccharomyces cerevisiae* [98]. Moreover, the SERCA inhibitor thapsigargin has no effect on ER Ca^{2+} levels in yeast [92]. Indeed, Pmr1 shares more homology to mammalian secretory pathway Ca^{2+} ATPases (SPCAs) than SERCA [101]. However, the expression of mammalian SERCA can rescue Δ*pmr1* ER Ca^{2+} defects [98]. Pmr1 is therefore thought to act as a SERCA functional homolog though it is mechanistically different [95,98].

Δ*pmr1* cells have high Ca^{2+} influx via Cch1 and Mid1 at the plasma membrane, likely to compensate for their lower ER and Golgi Ca^{2+} levels [95]. This HACS activation is reminiscent of SOCE induction after SERCA inhibition in mammalian cells [95]. However, this pathway differs

from mammalian SOCE in at least one key aspect: there is no evidence yet of luminal Ca^{2+} sensors like STIM1 in yeast [91]. Yeast also lack IP_3Rs, which can activate SOCE in mammals as previously described [84,91]. Thus, how yeast sense Ca^{2+} changes and respond to activate HACS is not yet known.

Ca^{2+} leak through the RTC has also been reported in *S. cerevisiae* [61]. No other mechanism of ER Ca^{2+} release has been identified in this species, though one untested model suggests Ca^{2+} can be released as a secretion along the secretory pathway [100]. It has also been suggested that the ER protein Csg2 forms a channel to export Ca^{2+} from the ER lumen [106,107]. However, multiple studies have shown its loss does not alter cytosolic Ca^{2+} levels, so its identity as a channel has been disputed [106,108]. Thus, more research is needed to fully understand Ca^{2+} release from the yeast ER.

Regulation of mitochondrial Ca^{2+} in *S. cerevisiae* is even less understood. One study has suggested a theoretical antiporter could import Ca^{2+} into mitochondria in place of two protons, but no evidence of this or a similar mechanism has been described yet [109]. Yeast also lack MCU or any other known functional homolog [109]. Nevertheless, there is significant evidence yeast mitochondria also take up Ca^{2+} and are regulated by it, which will be discussed below.

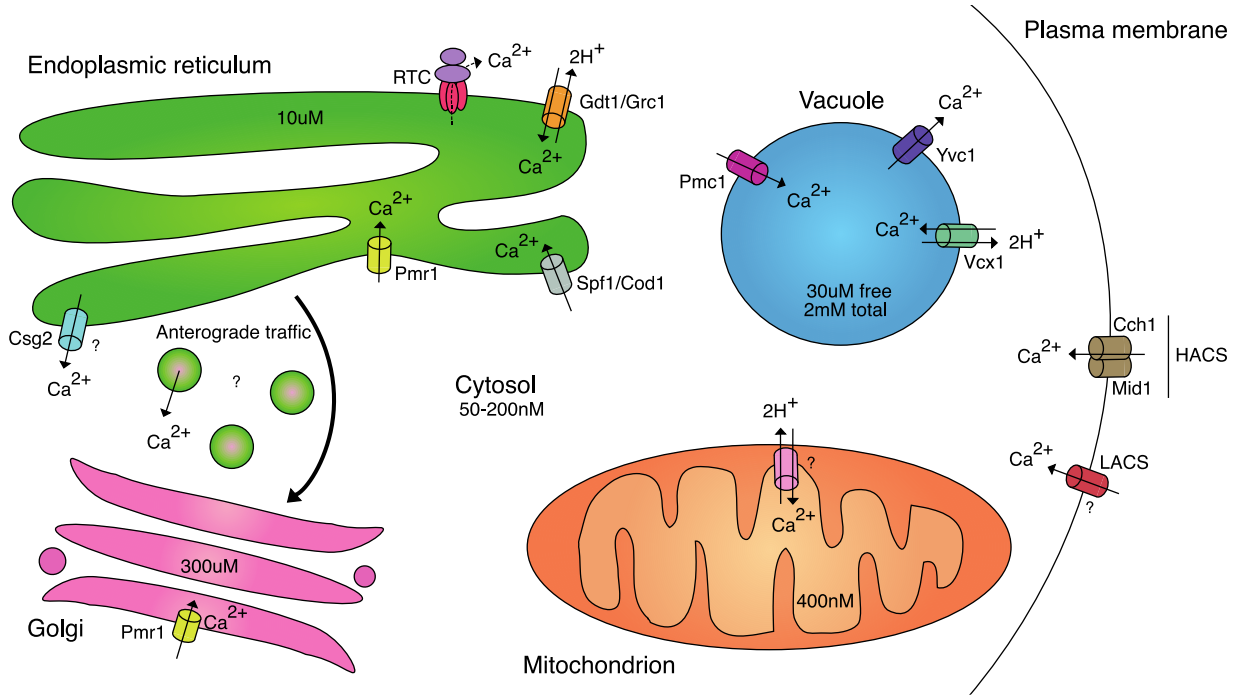

Figure 1.2 Ca^{2+} handling in *Saccharomyces cerevisiae*
Schematic diagram of Ca^{2+} channels and pumps in *S. cerevisiae.* Ca^{2+} from the extracellular medium enters the cell through two different mechanisms, the low affinity Ca^{2+} system (LACS) and the high affinity Ca^{2+} system (HACS). The identity of the LACS remains unknown while HACS is composed of Cch1 and Mid1. The average Ca^{2+} concentration of each organelle is indicated. Ca^{2+} in the vacuole is often complexed with inorganic phosphate, lowering the concentration of free Ca^{2+} to ~30μM. Vacuolar Ca^{2+} is maintained by the ATPase Pmc1, which pumps Ca^{2+} into the vacuole lumen, the Vcx H^+/ Ca^{2+} exchanger, and the Yvc1 channel that allows Ca^{2+} release. The mechanisms of mitochondrial Ca^{2+} uptake and release remain unknown but a theoretical H^+/ Ca^{2+} exchanger has been hypothesized to exist as depicted. Nevertheless, mitochondrial Ca^{2+} is maintained at ~400nM. At the Golgi, the ATPase Pmr1 maintains the Ca^{2+} concentration at ~300μM. Pmr1 also pumps Ca^{2+} into the ER lumen. The Spf1/Cod1 ATPase is hypothesized to also pump Ca^{2+} into the lumen. The Gdt1/Grc1 H^+/ Ca^{2+} exchanger also contributes to the Ca^{2+} concentration of ~10μM. The ribosome-translocon complex (RTC) allows for passive release of Ca^{2+} out of the ER. Csg2 has been described as a Ca^{2+} channel for the ion's release but its role as a channel has been disputed. ER Ca^{2+} release has also been hypothesized to occur through vesicular secretion during anterograde traffic.

1.1.3.3 Mitochondrial metabolism

One of the most important functions of mitochondria is to provide the cell with ATP via oxidative phosphorylation (OXPHOS). OXPHOS requires a minimum concentration of Ca^{2+} in the mitochondrial matrix since Ca^{2+} is used as a cofactor for pyruvate dehydrogenase, two tricarboxylic acid cycle (TCA) enzymes, [110] and the mitochondrial ATP synthase [111]. Mitochondria therefore require a constant supply of Ca^{2+} to operate. Given the low affinity for Ca^{2+} of the MCU, Ca^{2+} hotspots are required to promote Ca^{2+} influx into the mitochondrial matrix [64,110]. As previously described, Ca^{2+} hotspots occur specifically at MAMs, where IP_3R is enriched [62,63,65]. Therefore, IP_3R inhibition or KO decreases oxygen consumption and ATP synthesis [112]. Bringing the ER and mitochondrial membranes closer by expressing a synthetic linker, a construct with OMM and ER membrane targeting sequences, can instead significantly increase ATP synthesis [15].

MAM disruption via tethering deficiency impairs mitochondrial metabolism in yeast as well, given ERMES deletion mutants have significant growth defects when forced to perform OXPHOS [36]. This was investigated by assaying for growth on non-fermentable glycerol [36]. This is a common test for respiratory capacity in this model organism since glycolysis, the preferred metabolism of yeast, cannot be performed with non-fermentable carbons [113]. Instead, yeast catabolize glycerol via the L-glycerol-3-phosphate (L-G3P) pathway, which results in the catalytic conversion of glycerol into pyruvate through the action of three cytosolic enzymes [114]. The pathway also contributes electrons to the mitochondrial respiratory chain, which along with pyruvate, fuel the TCA cycle. Thus, yeast grown on glycerol switch entirely to respiratory metabolism, allowing researchers to study OXPHOS capacity in yeast. Another study showed certain ERMES deletion mutants have a lower respiratory capacity as determined by a tetrazolium assay [115]. This assay allows for the detection of respiration proficient colonies which metabolize the white compound into a reduced form that turns red upon the pH change invoked by respiration. The effect was mild though, as there was only a 10% decrease in the number of red colonies in ERMES mutants. The role of Ca^{2+} in this effect was not tested, so it remains unknown if Ca^{2+} is required for mitochondrial respiration as in mammals.

Nevertheless, there is significant evidence yeast mitochondria are also regulated by Ca^{2+}. Firstly, their oxidative dehydrogenases also require Ca^{2+} [116]. Secondly, their mitochondria take up Ca^{2+} in the range of that found in rat liver mitochondria, which is relatively high at 150-

400nM. Thirdly, Ca^{2+} chelators, increased extracellular Ca^{2+}, and mitochondrial uncouplers all alter matrix Ca^{2+}. This was assayed using the Ca^{2+}-sensitive fluorescent dye Fluo-3 to measure Ca^{2+} concentration in isolated mitochondria. When the extracellular Ca^{2+} chelator EGTA was used, mitochondrial Ca^{2+} decreased from roughly 400nM to 140nM. EGTA also decreased oxygen consumption in isolated mitochondria. Fourthly, increases in mitochondrial Ca^{2+} have been shown to increase ATP levels [117]. Therefore, multiple avenues of evidence indicate yeast mitochondria take up Ca^{2+} and that their metabolism is affected by it.

1.1.3.4 Apoptosis

Another critical role for Ca^{2+} flux at the MAM is apoptosis, since mitochondrial Ca^{2+} overload induces MOMP, resulting in cytochrome c release and the subsequent activation of caspases [19,118–120]. MOMP involves a massive increase in permeability that can be triggered by high Ca^{2+} levels activating a Ca^{2+}- and voltage-dependent high conductance channel on the IMM [120,121]. Opening of this channel results in loss of mitochondrial membrane potential, which disrupts mitochondrial function [120,121]. This channel is also known as the mitochondrial permeability transition pore (mPTP) and its opening results in mitochondrial swelling, rupture of the OMM, and release of mitochondrial contents [118,120]. mPTP composition has been difficult to uncover but is thought to include ATP synthase on the IMM [122]. On the OMM, VDAC1 has also been shown to participate in pore formation, although cells lacking VDAC1 can still undergo MOMP [123]. Deletion of two Bcl-2 family proteins, Bax and Bak, grants resistance to Ca^{2+}-induced mitochondrial swelling [120]. This led to the current model of MOMP, whereby Bax and Bak become activated during apoptotic signaling and oligomerize to form pores on the OMM, inducing MOMP [124].

Apoptosis is largely controlled by the Bcl-2 family of proteins, sometimes referred to as master regulators of apoptosis due to their regulation of the MOMP [124]. The family is composed of pro- and anti-apoptotic members which act in diverse pathways and manners [124]. Many anti-apoptotic members act by opposing the action of pro-apoptotic Bax and Bak [124,125]. This occurs either through direct binding of Bax and Bak to prevent their oligomerization, or indirectly by preventing mitochondrial Ca^{2+} overload [125]. On the other hand, pro-apoptotic members such as Bim can bind and activate Bax/Bak [126]. However, Bim is normally associated with the cytoskeleton, preventing Bax/Bak activation unless apoptotic signaling releases Bim [127]. To

regulate Ca^{2+} flux, some anti-apoptotic members interact with IP_3R and SERCA at the MAM [128–130]. For instance, anti-apoptotic Bcl-2 and Bcl-xL activate IP_3R to maintain pro-survival Ca^{2+} levels [128]. They have also been shown to inhibit VDAC1 and SERCA to prevent Ca^{2+} overload [131,132].

Unicellular organisms can undergo a cellular program similar to apoptosis called programmed cell death (PCD) [117,133]. PCD is distinct from necrosis or mechanically induced death in that inhibition of an intracellular signal or activity can prevent PCD [134]. Oppositely, death that is not programmed can be stopped by removing cells from the toxic stimuli causing death, such as removing an antifungal [133]. PCD in yeast is observed in response to physiological conditions such as pheromone release and ER stress due to disrupted lipid homeostasis or unfolded protein accumulation [135].

There are several hypotheses for why yeast would have a programmed death pathway to eliminate aged or unfit cells [134]. The main hypothesis proposed in the literature is that although yeast are unicellular organisms, a population of cells need to communicate with one another to survive, much like multicellular organisms [136]. Moreover, yeast colonies arise from a single clone, so programmed death of unfit cells in a colony could promote survival of the remaining cells, which carry the same genetic content. Indeed, experiments have demonstrated cells in the center of colonies can die once they have exhausted the resources available to them [137]. This in turn supports growth of more viable cells in the periphery.

Although the process is not exactly the same, several mammalian apoptosis trademarks have been observed during yeast PCD. For example, multiple studies have shown PCD induced either by pheromones, oxidative stress, or ER stress, triggers an increase in cytosolic Ca^{2+} [133,135,138]. This is reminiscent of the massive ER Ca^{2+} release that precedes mammalian MOMP [19,121]. *S. cerevisiae* also have a cytochrome c homolog, Ysp1, which is required for pheromone- and antifungal-induced PCD [133]. Further reproducing the system in mammals, increased cytosolic Ca^{2+} and mitochondrial Ca^{2+} overload has been shown to induce formation of the mPTP [139,140], though the existence of this structure in yeast remains controversial [140]. PCD also appears to require ER-mitochondria contact sites given a recent study demonstrated ERMES disruption impaired PCD induced by acetic acid [115]. Specifically, loss of subunits Mdm10 or Mdm34 prevented release of Ysp1 following exposure to acetic acid. In summary, there is evidence that

programmed cell death of *S. cerevisiae* also involves cytosolic Ca^{2+} changes, mitochondrial Ca^{2+} overload, and more recently, MAMs.

1.1.3.5 ER stress

Another important cell fate process linked to the MAM is ER stress, a perturbation of ER homeostasis that is characterized by two main features: aberrant protein accumulation and luminal Ca^{2+} imbalance [141]. To help nascent proteins achieve their correct conformation, the ER houses a group of enzymes referred to as folding assistants [141]. Folding assistants can be classified into three categories: chaperones, oxidoreductases, and glycosidases [142]. Glycosidases participate in protein folding by mediating the enzymatic addition and modification of glycan moieties to nascent proteins as they enter the ER through the translocon [143]. Oligosaccharyltransferase (OST) is the first glycosidase to act on nascent proteins, after which several other glycosidases participate to trim, add, remove, or otherwise modify the glycan[143]. Many glycan moieties are derived from glucose, so the process of glycosylation consumes glucose. Glycosylation is required for interaction with chaperones, enzymes that assist the folding of nascent proteins by binding to prevent protein aggregation.

Chaperones are also required for the re-folding of unfolded proteins, translocation of nascent proteins, and degradation of proteins that cannot be folded appropriately [142]. The different types of chaperones include lectins, heat shock proteins, and oxidoreductases. Lectins are chaperones that bind glycoproteins, such as Calnexin and Calreticulin [144,145]. Glycoprotein clients go through a series of glycan modifications to achieve adequate folding, re-entering the cycle several times if folding is not achieved after one attempt [145,146]. Another category of chaperones are heat shock proteins (HSPs), which can prevent protein aggregation by binding clients [147]. The heat shock family can also be further classified into ATP-dependent and ATP-independent chaperones [147]. The most abundant chaperone in many cells is the HSP member binding immunoglobulin protein (BiP), also known as 78-kDa glucose-regulated protein (GRP78) [148]. Lastly, the protein disulfide isomerase (PDI) family of chaperones catalyze the formation, isomerization, or hydrolysis of disulfide bonds, which are critical for proper protein folding [149]. These proteins are also known as oxidoreductases since they catalyze redox reactions. These reactions require the oxidizing environment that is maintained in the ER lumen. Formation of a disulfide bond in the client occurs via oxidation of cysteines in the oxidoreductase's thioredoxin (TRX) domain, which

consists of two cysteines (C) between any dipeptide sequence: CxxC [150,151]. This is an oxidase reaction, which can also catalyze disulfide bond isomerization [149]. Reduction of the cysteines hydrolyzes disulfide bonds in the client protein instead [149]. Given protein folding requires ATP, glucose, oxidizing conditions, and Ca^{2+} homeostasis, ER stress can be triggered by ER Ca^{2+} depletion, redox imbalance, and nutrient deprivation [141].

ER stress caused by an accumulation of unfolded proteins triggers the unfolded protein response (UPR), a multipronged approach to increase the ER's folding capacity and reduce the number of misfolded proteins [152]. This process is initiated by three ER transmembrane proteins: protein kinase R-like ER kinase (PERK), inositol-requiring enzyme 1 (IRE1), and activating transcription factor 6 (ATF6) [152]. There are two main proposed mechanisms for PERK and IRE1 activation. Normally, chaperones deal with unfolded proteins quickly and efficiently enough to prevent PERK and IRE1 binding misfolded proteins [152]. However, unfolded protein accumulation overwhelms chaperones and allows PERK and IRE1 to bind misfolded proteins [152,153]. This leads to their homodimerization and activation [152,154,155]. The other mechanism requires chaperones binding and inactivating PERK and IRE1 in basal conditions [155,156]. When unfolded proteins accumulate, the chaperones preferentially bind misfolded proteins, allowing PERK and IRE1 to homodimerize and become active [155,156]. For example, BiP interacts with both ER stress sensors in homeostasis, but preferentially binds unfolded clients as they accumulate [156]. BiP binding also prevents ATF6 activation, which requires its translocation to the Golgi [157]. Here, ATF6 is cleaved by proteases into a fragment that becomes a transcription factor [157]. This leads to the upregulation of genes that will alleviate ER stress, including the X-box-binding protein 1 (XBP1), a transcription factor that promotes transcription of UPR genes [152,157]. XBP1 mRNA must be cleaved into a smaller fragment to become a functional transcription factor [158]. This endonuclease activity is catalyzed by IRE1 [158]. This only occurs when ATF6 creates a sufficient amount of XBP1 mRNA, since XBP1 mRNA is found at low levels in homeostasis [158]. Finally, PERK activation results in phosphorylation of eukaryotic translation initiation factor 2 subunit-α (eIF2α) [159] eIF2α also upregulates genes involved in protein folding as well as attenuates protein synthesis to reduce the protein folding load. Another important downstream transcription factor is CCAAT/enhancer binding homologous protein (CHOP), which can be upregulated by all three UPR branches [152,160]. Rather than help alleviate ER stress, CHOP

induces apoptosis by upregulating pro-apoptotic proteins such as Bax, Bak, and Bim, or by repressing anti-apoptotic Bcl-2 and Bcl-xL [152,161].

These pathways can also induce degradation of misfolded proteins to alleviate ER stress via a process called ER-associated protein degradation (ERAD) [162]. ERAD involves the recognition of terminally misfolded proteins, proteins which can no longer be folded appropriately. The process of identifying and delivering terminally misfolded proteins often involves the action of glycosidases trimming glycans to tag these proteins as ERAD substrates. For example, ER degradation-enhancing α-mannosidase I-like (EDEM) interacts with terminally misfolded Calnexin clients and catalyzes mannose trimming to mark them as ERAD substrates [163]. However, not all proteins require a glycan modification to become degraded via ERAD [162]. BiP can also recognize ERAD substrates and deliver them to the ERAD complex on the ER membrane [164]. The ERAD complex contains several types of proteins, including chaperones and ubiquitin ligases [165]. Ubiquitin ligases mediate the addition of ubiquitin, which serves as a tag for degradation in the proteasome [166,167]. The proteasome is a large complex that recognizes ubiquitin-tagged proteins and catalyzes their degradation into small peptides [168]. The proteasome also interacts with the ERAD complex, immediately recognizing ERAD substrates as they are retro-translocated across the complex. Retro-translocation is partly induced by the ATPase p97 and can be facilitated by hydrolysis of disulfide bonds in ERAD substrates. ER-localized J protein 5 (ERdj5), an oxidoreductase that hydrolyzes disulfide bonds, has been shown to participate in this process [165].

Protein folding requires large amounts of ATP since many chaperones have ATPase activity, including one of the most abundant chaperones, BiP [169,170]. ATP is also required to maintain adequate Ca^{2+} conditions for folding assistants to operate [170]. This includes ATP consumed by the SERCA ATPase pump as well as ATP to allosterically activate IP_3R [72,79]. Ca^{2+} flux by SERCA and IP_3R in turn determines ER ATP levels by promoting mitochondrial respiration so that ER Ca^{2+} release coincides with an increase in ATP within the ER [171]. Ca^{2+} also affects the redox state of the ER, which must also be maintained for oxidoreductases to work adequately. For instance, Ca^{2+} loss has been shown to shift the lumen to a more reduced state.

Ca^{2+} is also important for protein folding as it is a co-factor for many folding assistants, including Calnexin, Calreticulin, and BiP [141]. Given these chaperones are required for folding of glycoproteins, secreted proteins, and integral membrane proteins, Ca^{2+} is absolutely essential for

protein folding [141,172]. Ca^{2+}-binding folding assistants also serve to buffer ER Ca^{2+} [172]. Thus, although the total Ca^{2+} concentration of the ER is roughly 0.1-1mM in mammalian cells [58], buffering by chaperones causes the concentration of free, available Ca^{2+}, to fall between 60-400μM [172].

Ca^{2+} dysregulation therefore triggers ER stress, which can activate SOCE to restore luminal Ca^{2+} levels [84]. SOCE is initiated when ER Ca^{2+} levels drop, activating PERK through a still unknown mechanism [173,174]. PERK then activates Calcineurin, a Ca^{2+}- and PERK-binding phosphatase that is required for STIM1 and Orai1 activation [84,173]. PERK also interacts with the actin cytoskeleton and can relocate STIM1 to the plasma membrane by promoting ER-plasma membrane contact sites upon ER Ca^{2+} loss [174].

The yeast UPR contains only one ER stress sensor, Ire1, which follows a pathway largely conserved from mammals [175]. Specifically, Ire1 is activated either by binding to unfolded proteins or via release from inhibitory binding of BiP homolog Kar2 [175,176]. Ire1 then homodimerizes and becomes active, binding and splicing *HAC1* mRNA, which encodes for a transcription factor [175,177]. Hac1 in turn binds and promotes the transcription of genes with a UPR responsive element (UPRE) in a pathway that is functionally homologous to XBP1 in mammals [158,177]. This includes genes encoding proteins required to alleviate ER stress, including chaperones such as Pdi1 and Kar2, as well as proteins required for ERAD [175,177].

ERAD is also well conserved in yeast. Their ERAD complex also consists of ubiquitin ligases, BiP homolog Kar2, and p97 homolog Cdc48 [168]. Moreover, research in yeast revealed the Sec61 complex acts as the channel involved in retro-translocation, since its loss prevented degradation of ERAD substrates [178]. Yeast are proposed to have three distinct types of ERAD complexes for substrates with folding lesions in their cytosolic (ERAD-C), luminal (ERAD-L), or membrane (ERAD-M) domains [168]. Similar ERAD subtypes have not been identified in mammals, where the process of lesion identification is likely more complicated [168].

Ca^{2+} is also broadly required for most protein glycosylation, sorting, and quality control in yeast [98,102]. For example, a key ERAD enzyme, ER mannosidase I, requires Ca^{2+} in both yeast and mammals [102]. It was therefore surprising to find Δ*pmr1* cells had only minor defects in bulk protein folding, secretion, or degradation [98,102,104]. Specifically, Δ*pmr1* cells have reduced degradation of a folding-incompetent mutant protein, carboxypeptidase Y (CPY*) [98,102]. They also have impaired trafficking of at least two native vacuolar protein and plasma membrane

proteins [98]. However, concomitant loss of Cch1 or Mid1, subunits of the HACS plasma membrane Ca^{2+} channel, triggered Hac1 activation [97]. Δ*pmr1* cells therefore likely compensate for their decrease in ER and Golgi Ca^{2+} by inducing Ca^{2+} influx via the HACS channel. This pathway is similar to mammalian SOCE, though as previously mentioned, no ER Ca^{2+} sensor has been identified in *S. cerevisiae* yet [91]. Moreover, this pathway can take up to an hour to create significant changes in cytosolic Ca^{2+} while SOCE in mammals takes seconds [97,179]. Indeed, tunicamycin-induced UPR was shown to activate HACS, but significant cytosolic Ca^{2+} accumulation only occurred after ~90 minutes [97]. Thus, ER stress and Ca^{2+} decrease also promote Ca^{2+} entry at the plasma membrane to restore Ca^{2+} homeostasis in *S. cerevisiae,* though the kinetics of this process are different compared to mammals.

As expected, Ca^{2+} chelation induces UPR signaling as assayed by a fluorescent UPRE reporter [97]. Similarly, Ca^{2+}-deficient medium upregulates proteins with a UPRE, including Kar2 [138]. Although Δ*pmr1* cells do not have high basal UPR signaling, likely due to their high HACS activity, they have high Kar2 amounts [98]. These mutants are also highly sensitive to reducing agent dithiothreitol (DTT) and tunicamycin [98]. This was also observed with Ca^{2+} chelation and Ca^{2+}-deficient medium [97,138].

Yeast also require cytosolic Ca^{2+} for transcriptional changes in response to ER stress [97]. This pathway is known as Ca^{2+} cell survival (CCS) and is particularly important during prolonged ER stress [97]. The CCS pathway activates Ca^{2+}-dependent pathways in response to a variety of insults, including ER stress [97,180]. One of the main proteins it activates is Calmodulin, a conserved Ca^{2+}-sensing protein [97,180]. When bound to Ca^{2+}, Calmodulin activates several kinases as well as Calcineurin, a Ca^{2+}/calmodulin-dependent phosphatase that is usually inactive during homeostasis [97,181]. Calcineurin then activates the calcineurin-dependent transcription factor Crz1, which upregulates genes required to restore Ca^{2+} homeostasis [182,183]. This includes the vacuole pump Pmc1, which transports Ca^{2+} into the vacuole and therefore decreases cytosolic Ca^{2+} [182,183]. Importantly, this pathway is independent of the UPR, since *IRE1* and *HAC1* null mutants had no defects in these responses [97]. Nevertheless, Ire1 and Hac1 signaling is also dependent on Ca^{2+} availability. Specifically, Ca^{2+} deprivation dampens Hac1-mediated transcription changes [97]. This includes transcription of the oxidoreductase Ero1, which is highly induced by Hac1 [97]. Interestingly, ER stress caused by Ca^{2+} chelation does not disrupt transcription of Ero1 at early time points, but prolonged stress eventually impairs its transcription [97]. Together, these results

suggest Ca^{2+} is dispensable for early UPR signaling but critical for cell survival during prolonged ER stress, particularly for transcriptional changes required to restore Ca^{2+} homeostasis.

The role of mitochondria in the ER stress response of yeast has only recently been explored. Recent studies have shown ER stress triggered by Ca^{2+} deprivation or tunicamycin can be relieved with increased mitochondrial respiration [138,184]. In one of these studies, cells grown in Ca^{2+}-depleted medium had UPR induction, growth and size defects, and reduced viability [138]. These cells were grown in glucose, where yeast preferentially perform glycolysis. In contrast, cells grown on non-fermentable carbons are unable to perform glycolysis and must rely on OXPHOS. Interestingly, when the carbon source was switched to non-fermentable acetate, Ca^{2+} depletion no longer caused growth defects or reduced viability. Cells with genetic deficiencies for glycolysis also had no Ca^{2+} depletion defects. Taken together, these experiments suggest mitochondrial respiration alleviates ER stress and growth defects caused by Ca^{2+} depletion. A more recent study has also shown ER stress induced by tunicamycin can activate mitochondrial respiration via Ire1 and Calcineurin [184]. Indeed, both proteins seem to promote the activity of cytochrome c, in turn increasing mitochondrial respiration. This was assayed by measuring cytochrome c oxidation and O_2 consumption in cells without Ire1 or Calcineurin. Whether this increase in mitochondrial respiration involves MAMs and Ca^{2+} flux, as it does in mammals, is unknown [185,186].

1.1.3.6 Mitochondrial fission and motility

The MAM is also a hub for mitochondrial motility since Ca^{2+} microdomains can halt mitochondrial movement [187,188]. This process is in part mediated by OMM protein Miro-2, which has Ca^{2+}-binding domains that regulate its GTPase activity [187]. Miro-2 promotes mitochondrial movement along microtubules by binding to the motor protein kinesin 1, but its GTPase activity is inhibited when exposed to high Ca^{2+} levels [187,189]. Thus, large ER Ca^{2+} bursts halt mitochondrial movement, which can stabilize MERCs and shorten the distances between these two organelles [185,188,189]. This process has been shown to occur during ER stress and helps restore homeostasis by increasing Ca^{2+} flux and OXPHOS [185].

Mitochondrial fission also occurs at the MAM and must be balanced with mitochondrial fusion, which is mediated by GTPases Mitofusin-1 and 2 in mammals and Fzo1 in yeast [190–192]. In mammals, the process requires the Mitofusins to form homo- and heterodimers on the OMM

of separate mitochondria[190,192]. Their dimerization activates their GTPase activity, which then drives membrane fusion [190]. The process is the same in yeast, though only Fzo1 homodimers form in this species [191,192]. Fission is instead performed by the GTPase dynamin related protein 1 (Drp1) in mammals and Dnm1 in *S. cerevisiae* [193,194]. Accumulation of this GTPase at MAMs immediately preceding fission has been observed in both organisms [195,196]. Microscopy studies in mammalian cells have demonstrated fission is initiated by an ER tubule extending and wrapping around mitochondria within membrane distances consistent with MCS (10-50nm) [196]. The ER tubule then constricts and reduces mitochondrial circumference through actin polymerization [196,197]. Drp1 simultaneously accumulates at these contact sites and forms a ring around the constricted mitochondrion [192,197]. Oligomerization at this site promotes its GTPase activity, which finishes the fission process [192]. This process is also regulated by Ca^{2+} since Ca^{2+} can activate Calcineurin and Ca^{2+}/calmodulin-dependent protein kinase I (CaMKI) in the cytosol, which then phosphorylate and activate Drp1 [192]. In summary, the MAM serves as a platform for mitochondrial motility, fusion, and fission.

1.1.3.7 Autophagy

Autophagy is an essential, highly conserved pathway that involves the formation of double membrane vacuoles to capture intracellular components and target them to lysosomes for their degradation [198]. This process is usually carried out at basal levels as a quality control system to degrade aged or damaged cellular components and is therefore also known as basal autophagy. This type of degradation is largely non-discriminate and usually degrades portions of the cytosol. Highly specific degradation of organelles is termed selective autophagy and is known to degrade mitochondria, ER, lipid droplets, and peroxisomes, amongst other organelles [199–201]. Autophagy also serves as a catabolic pathway that provides cells with energy via degradation of non-essential components while cells are under stress [201]. Thus, autophagy is massively upregulated with a variety of stressors such as nutrient deprivation, hypoxia, ER or oxidative stress, and DNA damage [202]. Autophagy begins with the formation of the membrane that will become the autophagosome, also known as the isolation membrane [201]. The second step involves autophagosome maturation and closure and the last step requires autophagosome-lysosome fusion and degradation of the enclosed contents [201].

Numerous studies have identified the ER, and more recently, the MAM subdomain of the ER, as a platform for isolation membrane formation [203–206]. This has led to the following detailed model of this first step in autophagy: firstly, key autophagy initiator complexes are recruited to the ER after inhibition of mammalian target of rapamycin complex 1 (mTORC1), the master regulator of autophagy [198]. In homeostasis, mTORC1 binds to and inhibits two key complexes: the Unc-51 like autophagy activating kinase-1 (ULK1) complex, and the phosphtatidyl-inositol-3-phosphate (PI3P) kinase class III (PI3K III) complex [201,207]. Autophagy inducers such as starvation inhibit mTORC1, allowing the ULK1 and PI3K III complexes to become active and translocate to the ER, where the isolation membrane will assemble [201,206]. Here, the ULK1 complex phosphorylates several proteins to promote autophagy [201,208]. One of its targets is vacuolar protein sorting 34 (VPS34), the catalytic component of the PI3K III complex [208]. Activating molecule in Beclin-1-regulated autophagy (AMBRA1), a scaffolding protein, also interacts with the PI3K III complex here and enhances its enzymatic activity [209]. The PI3K III complex is responsible for producing PI3P, which is not normally found on most organelles and therefore serves as a signal for the assembly of the autophagy machinery [210]. For example, the PI3P-binding WD-repeat domain phosphoinositide-interacting proteins (WIPIs) help recruit autophagy-related (Atg) proteins required for membrane elongation and closure [211]. These PI3P-enriched regions of the ER become the omegasome, a cup-shaped membrane extending from the ER that serves as a platform for the formation of the isolation membrane [206]. Interestingly, MCS have been observed between the ER membrane of the omegasome and the emerging isolation membrane [205,206,212]. These contact sites are thought to contribute to membrane expansion by serving as platforms for lipid transport [213]. This hypothesized *de novo* lipid synthesis and transfer at these MCS could be mediated by lipid biogenesis enzymes heavily enriched at the MAM, but this has not been tested. Isolation membrane expansion is also thought to occur via fusion with Golgi-derived vesicles containing the Atg9 protein, though this process is not fully understood yet [201].

Once at the omegasome, the ULK1 complex also activates Syntaxin 17, an ER soluble N-ethylmaleimide-sensitive factor attachment protein receptor (SNARE) [201,203]. Syntaxin 17 then interacts with Atg14L, a component of the PI3K III complex that anchors the complex to the omegasome [203]. Both Syntaxin 17 and Atg14L become enriched in biochemically isolated MAM fractions following starvation-induced autophagy [203]. This enrichment also occurs with several

other components of the PI3K III and ULK1 complexes, strongly suggesting the MAM is a site for autophagosome biogenesis during nutrient deprivation [203].

The second step in autophagy, autophagosome closure, requires the action of the Atg16L1 complex, which is composed of Atg12, Atg5, and Atg16 [201]. The Atg16L1 complex catalyzes the lipidation of LC3 I, a small protein found in the cytosol in basal conditions [214]. This modification results in the enrichment of LC3 II, the lipidated form of LC3 I, at the growing isolation membrane [201,215]. LC3 II localizes to both the inner and outer membrane of the autophagosome [215]. On the inner membrane, LC3 II is bound by autophagy receptors, proteins with LC3 interacting regions (LIRs) that also recognize and bind cargo proteins to be degraded [201,216]. Its role on the outer membrane is less understood, but LC3 II is also required for expansion and closure of the isolation membrane [201].

Once the autophagosome seals, it is usually transported along microtubules to the perinucleus, where most lysosomes usually reside [217]. Fusion with the lysosome is mediated by the concerted action of Rab GTPases, tethering proteins, and SNAREs [217]. Rab proteins regulate intracellular traffic through their ability to shuttle between specific membranes as they bind and release guanosine triphosphate (GTP) and guanosine diphosphate (GDP) in a cycle [218]. They do this by recruiting their binding partners, which include motors and tethering factors, to the different membranes they associate with [218]. Hence, Rab proteins are involved in multiple types and stages of vesicular formation, motility, and fusion [218]. The process of autophagosome-lysosome fusion is mainly mediated by Rab7, an endolysosomal Rab [217,219,220]. Rab7 is thought to be acquired on autophagosomes via fusion with endosomes in a process that has not been fully elucidated yet [217]. This fusion yields the amphisome, which is required prior to fusion with lysosomes [217]. Once the amphisome reaches the lysosome, Rab7 interacts with a tethering protein at the lysosomal membrane, which acts as a bridge to bring the membranes close enough to prime them for fusion, which is catalyzed by SNAREs [221]. SNAREs are categorized into Q or target/t-SNAREs and R or vesicular/v-SNAREs based on the SNARE domains they contain: Qa, Qb, Qc, or R [222]. SNAREs promote membrane fusion by assembling all four SNARE domains in a complex formed by an R-SNARE on one membrane and three Q-SNAREs on the other membrane. This brings the SNARE domains together in a “zippering” process that drives membrane fusion as the SNAREs form a stable four-helix bundle with all four SNARE domains. Thus, Syntaxin 17 on the amphisome interacts with a SNARE complex on the lysosomal

membrane and induces membrane fusion [217]. Once the membranes fuse, the contents of the amphisome are degraded by lysosomal hydrolases [213].

Autophagy in yeast largely relies on the same mechanisms described in mammals [223]. However, autophagosome biogenesis in yeast always occurs at a specific intracellular location: the pre-autophagosomal structure (PAS) [223,224]. The PAS is defined as the site of assembly of Atg proteins required for autophagosome biogenesis and is located adjacent to the vacuole [224]. No PAS has been described in mammals [201]. Furthermore, only one autophagosome at a time is formed in yeast while mammals usually produce multiple autophagosomes at multiple intracellular locations [223–225].

Indeed, the Golgi [226], plasma membrane [227], ER [205,212], mitochondria [228], and MAM [203,204] have all been described as platforms for basal autophagosome formation in mammals. However, the vast majority of these studies report the ER as a site of autophagosome biogenesis [201,203–205,212,229]. Thus, the ER is predominantly regarded as the main site of isolation membrane formation in mammals [201,230,231]. Strong evidence also suggests the MAM subdomain of the ER is the main site of autophagosome formation during starvation-induced autophagy [201,203,231]. As previously mentioned, one study demonstrated several subunits of the ULK1 and PI3K III complexes become enriched in biochemically isolated MAMs following starvation-induced autophagy [203]. Similarly, Atg14L as well as Atg5, another isolation membrane protein, colocalize with both the ER and mitochondria in fluorescence microscopy of starved cells. Additionally, essential autophagy protein Atg5 colocalized with the ER and mitochondria over 95% of the time following starvation. Separate electron tomography and electron microscopy studies have also observed isolation membranes originating at the MAM [203,204]. One of these studies identified isolation membranes via immuno-electron microscopy with LC3 antibodies and found almost 80% of these membranes were adjacent to the ER or mitochondria during starvation-induced autophagy [204]. Further supporting this model, cells lacking the MAM tether Mitofusin-2 or the tethering regulator PACS-2 have impaired basal and starvation-mediated autophagy [203,228]. These results strongly suggest the MAM is the main platform for autophagosome formation following nutrient deprivation [203,204,228].

Other studies have also reported MAM proteins regulate autophagosome formation [232,233]. One study found loss of the MAM tethering complex VAPB-PTPIP51 decreased IP_3R-mediated Ca^{2+} transfer to mitochondria and increased autophagy [232]. The overexpression of either VAPB

or PTPIP51 instead increased Ca^{2+} flux and impaired autophagy. Concomitant MCU silencing or IP_3R inhibition in these cells restored autophagy, strongly suggesting the effects of VAPB-PTPIP51 on autophagy are Ca^{2+}-dependent. Importantly, starvation-induced autophagy was not inhibited in these cells. These results therefore do not contradict those observed in Mitofusin-2 and PACS-2 KO cells, where starvation-induced autophagy was impaired [203,228]. Instead, VAPB/PTPIP51 overexpressing cells had impaired autophagy in response to chemical inhibitors of mTOR while starvation triggered autophagy normally [232]. Taken together, these studies suggest different MAM tethering complexes are required for different types of autophagy, where they could have activating or inhibiting effects.

Additional studies have also found impaired ER-mitochondria Ca^{2+} flux can activate autophagy, highlighting the importance of MAM signaling in autophagy regulation [112,232–234]. One of the first studies to report this effect found IP_3R disruption decreased the activity of Ca^{2+}-sensitive OXPHOS enzymes and lowered ATP levels [112]. This led to the activation of adenosine monophosphate (AMP)-activated protein kinase (AMPK), a master regulator of cell bioenergetics. AMPK signaling acts to restore homeostasis by activating catabolic pathways that will increase ATP biosynthesis. It simultaneously inhibits non-essential anabolic processes that consume ATP. One catabolic pathway it activates is autophagy, which releases carbohydrates, nucleic acids, amino acids, and fatty acids following lysosomal degradation [235]. These metabolites are then used by the cell either as substrates for biosynthesis or as sources for energy production.

Lastly, the lipid raft nature of the MAM also contributes to the process of autophagosome biogenesis [209]. Lipid rafts are membrane microdomains enriched in sphingolipids and cholesterol thought to facilitate lipid-protein interactions involved in signaling and membrane remodeling. They are also characterized by having extensive lipid biosynthesis and modification. Specifically, ganglioside 3 (GD3), a lipid commonly found in lipid rafts at the MAM, interacts with several autophagy initiating proteins including AMBRA1 and WIPI1. This interaction stabilizes these autophagy proteins, facilitating formation of the isolation membrane.

1.1.3.8 Reactive oxygen species (ROS)

ROS are another important signaling molecule at MAMs. The vast majority of ROS in homeostasis originates in mitochondria due to electron leak from OXPHOS after Ca^{2+} enters the

mitochondrial matrix [236]. However, ROS is also produced in the ER by oxidoreductases, including the MAM-localized Ero1α [170,237]. Studies have shown ROS release from the ER and mitochondria creates sites of high ROS concentration at MAMs called ROS microdomains [236,238]. Much like Ca^{2+} hotspots, ROS microdomains affect MAM functions and proteins [236,238]. Additionally, ROS and Ca^{2+} crosstalk at the MAM to regulate the activity of proteins mediating their production [236]. For example, Ca^{2+} overload from the ER can trigger high mitochondrial ROS production and MCU oxidation, which enhances MCU activity [239]. In turn, ROS can influence Ca^{2+} flux since SERCA2b and IP_3R are regulated via oxidation [170]. The redox reactions involved in this regulation are catalyzed by several MAM localized oxidoreductases [170]. This redox regulation of SERCA2b and IP_3R by ER folding assistants will be described in detail below.

1.2 MAM modulators

There are several factors known to regulate the number of ER-mitochondria contacts and the activity of MAM proteins. They include cell cycle stage [240], cell type, culture conditions, oxidation state, metabolic status [18], and ER stress [185]. The mechanisms behind this plasticity are not completely understood, though they usually fall into two main categories: i) modulation of Ca^{2+} channel/pump activity, and ii) modulation of tethers. However, there is a lot of diversity in how different conditions and stressors do this. The following sections will detail how ER stress, the most understood MAM regulator, directly promotes MAM tethering and Ca^{2+} modulation.

1.2.1 ER stress induces MAM formation

ER stress was one of the first stressors shown to promote MAM tethering [15]. Specifically, acute ER stress can increase the number of MERCs by up to 25% and their average length by over 50% (from 220nm). Numerous studies have shown this increase in ER-mitochondria tethering promotes Ca^{2+} flux to: i) stimulate OXPHOS to relieve ER stress by increasing ATP biosynthesis [15,185,241] or, ii) if the stress persists, induce Ca^{2+} overload and apoptosis [15,121,242]. For instance, a short 4hr incubation with tunicamycin induces mitochondria and the ER to move towards the perinuclear area, which significantly increases their co-localization in fluorescence microscopy analyses [185]. This increase in MERCs was also observed in electron microscopy in this and other studies [15,185]. These changes were coupled with an increase in IP_3R-mediated

mitochondrial Ca^{2+} uptake, oxygen consumption, and cellular ATP [15,185]. More recent studies have demonstrated MAM dysfunction triggers ER stress and UPR signaling, suggesting this pathway could be a mechanism by which MAM tethering is restored.

1.2.2 Disruption of MAM tethering induces ER stress

Several studies have demonstrated MAM tethering disruption induces ER stress [30,243,244]. For example, loss of the tethering regulator PACS-2 not only decreases the number of MERCs but also doubles BiP levels [30]. Several studies have also shown Mitofusin-2 KO cells activate all three branches of the UPR and contain more ER chaperones [243–245]. Indeed, loss of Mitofusin-2 increases BiP and CHOP transcription *in vitro* and *in vivo* [243,245]. PERK and its downstream mediator eIF2α are particularly active in Mitofusin-2 KO cells and mice [244]. Interestingly, Mitofusin-2 has been shown to bind PERK. Given its loss activates PERK, Mitofusin-2 is thought to act as an upstream inhibitor in basal conditions. These studies suggest there is a tight link between the MAM proteome and the UPR which allows MAM tethers to directly regulate ER stress mediators.

There are several ways ER stress directly regulates tethering to promote contact formation, including transcription [243]. For example, acute ER stress induced by tunicamycin or the SERCA inhibitor thapsigargin increased Mitofusin-2 mRNA and protein levels. This increase was preceded by eIF2α phosphorylation, suggesting PERK activation induces this upregulation. ER stress sensors can also directly support MAM tethering and functions. For instance, PERK is found in biochemically isolated MAM fractions and evidence suggests it can act as a tether and support ER-mitochondrial Ca^{2+} flux [246]. Indeed, PERK KOs are more resistant to ER stress-induced apoptosis, which is consistent with them having significantly fewer MERCs. These defects were rescued when PERK KOs were transfected with kinase-dead PERK, suggesting its catalytic activity is not required for MAM tethering. Conversely, transfection with a PERK mutant lacking its cytosolic portion did not reverse these effects. Given PERK is found on MAMs, these results suggest the cytosolic portion of PERK could act as an ER component of a tethering complex. Taken together, these results suggest PERK influences MAM functions by directly promoting tethering.

IRE1 is also found at the MAM and can regulate IP_3R activity [247–249]. Specifically, IRE1 deficient cells have higher apoptosis rates due to increased IP_3R-mediated Ca^{2+} release into the

cytosol and subsequent uptake by mitochondria [248]. Like PERK, this effect was independent of its catalytic domain, suggesting its role in the UPR is not responsible for these effects [249]. IRE1 binds two known regulators of IP_3R that mediate channel opening, which could explain why its loss dysregulates IP_3R activity [248]. Thus, IRE1 does not appear to act as a tether but instead as a scaffold to support IP_3R tethering and activity [249].

1.2.3 ER folding assistants regulate ER Ca^{2+} channels and pumps

The MAM contains numerous ER chaperones and oxidoreductases, underscoring their importance at these sites [170]. One of their common functions at the MAM is regulation of IP_3R and SERCA2b activity. This allows folding assistants to modulate mitochondrial ATP production by regulating the release and uptake of Ca^{2+} from the ER. Given ATP is required for protein folding, ERAD, and ER homeostasis, this function allows folding assistants to maintain the conditions that support their protein folding activities. Their MAM enrichment, as well as their binding to IP_3R and SERCA2b, changes in response to a variety of stressors and conditions, once again reflecting the complex and dynamic nature of the MAM. The main folding assistants regulating SERCA2b and IP_3R at the MAM include Calnexin, Ero1α, thioredoxin-related transmembrane protein 1 (TMX1), Sigma-1 receptor (SIGMAR1), ER-resident protein 44 (ERp44), ERdj5, and ERp57 [170,250].

IP_3R activity is in part regulated by BiP and SIGMAR1 [251]. SIGMAR1 is a Ca^{2+}-sensitive, membrane-bound chaperone that counteracts protein aggregation. SIGMAR1 and BiP interact during homeostasis, but unlike most chaperone complexes, their activities decrease when bound to each other. ER Ca^{2+} loss induced by ER stress triggers their dissociation, allowing SIGMAR1 to interact with IP_3R instead. This interaction in turn stabilizes IP_3R, which is otherwise degraded when activated by its agonist, IP_3. Thus, SIGMAR1 stabilizes IP_3R and promotes ER-mitochondria Ca^{2+} flux. IP_3R is also regulated by ERp44, a luminal oxidoreductase which binds IP_3R at the same site as SIGMAR1 [252]. ERp44 preferentially binds IP_3R during ER stress, when the ER has low Ca^{2+} and reducing conditions. This interaction inhibits IP_3R activity, preventing apoptosis due to large ER Ca^{2+} release. ERp44-mediated inhibition also results in increased ER Ca^{2+} levels, which helps resolve ER stress. ERp44-mediated inhibition requires cysteine residues on IP_3R[252], suggesting ERp44's oxidoreductase activity is required for these effects [253]. When ER stress is not resolved, IP_3R activity is sustained to induce apoptosis [254]. This activation is

mediated by Ero1α, which is upregulated during the UPR. Ero1α activates IP_3R by oxidizing it and disrupting ERp44 binding.

SERCA2b activity is largely controlled by the oxidation state of its luminal and cytosolic cysteines [81,255]. SERCA2b has several cytosolic cysteines but only mutation of the highly conserved cysteine 674 (C674) alters its ATPase activity [256]. Several studies suggest oxidation of C674 promotes SERCA2b's ATPase activity while hyperoxidation of its cytosolic cysteines inhibits it [256–258]. SERCA2b also has two well conserved luminal cysteines that regulate its activity [81]. The effect of these cysteines on SERCA2b activity is less understood but some studies suggest oxidation and disulfide bond formation between the cysteines inhibits its activity [81,255,257]. However, these studies also suggest a minimal level of oxidation of luminal and cytosolic cysteines is required for ATPase activity [81,255,257]. Indeed, SERCA2b appears to be most active when its cysteines are only partially oxidized while hyperoxidation causes inactivation [81,257,258]. Reduction of its luminal cysteines therefore activates SERCA2b [255].

The MAM-localized folding assistants that regulate SERCA2b activity include ERp57, ERdj5, Calnexin, and TMX1. During ER stress, the reductase ERdj5 hydrolyzes the disulfide bond between the luminal cysteines and therefore activates SERCA2b [255]. In oxidizing conditions, ERp57 is thought to inhibit SERCA2b, but the exact mechanism remains unknown [170,257]. During basal conditions, Calnexin binds SERCA2b and sustains its partially oxidized state, maintaining the ATPase in its active state [259]. TMX1 is instead thought to inhibit SERCA2b, since TMX1 overexpression significantly decreases ER Ca^{2+} compared to WT cells [260].

Calnexin and TMX1 are amongst the few proteins consistently found in MAM fractions in unbiased proteomic analyses [24,25,261]. This indicates Calnexin and TMX1 are highly MAM-enriched in a variety of tissues and organisms, suggesting they play a key role there. As previously discussed, ER-mitochondria Ca^{2+} flux has important consequences on mitochondrial metabolism, cell fate, and MAM properties. Thus, Calnexin and TMX1 regulation of SERCA2b activity has a wide number of effects on the MAM [259,260]. These effects, as well as their individual chaperoning functions, will be discussed in further detail in the following sections.

Regulation of ER Ca^{2+} uptake and release in *S. cerevisiae* is far less understood, partly because yeast lack IP_3Rs and no mechanism has been described for the ion's release yet [91]. Nevertheless, the ER/Golgi Ca^{2+} ATPase Pmr1 is thought to act as a SERCA functional homolog

[95], opening up the possibility it also influences ER-mitochondria Ca^{2+} flux and MAM functions. In support of this hypothesis, recent evidence has shown luminal redox changes disturb ER Ca^{2+} homeostasis [108]. Interestingly, this study showed loss of an oxidoreductase caused significant luminal oxidation and Ca^{2+} dysfunction, strongly suggesting folding assistants in yeast may also mediate redox-dependent regulation of Ca^{2+} channels and/or pumps. Specifically, cells without the ER-enriched oxidoreductase Glutaredoxin 6 (Grx6) have a highly oxidizing lumen as assayed by a redox-sensitive fluorescent probe. They also have lower ER Ca^{2+} and almost twice the level of cytosolic Ca^{2+} compared to WT cells. Their results suggest the decrease in ER Ca^{2+} occurred downstream of the luminal hyperoxidation, suggesting redox-dependent Ca^{2+} changes occur in yeast too. This was tested by assaying for growth of doxycycline-inducible Ero1-deficient mutants ($tetO_2$*ERO1*), which have severe growth defects and a highly reducing ER in the absence of the essential ER oxidase Ero1. $tetO_2$*ERO1* cells grew significantly better when treated with the oxidant diamide or when coupled with a Δ*grx6* mutation, suggesting the highly oxidizing lumen caused by loss of Grx6 could also rescue these cells. However, concomitant Δ*pmr1* mutations did not rescue $tetO_2$*ERO1* cells, suggesting the low ER Ca^{2+} due to loss of Pmr1 cannot rescue the effects of a highly reducing lumen; only the hyperoxidized lumen of Δ*grx6* can. Together, these results strongly suggest oxidoreductases can alter ER Ca^{2+} homeostasis in mammals as well as yeast. Whether this function extends to regulation of MAM tethering or ER-mitochondria Ca^{2+} flux in this model organism remains unknown.

Recent evidence has also shown redox regulation of Ca^{2+} channels and pumps exists in yeast. For example, one study found the vacuolar Ca^{2+} channel Yvc1 can be activated by glutathionylation of cytosolic cysteines [262]. This modification was catalyzed by the yeast glutathione S-transferase Gtt1, which induced a large release of Ca^{2+} from the vacuole into the cytosol during apoptosis. This modification was reversible via the action of the yeast thioredoxin protein Trx2. Another study demonstrated Cch1 is also redox regulated and is activated by Gtt1 and inhibited by Trx2 [263]. It is therefore plausible redox regulation of other Ca^{2+} channels and pumps, including Spf1/Cod1 or Pmr1, occurs in yeast.

1.2.3.1 Calnexin

Calnexin is a Ca^{2+}-binding ER chaperone that binds glycoproteins to slow down and facilitate their folding [264,265]. Calnexin clients include newly synthesized soluble and membrane-bound

glycoproteins [264,265]. Its folding clients go through a cycle to become properly folded, which also involves the following proteins: UDP-glucose glycoprotein glucosyltransferase (UGGT), Glucosidases Glu I and Glu II, and ERp57 [145]. The cycle starts when an N-glycan moiety is added to a protein as it enters the ER lumen while being transcribed. Glu I and II trim the N-glycan moiety to a form recognizable by Calnexin. Calnexin then interacts with the client and another chaperone, such as ERp57, to promote folding. If folding fails, UGGT glycosylates the client, starting the cycle once more to attempt correct folding. If the cycle fails multiple times, clients are instead targeted for degradation via ERAD.

Calnexin is an abundant ER transmembrane chaperone that can shift localization between ER subdomains to perform different functions [266,267]. Under basal conditions, Calnexin is mostly found at the MAM [267]. However, acute ER stress shifts it to the peripheral ER, which consists of ER tubules and sheets spread throughout the cytoplasm. At the peripheral ER, Calnexin often interacts with the RTC, which allows it to bind clients as they move across the complex [266]. Here, Calnexin also plays an important role as Ca^{2+}-buffering protein along with other Ca^{2+}-binding folding assistants such as Calreticulin and BiP [172].

MAM localization of Calnexin requires action of the sorting protein PACS-2, which is itself MAM-enriched [31]. MAM localization also requires a post-translational modification known as palmitoylation, which adds a highly hydrophobic palmitate to exposed cysteines, serines, or threonines [267]. Palmitoylation can contribute to membrane association, particularly when it occurs in membrane-proximal residues, such as in Calnexin. At the MAM, Calnexin interacts with SERCA2b and preserves its redox status, thereby allowing SERCA2b to maintain its activity [259]. This was determined by studying the abundance of reduced SERCA2b with a biotinylated iodoacetamide (BIAM) switch assay, which results in the biotinylation of reduced cysteines on proteins. Myc-tagged SERCA2b was then immunoprecipitated and biotin probed for by immunoblot in samples obtained from Calnexin WT and KOs cells. This assay revealed Calnexin KOs had almost twice as much reduced SERCA2b as WT cells, indicating Calnexin is required to maintain SERCA2b in an oxidized, and therefore active, state (Figure 1.3). On the other hand, loss of Calnexin caused SERCA2b to become highly reduced. Further supporting this model, Calnexin KOs also have significantly lower ATPase activity in isolated light membranes containing the ER, suggesting they have decreased SERCA2b activity. This effect is thought to occur via interaction with a known Calnexin binding partner and redox regulator of the ATPase

pump: the nicotinamide-adenine dinucleotide phosphate (NADPH) oxidase 4 (Nox4). This was determined by incubating both WT and Calnexin KOs with a Nox4 inhibitor, which decreased the ATPase activity of WT cells to similar levels as those observed in KOs. Inhibition of Ero1α had a similar effect, suggesting Calnexin regulates SERCA2b's oxidation state via Ero1α as well.

Loss of Calnexin-mediated SERCA2b activity resulted in several MAM-associated defects [259]. Firstly, Calnexin KOs had lower ER Ca^{2+} as assayed by ER-specific fluorescent Ca^{2+} probes. A mitochondrial Ca^{2+} probe revealed they also have low Ca^{2+} in this organelle, likely as a result of their decreased ER Ca^{2+}. Secondly, Calnexin KOs were more resistant to apoptotic insults, consistent with their low mitochondrial Ca^{2+}. Thirdly, Calnexin KOs had a lower respiration rate as assayed by their oxygen consumption. Interestingly, although their mitochondrial ATP output was roughly the same as in WT cells, they had a significantly higher citrate synthase activity. This suggests Calnexin KOs attempt to compensate for their low mitochondrial Ca^{2+} by increasing the enzymatic activity of their TCA enzymes. Consistent with their low respiration rate, they had higher levels of glycolytic enzymes and were more reliant on glycolysis. Fourthly, electron microscopy revealed they have tighter and longer MAMs. In summary, these results demonstrate loss of Calnexin results in lowered SERCA2b activity concomitant with low ER and mitochondrial Ca^{2+}, resistance to apoptosis, lower respiration rates, and closer and more extensive ER-mitochondria contact sites.

1.2.3.2 Cne1

The *S. cerevisiae* calnexin homolog, Cne1, shares roughly 23% identity with mammalian Calnexin and has similar chaperoning activities [268,269]. Specifically, Cne1 also binds glycoproteins and is also an ER-membrane protein [268]. *S. cerevisiae* lack a UGGT homolog, suggesting this organism has a slightly different, and likely simpler, protein glycosylation system [270]. Nevertheless, Cne1 is also able to resolve aggregation of glycoproteins [268,269]. Thus, Δ*cne1* cells have minor defects in protein folding of glycosylated proteins [269]. Otherwise, Δ*cne1* cells do not have major protein folding or growth defects [268,271]. One key difference with Calnexin is that Cne1 does not bind Ca^{2+} [268,269]. It is therefore possible Cne1 is not involved in Ca^{2+}-dependent pathways unlike its mammalian counterpart. There is also no evidence of Cne1 interacting with any ER Ca^{2+} channels or pumps [268,269].

1.2.3.3 TMX1

TMX1 is part of the PDI superfamily of chaperones which are defined by the presence of at least one TRX motif [272,273]. The cysteines in the CxxC motif cycle between reduced and oxidized states, allowing these enzymes to catalyze reversible redox reactions [149]. This grants oxidoreductases the ability to catalyse the formation or isomerization of disulfide bonds via oxidation of their cysteines. Conversely, disulfide bond hydrolysis is driven by their reduction. Correct disulfide bond formation is a rate-limiting step in protein folding, underscoring the importance of this superfamily [273]. Members with catalytically inactive TRX domains also exist and often perform general chaperoning functions [274].

TMX1 is one of only five transmembrane PDI superfamily members in mammals, which also include TMX2, TMX3, TMX4, and TMX5 [273]. TMX1 has a single TRX motif, CPAC, which is uncommon amongst mammalian TRX-containing proteins, where CGPC is the most common sequence [274,275]. It is usually found in its reduced form and is therefore thought to have a reductase activity in basal conditions [272,276]. TMX1 is highly selective as it appears to act almost exclusively on membrane-associated clients [272,275]. Calnexin is thought to help TMX1 identify glycosylated clients since together they form a functional complex that promotes folding of membrane-associated, N-glycosylated clients [277]. A recent study has demonstrated TMX1 not only promotes protein folding but also participates in ERAD [278]. Indeed, TMX1 was required for ERAD of certain membrane-bound substrates.

TMX1 is found throughout the ER but is particularly enriched at MAMs, showing a similar localization pattern as Calnexin [260,267]. Like Calnexin, TMX1 is also palmitoylated when enriched at the MAM [267]. Oxidative stress also promotes its enrichment at the MAM, where TMX1 can interact with SERCA2b and inhibit its activity [260]. This effect has not been directly demonstrated yet, but the following evidence strongly suggests TMX1 acts to inhibit SERCA2b [260]. After co-immunoprecipitations demonstrated TMX1 and SERCA2b are binding partners, SERCA2b activity was studied indirectly using organelle-specific Ca^{2+}-sensitive fluorescent probes. In support of the hypothesis that TMX1 inhibits SERCA2b, TMX1 overexpression decreased ER Ca^{2+} levels to roughly 50% compared to WT cells. TMX1 KOs instead had a significantly higher ER Ca^{2+} content. Ca^{2+}-depleted TMX1 KOs could also take up significantly more Ca^{2+} into the ER after the ion was reintroduced to the media, suggesting SERCA2b was more active. Cytosolic uptake of the ion following histamine-induced IP_3R Ca^{2+} release was

quicker in TMX1 KOs compared to WT cells, once more suggesting increased SERCA2b activity. Addition of the SERCA inhibitor thapsigargin eliminated this effect, confirming the change in Ca^{2+} uptake occurred due to SERCA2b activity.

Like Calnexin KOs, TMX1 KOs also had MAM-associated defects. For instance, TMX1 overexpressing cells had higher mitochondrial Ca^{2+} and respiration while KOs had low Ca^{2+} and respiration [260]. Consistent with this observation, TMX1 KOs had less mitochondrial Ca^{2+} uptake following histamine-induced IP_3R Ca^{2+} release, which is indicative of lower ER-mitochondria Ca^{2+} flux. Likely as a compensatory mechanism for their low mitochondrial metabolism, these cells had more glycolytic enzymes and were more resistant to glucose deprivation than WT cells. These results suggest loss of TMX1 shifts metabolism towards glycolysis. Lastly, TMX1 KOs had a significantly lower average MAM length of ~135nm compared to ~170nm in WT cells. This is likely also a compensatory mechanism for their low ER-mitochondria Ca^{2+} flux. In brief, these results strongly suggest TMX1 inhibits SERCA2b, though the mechanism remains unknown.

1.2.3.4 Eps1: candidate TMX1 functional homolog

The PDI superfamily is highly diverse both in terms of structure and function [274]. PDI superfamily proteins are often quite divergent and primary sequence identity between members can be as low as 10% [279]. Phylogenetic studies have also shown no functional phylogenetic group has complete active site conservation and roughly 50% of proteins from a wide variety of species do not conserve both cysteines in the CxxC motif [274]. A common substitution for these cysteines is serine or threonine, which can also participate in redox reactions [280]. All of these factors make the study of homologous relationships of thioredoxin proteins a complex process.

The mammalian PDI family contains 21 members while yeast contain only 5 members: Pdi1, Mdp1, Mdp2, Eps1 and Eug1 [281]. Of these, only Pdi1 has an established functional homolog in mammals: PDI [282]. Pdi1 catalyzes disulfide bond isomerization and oxidation and its loss causes lethality [282]. The remaining family members are not essential and are usually expressed at low levels in homeostasis [281]. Mdp1 is known to catalyze disulfide bond formation and can interact with Cne1, presumably to aid in the folding of Cne1-glycosylated clients [281,283]. Mdp2 function remains unknown [284]. Both Mdp1 and Mdp2 show no homology to any known mammalian protein [281]. Eug1 function is also unknown, though it does not appear to have any oxidoreductase

activity [281]. Other catalytically inactive PDI family proteins can promote folding of nascent proteins or participate in ERAD [274]. Therefore, it is possible Eug1 participates in similar redox-independent mechanisms. Eps1 is the only membrane-bound member of the family [285] and has therefore been hypothesized to be the closest functional homolog to TMX1 [283]. Its functions are still not fully understood but at least one study found it was involved in ERAD of membrane-bound proteins [286]. This function was also recently demonstrated for TMX1, suggesting Eps1 and TMX1 have similar functions [278].

Phylogenetic studies also suggest Eps1 is related to TMX1. Eps1 has two TRX-like domains: CPHC and CDKC [287]. One study suggests its CPHC motif and the CPAC motif of TMX1 form a phylogenetic group amongst thousands of TRX-containing proteins from all domains [274]. Its second motif, CDKC, is not easily reduced, suggesting it is catalytically inactive [288]. Eps1 loss impairs the normal secretion of proteins with disulfide bonds, likely due to loss of its first catalytically active TRX motif [286]. A more recent study suggested Eps1 has protein disulfide isomerase activity, although *in vitro* activity was not actually tested [289]. This was instead based on X-ray crystal structure comparison to other PDI isomerases as well as phylogenetic analysis of its first TRX domain. These analyses suggest the CPHC domain is catalytically active and could perform isomerization reactions required for protein folding and secretion. Δ*eps1* cells are viable, grow normally on YPD, and have no severe protein folding defects [285,286]. However, they have minor defects in ERAD of membrane bound substrates and processing of secretory proteins with disulfide bonds, suggesting Eps1 participates in these processes [286,287]. Additional studies have shown Δ*eps1* cells have higher UPR activation compared to WT cells, though *EPS1* itself is not transcriptionally upregulated during the UPR [287]. As with Cne1, there has been no research on its effect on Ca^{2+} homeostasis, mitochondrial metabolism, or MAMs.

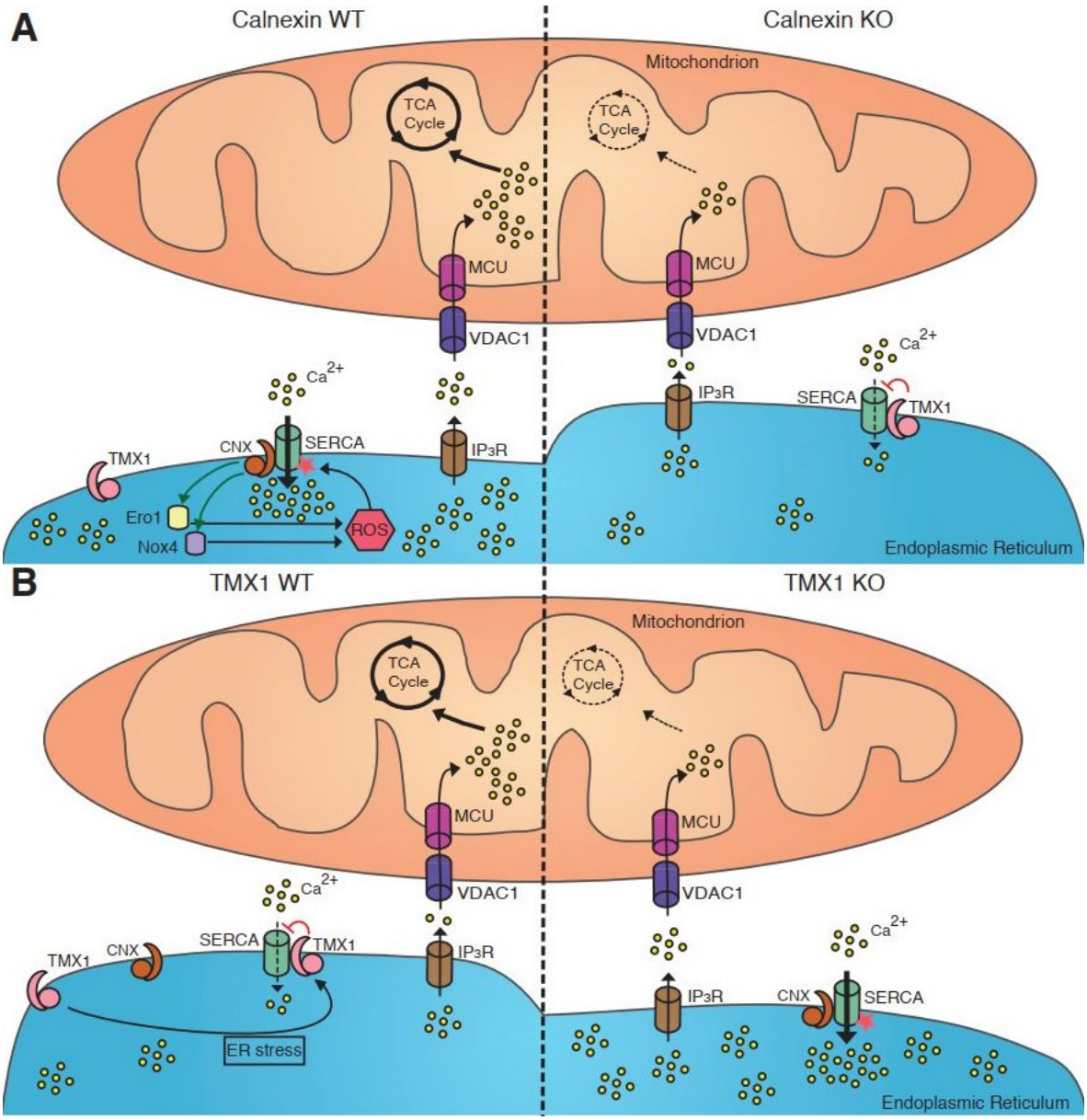

Figure 1.3 ER-mitochondria Ca^{2+} flux in TMX1 and Calnexin WT and KO cells
A. Schematic drawing of Ca^{2+} flux at MAMs in Calnexin (CNX) WT and KO cells. CNX WTs have looser MAMs, high ER Ca^{2+} and high SERCA2b activity. CNX interacts with SERCA2b and supports its ATPase activity via Ero1α and Nox4, which produce reactive oxygen species (ROS) that oxidize SERCA2b (indicated by star). CNX likely preferentially binds SERCA2b over TMX1. Mitochondria have high Ca^{2+} which fuels their tricarboxylic acid (TCA) cycle. In CNX KOs, TMX1 binds SERCA2b and inhibits its activity through a still unknown mechanism. This results in low ER and mitochondrial Ca^{2+}. **B.** TMX1 WT cells have tighter MAMs. TMX1 is enriched at the MAM with ER stress where it interacts with and inhibits SERCA2b. Mitochondria have high Ca^{2+} and TCA cycle activity. In TMX1 KOs, CNX bind SERCA2b and promote its activity resulting in high ER Ca^{2+}. These cells also have low mitochondrial Ca^{2+} and TCA cycle activity.

1.2.4 Rab32: a MAM modulator of the Rab GTPase family

Another protein that can regulate several aspects of the MAM is Rab32 [290]. Rab32 is part of the Rab GTPase family, a large group of conserved proteins that regulate intracellular traffic in all known eukaryotes [218]. Their high specificity for effectors and membrane residency allows Rabs to act as master regulators of traffic and establish membrane identity [218,291]. Rabs move effectors from a donor membrane to a target membrane via the GTP cycle [292,293]. Most Rabs do not interact with effector proteins in their inactive, GDP-bound state, while GTP-bound Rabs are usually active and can bind effectors [293]. Geranylgeranylation at one or two cysteines in their C terminus allows Rab proteins to insert into membranes, where two types of proteins regulate their GDP/GTP binding state: guanine exchange factors (GEFs) and GTPase activating proteins (GAPs) [294,295]. GEFs are usually associated with the donor membrane and catalyze the release of GDP, which prompts GTP binding due to the high GTP/GDP ratio in cells [218,295]. In this active state, the Rab protein can bind effectors and translocate to an acceptor membrane, allowing the effector to perform its function [296]. Here, GAPs promote GTP hydrolysis, leading to the formation of GDP-bound Rabs, which are removed from the membrane by GDP-dissociation inhibitors (GDIs) and recycled back to the donor membrane [297,298]. One of the ways Rabs maintain high membrane specificity is through GDI displacement factors (GDFs), which recognize specific Rab-GDI complexes and displace GDI, allowing the Rab protein to insert into its appropriate membrane [297,299]. Thus, Rabs act as master regulators of traffic by recruiting a variety of traffic-related effectors between membranes in a GTP-dependent manner.

Rab32 is found mainly in the ER, mitochondria, and MAM [290]. In melanocytes it is also present in melanosomes, where it participates in the biogenesis of this lysosome-related organelle (LRO) [290,300,301]. LROs are cell-type specific organelles with similar functions and morphologies that are partly derived from the endolysosomal system [302]. They are characterized by an acidic luminal pH, common lysosome-associated membrane proteins, and similar biogenesis. Some other examples of LROs include lytic granules, platelet-dense granules, and autophagosomes. In these cells, Rab32 transports Tyrosinase and Tyrosinase-related protein 1 (Tyrp1) and Tyrp2 from the trans-Golgi network (TGN) to the melanosome, a step required for melanosomes to become fully functional [300,301].

Rab32 membrane association is in part regulated by its GEF, biogenesis of lysosome-related organelles complex 3 (BLOC-3), which promotes its localization to melanosomes and

mitochondria [303]. Rab32 also interacts with other LRO biogenesis factors, including the adaptor protein complexes (APs) 1 and 3 [301]. AP complexes link cargo to the coat protein clathrin, thereby sorting cargo into clathrin-coated vesicles (CCV) destined for endosomal traffic. AP-1 and AP-3 recognize sorting signals in newly synthesized LRO proteins and participate in transport from the TGN to LROs. Both AP-1 and AP-3 interact with Rab32 and are required for the delivery of melanogenic enzymes. Taken together, these studies suggest Rab32 participates in early vesicle budding events and cargo recruitment to LROs.

Rab32 is also the only Rab known to function as an A-kinase anchoring protein (AKAP) [304]. AKAPs bind to and recruit protein kinase A (PKA) to membranes, providing specificity for the kinase by restricting the substrates it has access to. One of its substrates is the mitochondrial fission factor Drp1, which is also a Rab32 effector [305]. Drp1 can be phosphorylated at serine 656 (S656) by PKA, which inhibits its activity [290]. Loss of Drp1 activity can trigger the accumulation of mitochondria at microtubule organizing centers at the perinucleus, a phenotype known as mitochondrial collapse [304]. This phenotype is also observed in cells overexpressing the dominant negative mutant of Rab32, Rab32T39N [305]. This is likely caused by an increase in S656 phosphorylation by PKA, which Rab32T39N promotes [290]. T39N overexpression also increases Drp1 enrichment in mitochondria and MAMs [290]. Reducing the expression of T39N to more physiological levels revealed there were more elongated and interconnected mitochondria [304]. Together, these studies suggest Rab32T39N induces PKA-mediated Drp1 inhibition at mitochondria and/or the MAM, resulting in hyperfused mitochondria as a result of decreased mitochondrial fission.

Rab32 also interacts with Syntaxin 17, which promotes mitochondrial fission or autophagy depending on the cell's bioenergetics [306,307]. Under nutrient-rich conditions, Syntaxin 17 interacts with Drp1 and Rab32 at the MAM [307]. This interaction prevents Rab32 from recruiting PKA, allowing Drp1 to become active to promote mitochondrial fission during homeostasis. Starvation instead promotes MAM recruitment of Atg14L and its binding to Syntaxin 17. The simultaneous enrichment of other autophagy initiating proteins promotes isolation membrane biosynthesis as previously described. With Syntaxin 17 preferentially binding Atg14L, Rab32's AKAP activity is no longer inhibited. Thus, PKA is recruited to the MAM, where Drp1 is phosphorylated and inactivated by PKA, resulting in an overall elongation of mitochondria.

Rab32 is also amongst the group of Rabs known to participate in autophagy. Indeed, several members of the family regulate a variety of steps in autophagy through interaction with autophagy-related proteins. For example, Rab5 interacts with a component of the PI3K III complex, VPS34, and recruits the complex to the omegasome to initiate autophagosome formation [308]. Rab7 instead regulates autophagosome-lysosome fusion via its effector FYVE and coiled-coil domain containing protein 1 (FYCO1), a LC3-interacting protein that acts as an adaptor to link the autophagosome to motor proteins [309]. However, it is still unknown at what stage Rab32 acts, and if it has an autophagy-related effector. Early reports found Rab32 loss impaired autophagy in HeLa cells and *Drosophila* [310,311]. Rab32 overexpression in mouse embryonic fibroblasts (MEFs) was also shown to induce the formation of LC3-stained autophagosomes, a well-known autophagy hallmark [310,312]. Multiple studies have also found Rab32 colocalizes with the autophagosome [310,313]. Thus, although Rab32 clearly influences autophagy, its exact molecular involvement remains unknown.

ER Ca^{2+} homeostasis is another process influenced by Rab32, though the mechanism for its effects remain unclear. Specifically, overexpression of WT and T39N, but not the dominant-active mutant Q85L, increased cytosolic Ca^{2+} levels when coupled with the SERCA inhibitor thapsigargin [290]. This suggested WT and T39N increased IP_3R-mediated Ca^{2+} release and/or dampened SERCA activity. No differences in cytosolic Ca^{2+} were detected when IP_3R was activated with histamine regardless of the amount or activation state of Rab32, suggesting IP_3R activity remained unchanged. Thus, increase in cytosolic Ca^{2+} with thapsigargin observed with WT and T39N was likely a result of decreased SERCA activity. To test how mitochondrial Ca^{2+} uptake affected cytosolic Ca^{2+} in these experiments, the MCU inhibitor Ru360 was also added. Under these conditions, WT, T39N and Q85L all caused a significant increase in cytosolic Ca^{2+}. These results suggest overexpression of Q85L also increases IP_3R-mediated Ca^{2+} release, like WT and T39N, but there is a concomitant increase in mitochondrial Ca^{2+} uptake in Q85L that prevented detection of changes in cytosolic Ca^{2+} with thapsigargin incubation alone. In agreement with these findings, cells overexpressing Q85L were more sensitive to extrinsic and intrinsic apoptosis.

Rab32 also regulates the enrichment of the MAM protein Calnexin [290]. Specifically, overexpression of Q85L removes Calnexin from the MAM fraction and increases its relocation to the peripheral ER [267,290]. This could have indirect effects on ER-mitochondria Ca^{2+} flux since

Calnexin interacts with and activates SERCA2b [259]. Thus, Q85L-mediated removal of Calnexin would allow TMX1 to bind and inhibit SERCA2b, since these folding assistants are thought to compete for SERCA2b binding [260]. This would in turn decrease SERCA2b mediated ER Ca^{2+} uptake. However, it is still unknown if and how Rab32 regulates SERCA2b activity to induce these changes in ER-mitochondria Ca^{2+} flux.

1.2.4.1 Ypt: the Rab family in *S. cerevisiae*

Rab proteins can be further categorized into subfamilies based on subfamily-specific conserved motifs as well as pathway, organelle, and functional specificity [314]. Studies into Rab evolution suggest the last eukaryotic common ancestor (LECA) had between 19-23 subfamilies [314,315]. Rab32 is thought to be one of the Rabs found in the LECA [305,314,315]. Humans have 44 subfamilies and a total of 70 members, indicating a large expansion occurred in mammals since the LECA [305,314,315]. Phylogenetic studies suggest this expansion is largely due to gene duplication and lineage-specific diversification [316,317]. The Rab family in yeast is known as the yeast protein transport (Ypt) family and is considerably smaller [314,315,317]. For example, *S. cerevisiae* and other free-living fungi have only 6 subfamilies [317,318]. Many extant species, including *S. cerevisiae,* have fewer than 15 members in total, indicating a significant loss took place in this lineage since LECA [314,316,318]. This raises the question of how the Ypt family in *S. cerevisiae* operates with only 11 members [316,318]. This reduction of Ypt proteins is hypothesized to be at least in part due to the relative simplicity of the trafficking system in unicellular organisms compared to mammals [316]. Therefore, many mammalian Rabs, including Rab32, have no known Ypt homolog [296,316,318]. Nevertheless, several Ypt/Rab orthologs have been characterized. Some are represented by only one protein and can be referred to as 1:1 orthologs [319]. This includes Ypt1/Rab1, which are required for ER to Golgi transport [320]. Experiments have also demonstrated Rab1 can functionally replace Ypt1 in Δ*ypt1* cells, a common approach to establish functional homology in this model organism [315]. Other members are represented by two proteins and are referred to as 1:2 orthologs or co-orthologs, and those with multiple proteins as 1: >2 orthologs [319]. Protein families that have undergone lineage-specific duplications and diversification, such as human Rabs [316], often have co-orthologs or 1>2 orthologs in *S. cerevisiae* [319]. One such protein is Rab5, whose multiple roles in endolysosomal traffic are performed by four different Ypt proteins: Ypt51, Ypt52, Ypt53, and Ypt10 [321–323]. These and the remaining Ypt

proteins will be described in the following section to identify one or more potential Rab32 functional homologs.

1.2.4.2 Ypt candidates for Rab32 functional homology in *S. cerevisiae*

Ypt51, Ypt52 and Ypt53 were initially identified as Rab5 homologs since they all individually share roughly 50% identity with Rab5 [321]. Together they form a Ypt subfamily sometimes referred to as the Ypt5-like subfamily [323]. Like Rab5, the Ypt5-like subfamily is required for traffic from and to the endosome [321,324,325]. For example, single and double null mutants display defects in delivery of vacuolar proteins, particularly Δ*ypt51* mutants [321]. This is in line with Ypt51 being the closest homolog for Rab5 [321,325]. Rab5 is mainly found on early endosomes and is required for their homotypic fusion [326]. It also promotes early endosome traffic on microtubules [324] as well as TGN to lysosome traffic [327]. Rab5 is also found on the plasma membrane and on plasma membrane-derived endosomes, where it promotes endocytosis [328]. Endosomes can also originate from the TGN and serve to sort proteins for delivery to various organelles or to the plasma membrane for their secretion [327]. Endosomal traffic involves maturation of these vesicles from early to late endosomes. Early endosomes are characterized by the presence of Rab5 while late endosomes contain Rab7 [329]. Early to late endosome maturation requires the exchange of Rab5 with Rab7. This exchange is promoted by the Rab7/Ypt7 GEF Mon1-Ccz1, which is found on late endosomes [330].

Another name for several Ypt proteins is vacuolar protein sorting (Vps), since many of these proteins had been previously identified in studies characterizing deletion strains with abnormal vacuole morphology and/or function [331,332]. For example, although Ypt51 was identified in a study searching for a Rab5 homolog [321], an earlier study had described the same gene as Vps21 [331]. Thus, Ypt51 is also known as Vps21. Ypt51/Vps21, like Rab5, promotes early to late endosome maturation as well as TGN to late endosome traffic [333]. Multiple studies have shown Ypt51, Ypt52 and Ypt53 can interact with different effectors, suggesting they participate in distinctive pathways and have different degrees of functional homology with Rab5 [321,325]. A more recent addition to the Ypt5-like subfamily is Ypt10, which participates in endosome maturation [323].

Of the 11 Ypt proteins in *S. cerevisiae,* four regulate exocytosis: Ypt1, Ypt31, Ypt32, and Sec4 [334]. Ypt1 shares roughly 70% identity with Rab1 and mediates ER to Golgi transport as

well as intra-Golgi traffic [335,336]. Ypt1/Rab1 can promote tethering to aid membrane fusion by interacting with the transport protein particle (TRAPP)-I and -II complexes, which contain GEFs for Yp1/Rab1 [334]. Ypt1 also interacts with Atg11, a scaffolding protein required for PAS formation during selective autophagy in yeast [337]. Atg11 is required for mitophagy and pexophagy, the degradation of peroxisomes [338]. During non-selective autophagy, Ypt1 instead recruits Atg17, another PAS scaffolding protein [337]. Rab1 also participates in early autophagosome formation but there is no evidence it interacts with the Atg11/Atg17 mammalian homolog focal adhesion kinase family interacting protein of 200 kDa (FIP200).

Ypt31 and Ypt32 are most closely related to Rab11 with roughly 60% sequence identity [334]. These proteins regulate exocytosis by promoting intra-Golgi traffic. Ypt31 and Ypt32 often work in unison and are therefore usually referred to as Ypt31/32. The TRAPP complexes also act as GEFs for these proteins. Ypt31/32 also promote Golgi to plasma membrane traffic during exocytosis by binding the motor protein Myo2. They also promote traffic of Atg9 from the Golgi to the PAS, which is required for autophagosome formation in yeast [339].

Traffic from the Golgi to the plasma membrane is mainly regulated by Sec4, which was initially identified as a temperature sensitive secretory (sec) mutant strain with defective secretion [340]. Sec4 is most closely related to Rab8 [296]. Rab8 also regulates post-Golgi transfer and is mostly found at the TGN on budding vesicles, endosomes, exocytic vesicles, and the plasma membrane [296]. This traffic is partly mediated by Rab8 interacting with myosin V motor proteins [341]. Similarly, Sec4 interacts with Myo2 to promote post-Golgi traffic [284].

Ypt6 is most closely related to Rab6, with whom it shares roughly 55% identity [334]. Ypt6/Rab6 mainly promote the fusion of endosomes at the Golgi [342]. Indeed, Rab6 is enriched in the *trans* face of the Golgi and is required for retrograde transport to this organelle. Rab6 acts in conjunction with other Rabs, including Rab1, to maintain Golgi identity and structure by promoting intra-Golgi transport [336,342].

Ypt7 is 63% identical to Rab7 and performs many of the same functions [343,344]. For example, Ypt7/Rab7 are required for homotypic fusion of vacuoles/lysosomes as well as homotypic fusion of late endosomes, where they are mostly found [343–345]. Ypt7/Rab7 also promote fusion of autophagosomes and late endosomes with the vacuole/lysosome [345]. Thus, Ypt7 loss causes autophagosome accumulation [346]. Ypt7 is also involved in endosome maturation along with Ypt51/Vps21 as previously described [329,330]. The delivery of certain vacuolar proteins also

depends on Ypt7 [300,343]. Lastly, Ypt7 is the only Ypt protein identified at MCS in yeast [347,348]. Indeed, Ypt7 is part of the vacuole and mitochondria patch (vCLAMP), a complex that tethers mitochondria and vacuoles. Mammalian lysosome-mitochondria contact sites containing Rab7 and its GAP TBC1 domain family member 15 (TBCD151) have also been described recently [349]. Interestingly, vCLAMP can compensate for phospholipid defects in ERMES mutants, suggesting it can perform some of the MAM's functions.

Lastly, Ypt11 is the only known mitochondrial Ypt and is required for the inheritance of mitochondria to daughter cells [350]. Ypt11 mediates this function by promoting mitochondrial transport with its effector, Myo2 [351]. Phylogenetic analysis has not established homology to any known mammalian Rab but Ypt11 is most closely related to Rab8 [350,352]. Ypt11 can also localize to the Golgi, where it interacts with a Golgi-bound protein [350]. Interestingly, Ypt11 can also localize to the ER when overexpressed, though its function here is not well understood.

From these studies, three Ypt proteins emerge as likely candidates for functional homologs of Rab32: Ypt1, Ypt11, and Ypt7. In the case of Ypt1, this member could perform some of Rab32's autophagy functions. Indeed, Ypt1 temperature-sensitive mutants have impaired autophagy, as do Rab32 KD cells [310,353]. Although it is unclear how Rab32 regulates autophagy, it is plausible it participates in isolation membrane formation given it: i) is MAM-enriched, ii) interacts with Syntaxin-17, which recruits the PI3K III complex, and iii) its overexpression increases the number of autophagosomes, suggesting it promotes this pathway [203,290,310]. Similarly, Ypt1 is required for recruitment of Atg11 and Atg17 to the PAS, a process that is analogous to the formation of the isolation membrane in mammals [201,337]. Though highly speculative, one possibility is that Ypt1 and Rab32 perform similar functions by recruiting autophagy-related proteins to the site of autophagosome biogenesis in their respective species. It is possible Rab32 interacts with the Atg11/Atg17 homolog FIP200, a component of the ULK1 complex [337]. Rab32 would thus be responsible for recruitment of the ULK1 complex to the MAM in this scenario.

A case for Ypt11 can be built based on its localization to both the ER and mitochondria [350]. Indeed, both Ypt11 and Rab32 are the only known mitochondrial Ypt/Rab proteins [218,350]. Additionally, Ypt11 promotes mitochondrial movement via its effector Myo2, a motor protein [351]. Rab32 has also been recently implicated in mitochondrial movement since overexpression of its dominant negative mutant significantly decreases mitochondrial movement in neuronal cells

[354]. Rab32 could mediate this function by interacting with the related motor protein Miro-2, though this has not been tested.

Lastly, Ypt7 performs similar sorting functions as Rab32 in melanocytes. For instance, Ypt7 is required for targeting of membrane-bound vacuolar proteins, which is likely similar to Rab32-mediated traffic of membrane-bound melanosome enzymes [300,343]. Ypt7 could also have MAM regulatory abilities like Rab32 since it is the only known Ypt protein to localize to a MCS in yeast [347,348]. Indeed, Ypt7 is a component of vCLAMP, a tethering complex between mitochondria and vacuoles. More importantly, vCLAMP rescues the lipid traffic defects in ERMES mutants, suggesting the complex can perform or compensate for MAM functions.

1.3 Thesis outline and objectives

The MAM is a highly active structure with a large repertoire of functions and proteins moving in and out in response to a multitude of stimuli. There is also evidence of physically and functionally distinct types of MERCs, adding further complexity to this structure. MAMs are also highly dynamic as tethering is regulated to form and disassemble contacts in response to nutrient status, ER and oxidative stress, Ca^{2+} levels, and other factors in ways we are only just beginning to fully understand. Nevertheless, there are some well-established factors known to influence MAM properties and functions. This thesis focuses on some of these factors: Rab32 and ER folding assistants.

We know Rab32 influences multiple aspects of the MAM. This includes Ca^{2+} flux, apoptosis onset, MAM enrichment of MAM-localized Calnexin, and mitochondrial dynamics. However, its role in autophagy is still largely unknown. Thus, in our first project, we wanted to investigate the role of Rab32 in autophagy. Therefore, in Chapter 3 we first performed a number of assays to understand how Rab32 regulates autophagy. Additionally, we investigated if Rab32 had any autophagy-related effectors. We also wanted to know if the proteome, tethering, and apoptotic function of MAMs were altered during this process.

The highly interconnected nature of these processes, as described in this introduction, has complicated the study of the MAM. Therefore, one of the goals of this thesis is to return to a simple model organism previously used to great advantage in MAM research. Thus, in Chapter 4 we sought to identify a functional homolog for Rab32 amongst the Ypt family in *S. cerevisiae*. To do this we performed a phylogenetic analysis and proceeded to characterize MAM related

functions in mutant strains of the most likely candidate identified. This included growth assays with Ca^{2+} chelation and non-fermentable carbons as well as electron microscopy to analyze ER-mitochondria contact sites.

The recent characterization of Calnexin and TMX1 KOs has demonstrated these folding assistants activate and inhibit SERCA2b respectively, and therefore influence organellar Ca^{2+} levels and MAM functions such as mitochondrial respiration, apoptosis, and MAM tethering. In Chapter 5 we sought to investigate if folding assistants in *S. cerevisiae* conserve some of these functions. To investigate this, we used null mutants for their homolog counterparts: Δ*eps1* and Δ*cne1* strains. In this project, we performed growth assays, respirometry, and electron microscopy to investigate if loss of folding assistants in yeast also alters MAM functions and properties.

Taken together, the overarching goal of this thesis is to develop a better understanding of factors that can regulate ER-mitochondria contact sites and MAM functions in mammals and *S. cerevisiae.* The following chapter will detail the reagents, materials, and techniques used for the experiments performed in Chapters 3, 4, and 5.

Chapter 2: Materials and methods

2.1 Reagents, solutions, and buffers

Table 2.1 Chemicals and reagents

Chemical/reagent	Supplier
Acetic Acid	Fisher Scientific
Acetone	BDH Chemicals
Acetonitrile	Sigma
Acrylamide, 30%	BioRad
Ammonium Chloride	Sigma
Ammonium Persulfate (APS)	BioRad
Ammonium sulfate	Fisher Scientific
Ampicillin	Sigma
Bafilomycin A1	Millipore
Bacto™ agar	BD
β-Mercaptoethanol	BioShop
1,2-Bis(2-aminophenoxy)ethane-N,N,N′,N′-tetraacetic acid tetrakis(acetoxymethyl ester) (BAPTA-AM)	Sigma
Bovine serum albumin (BSA)	Sigma
Bromophenol Blue	BioRad
Cobalt chloride hexahydrate	Sigma
Carbonyl cyanide 4-(trifluoromethoxy) phenylhydrazone (FCCP)	Enzo
3-[(3-Cholamidopropyl) dimethylammonio]-1-propanesulfonate (CHAPS)	Sigma
25x Complete protease inhibitors	Roche
Dextrose	Fisher Scientific
4′,6-diamidino-2-phenylindole (DAPI)	Sigma
Dimethyl sulfoxide (DMSO)	Caledon
Dithiobis Succinimidyl Propionate (DSP)	Thermo Scientific
Dulbecco's Modified Eagle Medium (DMEM)	Gibco
Dulbecco's Phosphate Buffered Saline (DPBS) 10X	Cellgro Mediatech, Inc.
Earl's Balanced Salt Solution (EBSS)	Thermo Fisher
Embed 812	Electron Microscopy Sciences
Ethylene diamine tetraacetic acid (EDTA)	EMD
Ethylene glycol tetraacetic acid (EGTA)	OmniPur
Ethanol	Commercial Alcohols
Fetal Bovine Serum (FBS)	Gibco
Geneticin	Gibco
Glucose	Fluka
Glutaraldehyde grade I	Sigma
Glycerol	BDH
Glycine	Fisher Scientific
4-(2-hydroxyethyl)-1-piperazieethanesulfonic acid (HEPES)	Sigma
Isopropanol	Fisher Scientific
Lipofectamine 2000	Invitrogen
Lithium acetate	Fisher Scientific
L-glutamine, 200mM	Gibco
Luria-Bertani (LB) Agar, Miller	BD Biosciences

Luria Broth Base, Miller	BD Biosciences
Magnesium Chloride (Molecular Biology purity)	Finnzymes
Magnesium Chloride	EM Science
Metafectene Pro	Biontex
Methanol	Fisher Chemicals
Milk (skim milk powder)	Carnation
Nitrocellulose Trans-blot	BioRad
Nonyl phenoxypolyethoxylethanol (NP-40)	CalbioChem
Oligofectamine	Invitrogen
Opti-MEM	Gibco
Osmium tetroxide	Sigma
Paraformaldehyde (PFA)	Sigma
Peptone	Fisher Scientific
Percoll	GE Healthcare
Phosphate Buffer Saline with Ca^{2+} and Mg^{2+} (PBS++) 10X	Cellgro Mediatech, Inc.
Polyethylene glycol (PEG)	Sigma
Potassium permanganate	Sigma
Precision Plus Protein Dual Colour Standards	BioRad
ProLong Antifade Resin (PLAF)	Invitrogen Molecular Probes
Protein A Sepharose (PAS) Beads CL-4B	GE Healthcare BioSciences
Rapamycin	MP Biochemicals
Roswell Park Memorial Institute medium (RPMI)	Gibco (12633012)
Saponin	Fluka
Sodium Acetate trihydrate	EMD
Sodium Azide	ICN Biomedical Inc.
Sodium Bicarbonate	EMD
Sodium Carbonate	EMD
Sodium Chloride	Fisher Scientific
Sodium Deoxycholate	Sigma
Sodium Dodecyl Sulphate (SDS)	J.T. Baker
Sodium Hydroxide	BDH
Sodium periodate	Sigma
Sucrose	EMD
Tetramethylethylenediamine (TEMED)	OmniPur/EMD
Trans-blot nitrocellulose	BioRad
Tris	Bio Basic Inc.
Triton X-100	Sigma
Tunicamycin	Calbiochem
Trypsin 2.5%	Gibco
UltraPure water	Invitrogen
Yeast extract	Fisher Bioreagents

Table 2.2 Solutions and buffers

Buffer / Solution	Composition
CHAPS buffer	10mM Tris pH 7.4, 150mM NaCl, 1mM EDTA, 1% CHAPS
EM fixing solution	2% paraformaldehyde, 2% glutaraldehyde in 0.1M sodium cacodylate buffer, pH 7.4
IF blocking solution	DPBS, 2% BSA, 0.5% Saponin
IF fixing solution	DPBS, 4% Paraformaldehyde
IF permeabilization solution	PBS++, 0.2% BSA, 0.1% Triton X-100
Laemmli buffer	60mM Tris pH 6.8, 2% SDS, 10% Glycerol, 5% β-Mercaptoethanol, 0.01% Bromophenol Blue
Lithium acetate	1.0mM in ddH_20, pH 8.5
Mitochondria homogenization buffer	250mM Sucrose, 10mM HEPES pH 7.4, 1mM EDTA, 1mM EGTA
Osmium tetroxide	1% osmium tetroxide in 0.1M NaCaCod, pH 7.4
4x separating buffer	1.5M Tris pH 8.8, 0.4% SDS
4x stacking buffer	0.5M Tris pH 6.8, 0.4% SDS
Sodium cacodylate buffer	0.1M NaCaCod, pH 7.4
Tris Buffered Saline-Triton X100 (TBS-T)	10mM Tris pH 8.0, 0.15M NaCl, 0.05% Triton X-100
Tris-EDTA (TE) buffer	10mM Tris-HCl pH 8.0, 1.0mM EDTA
Uranyl acetate solution	1% uranyl acetate
WB antibody solution	TBS-T, 2% milk
WB blocking solution	DPBS, 2% BSA
WB transfer buffer	10mM $NaHCO_3$, 3mM Na_2CO_3, 20% Methanol
WB running buffer	25mM Tris, 200mM Glycine, 0.1% SDS

EM: electron microscopy
IF: immunofluorescence
WB: western blot

2.2 Antibodies

Table 2.3 Primary antibodies

Antibody	Host	Supplier	Working dilution	Application
Bad	Rabbit	#9239 Abcam	1:1000	WB
Bak	Rabbit	#12105 Abcam	1:1000	WB
Bax	Rabbit	#5023 Abcam	1:1000	WB
Bcl-2	Rabbit	#2872 Abcam	1:1000	WB
Bcl-xL	Rabbit	#2762 Abcam	1:1000	WB
Bim	Rabbit	#2933 Cell signaling	1:1000	WB
BiP	Mouse	610978 BD Biosciences	1:5000	WB
Calnexin	Rabbit	Inhouse, Bui et al., 2010	1:2000	WB
Caveolin	Mouse	610407 BD Transduction laboratories	1:1000	WB
CCPG1	Rabbit	13861-1-AP ProteinTech	1:500	WB
Climp 63	Mouse	C5840 US Biological	1:1000	WB
Complex II	Mouse	ab14714 Abcam	1:2500	WB
Complex IV-sub IV	Mouse	A21348 Life technologies	1:2500	WB
Cytochrome c	Goat	kind gift from Dr. Michelle Berry	1:1000	WB
Drp1	Mouse	ab56788 Abcam	1:2000	WB
FACL4	Goat	ab11007 Abcam	1:1000	WB
FAM134B	Rabbit	ab151755 Abcam	1:1000	WB
FLAG	Mouse	600-401-383 Rockland	1:5000	WB
			1:250	IF,IP
GAPDH	Rabbit	#5174 Cell signaling	1:1000	WB
Golgin 97	Mouse	A-21270- Molecular Probes	1:2000	WB
HA	Rabbit	#3724 Cell signaling	1:5000	WB
HA	Rabbit	901501 Biolegend	1:200	IF
LC3	Rabbit	#12741 Cell signaling	1:1000	WB
Mcl-1	Rabbit	#4572 Abcam	1:1000	WB
Mitofusin-1	Rabbit	#14739 Abcam	1:1000	WB
Mitofusin-2	Rabbit	M 6319 Sigma	1:1000	WB
p62	Mouse	610833 BD BioSciences	1:2000	WB
PACS-2	Rabbit	19508-1-AP ProteinTech	1:500	WB
PDI	Mouse	MA3-019 Thermo	1:5000	WB

Puma	Rabbit	#12450 Abcam	1:1000	WB
Rab32	Rabbit	HPA025731 Sigma	1:1000	WB
			1:100	IF
Reticulon 3	Rabbit	Boster Biological PA2256	1:500	WB
Reticulon 3	Rabbit	MA5-15538 clone 1E11 Thermo	1:100	IF
Reticulon 4	Rabbit	10740-1-AP ProteinTech	1:1000	WB
Sec 61B	Rabbit	07-205 Millipore	1:10 000	WB
Sec 62	Rabbit	HPA014059 Sigma	1:1000	WB
Syntaxin-17	Rabbit	ABC970 Sigma	1:1000	WB
Tubulin	Mouse	T 5168 Sigma	1:10 000	WB
TMX1	Rabbit	H008154-B01P Abnova	1:2000	WB
VDAC1	Mouse	ab14734 Abcam	1:2000	WB

WB: Western blot
IF: Immunofluorescence
IP: Immunoprecipitation

Table 2.4 Secondary antibodies

Antibody	Host	Supplier	Working dilution	Application
AlexaFluor 680 anti-Mouse	Goat	A21057 Invitrogen Molecular probes	1:10 000	WB
AlexaFluor 800 anti-Rabbit	Goat	A32735 Invitrogen Molecular probes	1:10 000	WB
AlexaFluor 680 anti-Goat	Donkey	A32860 Invitrogen Molecular probes	1:10 000	WB
AlexaFluor 800 anti-Goat	Donkey	A32930 Invitrogen Molecular probes	1:10 000	WB
Alexa Fluor 405 anti-Rabbit	Goat	A31556 Invitrogen Molecular probes	1:1000	IF
Alexa Fluor 594 anti-Mouse	Goat	A11005 Invitrogen Molecular probes	1:1000	IF

WB: Western blot
IF: Immunofluorescence

2.3 Commercial kits and equipment

Table 2.5 Commercially available kits

Kit	Supplier
Amaxa nucleofector kit V	Lonza
PE Annexin V apoptosis detection kit	BD Biosciences

2.4 Cell culture

Cell lines were cultured in indicated media (Table 2.6, below) and maintained in a humidified tissue culture incubator at 37°C with 5% CO_2. Cells were passaged after trypsinization usually 3 times per week, up to a maximum passage number of 30. Unless otherwise stated, cells were trypsinized, resuspended in media, counted with a hematocytometer or in an automatic cell counter (Countess™ II FL, life Technologies) and seeded onto 6-well plates.

Table 2.6 Cell lines

Cell line	Growth medium	Source
MCF7	RPMI + 10% FBS	ATCC
MCF7 LC3-GFP	RPMI + 10% FBS + 50mg/mL geneticin	Kind gift from Dr. Ing Swie Goping, University of Alberta
MCF7 pIRES2 MCF7 Q85L	RPMI + 10% FBS + 50mg/mL geneticin	This thesis (see point 6)
HeLa	DMEM + 10%FBS	ECACC
PACS-2 WT HeLa PACS-2 KO HeLa	DMEM + 10%FBS	Kind gift from Dr. Gary Thomas, University of Pittsburgh
MFN-2 WT MEF MFN-2 KO MEF	DMEM + 10%FBS	Kind gift from Dr. David Chan, California Institute of Technology

2.5 Plasmids and siRNA

Table 2.7 Plasmids and siRNA

Plasmid	Vector	Source
Rab32 WT-FLAG	pcDNA3	Kind gift from Dr. John Scott, University of Washington
Rab32 Q85L-FLAG	pcDNA3	Dr. John Scott
Rab32 T39N-FLAG	pcDNA3	Dr. John Scott
Rab32 WT-FLAG	pIRES2	Inhouse
Rab32 Q85L-FLAG	pIRES2	Inhouse
Rab32 T39N-FLAG	pIRES2	Inhouse
siRNA	**ID**	**Source**
Human Rab32	HSS116975	Invitrogen
Human RTN3	HSS145573	Invitrogen
Scrambled control	452001	Invitrogen

2.6 Transient transfections and generation of stable cell lines

Transient transfections were performed according to manufacturer's (Table 2.1) instructions. Unless otherwise stated, cells were transfected with plasmids in the pcDNA3 vector. Briefly, the morning after seeding into 6-well plates, cells were transfected with 2μg DNA (unless otherwise stated) and 7μL of Lipofectamine 2000 in Opti-MEM, or 10μL of Metafectene in PBS per well. Opti-MEM/PBS was replaced with the appropriate growth media (Table 2.5) after a 4hr incubation. Unless otherwise stated, transfections were carried out for 48hrs. siRNA knockdown was performed in Opti-MEM with 20pmol siRNA and 4μL of Oligofectamine per well for 72hrs, unless otherwise stated. Simultaneous siRNA knockdown and plasmid expression was performed by transfecting 1μg DNA and 20pmol siRNA with 7μL of Lipofectamine 2000.

Nucleofection for the immunofluorescence experiments was performed with the Lonza nucleofector kit V (#VVCA-1003) in their Nucleofector™ 2b device according to their MCF7 protocol. Briefly, cells were trypsinized and 2 million cells per condition were counted and pelleted in a centrifuge at RT (800rcf for 10 min). Cells were then resuspended in the nucleofection solution and transferred to cuvettes. Cuvettes were inserted into the Nucleofector™ 2b device and protocol P-020 was used. The cells were then resuspended with the appropriate growth media (Table 2.5) and transferred to a coverslip in a 6-well plate. The transfections were carried out for 48hrs.

MCF7 stably expressing vector control pIRES2 or Rab32Q85L-FLAG were generated as follows: MCF7 cells were transfected with lipofectamine as described above and after 24hrs trypsinized and counted. Serial dilutions from 200 to 2000 cells were transferred to 15cm dishes and the selection agent geneticin (50mg/mL) added. Clones were allowed to grow for 2-3 weeks, only replacing the media every 5 days. Clones were then isolated with cloning rings by adding trypsin and transferring into individual wells in 24-well plates. These were allowed to grow for roughly a week before being tested via immunofluorescence (to detect FLAG positive cells) and western blot (to detect FLAG and Rab32 signal).

2.7 Immunoblotting and densitometry analysis

After lysates were mixed with Laemmli buffer, they were boiled for 10 min, loaded onto SDS-PAGE with WB running buffer, and run at 150V for roughly 1hr. After protein separation by SDS-PAGE, samples were transferred onto a nitrocellulose membrane using a Mini Trans-blot Cell

apparatus (BioRad) at 400mA for 2hrs at 4°C, in WB transfer buffer (Table 2.2). The membrane was then incubated on a rocker in WB Blocking Solution for 1hr at room temperature and then with WB antibody solution with a primary antibody either overnight at 4°C or 1hr at room temperature, according to the specifications of each antibody. The membrane was then washed 3 times with TBS-T on a rocker for 5min at room temperature and then incubated with WB antibody solution containing secondary antibody for 1hr at room temperature. Lastly, the membranes were washed again as described above and visualized with the Odyssey Infrared Scanner (LI-COR, Lincoln, NE). Densitometry analysis was performed with LI-COR ImageStudio Lite 5.2.5 software. Rectangles or ovals were manually selected around bands and automatically corrected for background based on the median pixel intensity of a 3-pixel region around the shape. The resulting values were then statistically analyzed (see below).

2.8 Immunofluorescence and co-localization analysis

MCF7 were nucleofected as described above and grown on glass coverslips. RPMI was replaced with EBSS for 2hrs where indicated. Cells were washed twice with PBS++ (PBS 1mM $CaCl_2$ and 0.5mM $MgCl_2$) and fixed with 4% paraformaldehyde for 20 min. Cells were washed again with PBS++ and permeabilized with 0.1% Triton X-100 + 0.2% BSA in PBS++ for 2 min. They were then incubated with DAPI for 5 min, washed twice with PBS++ and incubated with primary antibodies (Table 2.3) for 1 hr in IF blocking solution (2% BSA + 0.5% Saponin in PBS++). The cells were washed again and incubated with secondary antibodies (Table 2.4) for 30 min in IF blocking solution before being mounted in Prolong AntiFade (PLAF) resin and allowed to dry overnight at room temperature.

For co-localization, MCF7 cells transfected as indicated were fixed in 3% paraformaldehyde + 0.1% glutaraldehyde in PBS++ for 20 min. Cells were permeabilized with 0.1% Triton X-100 + 0.2% BSA in PBS++ for 1 min. Cells were blocked for 15 min in 0.2% Saponin + 2% BSA in PBS++. Primary antibodies were added for 1 h in the same buffer, while secondary antibody incubation was for 30 min. Cells were washed in 0.2% Saponin + 0.2% BSA in PBS++ and mounted as above.

Coverslips were then imaged with an Axiocam on an Axio Observer microscope (Carl Zeiss, Jena, Germany) using a 63X plan-Apochromat oil lens. Representative images were prepared after iterative deconvolution with the Axiovision software Photoshop (Adobe, San Jose, CA) was used,

using the levels function only, to achieve near-saturation levels in the brightest areas of each channel. For the LC3 puncta assay, ImageJ software [355] (ImageJ, U.S. National Institutes of Health, http://rsb.info.nih.gov/ij/) was used to annotate images by denoting whether each cell had ≥10 LC3 puncta to facilitate counting. Cells with ≥10 LC3 puncta were considered to have higher than normal levels of autophagy. Samples were analyzed in a blinded manner. ≥100 cells per condition were counted in each independent experiment (n=3). For the co-localization assay, the images were deconvolved by AxioVision then analyzed using ImageJ Coloc 2. The Manders coefficient of each condition was calculated from the average of 5 cells. In each cell, 3 ROI (region of interest) were chosen for Coloc2 analysis.

2.9 Co-immunoprecipitations

MCF7 were plated at 10^6 cells per well in 6-well plates and transfected the following morning. Each construct was transfected into 3 wells and allowed to express for 48hrs. Before lysis, a crosslinking solution was made by preparing a 2mM DSP working solution in DMSO that was added to room temperature DPBS with protease inhibitors. The final 200mM DSP solution was filtered through a 0.2µm syringe filter. Cells were washed twice with room temperature PBS++ and then crosslinked at room temperature for 30 min. Afterwards, cells were washed twice with 10mM NH_4Cl in PBS++ to quench the cross-linking reaction and harvested on ice with 150µL CHAPS buffer supplemented with protease inhibitors. The 3 wells transfected with the same construct were pooled together into one microcentrifuge tube and centrifuged at 1000 rpm for 15 min at 4°C to remove cellular debris. Then 0.2 g of Protein A Sepharose (PAS) beads were washed 3 times with distilled water and resuspended into a 1.5mL solution. The sample supernatants were precleared by incubating with 20µL of PAS beads for 1hr on a rocker at 4°C after taking 25 µL to combine with Laemmli buffer to serve as input (5%). Samples were then centrifuged at 800rpm for 2 min and the resulting supernatant incubated with 5µL of anti-FLAG antibody overnight on a rocker at 4°C. 25µL of PAS beads were added for protein precipitation for 1hr on a rocker at 4°C the next day. Lastly, the samples were washed 3 times with 400µL CHAPS and the pellets resuspended in 25µL of Laemmli buffer before being analyzed by western blot.

2.10 Percoll fractionation

The protocol was adapted from Rusiñol *et al.* (1994). MCF7 cells were seeded to 90% confluence in fifteen 15cm dishes, washed twice with PBS++ and harvested on ice with 4mL of mitochondrial homogenization buffer (Table 2.2) supplemented with protease inhibitors. The cell suspension was centrifuged 5 min at 1,500rpm in a JA-12 rotor at 4°C, the supernatant discarded, and the entire sample resuspended in 5mL of the buffer. The sample was then passaged 8 times back and forth through a ball bearing homogenizer (Isobiotech, Heidelberg, Germany) with a 14µm clearance ball before being centrifuged twice at 1,810rpm for 10min in a JA-12 rotor to remove nuclei and debris. A sample of 160µL of supernatant was taken and 40µL of 5X Laemmli buffer added to be used as the homogenate fraction while remaining supernatant was spun at 8,500rpm for 10min in a JA-12 rotor at 4°C. The resulting pellet, the crude mitochondria fraction, was resuspended in 1mL of buffer supplemented with protease inhibitors. An 80µL aliquot was taken and 20µL of 5X Laemmli buffer added to serve as the crude mitochondrial fraction. The remaining sample was carefully layered on top of 7.9mL of 18% Percoll solution (in ddH_2O) in a polycarbonate tube. Samples were then centrifuged at 33,333 rpm for 35min in a 90Ti rotor at 4°C. The MAM fraction was harvested roughly ¾ down the tube with an 18G ½ needle and a 1mL syringe while the pure mitochondria fraction was found directly underneath the MAM fraction. To remove Percoll, the MAM fraction was centrifuged at 60,000rpm for 1hr in a TLA 120.2 rotor at 4°C. The fraction pelleted on top of a Percoll pellet and was isolated with a syringe equipped with an 18G ½ needle and resuspended with Laemmli buffer to a final 300µL volume. The pure mitochondrial fraction was also cleared of Percoll similarly but was instead distributed into 4 microcentrifuge tubes and centrifuged twice at 10,000rcf at 4°C for 10min, removing supernatant and adding fresh buffer in between spins. The supernatant of the 8,5000rpm was evenly distributed into four Beckman 1.4mL tubes, balanced with fresh buffer as necessary, and centrifuged at 60,000rpm in a TLA120.2 rotor for 1hr at 4°C. The resulting pellets represents the microsomal fraction and were resuspended with 300µL of 1X Laemmli to a final volume of 1.2mL. The supernatant was distributed into twelve microcentrifuge tubes (roughly 300µL per tube) and 1mL of pure acetone added to precipitate overnight at -20°C. The next morning, the samples were centrifuged at 13,000rpm for 20min at 4°C before aspirating the acetone, allowing the pellets to

dry, and resuspending in 100µL of 1X Laemmli buffer. Equal proportional amounts of each fraction were analyzed by immunoblot.

2.11 Electron microscopy and analysis for mammalian samples

2 million MCF7 cells were grown on 6cm dishes and fixed with filtered EM fixing buffer for 30 min at 37°C 5% CO_2. Cells were then quickly washed on ice 3 times with sodium cacodylate buffer and harvested in 500µL of the same buffer before being centrifuged at 1000g for 5 min. They were then spun 5 min at 3000g, 6000g, and finally 12,000g. Post fixation was done with 1% osmium tetroxide in the sodium cacodylate buffer for 1hr on ice. Samples were quickly rinsed twice with ddH_2O before staining with 1% aqueous uranyl acetate for 18hrs at 4°C in a rocker protected from light. Dehydration was done the following day, starting by replacing uranyl acetate solution with 70% ethanol and incubating on ice for 5min. The sample was then centrifuged 30s at 13,000rpm to maintain the integrity of the pellet before doing another 70% ethanol wash. This step was repeated with 80%, 90%, and 100% ethanol. Samples were then incubated twice with acetonitrile for 10 min on ice before being covered with a 1:1 mixture of acetonitrile and Embed 812 and placed under vacuum overnight. The following morning, samples were placed in 100% Embed 812 and under vacuum for 7hrs, and then allowed to polymerize at 65°C for 48hrs before sectioning. We used an Ultracut E (Reichert-Jung) for sectioning and imaged the samples using a CCD camera (iTEM; Olympus Soft Imaging Solutions) mounted on a 410-transmission electron microscope (Philips).

Images were analyzed for ER tubules in close proximity to mitochondria and quantified with ImageJ. Two types of measurements were taken: MCS distance and MCS length. Distance was defined as the space between the ER outer leaflet and the mitochondrial outer leaflet. Only measurements ≤50nm were considered a MCS, as defined previously [14]. Length was defined as the space along the ER membrane where the MCS distance was ≤50nm. Data was derived from over 50 images per condition, with n=100 measurements each.

2.12 Statistical analysis

All the data are expressed as mean ± standard deviation. Bar graphs include standard errors. Statistical significance was determined with student's unpaired *t*-test using QuickCalcs by GraphPad (https://www.graphpad.com/quickcalcs/ttest1/).

2.13 Flow cytometry and apoptosis analysis

500,000 MCF7 cells per well were seeded onto a 12-well plate and transfected with Rab32-Q85L and Rab32-T39N in the pIRES2-EGFP vector with metafectene for 24hrs. Apoptosis was induced with 2μM of tunicamycin for 16h before being collected and centrifuged at 800rcf for 10min at room temperature (JA-12 rotor). The samples were then washed once with PBS, centrifuged again and washed in 1X Binding buffer (BD Biosciences kit) before being resuspended in 100μL of buffer and stained with 2μL of Annexin V and 2μL of 7-AAD (BD Biosciences kit) for 15min in the dark, at room temperature. The cells were then analyzed by BD LSRFortessa flow cytometer with the FL-2 and FL-4 channels in the BD Accuri C6 acquisition software (BD Biosciences). Only GFP positive populations (transfected cells) were gated for analysis. 10,000 individual events were collected.

2.14 Human breast cancer patient data analysis

The gene expression microarray dataset was generated from a human breast cancer cohort consisting of 176 treatment-naïve primary tumor samples as previously described [356]. The data are accessible from the NCBI website (www.ncbi.nlm.nih.gov/geo/) through GEO series accession number GSE22820. Patient material and clinical information were collected under Research Ethics Board Protocol ETH-02-86-17. Patients received standardized guideline-based chemo- and hormone therapies: i.e., hormone therapy for all patients with ER-positive tumors, trastuzumab for those with HER2-overexpression tumors, anthracycline chemotherapy for high risk node-negative disease and anthracycline plus taxane chemotherapy for node-positive disease. The median follow-up time for surviving patients was 4.5 years. The patient population was stratified with *RAB32* or *RTN3* mRNA levels at a cutting-off point determined by Receiver Operating Characteristic (ROC) curve analysis. Prognostic significance was analyzed using logrank test on Kaplan-Meier survival probabilities with MedCalc Version 14.12.0 (MedCalc Software).

2.15 Yeast maintenance

Yeast were grown at 30°C with constant agitation at 220rpm in either YPA or YPD. Strains used in this work are listed in Table 2.8 (below).

Table 2.8 Yeast strains

Name	Parental Strain	Genotype	Source	Reference
	BY4742	MATa *his3Δ1 leu2Δ0 ura3Δ0 met15Δ0*	Kind gift from Dr. Richard Rachubinski, University of Alberta, Edmonton AB	[357]
Δ*cne1*	BY4739	MATa/ MATα *leu2/leu2 his3/his3 /trp1/trp1 ura3/ura3 ade2/ade2 can1/can1 Δcne1::LEU2*	Dr. Richard Rachubinski	[268]
Δ*eps1*	BY4742	MATα *ura3-1 leu2-3,112 his3-11,15 trp1-1 ade2-1 can1- 100 eps1::HIS3*	Dr. Richard Rachubinski	[285]
Δ*mdm34*	BY4742	MATa *his3Δ1 leu2Δ0 ura3Δ0 met15Δ0 mdm34Δ::KanMX*	Dr. Richard Rachubinski	[35]
Δ*gem1*	BY4739	MATα *ade2-1 leu2-3 his3-11,15 trp1-1 ura3-1 can1-100 gem1::HIS3*	Dr. Richard Rachubinski	[358]
	BJ3505	MATa *lys2-208, trp1-Δ101, ura3-52, his3-Δ200, gal2, can, prb1-Δ1.6R, pep4::HIS3*	Kind gift from Dr. Gary Eitzen, University of Alberta, Edmonton AB	[359]
Δ*ypt7*	BJ3505	*MATa lys2-208, trp1-Δ101, ura3-52, his3-Δ200, gal2, can, prb1-Δ1.6R, pep4::HIS3, ypt7::URA3*	Dr. Gary Eitzen	[360]
Ypt7 T22N	BJ3505	*MATa lys2-208, trp1-Δ101, ura3-52, his3-Δ200, gal2, can, prb1-Δ1.6R, pep4::HIS3, ypt7::URA3, ypt7::YPT7(T22N)*	Dr. Gary Eitzen	[360]
Ypt7 Q68L	BJ3505	MATa *lys2-208, trp1-Δ101, ura3-52, his3-Δ200, gal2, can, prb1-Δ1.6R, pep4::HIS3, ypt7::YPT7(Q68L)*	Dr. Gary Eitzen	[360]

2.16 Agar plates and liquid media

Yeast were grown and tested on either YPD or YPA (Table 2.9).

Table 2.9 Yeast media and plates

Liquid media	Composition
YPD*	1% yeast extract, 2% dextrose, 2% peptone
YPA*	1% yeast extract, 2% sodium acetate, 2% peptone

*plates were prepared with 2% agar

2.17 Optical density measurements

Yeast were grown overnight in YPD at 30°C 220rpm and optical density (OD) was measured by spectrophotometer at 24hrs. Samples were diluted by adding 900µL of milliQ water into a 1.5mL microcentrifuge Eppendorf, culture was vortexed well, and 100µL of sample then added. Contents of the tube were transferred into a cuvette and measured individually by the spectrophotometer. A blank with 900µL of milliQ water and 100µL of YPD was measured first. The recorded absorbance measurements were then multiplied by 10 to obtain the final OD. Bar graphs were performed with an average of at least n=3 independent experiments.

2.18 Spot assay

Yeast were grown overnight in YPD at 30°C 220rpm and previously prepared YPD or YPA plates were warmed to room temperature and labelled. The absorbance of each strain was measured as indicated above and enough autoclaved ddH_2O added to 100µL of sample to obtain OD=1.0, which is the first spot plated. 90µL of autoclaved ddH_2O were added to four more 1.5mL microcentrifuge Eppendorfs to prepare a 1:10 serial dilution by adding 10µL from the OD=1.0 tube and 10µL from each tube subsequently. 1.5µL per dilution was plated starting with OD=1.0 from the left. Plates were incubated at 30°C from 2-5 days depending on drugs added. All treated plates except BAPTA-AM plates were prepared by adding a filtered solution of the compound after autoclaving the solid media culture. BAPTA-AM was instead added as a filtered solution to the serial dilutions to reduce amount of compound needed per plate.

2.19 BLASTp

The human Rab32 and TMX1 sequences were used as query sequences in the Basic Local Alignment Search Tool (BLAST) algorithm for proteins (BLASTp 2.11.0+) from the National Centre for Biotechnology Information (NCBI) website (https://blast.ncbi.nlm.nih.gov/Blast.cgi). Genomic sequences were obtained from the Uniprot databases (Uniprot.org). The search was restricted to the nr (non-redundant) database of the *Saccharomyces cerevisiae* genome. A reciprocal BLASTp was also performed using the yeast Ypt7, Cne1 and Eps1 amino acid sequences as query. An E-value cut-off of 0.05 was used for all queries. Sequences were aligned in a pairwise manner within the NCBI website. The cladograms were also generated within the NCBI website with the Fast-Minimum Evolution method with at least the first 5 gene products with highest sequence similarity to the query. The Rab32 (ATIGVDFALK) and TMX1 (CPAC) active sites were also used as query sequences in the same manner.

2.20 Electron microscopy and analysis for yeast samples

For electron microscopy, strains were grown in YPD overnight at 30°C 220rpm. The following morning, their absorbance was measured (see above) and 1mL of OD_{600} 1.0 was prepared in 1.5mL microcentrifuge tubes. Samples were centrifuged at 3000rpm for 1 min at room temperature, the supernatant aspirated, and the pellet resuspended with 1mL ddH_2O for two quick washes. Samples were centrifuged one more time, the supernatant aspirated, and fixed by adding 1mL of 3% $KMnO_4$ (in ddH_2O) while rocking for 15 mins at room temperature. The samples were centrifuged and washed twice with ddH_2O as described above. 1mL of 1% NH_4Cl (in ddH_2O) was added while rocking for 15 mins at room temperature before washing with ddH_2O once and replacing ddH_2O with 60% ethanol. The samples were then incubated overnight on a rocker at 4°C. The following day the samples were centrifuged as previously, the supernatant aspirated and replaced with 1mL of 80% ethanol and incubated for 4 mins at room temperature. This step was repeated with 95% and 100% ethanol, and then three times with acetonitrile instead. Acetonitrile was aspirated and replaced with a 1:1 embed 812: acetonitrile solution and the samples were placed under vacuum at room temperature overnight. The following day, the acetonitrile was discarded, and the samples returned to the vacuum for 2hrs, placed in pure embed 812 and allowed to polymerize at 65°C for 48hrs. An Ultracut E (Reichert-

Jung) was used for sectioning and the samples were imaged using a CCD camera (iTEM; Olympus Soft Imaging Solutions) mounted on a 410-transmission electron microscope (Philips).

Images were analyzed for ER tubules in close proximity to mitochondria and quantified with ImageJ as described above for mammalian samples. Data was derived from over 25 images per condition, with n≥75 measurements per condition.

2.21 Respirometry

Oxygraph-2k (O2k)(Oroboros Instruments Inc., Innsbruck, Austria) was used and based on their protocol designed for analysis of yeast [361]. Yeast were grown overnight in YPD at 30°C 220rpm and prepared the following morning by measuring their OD and calculating the amount of culture and fresh media required for 2.5mL of 0.05mg/mL given $1OD_{600}$ =0.62mg/mL. The sample was mixed before adding 2.2mL to the O2k chambers and the rest set aside and frozen at -80°C for the citrate synthase assay.

Before experimental analysis, the instrument was washed as follows: the chambers and stoppers were washed 3 times milliQ water, then 3 times with 70% ethanol and then incubated in the chambers with the stoppers in the loose position for 10 mins. This wash was repeated with 90% ethanol before filling the chambers with milliQ while washing the stoppers with hot running tap water, milliQ water, 70% ethanol, 90% ethanol, and milliQ water. The oxygraph is then calibrated by filling the chamber with 2.1mL of YPD and allowing an air phase to form in the chamber by using the stopper-spacer. The oxygen signal is allowed to stabilize, roughly in 20-30 min. Background corrections were applied for oxygen consumption by the polarographic oxygen sensor and oxygen diffusion in the chambers. Zero calibration was also performed by closing the chamber and removing all the oxygen available with the addition of dithionite.

Calibrations and cell respiration measurements were performed at 30°C and data acquisition was performed with DatLab software (Oroboros Instruments Inc., Innsbruck, Austria). First, respiration was measured under routine conditions before adding 40µL of pure ethanol to serve as a vehicle control. Uncoupling with carbonyl cyanide p-(trifluoromethoxy) phenylhydrazone (FCCP) was done in stepwise titrations of 0.2µL of 10mM FCCP (prepared in 100% ethanol) and used to induce maximal noncoupled respiration as a measure of electron transfer system capacity (ET state). Lastly, 50µL of 4M Azide was added to completely block

mitochondrial respiration and measure residual oxygen consumption (ROX). Fluxes in all states were corrected for ROX and expressed per gram.

Chapter 3: Rab32 promotes autophagic degradation of the MAM

3.1 Abstract

Autophagy is a conserved essential pathway whereby intracellular components are enveloped within the autophagosome, a vesicle that fuses with lysosomes to promote degradation of the enclosed contents. Autophagy is induced by a variety of stressors, including nutrient starvation, and acts as a catabolic pathway to restore homeostasis. Autophagy in mammals begins at the omegasome, a subdomain of the endoplasmic reticulum (ER) enriched in phosphtatidyl-inositol-3-phosphate (PI3P) that serves as a platform for the formation of the autophagosomal membrane, also known as the isolation membrane. Several studies have found nutrient starvation induces biosynthesis of the isolation membrane at the mitochondria-associated membrane (MAM), an ER subdomain that forms membrane contact sites (MCS) with mitochondria. The MAM is a highly dynamic structure with numerous functions, including autophagy, apoptosis, and regulation of mitochondrial metabolism. We sought to investigate the role of the small GTPase Rab32, a known MAM regulator, in the process of autophagy. We demonstrate overexpression of the dominant active mutant of Rab32, Rab32Q85L, promotes autophagy. We also show Rab32 induces selective autophagy, a highly specific degradation that often targets old or damaged organelles. This specificity is granted by autophagy receptors, organelle-specific proteins that link cargo proteins to the autophagosomal membrane. Our results show Rab32 interacts with the long isoform of Reticulon-3, an autophagy receptor for ERphagy, selective autophagy of the ER. Increasing evidence suggests the specificity of selective autophagy goes beyond the organellar level. Indeed, evidence has shown different ER-associated receptors participate in specific degradation of ER subdomains, including sheets, tubules, or peripheral ER. Therefore, we also investigated the substrates of Rab32-mediated autophagy and found MAM-localized proteins were specifically degraded. This included degradation of TMX1 and VDAC1 as well as MAM-localized Bcl-2 family proteins. This degradation also reduced the number of mitochondria-ER contacts (MERCs) as assayed by electron microscopy. We also observed a delay in apoptosis for cells overexpressing Rab32Q85L. Thus, we demonstrate Rab32 triggers “MAMphagy”, a distinct type of selective autophagy that appears to be implicated in the survival of a subset of breast cancer patients.

3.2 Background

3.2.1 Rab32 and autophagy

The ubiquitous small GTPase Rab32 is a multifunctional traffic regulator that localizes to mitochondria, ER, and lysosome-related organelles (LROs) [290,300]. In melanocytes, Rab32 is mostly found on the melanosome, a LRO responsible for melanin synthesis [300]. This process requires several enzymes, including Tyrosinase and Tyrosinase-related protein 1 (Trp1) and 2 (Trp2). Delivery of these enzymes from the TGN to the melanosome requires Rab32 interaction with its GEF, biogenesis of lysosome-related organelles complex 3 (BLOC-3) [300,303]. Rab32 also promotes traffic to the melanosome together with adaptor protein (AP) complex 1 and 3, which link cargo to clathrin in emerging clathrin-coated vesicles (CCVs) [301]. Together, these studies suggest a model where Rab32 recruits cargo to the TGN and promotes vesicle traffic to LROs.

Rab32 is particularly abundant on the ER in non-melanogenic cells [290]. Here, Rab32 is enriched within ER subdomains in close apposition with mitochondria, also known as mitochondria-associated membranes (MAMs). Although a GEF on these membranes has not been identified yet, Rab32 is known to interact with several proteins at MAMs and participates in various processes originating at these membrane contact sites (MCS). One of its functions here is as an A-kinase anchoring protein (AKAP) [304]. Rab32-mediated recruitment of PKA can lead to inhibitory phosphorylation of Drp1, another of its effectors [290,305]. Specifically, overexpression of dominant negative Rab32, Rab32T39N, increases PKA mitochondrial localization and inhibitory Ser656 phosphorylation on Drp1 [290]. This process is in part regulated by another Rab32 effector, the ER SNARE Syntaxin-17 [307]. Syntaxin-17 interacts with Drp1 and Rab32 at MAMs during homeostasis and inhibits Rab32 from binding and recruiting PKA. This allows Drp1 to function normally and mediate mitochondrial fission from the MAM as necessary. Oppositely, starvation inhibits mitochondrial fission. Starvation also induces autophagy, which also occurs at the MAM [203]. Under these conditions, Syntaxin-17 dissociates from Drp1 and Rab32 and instead binds Atg14L, a component of the PI3K III complex [203,307]. This process enriches the PI3K III complex at the MAM, where it synthesizes PI3P to recruit PI3P-binding proteins required for the formation of the isolation membrane [203,210]. This process also releases Rab32 from Syntaxin-17, allowing it to recruit PKA and cause inhibition of Drp1 and mitochondrial fission [307]. Thus, homeostasis promotes Rab32-Syntaxin17 binding while starvation dissolves this interaction and

shifts Syntaxin-17 to its role in autophagosome biogenesis. Since Rab32 has been implicated in autophagy it is possible Rab32 also shifts to a pro-autophagy function under these conditions.

Studies in non-melanogenic cells have shown Rab32 is also found on another LRO: the autophagosome [310,312]. Additionally, its overexpression can increase autophagosome number, suggesting Rab32 could activate autophagy [310,312]. Its loss instead inhibited autophagy in mammalian cells and *Drosophila* [310,311]. Evidence from melanocytes indicates Rab32 participates in cargo recruitment and traffic required for LRO biogenesis. It is possible Rab32 performs a similar function in non-melanogenic cells. Therefore, we hypothesize Rab32 participates in cargo recruitment and/or traffic required for autophagosome biogenesis. Consistent with this hypothesis, autophagosome biogenesis following nutrient starvation occurs mostly at the MAM, where Rab32 is enriched [201,290]. However, autophagosome formation has also been detected at other membranes, including the Golgi and mitochondria [201,226,228]. Moreover, Rab32 could also be involved in selective autophagy of the ER and mitochondria, making it unclear where Rab32 is likely to promote autophagy from.

3.2.2 Selective autophagy

Selective autophagy targets organelles in a highly specific manner as opposed to indiscriminate, basal autophagy [201]. This specificity is granted by autophagy receptors, organelle-specific proteins that recognize and bind cargo that is to be degraded [362]. Simultaneously, autophagy receptors also bind LC3 II via their LC3-interacting regions (LIRs), linking cargo to the autophagosomal membrane. For example, selective autophagy of mitochondria, also known as mitophagy, has several known mitophagy receptors. Amongst them is Optineurin (OPTN), which participates in Parkin- and phosphatase and tensin homolog-induced kinase 1 (PINK1)-mediated mitophagy [363]. In this pathway, PINK1 activates the ubiquitin ligase Parkin, which ubiquitinates OMM proteins to tag them as cargo. OPTN then binds these ubiquitin-tagged proteins and bridges them to the growing autophagosome. Several other mitophagy receptors also recognize ubiquitin-tagged substrates during PINK1-Parkin mitophagy, including nuclear dot protein 52 kDa (NDP52) [362,363]. Therefore, mitophagy can occur through the cooperation of multiple mitophagy receptors [362].

Cargo recognition in ERphagy, the selective degradation of the ER, is less understood. For instance, while ubiquitin acts as a cargo tag in mitophagy [363], a cargo tagging mechanism has not been identified in ERphagy [364]. Moreover, ERphagy receptors do not cooperate with one another. Indeed, only one type of receptor protein is recruited to any ER-derived autophagosome. Several studies have also shown ERphagy receptors target distinct ER structures or subdomains [200,365–368]. For instance, the ERphagy receptor cell cycle progression 1 (CCPG1) specifically degrades peripheral ER enriched in aggregated proteins following starvation [366]. Some evidence suggests CCPG1 could specifically recognize and recruit unfolded proteins during this process [364,366]. This could represent an additional mechanism to reduce misfolded proteins during the UPR, which is known to trigger autophagy [369]. Moreover, ER stress induces CCPG1 transcription, which increases degradation of ER with aggregated proteins [366].

FAM134B is another ERphagy receptor that promotes the specific degradation of ER sheets [365,370], while the long isoform of Reticulon-3 (RTN3L) [200] and Atlastin 3 target ER tubules [367]. Interestingly, RTN3L and Atlastin 3 are also ER-shaping proteins [371,372]. Specifically, Atlastin 3 catalyzes the fusion of ER tubules while RTN3L stabilizes membrane curvature to maintain ER tubules. Both RTN3L and FAM134B have reticulon homology domains (RHD), which promote membrane bending when these proteins cluster together [364,365,373]. Thus, FAM134B clustering induces membrane bending in ER sheets, where it is mostly localized [365]. This activity is also required for FAM134B's role in ERphagy, since mutation or loss of its RHD impairs degradation. RTN3L, which is instead enriched in ER tubules, also induces membrane curvature [200,373].

Another ERphagy receptor that is transcriptionally upregulated during the UPR is Sec62 [374]. Sec62 specifically degrades membranes enriched in chaperones during ER stress resolution, after the ER has expanded to accommodate more protein folding. This process is also called recovERphagy since it helps return the ER to its homeostatic size and content. Lastly, a recent study in *S. cerevisiae* has described autophagic degradation of nuclear pores [368]. This degradation involved a cytoplasmic facing nucleoporin, a component of the nuclear pore, acting as an autophagy receptor by interacting directly with the LC3 homolog Atg8. Together, these studies strongly suggest degradation of specific ER subdomains is possible. Although selective

autophagy of the MAM subdomain of the ER has not been observed, this degradation could have implications in diseases with dysregulated MAMs such as cancer.

3.2.3 Rab32, MAMs, and cancer

Rab32 has been previously described as a marker for the development of melanoma since it is significantly upregulated in primary melanoma compared to benign nevi [375]. This effect is likely tied to its role in melanosome enzyme delivery, which is required for adequate melanosome biogenesis [300,301]. Interestingly, Rab32 is also upregulated in almost 25% of breast cancers [376,377]. This suggests Rab32 could be a relevant potential biomarker for this disease, though it is unclear if and how high Rab32 levels could affect breast cancer patients. There is also significant evidence linking cancer and MAM dysregulation, though the frequency and significance of this link is still unclear [34,260]. For example, several well-known tumor suppressors use the MAM as a platform to control mitochondrial activity [34]. For example, p53 binds SERCA2b and promotes its activity to induce apoptosis. Additionally, several Bcl-2 family proteins are found on MAMs, including anti-apoptotic members Bcl-2 and Bcl-xL, which can activate IP_3R to support pro-survival Ca^{2+} flux [128,129,378]. Therefore, degradation of the MAM could influence cell fate by removing tumor suppressors.

3.3 Results

3.3.1 Rab32 activation promotes autophagy

Given Rab32 overexpression has been shown to increase autophagosome number [310], we first sought to investigate the effect of WT, dominant-active, and dominant-negative Rab32 overexpression on autophagosome number. To do this, we quantified LC3 puncta generated by stably expressed GFP-tagged LC3 in cells transfected with FLAG-tagged WT Rab32, dominant-active Rab32Q85L, or dominant-negative Rab32T39N. We used a cutoff of ≥10 puncta per cell to categorize a cell as having an unusually high number of autophagosomes. This cutoff has been previously used for this assay [310]. We found roughly 20% of vector control cells had increased numbers of autophagosomes, establishing a baseline for basal autophagy which is consistent with other reports [310]. Over-expression of either WT Rab32 or Rab32T39N did not significantly increase this percentage (Figure 3.1A). However, Rab32Q85L more than doubled the baseline

percentage to roughly 55% (Figure 3.1A). We also observed Rab32Q85L partially co-localized with LC3-GFP puncta, confirming reports that Rab32 is found on autophagosomes (Figure 3.1A) [310,312]. To compare this increase to autophagy-inducing conditions, we starved cells by incubating them in Earl's Balanced Salt Solution (EBSS) for 2hrs. Under these conditions, roughly 60% of vector control cells had increased autophagosome numbers (Figure 3.1B). Interestingly, cells overexpressing WT, Q85L and T39N Rab32 all had similar percentages and no statistically significant differences were observed (Figure 3.1B). Taken together, these results suggest Rab32Q85L activates autophagy to levels similar to those induced by short-term nutrient starvation.

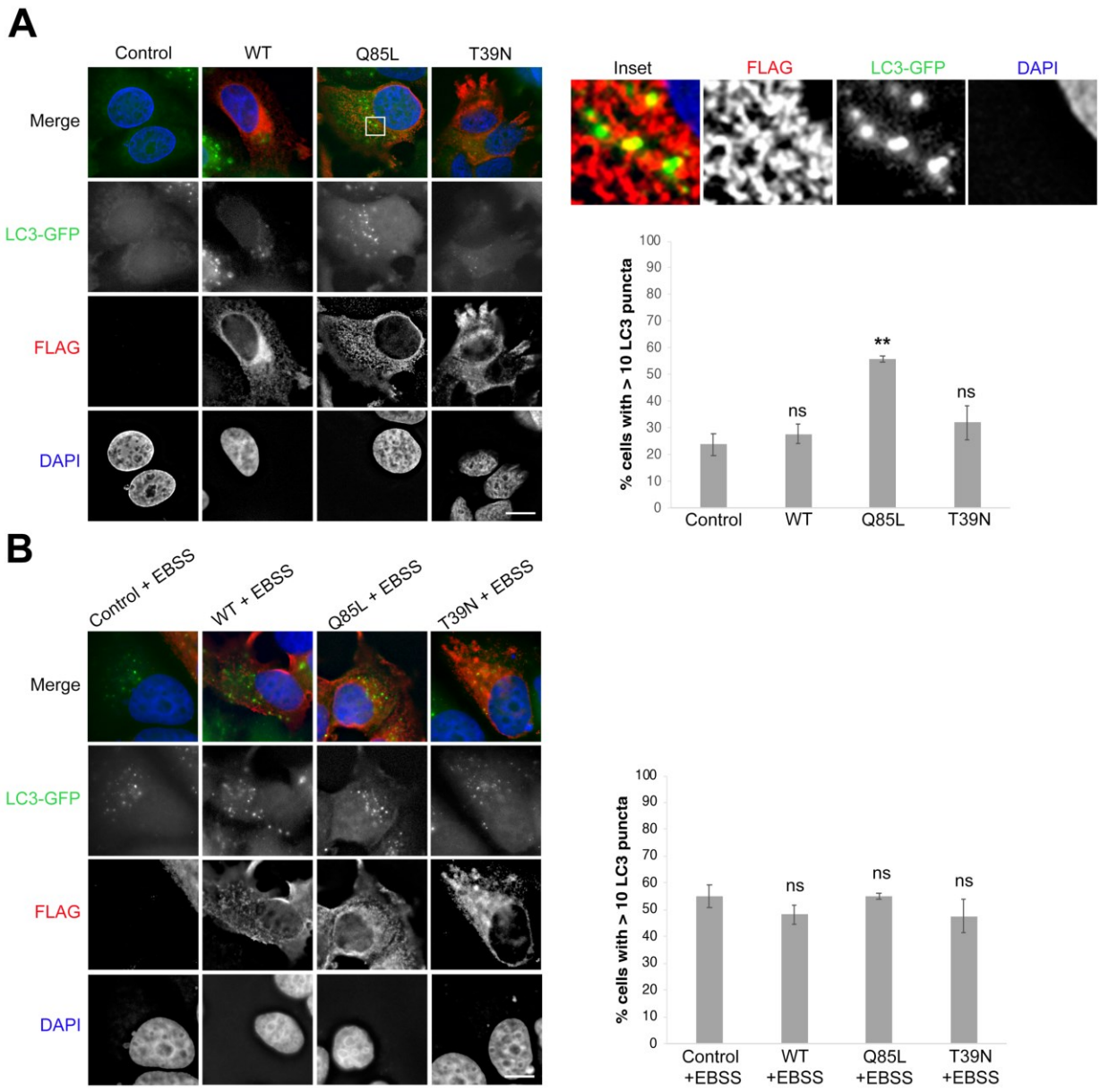

Figure 3.1 Active Rab32 increases autophagosome number
A. Representative immunofluorescence images of MCF7 cells stably expressing LC3-GFP and transfected with FLAG-tagged wild type (WT), dominant active (Q85L) or dominant negative (T39N) Rab32. Cells were probed for FLAG-tagged Rab32 (red) and nuclei (DAPI, blue) in parallel. Bar indicates 15µm. Quantification of cells with ≥10 LC3 puncta, indicating increased autophagy, were expressed as a percent of total cells counted. ≥100 cells per condition were counted in each (n=3) independent experiment. **p≤0.001. ns=not significant. Inset shows magnification of a representative area, evidencing overlap between FLAG-Rab32Q85L and LC3-GFP. **B.** Representative immunofluorescence images after a 2hr incubation with EBSS of MCF7 cells stably expressing LC3-GFP and transfected with FLAG-tagged WT, Q85L, or T39N Rab32. Cells were probed for FLAG-tagged Rab32 (red) and nuclei (DAPI, blue) in parallel. Bar indicates 15µm. Quantification as in A. ns=not significant.

Next, we sought to confirm these results by probing for LC3 II within lysates. Consistent with our immunofluorescence results (Figure 3.1A), only Rab32Q85L doubled baseline LC3 II amounts relative to tubulin (Figure 3.2A). This Q85L-mediated LC3II increase was lost when cells were starved (Figure 3.2B). These results are in line with those observed in the LC3 puncta assay, where starvation eliminated any differences between control and Q85L overexpressing cells (Figure 3.1B). To test if the Q85L-mediated increase in LC3 puncta (Figure 3.1A) and LC3 II protein levels (Figure 3.2A) are due to increased autophagy or a block along the pathway, we incubated cells with Bafilomycin A1, an inhibitor of lysosomal degradation. Under these conditions, an increase in LC3 II is indicative of autophagy induction. This is because LC3 II levels increase as autophagy is induced, but LC3 II cannot be degraded due to the block in lysosomal degradation, resulting in LC3 accumulation. Therefore, relative to control cells, LC3 II accumulates in cells with autophagy activation. On the other hand, a block in the pathway, such as inhibition of autophagosome-lysosome fusion, would yield no differences in LC3 II amounts. This is because equal amounts of autophagosomes are produced, therefore, lysosomal inhibition would result in similar accumulation of LC3 II. As seen in Figure 3.2B, incubation with Bafilomycin A1 resulted in a larger LC3 II increase in Rab32Q85L overexpressing cells compared to vector control cells. Therefore, these findings suggest Rab32Q85L did not increase autophagosome number by blocking autophagosome-lysosome fusion or by otherwise altering autophagic flux. Instead, these results strongly suggest Rab32Q85L induces autophagy.

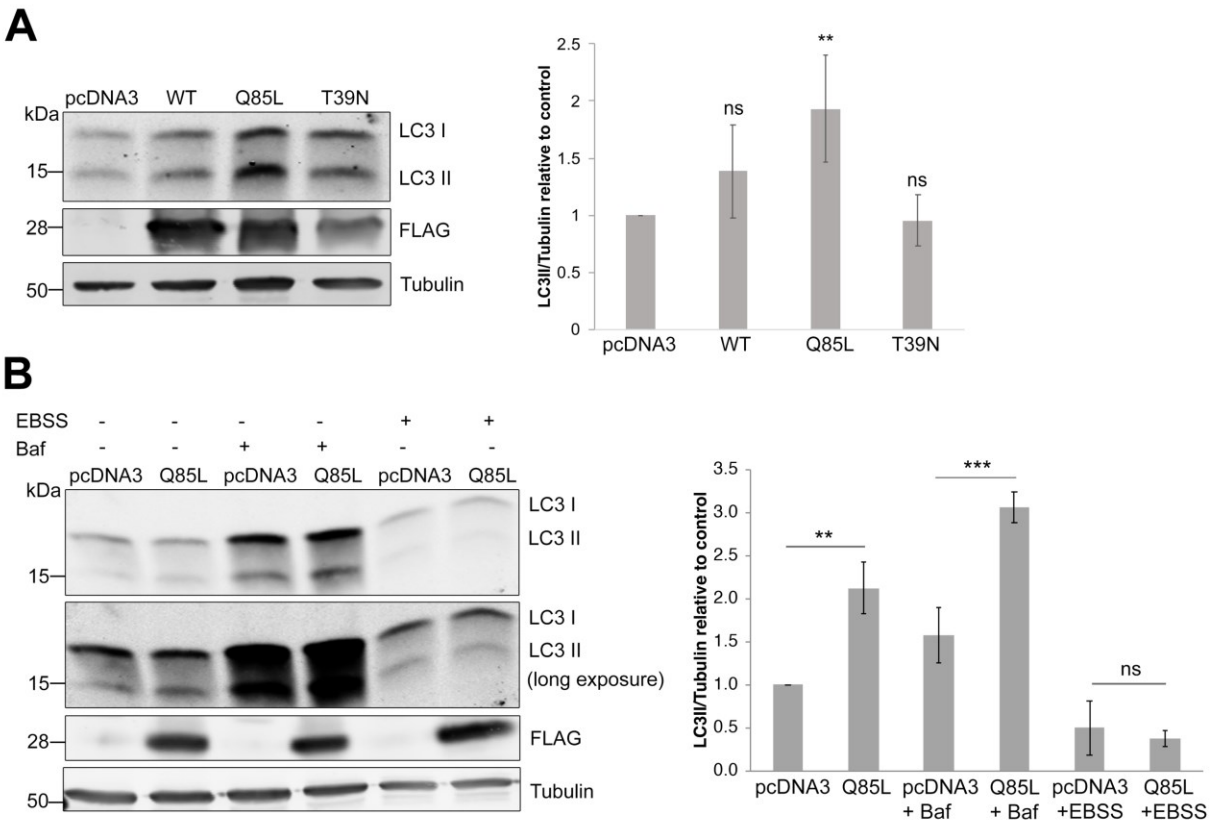

Figure 3.2 Active Rab32 promotes autophagy

A. Immunoblot of MCF7 cells transfected with pcDNA3 vector as a control or with FLAG-tagged WT, Q85L, or T39N Rab32. Blots were probed for LC3, FLAG, and Tubulin as a loading control. Densitometry analysis of LC3II/Tubulin is shown on the right. n=3. ns=not significant. **p≤0.001. **B.** Immunoblot of MCF7 cells transfected with pcDNA3 vector as a control or FLAG-tagged WT, Q85L, or T39N Rab32 following a 4hr EBSS or 48hr 100nM Bafilomycin incubation where indicated. Densitometry analysis of LC3II/Tubulin on the right. n=3. ***p≤0.0001. **p≤0.001. ns=not significant.

3.3.2 Rab32 knockdown impairs starvation-mediated autophagy

Next, we wanted to investigate if Rab32 is necessary for autophagy induction. To test this, we knocked Rab32 down using RNAi. This had no effect on the number of cells with unusually high numbers of GFP-LC3 puncta (Figure 3.3A), suggesting basal autophagy was not disrupted. Upon starvation, ~60% of control cells had increased autophagosomes compared to only ~40% of siRab32 cells (Figure 3.3B). We also verified Rab32 knockdown (KD) in protein lysates, which had roughly an 80% decrease (Figure 3.3C). Rab32 KD did not alter the protein levels of LC3 II in untreated conditions, once again indicating basal autophagy was not altered (Figure 3.3D). Consistent with these results, there was also no change in LC3 II levels in the presence of Bafilomycin A1 (Figure 3.3D). Consistent with the reduced formation of LC3 aggregates in starved siRab32 cells (Figure 3.3B), LC3 II protein levels decreased significantly in these cells (Figure 3.3D). In brief, these results suggest Rab32 KD impairs starvation-induced autophagy but does not alter basal autophagy.

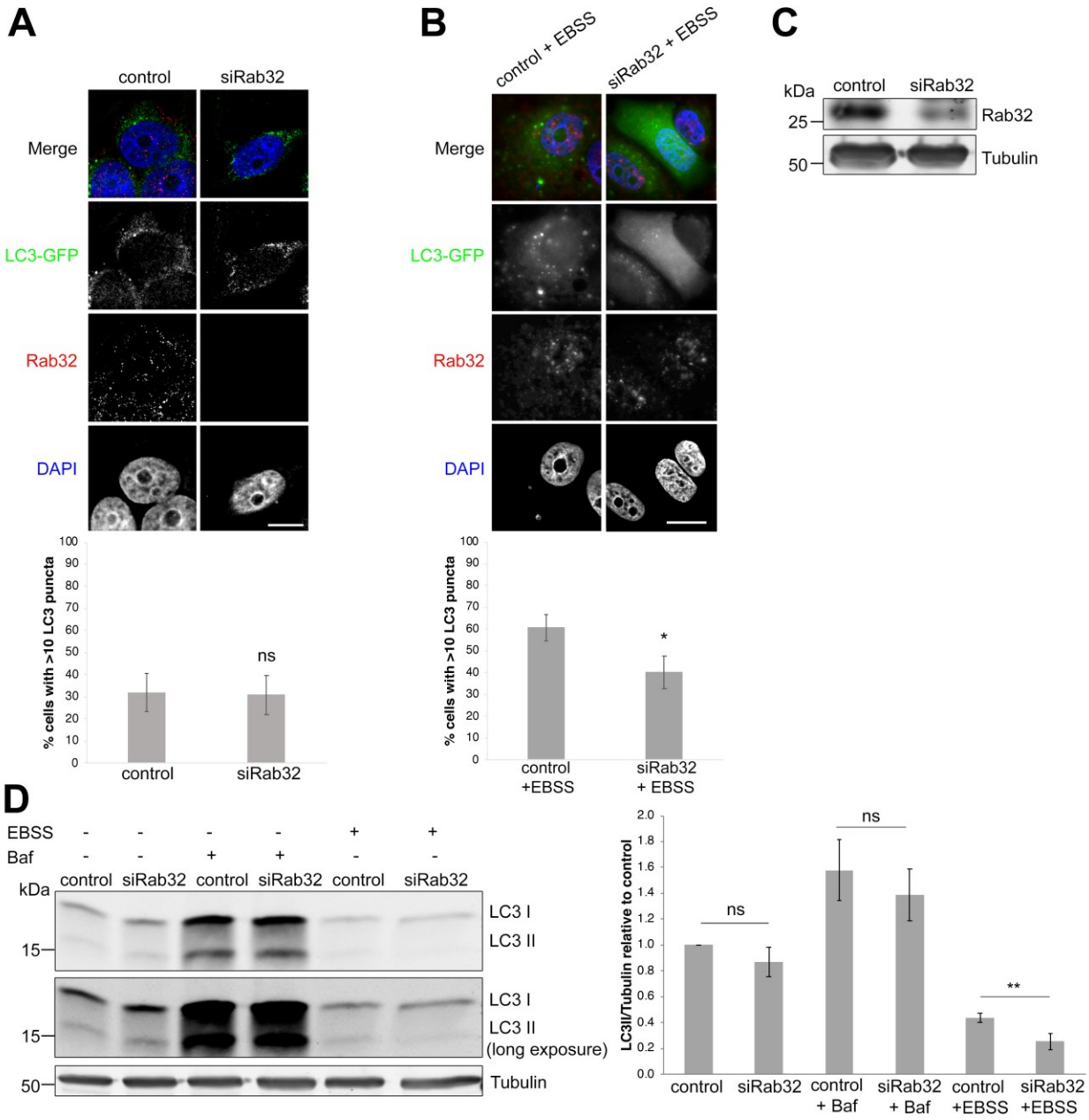

Figure 3.3 Rab32 knockdown impairs starvation-induced autophagy

A. Representative immunofluorescence images of MCF7 cells stably expressing LC3-GFP with control siRNA or siRNA against Rab32. Cells were probed for endogenous Rab32 (red) and nuclei (DAPI, blue) in parallel. Bar indicates 10µm. Quantification of cells with ≥10 LC3 puncta, indicating increased autophagy, were expressed as percent of total cells counted. ≥100 cells per condition were counted in n=3 independent experiment. ns=not significant. **B.** Representative immunofluorescence as in A with 2hr EBSS incubation. *p≤0.05. **C.** Immunoblot of MCF7 cells with control siRNA or siRab32 probed for endogenous Rab32 indicating Rab32 KD. Tubulin was used as a loading control. **D.** Immunoblot as in C after 4hr EBSS or 48hr 100nM Bafilomycin incubation where indicated. Long exposure of LC3 reveals a decrease in LC3 II in the last lane. Densitometry analysis on the right LC3II/Tubulin. n=3. **p≤0.001. ns=not significant p>0.05.

3.3.3 Rab32 targets the MAM for autophagic degradation

To identify the targets of Rab32-mediated autophagy we probed for organelle-specific substrates in the presence of active Rab32Q85L versus empty plasmid-transfected control cells. We observed no significant changes for a variety of candidate substrates in the cytosol, Golgi, endosomes, mitochondria, or ER (Figures 3.4A-D). These results therefore strongly suggest Rab32Q85L does not trigger bulk autophagy or selective degradation of Golgi, ER, or mitochondrial membranes.

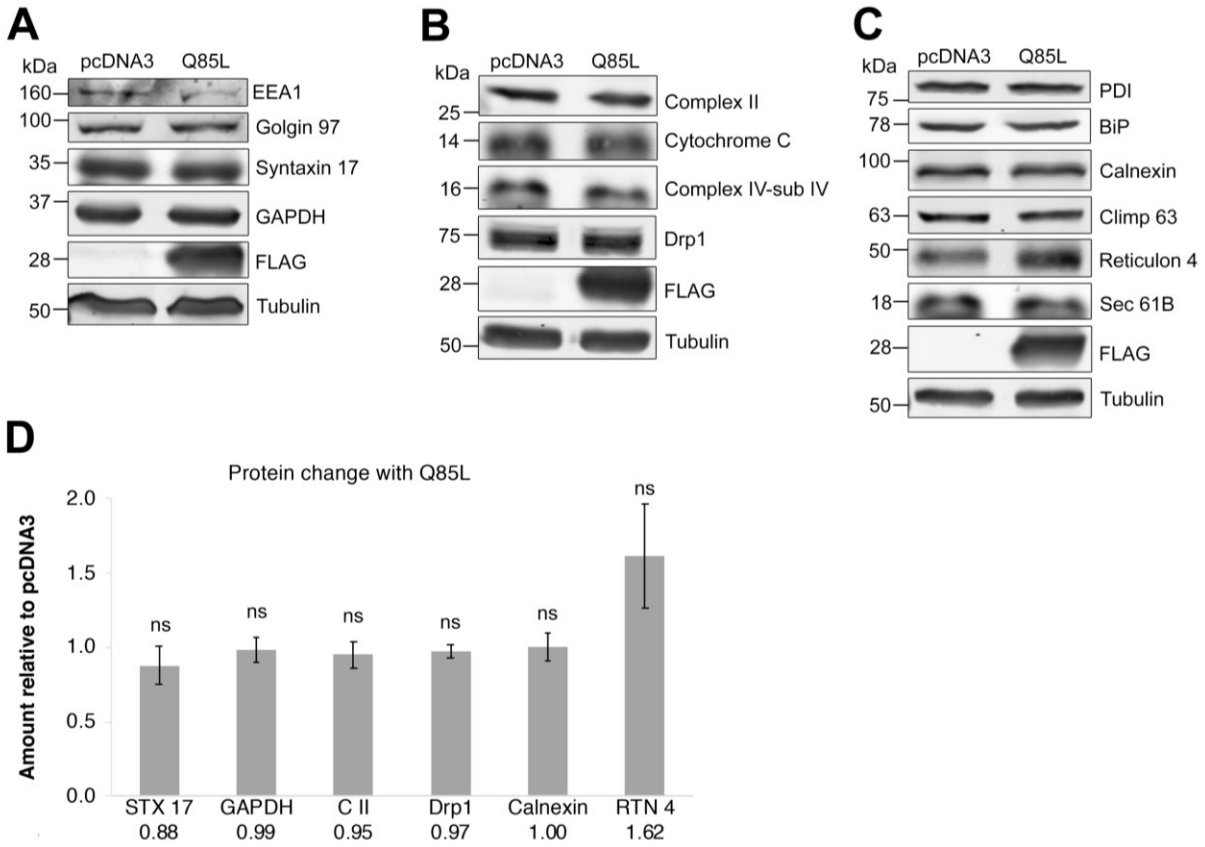

Figure 3.4 Active Rab32 does not alter cytosolic, Golgi, endosomal, mitochondrial, or ER protein levels

A. Immunoblot analysis of transfected MCF7 cells for the amounts of cytosolic, endosomal and Golgi proteins GAPDH, EEA1, and Golgin 97, respectively. Tubulin acts as a loading control while FLAG signal indicates transfected FLAG-tagged Rab32Q85L cells. **B.** Immunoblot analysis as in A for the amounts of several mitochondrial proteins. **C.** Immunoblot analysis as in A for the amounts of several ER proteins. **D.** Densitometry analysis from n=3 independent experiments for representative members of cytosolic, mitochondria, and ER proteins. Amounts were compared to control pcDNA3 samples. Average densitometry values are indicated below each bar. ns=not significant $p>0.05$.

Since Rab32 also localizes to the MAM, we also probed for MAM proteins. Our results showed MAM proteins FACL4, PACS-2, Caveolin, VDAC1, TMX1, and IP_3R decreased significantly between ~75% to ~45% in the presence of dominant-active Rab32Q85L (Figure 3.5A). Although we also observed the same trend for Mitofusin-2, this change was not statistically significant (Figure 3.5A). To continue characterizing this pathway we used TMX1 and VDAC1 as markers for Rab32-mediated degradation since they are more abundant and therefore easier to detect than the other MAM proteins we analyzed. We also chose to focus on TMX1 because it was heavily targeted by Rab32Q85L, causing a 48% decrease in lysates (Figure 3.5A). To confirm the degradation of MAM proteins was specific to active Rab32 we also tested the effect of WT and dominant-negative Rab32T39N overexpression (Figure 3.5B). These results confirmed only cells overexpressing Q85L, and not WT or T39N, decreased TMX1 and VDAC1 (Figure 3.5B). We also observed no changes for cytosolic, mitochondrial, or ER proteins with overexpression any of the Rab32 constructs, confirming the MAM-specific nature of Rab32Q85L-mediated autophagy (Figure 3.5B).

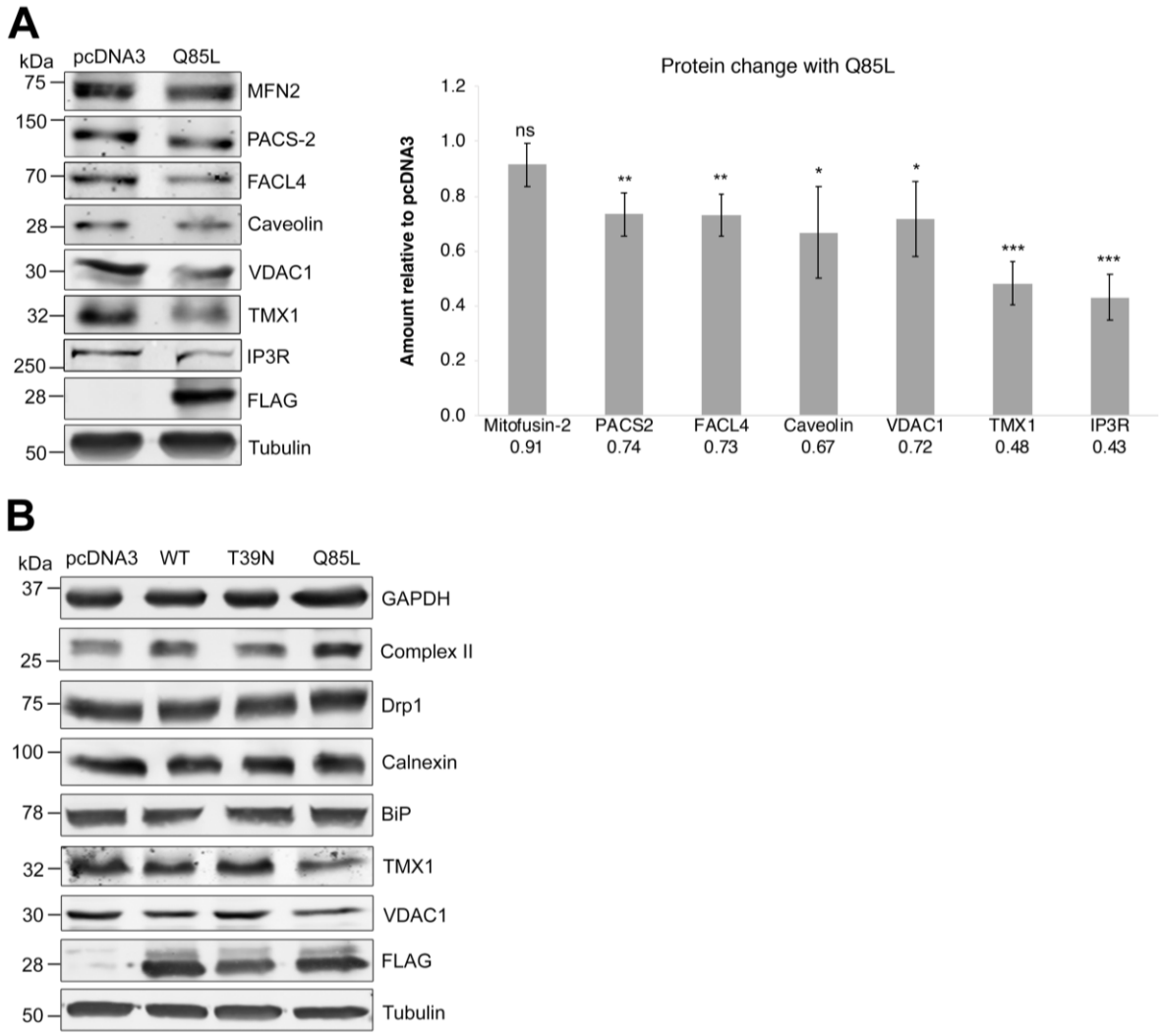

Figure 3.5 Active Rab32 promotes autophagic degradation of MAM proteins
A. Immunoblot and densitometry analysis of transfected MCF7 cells demonstrate MAM proteins decrease with Rab32Q85L. Densitometry analysis from n=3 independent experiments. Tubulin acts as a loading control while FLAG indicates transfected FLAG-tagged Rab32Q85L. Average densitometry values are indicated below each bar. ns=not significant. *p≤0.05. **p≤0.01. ***p≤0.001. **B.** Immunoblot for MCF7 cells transfected with control pcDNA3 or WT, T39N, and Q85L-FLAG tagged Rab32 shows only Q85L degrades MAM proteins TMX1 and VDAC1. Markers for other organelles were used to indicate specificity for MAM proteome as follows: GAPDH for cytosol, Complex II and Drp1 for mitochondria, Calnexin and BiP for ER. Tubulin was used as a loading control and FLAG to indicate transfection.

Next, we treated cells with Bafilomycin A1 and performed densitometry analysis. This eliminated the statistically significant Q85L-mediated TMX1 decrease, confirming the autophagic nature of the degradation (Figure 3.6A). Bafilomycin A1 also led to the accumulation of VDAC1 in the presence of Q85L, suggesting the decrease in VDAC1 observed in untreated Q85L overexpressing cells is also due to autophagy (Figure 3.6A). There were no significant changes for mitochondrial marker Complex II or ER marker Calnexin in this experiment, confirming the MAM specificity of Q85L-mediated degradation (Figure 3.6A).

Lastly, we wanted to know if Rab32 participates in the degradation of these proteins in basal conditions. Therefore, we knocked down Rab32 and probed for VDAC1 and TMX1. This caused a significant increase in TMX1, which suggests Rab32 does indeed degrade this protein in basal conditions (Figure 3.6B). VDAC1 also accumulated, suggesting other MAM proteins behave similarly (Figure 3.6B). TMX1 accumulation was no longer statistically significant when cells were starved, however (Figure 3.6B). This is in contrast to the results obtained in Figure 3.3D, where the same conditions led to a statistically significant LC3 II decrease. One possible explanation for this is that TMX1 is relatively abundant in these cells and a longer starvation period is required to observe a significant difference. Together, these results suggest active Rab32 induces a distinct type of selective autophagy that specifically targets MAM proteins.

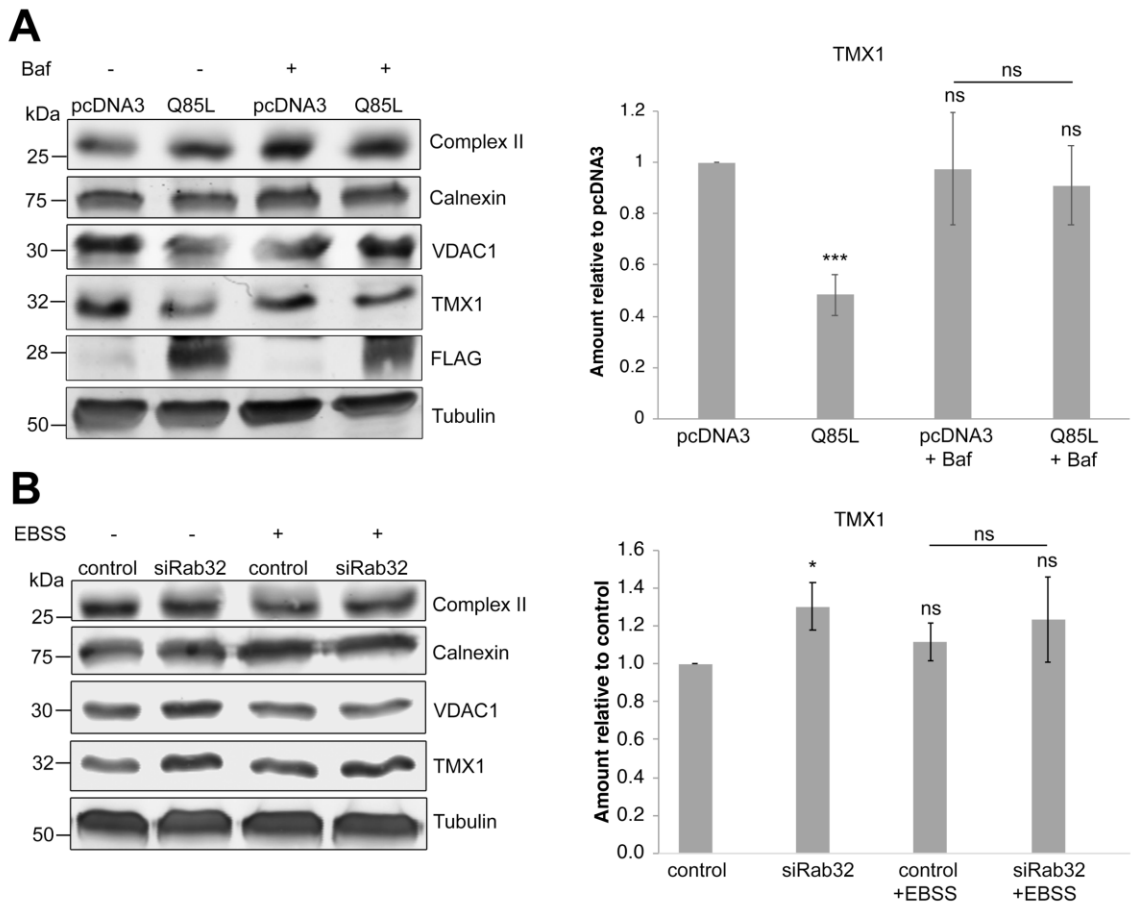

Figure 3.6 Rab32 knockdown causes an accumulation of MAM marker TMX1
A. Immunoblot analysis of transfected MCF7 cells with and without 48hr 100 nM Bafilomycin A1 incubation. Tubulin acts as a loading control while FLAG indicates transfected FLAG-tagged Rab32Q85L. TMX1 and VDAC1 were used as MAM markers and TMX1 amounts analyzed by densitometry from n=3 independent experiments. Complex II and Calnexin served as markers for mitochondria and ER, respectively, demonstrating Rab32Q85L does not target these organelles. ns=not significant. ***$p \leq 0.001$. **B.** Immunoblot of MCF7 cells transfected with control siRNA or siRNA against Rab32 with and without 4hr EBSS incubation. TMX1 and VDAC1 were used as MAM markers. Tubulin acts as a loading control. Complex II and Calnexin served as markers for mitochondria and ER, respectively, demonstrating Rab32Q85L does not target these organelles. TMX1 densitometry analysis from n=3 independent experiments. ns=not significant. *$p \leq 0.05$.

To further investigate Rab32-mediated autophagy we analyzed ER-mitochondria contact sites via electron micrograph quantifications (Figure 3.7A). Specifically, we obtained the average distance between the ER and mitochondrial membranes in individual ER-mitochondria contact sites to determine the tightness of the contacts (Figure 3.7C). We also obtained the length of individual contacts by measuring the length of a continuous ER membrane ≤50nm from the membrane of a mitochondrion (Figure 3.7D). We then calculated a MAM coefficient by dividing the length of each contact by its corresponding average distance between the membranes (Figure 3.7B). This allows us to obtain a factor proportional to MAM content.

These analyses revealed the MAM coefficient decreased to roughly half that of control cells when cells were stably expressing dominant-active Rab32Q85L (Figure 3.7B). We also observed a significant increase of ~5nm in the distance between ER and mitochondrial membranes engaged in MERCs (Figure 3.7C). Rab32Q85L also caused a significant decrease of ~50nm in MERC length (Figure 3.7D). Together, these results indicate Rab32Q85L caused a profound change in MAM structure that resulted in an overall decrease in MAM content concomitant with an increase in the distance between ER and mitochondrial membranes and a decrease in the length of these MCS.

To investigate whether ER-mitochondria tethering is necessary for Rab32-mediated autophagy, we used knockout (KO) cells for PACS-2 (HeLa) and Mitofusin-2 (mouse embryonic fibroblasts, MEFs). Consistent with the results observed in MCF7s (Figure 3.5A), Rab32Q85L decreased TMX1 levels in both PACS-2 and Mitofusin-2 WT cells (Figure 3.7 E,F). This effect was lost in the KOs, suggesting MAM tethering is required for Rab32-mediated degradation of MAM proteins (Figure 3.7 E,F). Given the narrow substrate specificity of this degradation, we propose active Rab32 triggers selective autophagy of the MAM, a process which we propose to call “MAMphagy”.

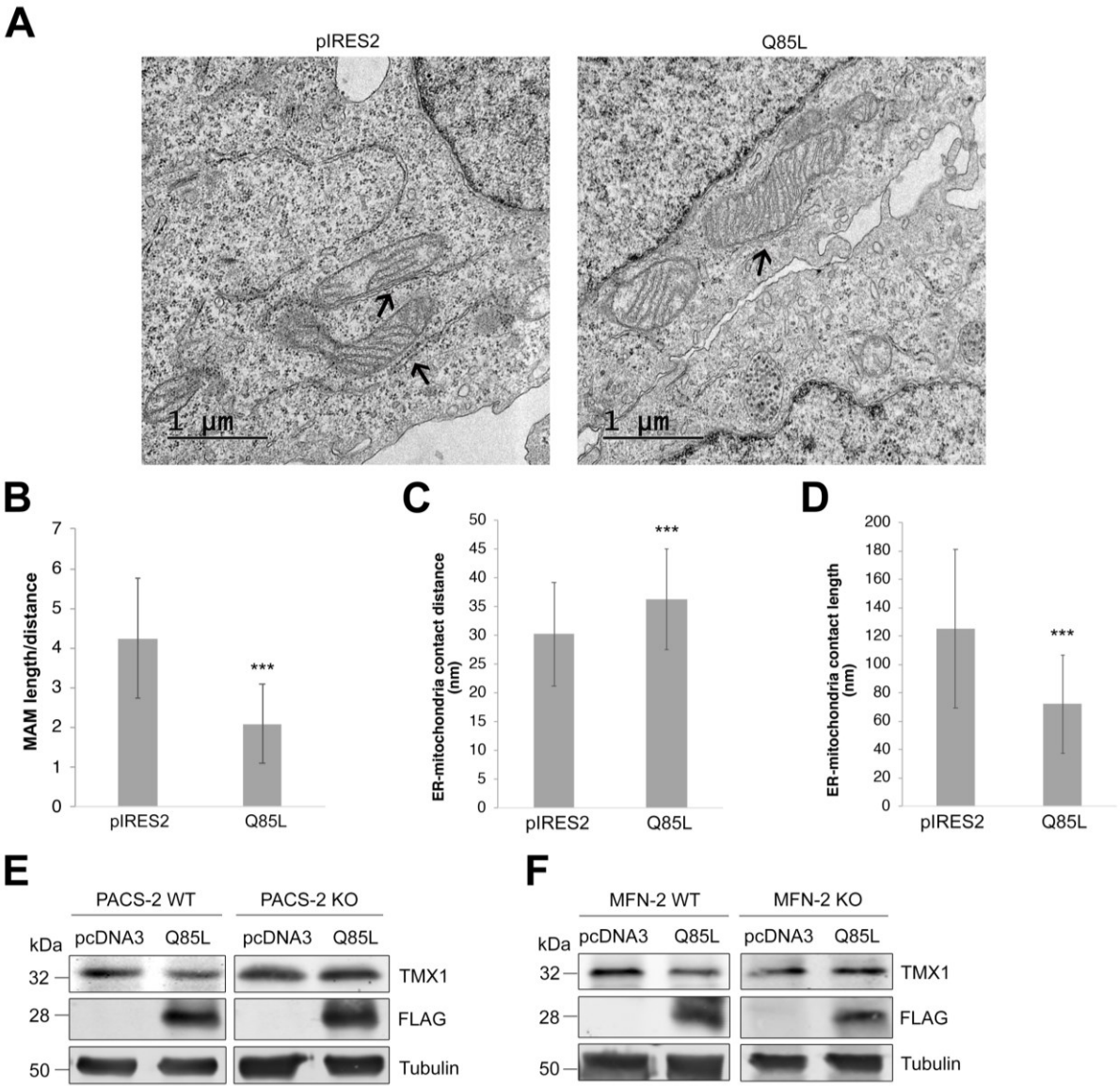

Figure 3.7 Active Rab32 decreases ER-mitochondria contact site length, tightness, and marker TMX1 in a tethering-dependent manner

A. Representative electron microscopy images of stably expressing control pIRES2 or Rab32Q85L MCF7s. Arrows indicate ER-mitochondria membrane contact sites ≤50nm apart. Images obtained by Dr. Nasser Tahbaz. **B.** ER-mitochondria length/distance ratio or MAM coefficient was obtained from n=100 individual measurements. ***p≤0.001. **C.** ER-mitochondria contact distance was graphed after obtaining an average measurement of the distance between a continous stretch of ER and mitochondria membranes 10-50nm apart for n=100 MCS. **D.** ER-mitochondria contact length was graphed after measuring the length along a continous stretch of ER engaged in a MCS (membranes 10-50nm apart) with a mitochondrion for n=100 MCS. **E.** Immunoblot of transfected WT and KO PACS-2 HeLa shows degradation of TMX1 in WT HeLas but not KOs. TMX1 was used as a MAM marker, tubulin as a loading control, and FLAG to indicate FLAG-tagged Rab32Q85L transfection. **F.** Immunoblot of transfected WT and KO Mitofusin-2 MEFs as in E shows TMX1 is degraded in WT MEFs but not KOs.

3.3.4 Rab32 interacts with RTN3L

Next, we sought to characterize the machinery used by Rab32 to trigger MAMphagy. This type of selective autophagy would require Rab32 to interact with an effector at the point of autophagosome origin. Given MAMs are a subdomain of the ER, we first tested if any known ERphagy receptors co-immunoprecipitated with Rab32. As effectors tend to preferentially bind to GTP-bound Rabs [218], we assessed for preferential binding to Rab32Q85L over WT or T39N Rab32. As shown in Figure 3.8A, FAM134B binding to Rab32 was non-specific, Sec62 bound preferentially to T39N, and CCPG1 showed no binding at all. In contrast, the long isoform of Reticulon-3 (RTN3L) bound markedly better to Q85L (Figure 3.8A). Densitometry analysis revealed this difference was statistically significant and RTN3L bound ~3.5 times better to Q85L compared to WT Rab32 (Figure 3.8A). We also tested for co-immunoprecipitation of Atg14L, which is recruited to the MAM upon starvation-mediated autophagy [203]. However, we observed no pulldown except for a small amount with Rab32T39N, suggesting Atg14L does not behave like a Rab32 effector (Figure 3.8A). We also tested for interaction with FUN14 domain containing protein 1 (FUNDC1), a mitophagy receptor recruited to the MAM during hypoxia via Calnexin binding [379], but found preferential binding to WT and T39N rather than Q85L (Figure 3.8A).

Next, we tested if any of these ERphagy receptors localized to the MAM. We hypothesized RTN3L would be found on the MAM since it preferentially bound Q85L. To do so, we performed a biochemical separation of membranes on a Percoll gradient from a MCF7 cell homogenate. On this classic isolation method, Rab32 localized mostly to the microsomal, mitochondrial, and MAM fractions (Figure 3.8B), as previously published [290]. As expected, MAM proteins TMX1, Calnexin, and PACS-2 were also found in the MAM fraction (Figure 3.8B). However, we observed minimal or no presence of RNT3L on the MAM (Figure 3.8B). It is possible RTN3L only accumulates at the MAM when Rab32 activity is high and induces MAMphagy.

Therefore, to test the specificity of a Rab32-RTN3L interaction during MAMphagy we probed for protein levels of these autophagy receptors with Rab32Q85L (Figure 3.8C). Given receptors are degraded along with the cargo they recruit to autophagosomes, an autophagy receptor required for MAMphagy should be degraded with Rab32Q85L. This was indeed the case, as RTN3L was the only ERphagy receptor whose levels decreased significantly with Q85L (Figure 3.8C). Furthermore, this decrease was prevented by the addition of Bafilomycin A1, once again confirming the autophagic nature of the degradation (Figure 3.8D).

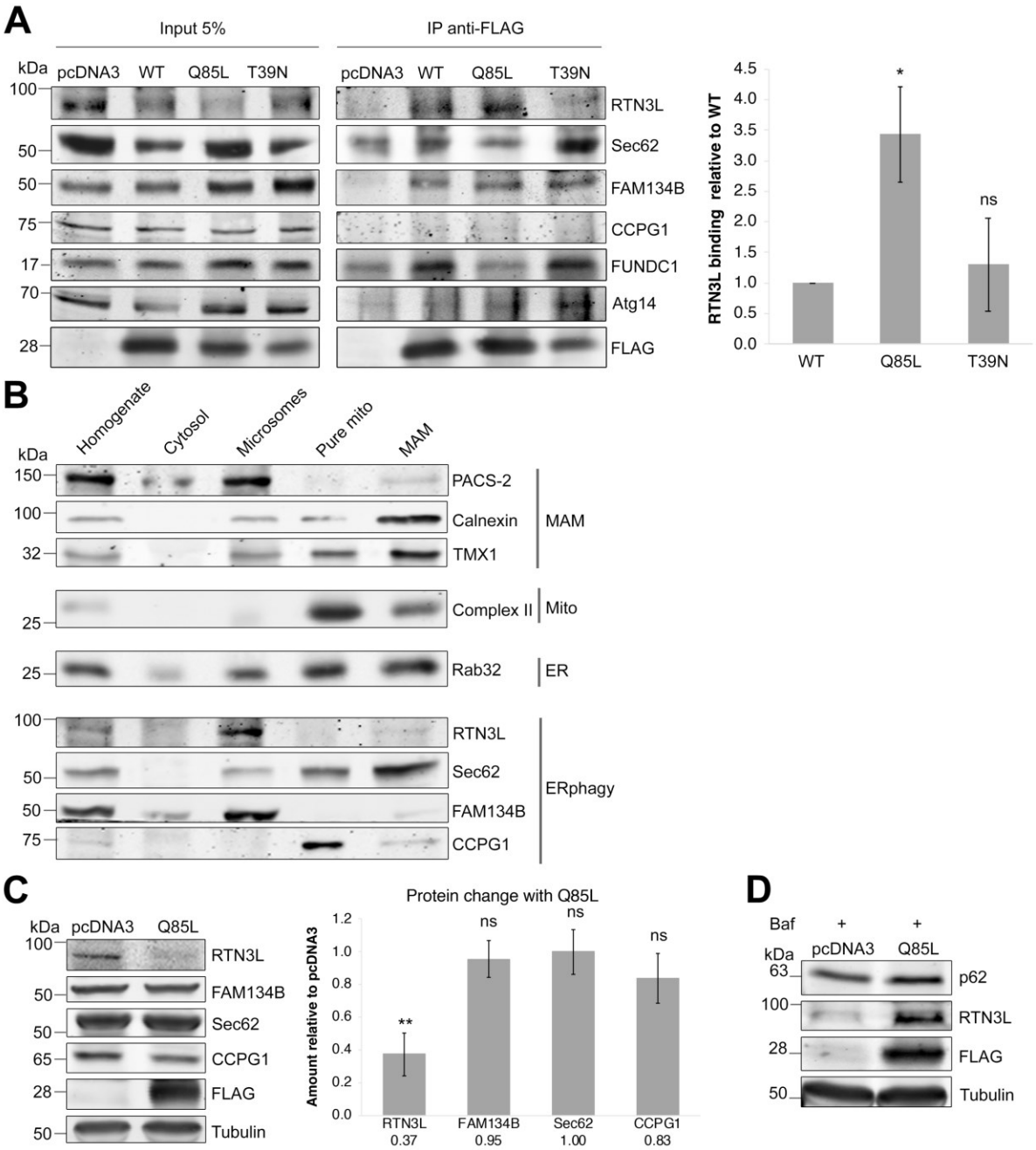

Figure 3.8 Rab32 interacts with ERphagy receptor Reticulon-3L

A. Co-immunoprecipitation of Rab32 constructs with endogenous autophagy receptors. MCF7 cells were transfected with FLAG-tagged Rab32, crosslinked with 2mM DSP, lysed and incubated with anti-FLAG antibodies. Immunoprecipitates were analyzed for anti-FLAG and co-immunoprecipitating endogenous autophagy receptors. Densitometry analysis of RTN3L binding to Rab32 was normalized to respective input signals. ns=not significant. *p≤0.05. **B.** Percoll fractionation of untransfected MCF7 cells for ERphagy receptors. Equal amounts of fractions were loaded. **C.** Immunoblot and densitometry analysis of control pcDNA3 and Q85L-FLAG transfected cells indicates only RTN3L levels decrease with Q85L. ns=not significant. **p≤0.01. n=3. **D.** Immunoblot as in C with 48hr 100nM Bafilomycin incubation shows RTN3L decrease with Q85L is prevented with autophagy inhibition.

We also tested for binding with the short isomer of RTN3, RTN3S, which is not involved in ERphagy [200]. We did not observe preferential binding with Rab32Q85L with RTN3S (Figure 3.9A), nor was this isomer degraded by Q85L (Figure 3.9B). To confirm Rab32-RTN3L binding we also performed a reciprocal co-immunoprecipitation, which successfully pulled down endogenous Rab32 with HA-tagged RTN3L (Figure 3.9C). Together, these results suggest RTN3L is a *bona fide* Rab32 effector.

To gain further evidence of a functional connection between Rab32 and RTN3L we simultaneously knocked down RTN3 with siRNA and transfected cells either with pcDNA3 or Rab32Q85L (Figure 3.9D). If RTN3L is required for Q85L-mediated MAMphagy, then TMX1 degradation in cells with both Q85L and siRTN3 should be impaired. Consistent with Figure 3.5A, TMX1 decreased with Rab32Q85L as compared to a pcDNA3 vector control (Figure 3.9D, lane 1 vs lane 3). TMX1 levels increased in cells with both pcDNA3 and siRTN3 (Figure 3.9D lane 1 vs lane 2), suggesting RTN3L is required for basal degradation of TMX1. In the presence of Rab32Q85L and siRTN3L, TMX1 levels were instead very similar to pcDNA3 control levels (Figure 3.9D, lane 1 vs lane 4). These results suggest siRTN3L impaired Q85L-mediated TMX1 degradation.

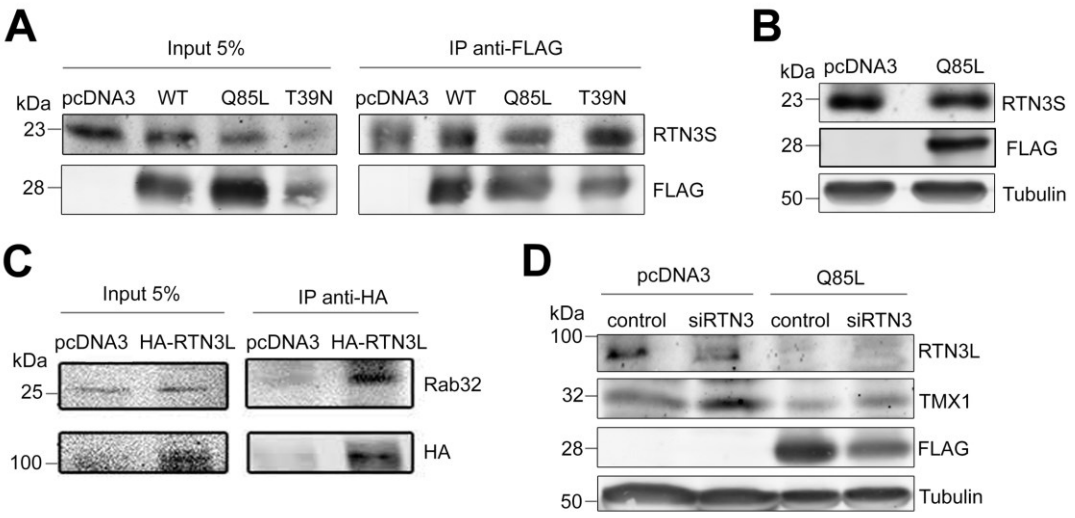

Figure 3.9 Reticulon-3L acts as an effector for Rab32Q85L-mediated autophagy
A. Co-immunoprecipitation of the endogenous short isoform of Reticulon-3, RTN3S, with FLAG-tagged Rab32 constructs shows non-selective binding. MCF7 cells were transfected with FLAG-tagged Rab32 constructs, crosslinked with 2mM DSP, followed by lysis and incubation with anti-FLAG antibodies. Immunoprecipitates were analyzed for anti-FLAG and co-immunoprecipitating endogenous RTN3S. **B.** Immunoblot of control pcDNA3 and Q85L-FLAG transfected cells indicates RTN3S levels do not decrease with Q85L. Tubulin was used as a loading control and FLAG to indicate transfection. **C.** Co-immunoprecipitation of endogenous Rab32 with HA-tagged RTN3L. MCF7 cells were transfected with HA-tagged RTN3L, crosslinked with 2mM DSP, lysed and incubated with anti-HA antibodies. Immunoprecipitates were analyzed for anti-HA and co-immunoprecipitating endogenous Rab32. Experiment performed by Megan Yap. **D.** Immunoblot of MCF7 cells transfected with pcDNA3 and Rab32Q85L co-transfected with control or siRNA against RTN3. TMX1 amounts were used to assay for MAMphagy, Tubulin was used as a loading control, and FLAG to identify FLAG-tagged Rab32Q85L.

Next, we decided to perform immunofluorescence microscopy and assess co-localization between Rab32 and RTN3L. This experiment revealed an overlapping distribution between endogenous Rab32 and HA-tagged RTN3L on perinuclear structures (Figure 3.10A). This is consistent with both proteins being mostly ER-bound [200,290]. We also calculated a Mander's coefficient to determine the extent of their colocalization. We compared these results against colocalization with Rab32T39N, which did not significantly pull down RTN3L (Figure 3.8A). This analysis demonstrated Rab32T39N co-localized with RTN3 roughly half as much as Rab32Q85L (Figure 3.10B). These findings are consistent with the hypothesis that Rab32Q85L and RTN3L act together to mediate MAMphagy.

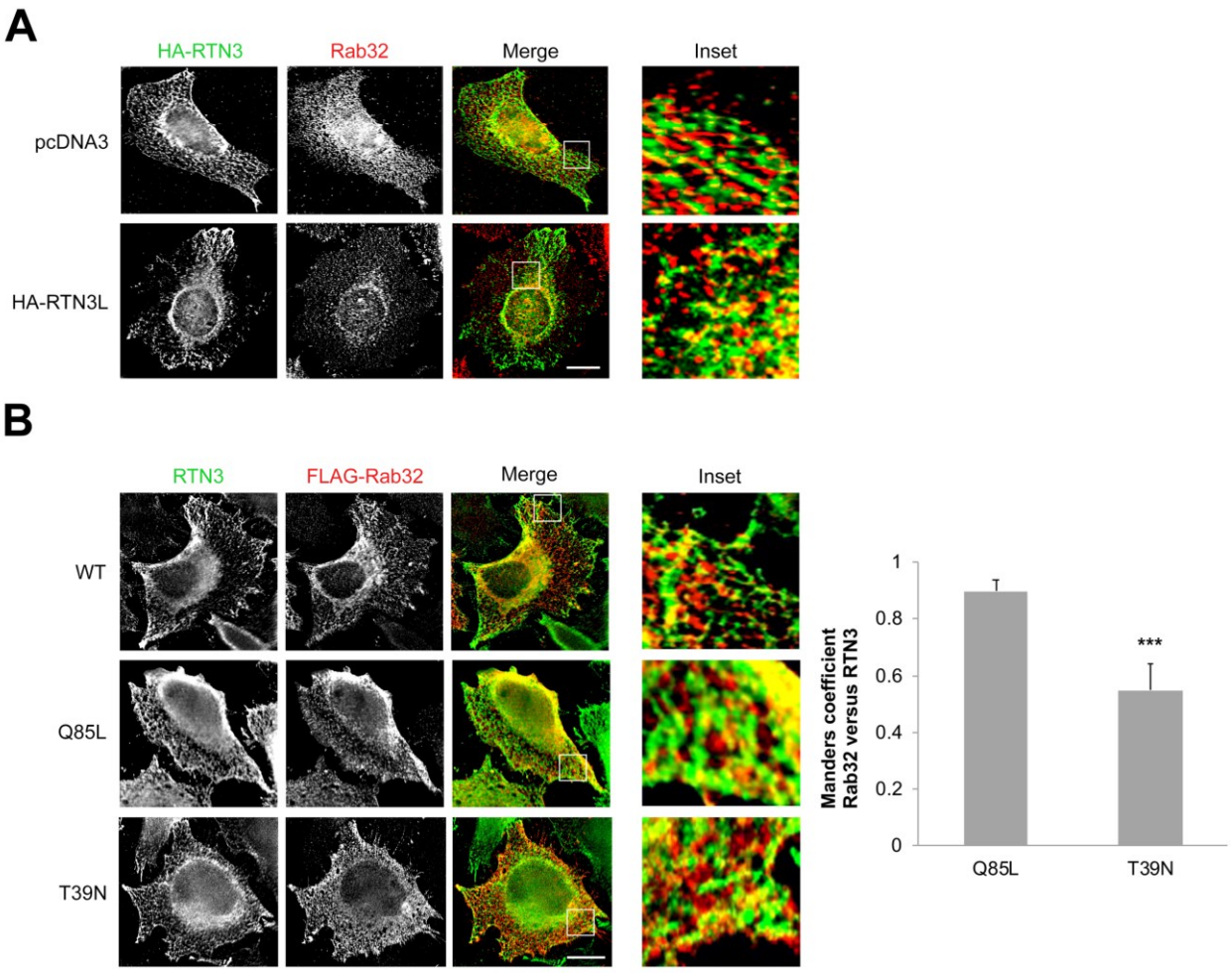

Figure 3.10 Active Rab32 co-localizes with Reticulon-3L
A. Representative immunofluorescence images of MCF7 cells transfected with HA-tagged RTN3L (bottom) or empty pcDNA3 (top). Cells were incubated with antibodies against Rab32 (red) and RTN3 (green). Bar indicates 15µm. Inset shows magnification of a representative area. **B.** Representative immunofluorescence images of MCF7 cells transfected with FLAG-tagged wild type (WT), dominant active (Q85L) or dominant negative (T39N) Rab32. Cells were incubated with Rab32 (red) and RTN3 (green) antibodies. Bar indicates 15µm. Mander's coefficient was calculated for Q85L and T39N. ***$p \leq 0.001$. Experiments and data analysis performed by Megan Yap.

3.3.5 MAM-localized Bcl-2 proteins are degraded by active Rab32

Next, we aimed to understand the larger significance of MAMphagy by investigating whether this process affects cell fate and/or apoptosis. To answer this question, we first turned to the status of Bcl-2 family proteins since anti-apoptotic members Bcl-2 and Bcl-xL partially reside on MAMs, where they bind IP_3R to promote pro-survival Ca^{2+} release [128,129]. Under resting conditions, Bcl-2, Bim_{EL}, Mcl-1 and Puma were found in the MAM fraction (Figure 3.11A). Of these proteins, only Bcl-2 has been previously reported to localize to MAMs [129]. As previously mentioned, Bcl-xL has also been reported to localize to MAMs [129]. However, our MAM fraction was almost completely devoid of Bcl-xL, a discrepancy that could be due to cell type differences [124] (Figure 3.11A). When we assayed for Rab32Q85L degradation, we found only the MAM-localized Bcl-2 family proteins were significantly degraded, while the MAM-excluded Bcl-xL was not (Figure 3.11B). As with the other MAM proteins probed in Figure 3.5, these Rab32-mediated decreases could be inhibited with Bafilomycin A1 (Figure 3.11B). These results further highlight the MAM-specific nature of Rab32-mediated autophagy.

We also investigated if Bim_{EL} degradation depended on RTN3L since this was the most consistently degraded Bcl-2 family protein (Figure 3.11B). This was indeed the case, as Bim_{EL} behaved like TMX1 in Figure 3.7D and did not decrease with Q85L when RTN3 was also knocked down (Figure 3.11C). Lastly, Rab32 KD caused a statistically significant accumulation of Bim_{EL} that was slightly mitigated when the cells were placed under starvation (Figure 3.11D). These results were also similar to those observed with TMX1 (Figure 3.5C). Taken together, these results suggest MAMphagy can also degrade MAM-localized Bcl-2 proteins, which at least in MCF7, includes anti-apoptotic Bcl-2 and Mcl-1, and pro-apoptotic Bim_{EL} and Puma.

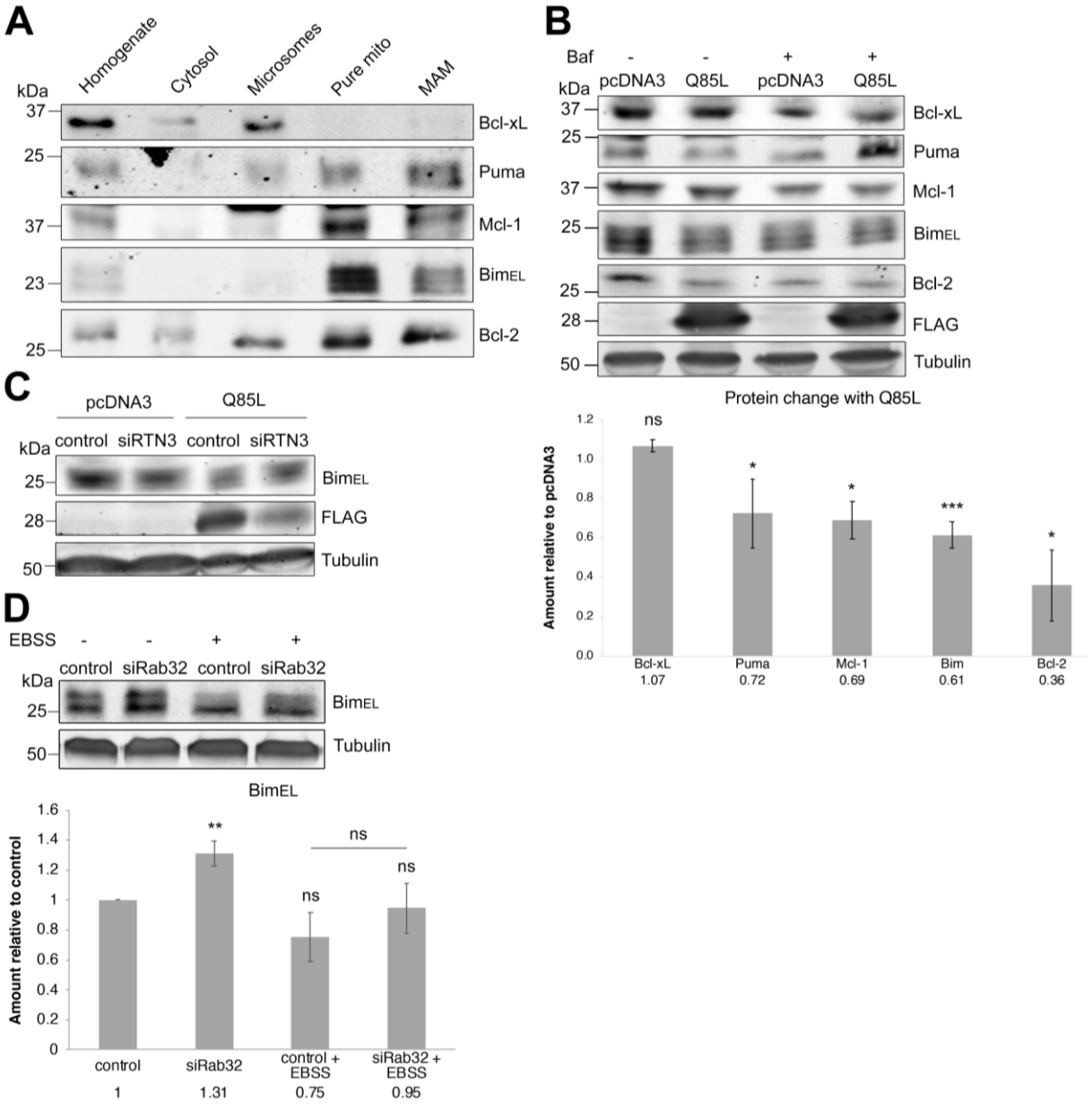

Figure 3.11 Active Rab32 degrades Bcl-2 family proteins localized to the MAM
A. Percoll fractionation of untransfected MCF7 cells. Equal amounts of fractions were loaded. **B.** Immunoblot of MCF7 cells transfected with pcDNA3 or Rab32Q85L and incubated with 100nM Bafilomycin for 48hrs where indicated. FLAG was used to detect FLAG-tagged Rab32Q85L and Tubulin was used as a loading control. Densitometry analysis for n=3 independent experiments. Average densitometry values are indicated below each bar. ns=not significant. *p≤0.05. ***p≤0.001. **C.** Immunoblot of MCF7 cells co-transfected with pcDNA3 or Rab32Q85L and control siRNA or siRNA against RTN3. Bim_{EL} was used to assay for MAMphagy. FLAG was used to detect FLAG-tagged Rab32Q85L and Tubulin was used as a loading control. **D.** Immunoblot and densitometry analysis of MCF7 cells transfected with control siRNA or siRNA against Rab32 after a 4hr EBSS incubation where indicated. Bim_{EL} was used to assay for MAMphagy and Tubulin was used as a loading control. Average densitometry values for Bim_{EL} are indicated below each bar. n=3. ns=not significant. **p≤0.01.

3.3.6 Active Rab32 delays apoptosis

Our results suggest Rab32 could play a role for cell survival since MAM-localized Bcl-2 family proteins regulate ER-mitochondria Ca^{2+} flux to promote survival or apoptosis [128,129]. Moreover, autophagic degradation of Bim has been shown to cause resistance to chemotherapy [380], suggesting autophagy-promoting proteins could sustain tumors in a similar fashion. As previously mentioned, high Rab32 expression levels correlate to tumor progression in melanoma [375]. Thus, Rab32 has been proposed to act in a tumor-promoting manner. To investigate whether Rab32 could influence cell fate, we treated Q85L and T39N overexpressing cells with tunicamycin to trigger ER stress-dependent apoptosis. We decided on this stimulus since ER stress has been previously used to induce ERphagy mediated by CCPG1 [366] and Sec62 [374]. Conversely, RTN3L ERphagy was triggered by starvation [200]. Therefore, in an effort to avoid RTN3L-mediated ERphagy, we triggered ER stress with tunicamycin instead. To identify apoptotic cells, we stained MCF7 cells with annexin V and analyzed them via flow cytometry. We transfected the cells using a vector tagged with eGFP and analyzed only eGFP positive cells to study only transfected cells. Our results demonstrated cells overexpressing Rab32T9N were significantly more prone to undergo apoptosis compared to cells overexpressing Rab32Q85L (Figure 3.12A). In brief, our results suggest Rab32 activation delays ER stress-dependent apoptosis in breast cancer cells.

3.3.7 RTN3L and Rab32 act synergistically to worsen breast cancer patient outcomes

Next, we decided to investigate if Q85L-dependent apoptosis delay is relevant in breast cancer given Rab32 is upregulated in almost 25% of breast cancers [376,377]. To do this, we generated a gene expression microarray dataset from a human breast cancer cohort of primary tumor samples as previously described [356]. This analysis revealed high mRNA levels of either Rab32 or RTN3 in breast tumor tissues are significantly associated with poor patient prognosis with hazard ratios of 2.32 ($p=0.01$) and 2.43 ($p=0.003$), respectively (Figure 3.12B). Consistent with a potential synergetic role of Rab32 and RTN3, there was an acceleration of the disease when high levels of Rab32 coincided with high levels of RTN3 (Figure 3.12B, right). Under this condition, the difference between Rab32/RTN3 double high and double low levels was further magnified (HR=3.82, $p=0.001$). Therefore, MAMphagy mediated by Rab32 and RNT3L could delay apoptosis in breast cancer cells, a phenomenon that may compromise the survival of these patients.

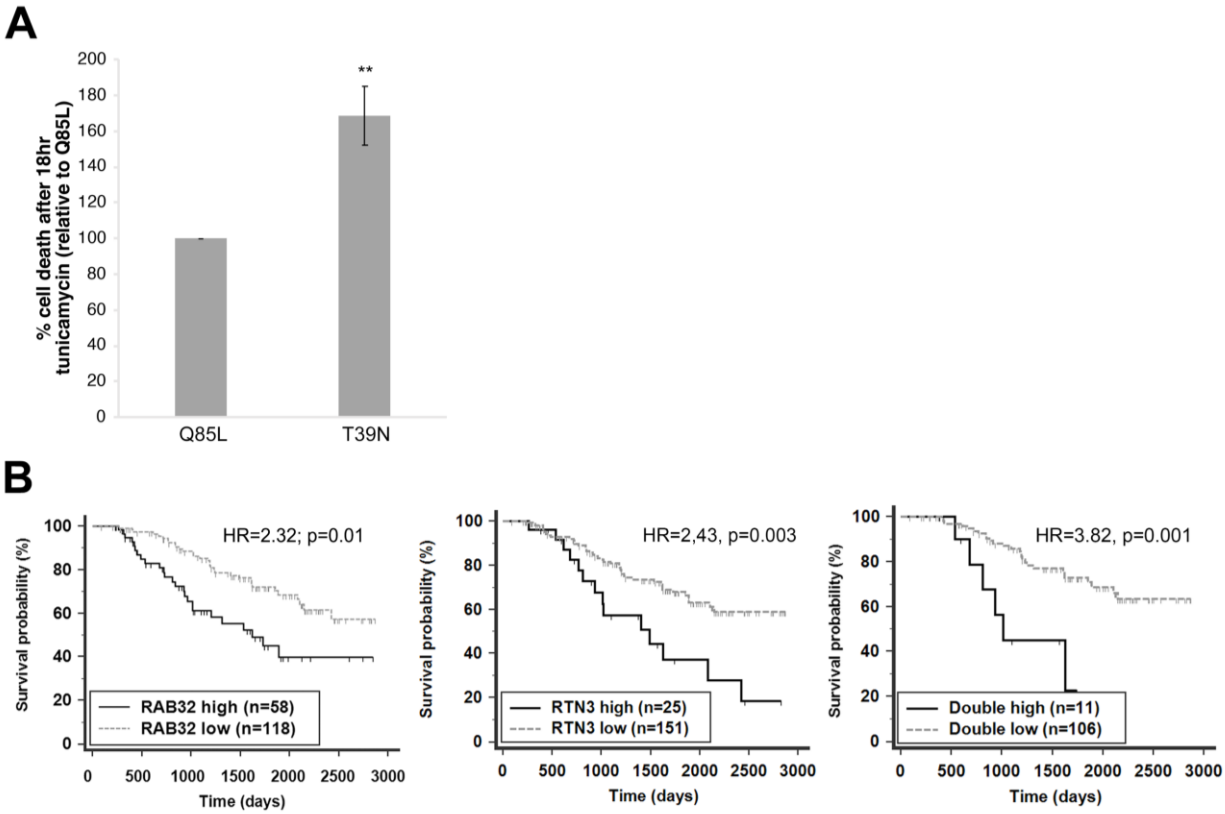

Figure 3.12 Rab32 delays apoptosis and acts as a negative prognostic marker in breast cancer patients

A. Percent of apoptotic cells was analyzed by flow cytometry via annexin V staining. MCF7 cells were transfected with eGFP tagged plasmids and only eGFP positive cells were analyzed to remove effects of untransfected cells. Cells were treated with 2 μM of Tunicamycin for 16 h before staining. n=3. **p≤0.01. Experiment and data analysis performed by Megan Yap. **B.** Kaplan-Meier patient survival curves generated based on mRNA levels of *RAB32* (high vs low; left panel), *RTN3* (high vs low; middle panel) or *RAB32/RTN3* combined (double high vs double low; right panel) in patient tumor tissues. n denotes sample size; HR, hazard ratio; p, probability value of statistical significance. Analysis performed by Dr. Rongzong Liu.

3.4 Discussion

3.4.1 Model for Rab32- and RTN3L- induced MAMphagy

The origin of the autophagosomal membrane has been a highly researched topic in the field of autophagy. As previously mentioned, the Golgi, ER, mitochondria, MAM, and plasma membrane have all been reported as sources for the isolation membrane [203,212,226–228]. However, a consensus has largely emerged that bulk autophagy, particularly due to amino acid starvation, derives from the omegasome in the ER [201]. Other organelles could then act as a platform for the isolation membrane with other types of stimuli. This model could also explain how so many organelles can undergo selective autophagy. In support of this hypothesis, mitochondria have been observed to contribute their membrane during autophagosome biogenesis in PINK1-Parkin-mediated mitophagy [381]. This study demonstrated mitochondria formed a continuous membrane with an LC3-tagged isolation membrane.

Recent studies have provided evidence for even more specialized autophagy: autophagy of ER subdomains. Indeed, ER tubules are targeted by the autophagy receptors RTN3L [200] and Atlastin 3 [367], ER sheets by FAM134B [370], and peripheral ER by CCPG1 [366]. Most of these studies were performed with starvation or ER stress as autophagy triggers, so more research is required to fully tease apart these different types of selective autophagy. Further complicating our ability to discern these pathways apart, evidence suggests multiple ERphagy receptors can be activated by the same stimuli. They also appear to participate in different stages of stress progression and recovery. For example, CCPG1 acts to remove insoluble proteins during ER stress [366] while Sec62 acts after ER stress has been resolved in order to remove excess chaperones [374]. Other ERphagy receptors could also be activated by the same stimuli but act at different timepoints, though this has not been tested.

Our results support this model for ER subdomain selective autophagy by demonstrating overexpression of active Rab32 promotes autophagic degradation of the MAM subdomain. Interestingly, the susceptibility of MAM proteins to Rab32-mediated MAMphagy varied. In particular, Calnexin was not subject to this degradation (Figure 3.4C,D) although it was enriched in our MAM fraction (Figure 3.8B). A possible explanation for this effect could be that Rab32Q85L is known to move Calnexin away from the MAM towards the peripheral ER [290], which would remove it from the degradative area. Another protein that is highly associated with MAMs

is TMX1, which consistently showed autophagic degradation. A potential explanation for this difference could be their distinct MAM targeting, since TMX1 is associated with detergent-resistant membranes while Calnexin is not [267]. The difference could therefore be based on their localization to detergent-resistant, lipid raft-like domains, which have been observed at the MAM [209,307]. Lipid rafts are lipid-rich regions that act as microdomains to facilitate lipid-protein and protein-protein interactions [18]. For instance, Syntaxin-17 moves from a raft-like MAM domain to a non-raft like domain when starvation triggers autophagy [307]. This movement allows Syntaxin-17 to recruit the PI3K III complex to the isolation membrane at the MAM [203]. Calnexin could therefore behave similarly and also move in and out of these domains in an autophagy-dependent manner. Potentially, this explanation could also explain why Calnexin associates with core autophagy initiators such as AMBRA1 and WIPI1 [209]. These and other autophagy initiating proteins are removed from the isolation membrane before closure of the autophagosome and are therefore not degraded [382]. Thus, it would make sense for Calnexin to also be spared from degradation in MAMphagy.

Interestingly, Calnexin is also involved in selective autophagy of the ER and mitochondria. A recent study demonstrated Calnexin acts as an autophagy co-receptor, binding both misfolded proteins and FAM134B during FAM134B-mediated ERphagy [383]. Unlike Rab32-mediated MAMphagy however, Calnexin was degraded in this type of ERphagy. This finding is further evidence that FAM134B and Calnexin are not directly involved in the selective degradation of the MAM described here. Calnexin also binds the mitophagy receptor FUNDC1, which accumulates at the MAM during hypoxia via Calnexin binding [379]. This binding decreases as mitophagy proceeds, sparing Calnexin from degradation. FUNDC1 then binds Drp1 to promote mitochondrial fission, a process required for mitophagy to proceed. Thus, these studies are consistent with our model of MAMphagy where Calnexin is not degraded although other MAM proteins are. Importantly, RTN3L-mediated ERphagy described by Grumati *et al.* (2017) triggered Calnexin degradation, which we repeatedly did not observe with Rab32Q85L overexpression (Figures 3.4D; 3.5B, 3.6A). Similarly, RTN3L ERphagy identified by Grumati *et al.* (2017) degraded Reticulon-4, which instead accumulated during Rab32Q85L-mediated degradation (Figure 3.4C,D), possibly as a compensation for the degradation of RTN3. This is further evidence that the process triggered by Rab32Q85L is not the same type of ER tubule-specific autophagy described by Grumati *et al.* (2017).

Nevertheless, an important question remains unanswered: how could RTN3L mediate selective autophagy of both ER tubules and MAMs? Firstly, it should be noted that there is precedent for an autophagy receptor operating in multiple types of autophagy. For example, p62 acts as a receptor for protein aggregates [216], sometimes called aggresomes, as well as mitophagy [384]. This could be due to the fact that p62 binds ubiquitinated cargo, which is involved in both mechanisms of degradation [216,384]. Indeed, p62 was required for the clearance of polyubiquitinated aggresomes [216]. Similarly, PINK1-Parkin mitophagy ubiquitinates OMM proteins to tag them as substrates [363]. These proteins are then bound by mitophagy receptors that bind ubiquitin, including p62 [384].

Autophagy receptors like p62 must have two properties to be considered canonical receptors: i) they must have a LIR motif to bind LC3 and ii) they must also directly bind cargo [201]. Another important characteristic of receptors is their ability to oligomerize, which creates cargo-rich areas to facilitate autophagy. Although RTN3L has several LIR motifs, it does not bind cargo, making it a non-canonical receptor [200]. Instead, RTN3L could act by omitting the cargo binding step and oligomerizing within ER tubules directly. This mechanism could be regulated within ER tubules, where RTN3 is exclusively found [385], by maintaining a balance between RTN3L and RTN3S, since only RTN3L has a LIR motif and heterodimers did not trigger ERphagy [200]. Thus, both isoforms could be present without triggering autophagy, but RTN3L accumulation, via transcription, degradation, enrichment, or other changes, would induce ERphagy. This process of RTN3L enrichment at tubules to trigger selective autophagy could also happen during MAMphagy, since ER tubules can establish MERCs [188]. In fact, MAMs are thought to be formed mostly by ER tubules rather than sheets [386]. ER tubulation at MAMs also helps constrict mitochondria to promote mitochondrial fission [196], a process that must precede mitophagy [387]. This model could also explain why there was little to no RTN3L on the MAM fraction under basal conditions (Figure 3.8B). Namely, since RTN3L accumulation at the MAM would trigger MAMphagy, RTN3L would likely only be recruited there when MAMphagy is triggered, such as with Rab32Q85L overexpression. In this model, the mechanistic switch between degradation of ER tubules as described by Grumati *et al.* (2017), or MAMphagy, would be *where* RTN3L accumulates. These observations could all come together to establish a model where the cell could prime for Rab32-mediated MAMphagy by triggering mitochondrial fission first, which would presumably be needed for the degradation of MAMs

similarly to mitophagy [387]. This model is also consistent with previous studies demonstrating Rab32T39N promotes PKA-mediated inhibition of Drp1 at mitochondria [290]. Given Rab32Q85L did not increase mitochondrial localization of PKA, Drp1 would not be inhibited with activation of Rab32, and would thus be able to promote fission preceding MAMphagy. Similarly, both RTN3S and RTN3L at the MAM could act to promote ER tubulation required for mitochondrial fission. After this step, RTN3L could accumulate, oligomerize, and promote MAMphagy via its interaction with Rab32Q85L.

A question that arises from this model is: how or why would RTN3L accumulate if it cannot recognize or bind cargo? It seems more likely that chaperones, which constantly monitor the ER for unfolded or accumulated proteins, would act as sensors for ERphagy. As previously mentioned, Calnexin binds FAM134B when also bound to unfolded proteins, thus acting as a co-receptor for FAM134B-mediated ERphagy [383]. It is possible Calnexin acts as a co-receptor for RTN3L as well. This hypothesis could be tested by performing a co-immunoprecipitation for Calnexin with HA-RTN3L. We could also test this hypothesis by analyzing degradation of MAM proteins with Rab32Q85L in the absence of Calnexin. If Calnexin indeed acts as a co-receptor, then loss of Calnexin in the presence of Rab32Q85L should prevent degradation of TMX1, VDAC1 and other MAM substrates we identified (Figure 3.5A)

3.4.2 How could MAMphagy worsen breast cancer patient outcome?

In the context of breast cancer, MAMphagy could play a role in decreasing patient survival if combined high levels of Rab32 and RTN3 are found within patient tissue. This suggests that Rab32 activation contributes to a worse patient survival, though it is still unclear how. One possibility is that MAMphagy alters the balance of Bcl-2 family proteins towards an anti-apoptotic state, which can favor the development of chemotherapy-resistant tumorigenic cells [388,389]. This could explain why Rab32Q85L cells had lower apoptosis rates compared to Rab32T39N (Figure 3.12A). However, Rab32Q85L led to the degradation of two anti-apoptotic proteins: Bcl-2 and Mcl-1, and two pro-apoptotic proteins: Bim_{EL} and Puma (Figure 3.11B), which could result in no overall change in pro- and anti-apoptotic proteins. Thus, it is hard to determine, without additional experiments, if the degradation of Bcl-2 proteins is responsible for the changes in apoptosis observed here.

Additionally, while our results show Rab32Q85L slows ER stress-mediated apoptosis from incubation with tunicamycin (Figure 3.12A), our lab has previously shown Rab32Q85L accelerates staurosporine and TNF-related apoptosis inducing ligand (TRAIL)-mediated apoptosis [290]. This difference could simply be due to the nature of stress triggering apoptosis or the cell line used. Nevertheless, our latest data suggests ER stress coupled with Rab32Q85L could worsen breast cancer patient outcomes. In support of this hypothesis, Rab32 mRNA and protein levels increase with ER stress [390]. This could explain why patients with high Rab32 levels have a worse prognosis. To test if this is at least in part due to MAMphagy, we could silence RTN3L, which should eliminate this tunicamycin-induced apoptosis delay with Rab32Q85L.

Another potential explanation could be that the Rab32/RTN3L axis would improve bioenergetics in advanced tumor tissue. This could occur in several ways. One mechanism would rely on MAMphagy acting simply as an energy generating pathway, much like bulk autophagy does during starvation. Another plausible mechanism would involve MAMphagy specifically degrading certain portions of the MAM to beneficially modulate ER-mitochondria Ca^{2+} flux and mitochondrial ATP production. This scenario seems at first unlikely since Rab32Q85L-expressing cells actually had a significantly lower MAM coefficient as assayed by electron microscopy (Figure 3.7B), suggesting OXPHOS would decrease. However, MAMphagy likely targets certain MAM domains but not others given that it did not significantly degrade Calnexin or Mitofusin-2 (Figure 3.4D, 3.5A). This could be beneficial to the tumor if it degraded certain domains to provide energy as a catabolic pathway but also spared domains to maintain Ca^{2+} flux and therefore mitochondrial ATP production. On the other hand, if MAMphagy is indiscriminate, degradation would result in lower ER-mitochondria Ca^{2+} flux and therefore, lower mitochondrial metabolism. Overall, this could help shift the cell towards glycolysis. In support of a model where MAMphagy provides energy to tumors, a recent study in leukemia cells demonstrated lipophagy, the selective degradation of lipid droplets (LDs), releases free fatty acids stored in LDs, which are then used by mitochondria for OXPHOS [391]. This pathway increased proliferation of leukemia cells but did not operate in normal hematopoietic cells. These results suggest selective autophagy can provide substrates for the TCA cycle, promote OXPHOS, and therefore provide energy for tumor cells. Thus, MAMphagy could act in a similar way in breast cancer.

3.4.3 When is MAMphagy activated?

Another unanswered question is what conditions or stressors turn on MAMphagy. A co-immunoprecipitation of RTN3L with FLAG-WT under different conditions could help answer this question. Given Rab32WT can bind either GTP or GDP, unlike Q85L or T39N, a condition that triggers MAMphagy should promote Rab32WT to bind GTP and thus behave like Rab32Q85L. Consequently, this condition would increase RTN3L co-immunoprecipitation compared to untreated Rab32WT. Interestingly, a recent study found bulk autophagy is impaired when MAM tethers are manipulated, but only with certain stimulus [232]. Specifically, silencing the MAM tethers VAPB or PTIPIP51 promoted this process, while their overexpression impaired rapamycin-mediated autophagy but not starvation-induced autophagy. Given Mitofusin-2 and PACS-2 KOs have impaired starvation-induced bulk autophagy [203], as well as impaired MAMphagy (Figure 3.7 E,F), this data suggests different MAM tethers participate in distinct types of autophagy triggered by different stimuli.

Bulk autophagy induced by VAPB/PTPIP51 overexpression was dependent on Ca^{2+} flux at the MAM, since MCU KD or inhibition of IP_3Rs eliminated the effect [232]. Multiple other studies support this idea that IP_3R-mediated Ca^{2+} flux disruption triggers autophagy. One study had opposite results, however, demonstrating starvation-induced autophagy required IP_3R Ca^{2+} release [392]. Additionally, a recent study demonstrated Mitofusin-2 was required for bulk autophagy triggered by mitochondrial inhibitors [393]. Thus, it seems likely that the type of autophagy induced, and the machinery it requires, is highly dependent on the type of stimulus and MAM tether involved. Therefore, a wide array of conditions and stressors should be tested to identify a physiological trigger for MAMphagy. In addition to starvation-induced autophagy, this could include ER stressors like tunicamycin, Ca^{2+} chelation or depletion, and mitochondrial inhibitors.

Chapter 4: Ypt7 regulates mitochondrial metabolism and ER-mitochondria contact sites

4.1 Abstract

The Rab family of small GTPases is a conserved group of proteins that regulate intracellular traffic. Humans have up to 70 members while the model organism *Saccharomyces cerevisiae* has only 11 members. Amongst these 70 members, Rab32 is the only Rab protein known to localize to mitochondria. Our lab has shown Rab32 participates in several important processes here, including mitochondrial fission and selective autophagic degradation of the mitochondria-associated membrane (MAM), a membrane contact site (MCS) of the endoplasmic reticulum (ER) and mitochondria. This latter process, which we have called MAMphagy, causes a significant decrease in ER-mitochondria contact sites. Therefore, Rab32 is an important determinant of the extent of ER-mitochondria tethering in cells. However, no Rab32 homolog has been identified in yeast. To investigate if such a homolog exists, and if it also regulates MAM tethering and function, we performed a simple phylogenetic analysis based on protein-protein basic local alignment search tool (BLAST) queries to identify reciprocal best BLAST hits (RBH). This methodology revealed Ypt7 shares roughly 37% identity with Rab32. Additional analysis of conserved Rab subfamily residues suggests Ypt7 is the closest Rab32 ortholog in yeast. We also demonstrate Ypt7 can significantly alter MAM tethering, suggesting Ypt7 could be functionally homologous to Rab32. Additionally, we investigated the effects of these Ypt7-dependent changes in MAM tethering by assaying for growth on non-fermentable acetate, where yeast metabolism shifts entirely to mitochondrial respiration. Our results demonstrate Ypt7 mutants have growth defects under these conditions, suggesting Ypt7-mediated changes in MAM tethering can lead to changes in mitochondrial respiration. Lastly, we also show growth on non-fermentable acetate is facilitated by Ire1, since its inhibition caused growth defects in all strains tested. These results suggest Ire1 can promote mitochondrial respiration and are in line with reports that respiration can help resolve ER stress in *S. cerevisiae.* In brief, our results suggest Ypt7 is the closest homolog of Rab32 and also regulates MAM tethering, which likely explains why Ypt7 negatively affects growth based on mitochondrial respiration.

4.2 Background

4.2.1 The Ypt/Rab family

Saccharomyces cerevisiae has been used as a model organism to understand basic cell biology for several reasons, including the fact that it can be grown and maintained easily and inexpensively. *S. cerevisiae* also have a small proteome and are easier to manipulate genetically compared to mammalian cells. The wide availability of whole genome libraries of deletions and mutations also makes yeast an ideal model. Their short replication time, roughly between 60-90 minutes [394], is also amenable. Although humans and yeast have obvious differences in their metabolism, cell organization, and several other aspects, there is good evolutionary conservation between them [319]. This has led to the identification of hundreds of orthologs: gene products from different organisms with similar functions due to shared evolutionary ancestry [319]. One field that has greatly benefitted from studies done in *S. cerevisiae* is that of intracellular traffic. For example, the first Ypt/Rab protein was described in the late 80's as Ypt1 in *S. cerevisiae* [395]. This led to the quick identification of Rab1 in mammals [299]. The use of *S. cerevisiae* as a model for protein traffic research has led to the identification of 10 other Ypt proteins as well as their regulators and effectors, many of which are conserved in humans [336]. These and later studies have informed our current model of Ypt/Rab proteins as master regulators of cellular traffic [336].

Ypts/Rabs GTPases have highly specific membrane residency and therefore contribute to intracellular membrane identity [218,291]. Ypt/Rabs interact with a variety of effectors that promote different traffic steps, including motor proteins, sorting adaptors, and tethering factors [218,291]. Most Ypt/Rab proteins interact with effectors in their active, GTP-bound state [293]. Their traffic between membranes is in part regulated by the exchange of GTP and GDP, also known as the GTP cycle [292,293]. Two types of membrane proteins regulate their GTP/GDP binding state: GEFs, which catalyze the release of GDP and induce GTP binding due to the high GTP/GDP ratio in cells, and GAPs, which promote GTP hydrolysis [294,295]. GAPs and GDP-bound Ypts/Rabs are removed from acceptor membranes by GDIs following GTP hydrolysis [297–299]. Lastly, GDFs help Ypts/Rabs to maintain high membrane specificity since they recognize specific Rab-GDI complexes and displace GDI, allowing the Ypt/Rab protein to associate with its specific donor membrane once more [218,297,299].

Ypt effectors, as well as GEFs and GAPs, are also well conserved between humans and yeast [315]. However, the Rab family is much larger, with up to 70 members in humans, while the Ypt family in *S. cerevisiae* only has 11 members [314,318]. In order to investigate if Rab32 has a functional ortholog in *S. cerevisiae*, and whether this ortholog also regulates the MAM, we turned to comparative genomics and decided to use the reciprocal best BLAST hit (RBH) method [396]. This method defines RBHs as genes from two species that are each other's best match in reciprocal BLAST searches [396]. We chose this method since it has been successfully used to study Ypt/Rab proteins in the past [284,318]. Additionally, this method has a relatively high specificity and can be performed easily and quickly compared to other methods used to study orthologs [397]. Thus, we used the *Homo sapiens* Rab32 sequence as query in the *S. cerevisiae* genome, which revealed Ypt7 as the best match with 36.8% identity (Figure 4.1A). The results of the reciprocal BLAST using Ypt7 as a query will be discussed in the results portion of this chapter.

4.2.2 Ypt7 in endolysosomal traffic

Ypt7 was first described in an attempt to uncover the function of mammalian Rab7 by using *S. cerevisiae* [343]. This study found Rab7 and Ypt7 have 63% identity and identical effector-binding sequences. This and additional studies in yeast in the early 90's revealed Ypt7/Rab7 is a multi-functional protein involved in endolysosomal traffic and autophagy due to its ability to promote membrane fusion events [343,344,398]. Ypt7 localizes mostly to late endosomes and is commonly used as a marker for this organelle [343,344]. Here, Ypt7 can promote several types of fusion events, including homotypic fusion of late endosomes and vacuoles as well autophagosome-vacuole and late endosome-vacuole fusion [343,344,399]. Ypt7 mediates these events in concert with its effector, the homotypic vacuolar fusion and protein sorting (HOPS) complex, which localizes to late endosomes and vacuoles [400]. Together, Ypt7-HOPS establish membrane tethering that precedes SNARE-mediated fusion of vesicles [398,401].

Ypt7 is also required for the maturation of early endosomes into late endosomes [330]. Early endosomes are characterized by the presence of Vps21/Ypt5 while late endosomes specifically contain Ypt7 [321,343]. At their respective membranes, Vps21 and Ypt7 bind tethering complexes to tether the membranes of vesicles and prepare them for fusion [402,403]. In the case of Ypt7, this is the HOPS complex, while Vps21 in early endosomes binds the tethering complex class C core

vacuole/endosome tethering (CORVET) [403,404]. Early to late endosome maturation requires the exchange of Vps21 with Ypt7, which is promoted by the Ypt7 GEF Mon1-Cz1 found on late endosomes [330].

The Mon1-Ccz1 complex is conserved in mammals as biogenesis of lysosome-related organelles complex 3 (BLOC-3), a melanosomal Rab32 GEF [330,405]. GEFs promote GDP to GTP exchange by displacing Mg^{2+}, a Ypt/Rab cofactor which usually hides their GTPase active site [406]. Recent research has shown Mon1-Ccz1 activity requires interaction with a lysine (K) at position 38 (K38) in Ypt7 [405]. This positively charged lysine is thought to insert into Mon1-Ccz1's nucleotide-binding pocket, displacing Mg^{2+} and allowing GDP release. This residue is well conserved in the Rab7 subfamily but variable in other Rabs. Interestingly, Rab32 has an arginine (R) in its equivalent position when aligned with Rab7: R55 (Figure 4.1D). This positively charged amino acid could also promote displacement of the Mg^{2+} cofactor, suggesting both Ypt7 and Rab32 have a conserved residue that is used to insert into the nucleotide-binding pocket of this GEF. In turn, this suggests these proteins share a certain degree of homology.

Δ*ypt7* cells have vacuole fusion defects and exhibit vacuolar fragmentation [343,344]. They also have defects in sorting of membrane-bound vacuolar proteins dependent on AP-3, which Ypt7 also regulates [407]. Rab32 performs a very similar function in melanogenic cells since it also mediates AP-3 traffic and its loss results in defects in delivery of membrane-bound Tyrosinase to the melanosome [300,301,343]. On late endosomes, Ypt7 can also interact with the retromer complex, which mediates retrograde traffic [399]. An example of this type of transport is a process called endosome recycling, whereby endosomes originating at the plasma membrane are processed to return content to the plasma membrane [329]. During endosome recycling, retromer assembly on the endosomal membrane eventually releases Ypt7, allowing it to instead participate in fusion by interacting with the vacuole-localized HOPS complex. Thus, Ypt7 is able to mediate both endosome fusion and recycling. Additionally, Ypt7 is required for autophagosome-vacuole fusion via the HOPS complex [399]. Hence, *Δypt7* cells also have autophagosome accumulation defects [346]. More recent research has found Ypt7 is present in a mitochondria-vacuole tethering complex which has been implicated in mitochondrial metabolism, potentially expanding the list of Ypt7 functions [347,348].

4.2.3 Ypt7 participates in vacuole-mitochondria contact tethering

Recent studies have shown Ypt7 also localizes to mitochondria-vacuole MCS as demonstrated by fluorescence microscopy colocalization with a mitochondrial marker [347]. These MCS are maintained by the vacuole and mitochondria patch (vCLAMP), which is composed of the mitochondrial proteins Mcp1 and Tom40 and the vacuolar proteins Vps13, Vps39, and Ypt7 [347,408]. vCLAMP was first described in a genetic screen for synthetic lethality of ERMES mutants, suggesting vCLAMP could compensate for ERMES [348]. Although three of the four ERMES subunits bear lipid-binding motifs, their deletion causes only a minor decrease in mitochondrial phospholipid content [35]. However, concomitant loss of vCLAMP subunits results in mitochondria with significantly lower phospholipid levels and eventual cell death [347,348]. ERMES loss also results in small growth defects [36,409] which can be rescued by overexpressing vCLAMP component Vps39 [347]. Together, these observations suggest vCLAMP can compensate for phospholipid transfer defects in ERMES mutants [348]. Recent evidence has shown vCLAMP component Vps13 can bind and transport phospholipids between liposomes *in vitro*, supporting this hypothesis [410]. Thus, vCLAMPs could compensate for lipid transfer by acting as a bypass route in ERMES mutants [39]. This is thought to occur via the nucleus-vacuole junction (NVJ), so that lipids synthesized in the ER would be transferred to the vacuole at the NVJ and then transferred to mitochondria at vCLAMPs [39,347]. This model has not been tested, however.

Both ERMES and vCLAMP formation appear to be dynamically regulated. Specifically, deletion of vCLAMP components massively upregulates ERMES as determined by fluorescence and electron microscopy [347,348]. Similarly, deletion of ERMES subunits significantly increases vCLAMPs. vCLAMP and ERMES formation are also influenced by the carbon source available to yeast. Yeast preferentially perform glycolysis in the presence of fermentable carbons such as glucose, though they can also survive on non-fermentable carbons like acetate [113]. *S. cerevisiae* can use acetate in two main pathways: the TCA cycle or the glyoxylate cycle. In the former, acetate is converted into acetyl coenzyme A (acetyl-CoA) via the action of acetyl-CoA synthase. Acetyl-CoA can then be oxidized in the mitochondrial matrix via the TCA cycle and therefore fuels OXPHOS. Acetate can also be used in the glyoxylate cycle, an anabolic pathway that produces TCA cycle intermediates, including succinate, malate, and oxaloacetate. This pathway therefore exclusively supports catabolism through OXPHOS. Thus, yeast can only catabolize this non-fermentable carbon through OXPHOS, allowing researchers to use acetate and similar non-

fermentable carbons to assay exclusively for respiration. Interestingly, yeast grown in non-fermentable carbon have significantly more ERMES complexes compared to yeast grown in glucose [347]. These cells also had a concomitant decrease in vCLAMPs. On the contrary, yeast grown on glucose had significantly more vCLAMPs and fewer ERMES complexes. Together, these results suggest yeast forced to rely on mitochondrial respiration have more ER-mitochondria contacts and fewer vacuole-mitochondria contacts.

Mammalian lysosome-mitochondrial contacts have also been recently described using electron microscopy [349]. Interestingly, these MCS contain Rab7. This research has also shown dominant active Rab7 increases mitochondria-lysosome contacts. Recruitment of the Rab7 GAP TBC1 domain family member 15 (TBCD151) to mitochondria instead decreased these contact sites. Thus, Rab7 activation appears to decrease mitochondria-lysosome contacts, which suggests activation of Ypt7 could decrease vCLAMP formation. Given a decrease in vCLAMPs was previously shown to increase ERMES [347,348], this also suggests Ypt7 activation could promote ER-mitochondria tethering.

4.2.4 Are ERMES and mitochondrial metabolism in yeast regulated by ER stress?

ER stress is a well-known inducer of MAMs in the mammalian system, since starvation, tunicamycin, and other ER stressors have repeatedly been shown to increase the number of MERCs as assayed by fluorescence and electron microscopy [15,185,411]. This increase in ER-mitochondria contact sites promotes ER Ca^{2+} release coupled with mitochondrial Ca^{2+} uptake, which in turn promotes OXPHOS and ATP synthesis to improve cell survival [185,411]. Whether ER stress also modulates ER-mitochondria contact site formation and MAM functions in yeast is poorly understood. Nevertheless, yeast also: i) increase cytosolic Ca^{2+} in response to ER stress [97] ii) alter mitochondrial metabolism and begin programmed cell death (PCD) in response to Ca^{2+} flux [133,135,138] iii) require Ca^{2+} for transcription changes in an Ire1-dependent and -independent manner during prolonged ER stress as part of the Ca^{2+} cell survival (CCS) pathway [97] iv) increase mitochondrial respiration to resolve ER stress [138,184], and v) require adequate ER Ca^{2+} levels to resolve ER stress, since cells without the ER Ca^{2+} pump Spf1/Cod1 have severe protein folding defects [102,138]. This suggests *S. cerevisiae* also have Ca^{2+}-induced changes in mitochondrial metabolism, mitochondrial PCD, and ER stress resolution. Taken together, this

evidence suggests yeast also coordinate ER stress, Ca^{2+} flux, respiration, and PCD in an integrated response that resembles the mammalian MAM system.

Taking all this information together, changes in vCLAMP tethering via Ypt7 activation state could alter ERMES content and in turn influence mitochondrial metabolism. Therefore, we hypothesize Ypt7 inactivation can increase the number of mitochondria-vacuole contact sites and also decrease ER-mitochondria contact sites. We also hypothesize Ypt7 inactivation can promote mitochondrial respiration as a consequence of these changes. To investigate if ER stress can also induce ER-mitochondria contact sites and mitochondrial metabolism in yeast, we also used an Ire1 inhibitor and hypothesized this would reduce the amount of ER-mitochondria contacts.

4.3 Results

4.3.1 Ypt7 as a potential Rab32 *S. cerevisiae* functional homolog

To perform a RBH analysis we used the human Rab32 sequence as a query in a protein-protein BLAST search in the *S. cerevisiae* genome. The best match obtained was Ypt7, which had an amino acid identity of 36.8% (Figure 4.1A). A threshold of 30% identity is usually applied to these analyses [396], so Ypt32 at 36.3%, Ypt1 at 35.3%, Ypt31 at 34.5%, and Ypt6 at 33.8%, are also closely related to Rab32 (Figure 4.1A). Additionally, 3 of the 4 members of the Ypt5-like subfamily also shared identity percentages above 30%, suggesting this family could also be in part functionally homologous to Rab32 (Figure 4.1A). Next, we used the sequence of the best match, Ypt7, as query in a protein-protein BLAST of the human genome. As seen in Figure 4.1B, the best scoring match was Rab7 with 61.3% identity, as previously published [344]. The second-best match was Rab9 at 52% identity, while Rab32 was the 14th best match, with 35.1% identity (Figure 4.1B). Taken together, these results suggest Rab32 is best represented by Ypt7 in *S. cerevisiae,* although Ypt7 is best represented in the human genome by several Rabs other than Rab32. To gain a better understanding of the relationship between Rab32 and Ypt7 we also performed a sequence alignment and BLAST search for Rab32's active site, defined as the region that interacts with GTP/GDP [412]. This site contains the ultra-conserved FALK sequence within the Rab32 subfamily, which is also composed of members Rab38 and Rab29 [413]. This alignment showed good conservation, with the FALK motif altered to FLTK in both Ypt7 and Rab7 (Figure 4.1D). This BLAST search also found Ypt7 as a close hit, though Ypt1, Ypt32, and Ypt6 were more closely related (Figure 4.1C). Taken together, these results suggest Ypt7 is the

most closely related Ypt protein to Rab32. To understand if this extends to functional homology, we next investigated whether Ypt7, like Rab32, could influence ER-mitochondria contact sites.

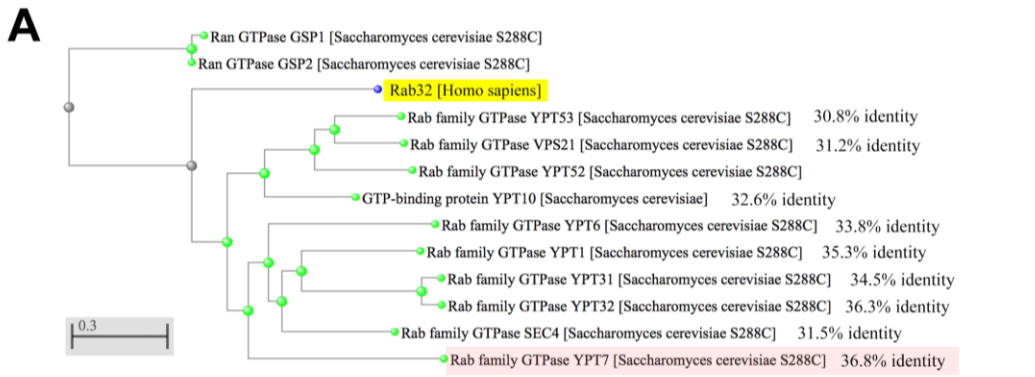

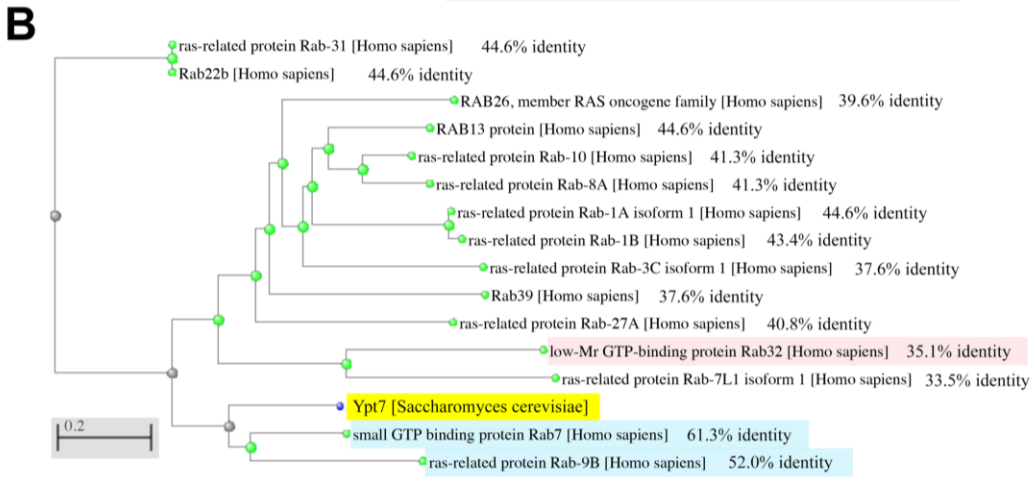

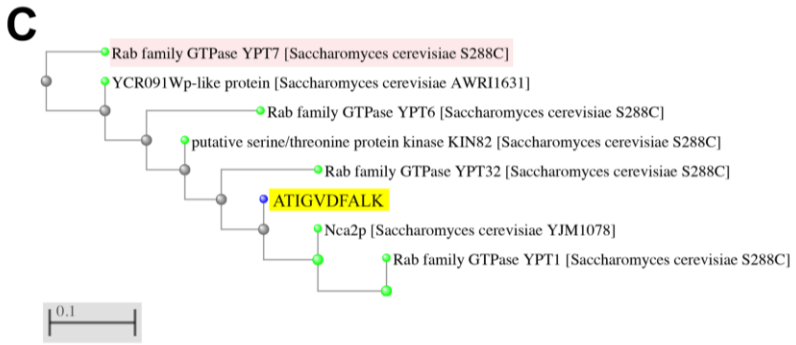

D

```
Rab32     22   REHLFKVLVIGELGVGKTSIIKRYVHQLFSQHYRATIGVDFALKVLNWDSRTLVRLQLWD  81
Ypt7       5   KKNILKVIILGDSGVGKTSLMHRYVNDKYSQQYKATIGADFLTKEVTVDGDKVATMQVWD  64
Rab7       5   KKVLLKVIILGDSGVGKTSLMNQYVNKKFSNQYKATIGADFLTKEVMVDDR-LVTMQIWD  63

Rab32     82   IAGQERFGNMTRVYYKEAVGAFVVFDISRSSTFEAVLKWKSDLDSKVHLPNGSPIPAVLL  141
Ypt7      65   TAGQERFQSLGVAFYRGADCCVLVYDVTNASSFENIKSWRDEFLVHANVNSPETFPFVIL  124
Rab7      64   TAGQERFQSLGVAFYRGADCCVLVFDVTAPNTFKTLDSWRDEFLIQASPRDPENFPFVVL  123

Rab32    142   ANKCDQNKDSS-QSPSQVDQFCKEHGFAGWFETSAKDNINI----EEAARFLVEKILVNH  196
Ypt7     125   GNKIDAEESKKIVSEKSAQELAKSLGDIPLFLTSAKNAINVDSAFEEIARSALQQNQADT  184
Rab7     124   GNKIDLENRQVATKRAQA--WCYSKNNIPYFETSAKEAINVEQAFQTIARNALKQETEVE  181

Rab32    197   QSFPNEENDVDKIKLDQETLRAENKSQCC  225
Ypt7     185   EAFEDDYNDAINIRLD-----GENNSCSC  208
Rab7     182   ----LYNEFPEPIKLDKND-RAKASAESC  205
```

Figure 4.1 Ypt7 shares homology with Rab32
A. Homology tree generated by a protein-protein BLAST search (NCBI) with *Homo sapiens* Rab32 as query (yellow box) in the *Saccharomyces cerevisiae* genome. The best match, Ypt7, is highlighted in the red box. Percent identities above 30% are also indicated. The *S. cerevisiae* strain of the genomic sequences queried are indicated in square brackets. **B.** Homology tree generated by a protein-protein BLAST search (NCBI) with *Saccharomyces cerevisiae* Ypt7 (yellow box) as query in the *Homo sapiens* genome. The best two matches, Rab7 and Rab9, are highlighted in the blue box. Rab32, the 14th best match, is highlighted in the red box. Percent identities above 30% are also indicated. **C.** Homology tree generated as in A but with the Rab32 active site sequence highlighted in yellow as the query. The sequence was obtained from amino acids 56-65 of Rab32 and is also highlighted in red in panel D. The *S. cerevisiae* strain of the genomic sequences queried are indicated in square brackets. **D.** Sequence alignment for Rab32, Ypt7, and Rab7. The Rab32 effector binding domain is highlighted by the red box and the highly conserved Rab7/Ypt7 residue K38 by the blue box.

4.3.2 Dominant negative Ypt7 mutants have more ER-mitochondria contacts

Next, we performed electron microscopy to quantify ER-mitochondria and vacuole-mitochondria contacts in cells with WT or dominant negative Ypt7, Ypt7T22N. In the mammalian system, Rab7 GAP overexpression decreased mitochondria-lysosomes contact sites [349]. This suggests an increase in inactive Rab7 decreases these contacts. Therefore, we hypothesized Ypt7T22N would have fewer vacuole-mitochondria contacts compared to WT. Moreover, since a decrease in vCLAMPs has been shown to increase ERMES [347,348], we also hypothesized Ypt7T22N would have more ER-mitochondria contact sites. Thus, WT and Ypt7T22N strains were grown overnight in 2% yeast extract peptone dextrose (YPD), processed for electron microscopy, imaged, and quantified. These quantifications revealed Ypt7T22N has significantly more MAM compared to WT cells with almost double the ratio of ER-mitochondria length/distance (Figure 4.2A). Ypt7T22N also had a statistically significant increase in the number of ER-mitochondria contact sites per cell, with over twice as many MERCs compared to WT (Figure 4.2A). We did not observe a statistically significant difference in vacuole-mitochondria contact site length/distance, suggesting these MCS were not altered (Figure 4.2B). In terms of number of vacuole-mitochondria contacts per cell, WT cells had an average of 0.54, suggesting most cells had between 0 and 1 contacts, while Ypt7T22N cells had a statistically significant higher average of 1.07 contacts (Figure 4.2B). In summary, these results show dominant negative Ypt7 increases the number of MERCs as well as their overall length and distance. However, this change was not coupled with a decrease in vacuole-mitochondria contacts as we had hypothesized. Instead, these contact sites increased in Ypt7T22N mutants. Next, we wanted to investigate if this increase in MERCs affected mitochondrial metabolism.

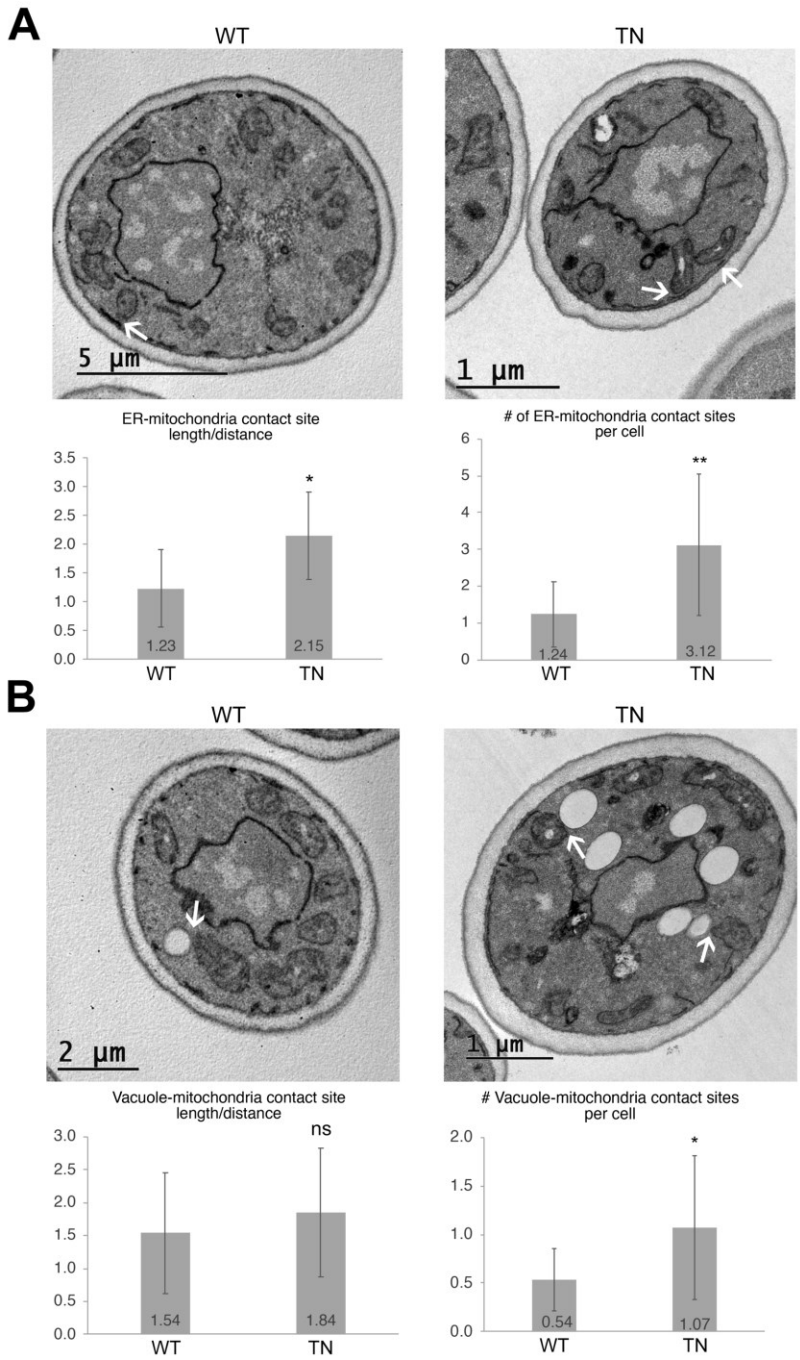

Figure 4.2 Dominant negative Ypt7 mutants have more ER-mitochondria and vacuole-mitochondria contacts.

A. Representative images of electron microscopy for WT and Ypt7T22N cells maintained in 2% YPD. The average distance between a continous stretch of ER and mitochondria membranes between 10-50nm apart was measured and divided by the length along the ER membrane contacting this mitochondrion. These values were graphed to obtain a length/distance ratio or MAM coefficient. White arrows indicate ER-mitochondria contact sites. The number of ER-mitochondria contacts per cell was also counted. Average values for each condition graphed are indicated at the base of each bar. n≥75. *p≤0.05. ** p≤0.01. **B.** Electron microscopy as in A for vacuole-mitochondria contacts, which are indicated by white arrows. n≥50. *p≤0.05. Images obtained by Dr. Nasser Tahbaz.

4.3.3 Dominant active and negative Ypt7 mutants have growth defects in acetate

As previously described, vCLAMPs outnumber ERMES when glucose is present, while growth on a non-fermentable carbon promotes ERMES and decreases vCLAMPs [347]. Given Ypt7T22N had more ER-mitochondria MCS (Figure 4.2A), we hypothesized these cells would have better growth on a non-fermentable carbon. To investigate if Ypt7 influences growth when cells are forced to respire, we assayed for growth of WT and Ypt7 mutants on yeast extract peptone glucose (YPD) or acetate (YPA). To do this, we assayed for growth in liquid media by measuring absorbance in a spectrophotometer after 24hrs of growth from an initial optical density (OD) of 0.2. We simultaneously plated serial dilutions on agar and observed colony growth. Although there were no significant growth differences in YPD (Figure 4.3A), both the dominant active (Ypt7Q68L) and dominant negative (Ypt7T22N) mutants grew significantly worse in YPA (Figure 4.3B). This effect was more moderate in Ypt7Q68L mutants, which had roughly a 20% decrease while Ypt7T22N had almost a 40% decrease (Figure 4.3B). These results were similar on solid media (Figure 4.3B). Interestingly, Δ*ypt7* behaved similarly to WT in both YPD and YPA (Figure 4.3A,B). Together, these results suggest both dominant active and dominant negative Ypt7 have a negative effect on growth when respiration is required, while curiously, the absence of Ypt7 has no effect (Figure 4.3B). This suggests these GTP-binding mutants have impaired respiration. Therefore, we focused on these mutants for the remaining experiments.

4.3.4 Ire1 facilitates growth in acetate, particularly in dominant negative Ypt7 mutants

In mammals, IRE1 acts as a scaffold for IP_3R at MAMs, so that IRE1 loss causes a decrease in ER-mitochondria Ca^{2+} flux and mitochondrial respiration [249]. To test if Ire1 is also required for mitochondrial respiration in yeast we used the Ire1 inhibitor I, STF-083010. This treatment significantly inhibited growth in WT cells to roughly 85% compared to untreated conditions, though the effect was more profound on solid versus liquid media (Figure 4.3C). Ypt7Q68L had a very similar decrease of roughly 85% in liquid media compared to untreated conditions (Figure 4.3C). Lastly, Ypt7T22N had a decrease of almost 50% when STF was added in liquid media while on agar the decrease appeared even larger (Figure 4.3C). Ire1 therefore seems to boost mitochondrial respiration in yeast as well as in mammals, since inhibition of Ire1 decreased growth on acetate in all strains.

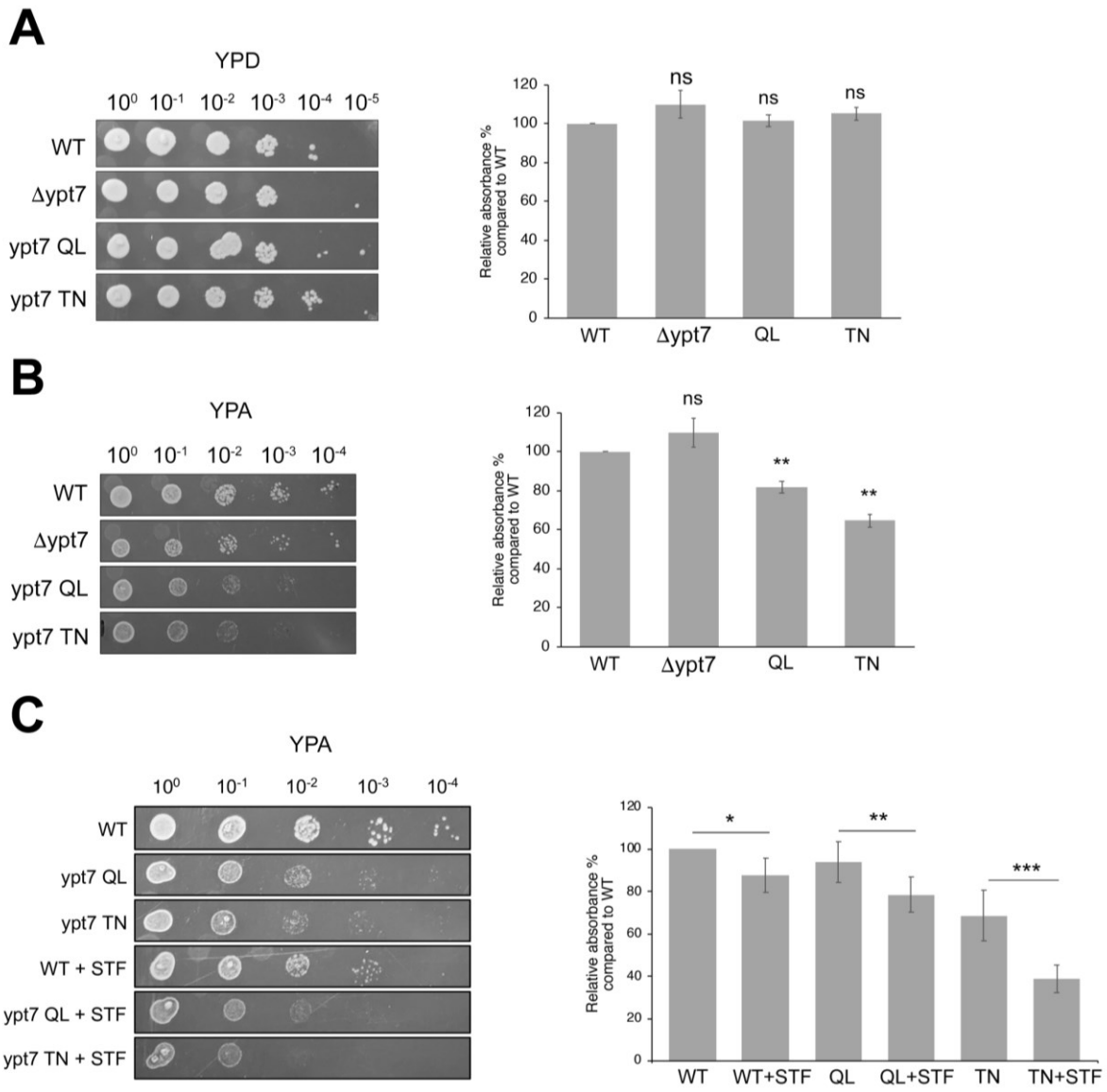

Figure 4.3 Ypt7 dominant active and negative mutants have defective growth on non-fermentable acetate

A. Spot assay in YPD shows Ypt7 mutants have no significant growth defects. Strains were serially diluted from an initial optical density (OD) of 1 and spotted onto 2% YPD plates. Absorbance measurements in YPD after 24hrs of growth were also graphed. Strains were grown at 30°C from an initial OD of 0.2 and absorbance was measured at 24hrs. n=3 independent experiments. ns=not significant. **B.** Spot assay performed in 2% YPA shows Ypt7 mutants have growth defects. Absorbance measurements as in A. n=3. **p≤0.01. **C.** Spot assay as in B with and without 60μM of Ire1 inhibitor STF-083010 shows WT and Ypt7 mutants have decreased growth on acetate with Ire1 inhibition. n=3. *p≤0.05. **p≤0.01. ***p≤0.001.

4.4 Discussion

4.4.1 Is Ypt7 a functional homolog of Rab32?

Although pairwise alignments with BLAST are used often to identify Rabs [414], RBHs and similar genomic methods based on sequence similarity have a number of drawbacks. One of these is that ortholog detection becomes increasingly difficult with gene duplication, deletion, transposition, and similar genetic and evolutionary events [396]. Gene loss and high number of paralogs are common in species that have undergone whole genome duplication events, such as *Saccharomyces cerevisiae*. Additionally, the Rab family in humans has undergone dramatic expansion and lineage-specific diversification, further complicating the identification of homologs [314,315]. Some of these issues are exacerbated when sequence identity falls below 30% [396]. Since our BLAST queries revealed sequence identity between Rab32 and Ypt7 to be above 30% (Figure 4.1), these problems are unlikely to significantly affect our RBH analysis. Nevertheless, other phylogenetic approaches can be used in the future to verify the validity of the homology described here. For example, software such as InParanoid [415] and ScrollSaw [316] has been previously used to identify human orthologs in model organisms and to resolve gene duplications events undergone by the Rab family, respectively.

Although our phylogenetic analysis suggests Ypt7 and Rab32 share some homology, our functional assays are less clear. Our earlier results (Figure 3.6A) demonstrated Rab32Q85L significantly decreased ER-mitochondria contact sites as assayed by electron microscopy. Therefore, in Figure 4.2 we sought to investigate whether Ypt7 could also influence these MCS. Specifically, we decided to perform electron microscopy on the dominant negative Ypt7 mutant since we observed larger effects with this mutant on our growth assays (Figures 4.3B,C). Our results demonstrate Ypt7T22N caused a statistically significant increase in ER-mitochondria contact sites (Figure 4.2A). These results are in line with our hypothesis that Ypt7T22N would have more MAM since i) Rab7 GAP overexpression decreased vacuole-mitochondria contacts and ii) vCLAMP and ERMES are inversely proportional [347–349]. However, we did not observe a concomitant decrease in vCLAMP content and instead observed a significant increase in the number of vCLAMPs per cell (Figure 4.2B). This discrepancy could be explained in light of recent evidence suggesting the type of vCLAMP, rather than the total number of vCLAMPs, is the determining factor in whether or not vCLAMPs can compensate for ERMES defects [408,416].

These studies have found two types of functional vacuole-mitochondria contacts exist in yeast: one containing Vps39, Ypt7, and Tom40, which acts only to tether these membranes, and another containing Vps13 and Mcp1. These studies also showed the latter complex is enough to compensate for growth defects of ERMES mutants in YPD. Interestingly, there were no differences in total or mitochondrial phospholipid content when an ERMES mutant also had a deficient Vps39-Ypt7-Tom40 vCLAMP. Thus, the amount and number of vCLAMPs containing Vps13 was the determining factor for compensation of the growth defects. This suggests comparing the number of vCLAMPs, or their relative abundance compared to MERCs, may not be enough to determine if ERMES function is altered. Moreover, this evidence suggests there are different functional vCLAMP units. Therefore, it will also be important to test if there are changes in these functionally different complexes. This can be done by assaying for Vps13 positive puncta co-localization with mitochondria via immunofluorescence.

Nevertheless, our results demonstrate the activity of both Rab32 and Ypt7 can determine the number and tethering of MERCs. It remains unclear if they do so via similar mechanisms, though. To explore the mechanistic basis for these effects, these MCS could be quantified in an autophagy-deficient genetic background, such as Atg5 KO cells, which cannot form isolation membranes [198]. If MAMphagy is responsible for the decrease in MAMs with Rab32Q85L overexpression, as we hypothesize, then these conditions should prevent the decrease in ER-mitochondria contacts. This should also occur in cells with RTN3L siRNA. Another possibility is that Ypt7 regulates MAM formation through its role as a component of vCLAMP, as we had originally hypothesized. This could be tested by assaying for Vps13-positive vacuole-mitochondria MCS as suggested above. Lastly, although we did not observe a statistically significant difference in vacuole-mitochondria length/distance, there was a significant increase in the number of these MCS with Ypt7T22N (Figure 4.2B). We could therefore test if the changes in MERCs we observed in Figure 4.2B are due to its role in vCLAMP formation with synthetic linkers. Synthetic linkers are constructs which artificially tether two organellar membranes [35]. This method has been employed in yeast in the past, such as the use of the construct helping in mitochondria-ER association (ChiMERA) used to identify ERMES. If Ypt7T22N increases MAMs due to a decrease in vCLAMP, as we hypothesized based on previous Rab7 research [349], then vacuole-mitochondria synthetic linkers should reverse this effect and decrease the number of MERCs.

Interestingly, Ypt7 participates in ERphagy, since rapamycin-induced degradation of Sec63-labelled ER fragments was impaired in Δ*ypt7* mutants [417]. Additionally, Rab7 participates in isolation membrane expansion during mitophagy [418]. This suggests Ypt7 could also be involved in selective degradation of the ER and/or mitochondria. Though this model is highly speculative, if Ypt7 has a similar function to Rab32-mediated MAMphagy, then it is possible Ypt7 activation triggers one or both of these types of selective autophagy.

It will also be important to further test for functional homology in the future. This is commonly done by expressing the mammalian homolog in null strains to rescue defects or reverse phenotypes. These types of experiments are commonly used to establish functional homology for essential *S. cerevisiae* genes [319] and can be performed via Drag&Drop cloning, which uses *in vivo* homologous recombination in *S. cerevisiae* to introduce a mammalian gene of interest in an inducible vector [419]. However, we did not observe significant changes in Δ*ypt7* growth in YPD or YPA (Figure 4.3B), making this experiment unsuitable for such a test. Instead, we could turn to ER-mitochondria contact site quantification, where we observed highly significant increases with Ypt7T22N (Figure 4.2A). We could also assay for growth on acetate with and without Ire1 inhibition, where we observed statistically significant decreases in WT, Ypt7Q68L, and Ypt7T22N (Figure 4.3C). If we still do not observe significant changes for Δ*ypt7* in these experiments, we could assay for vacuolar protein sorting defects in Δ*ypt7* as previously published [407]. Since Rab32 is required for the similar process of melanogenic enzyme sorting [300,301], it is plausible Rab32 could rescue this mutant and therefore establish at least partial functional homology with Ypt7.

4.4.2 Ypt7 regulates ER-mitochondria contact site formation

Our results show Ypt7T22N significantly increases MERCs (Figure 4.2A). These cells were maintained in glucose before imaging, where ERMES have been previously reported to be outnumbered by vCLAMPs [347]. However, we found both WT and Ypt7T22N cells had at least twice as many MERCs as vacuole-mitochondria contact sites when grown in glucose (Figure 4.2B), contradicting this previous report. As detailed above, one possible explanation for this discrepancy is evidence suggesting only Vps13-Mcp1 vCLAMPs, but not Vps39-Ypt7-Tom40 vCLAMPs, can compensate for ERMES growth defects [408,416]. Thus, it is possible Ypt7T22N

specifically increased Vps39-Ypt7-Tom40 vCLAMPs, which cannot compensate for ERMES. Therefore, ERMES are unlikely to decrease in this genetic background.

Another possible explanation for our result is that vCLAMP participates in mitochondrial fission, which would in turn affect the number of MERCs in cells. This potential function of vCLAMP as both a tethering complex and mitochondrial fission machinery is reminiscent of Mitofusin-2, which mediates both ER-mitochondria tethering and mitochondrial fusion at the MAM [16]. Indeed, expression of a dominant negative mutant of Drp1 in mammalian cells induces mitochondrial elongation and a significant increase in MERCs [420]. In support of our hypothesis, a recent study in mammalian cells showed almost 80% of mitochondrial fission events in healthy cells occurred at mitochondria-lysosome MCS [349]. Moreover, 100% of these mitochondria-lysosome fission events also colocalized with the ER, suggesting this process occurs at tripartite, mitochondria-lysosome-ER MCS. Interestingly, fission at these MCS could be induced by recruitment of the Rab7 GAP TBC1D15 to mitochondria via Fis1 binding. [349]. This recruitment also resulted in mitochondria-lysosome untethering. Therefore, Rab7 GTPase activity appears to untether mitochondria-lysosome contacts, likely allowing Drp1-mediated fission to occur at the ER-mitochondria contact site left behind. It is therefore possible YptT22N also promotes mitochondrial fission in a similar manner, which would result in an increase in MERCs required to perform Drp1-mediated fission [196]. This is consistent with our results, which indicate Ypt7T22N significantly enhanced ER-mitochondria contact formation (Figure 4.2A). To begin to investigate if mitochondrial morphology or fission changes occurred in Ypt7T22N cells we could assess mitochondrial swelling as well as mitochondrial length in our electron microscopy images.

It is also tempting to speculate whether these tripartite MCS, if they do indeed exist in yeast, could allow the vacuole to buffer Ca^{2+} at these organelles. Given vacuolar Ca^{2+} uptake is the main mechanism of cytosolic Ca^{2+} buffering in yeast [186], this could allow for quick and efficient regulation of mitochondrial Ca^{2+} uptake due to the short membrane distances of MCS. In this hypothetical model, when vacuole-mitochondria-ER contact sites increase, mitochondrial Ca^{2+} levels would drop due to increased vacuolar Ca^{2+} uptake, resulting in lower mitochondrial respiration. This is a highly speculative model since no evidence of these tripartite contact sites has been reported in *S. cerevisiae,* or of vacuolar Ca^{2+} uptake affecting mitochondrial Ca^{2+}

levels. Therefore, extensive testing of vacuole-mitochondria-ER contacts in fluorescence and electron microscopy would be necessary, as well as organellar Ca^{2+} measurements.

4.4.3 Ypt7 activity impairs growth during mitochondrial respiration

Growth on acetate has been used as a proxy for mitochondrial respiration in the past since acetate can only be metabolized via the TCA cycle [113]. Therefore, we assayed for growth of Ypt7 mutants in acetate as a proxy for the state of their respiration and in turn, their MAM tethering. Our results show both dominant active and dominant negative Ypt7 mutants had impaired growth when forced to respire (Figure 4.3B). Previous results from our lab showed Rab32Q85L overexpression increases IP_3R-mediated Ca^{2+} release as well as mitochondrial Ca^{2+} uptake [290]. This suggests these cells likely have higher respiration rates, though this has not been tested. Our results in Chapter 3 suggest Rab32Q85L-mediated autophagic degradation of MAMs could decrease ER-mitochondria Ca^{2+} flux and therefore, mitochondrial respiration. However, autophagy provides cells with fatty acids, amino acids and sugars, which can be used to support mitochondrial metabolism [235]. For example, amino acids can have their amino group removed in order to be used in the TCA cycle, such as deaminated aspartate, which is converted to oxaloacetate [421]. This effect could counterbalance a decrease in ER-mitochondria Ca^{2+} flux due to MAMphagy, so it is still unclear what overall effect Rab32Q85L has on mitochondrial respiration. Therefore, it would be beneficial to measure oxygen consumption in both models to fully understand the effects of Rab32- and Ypt7-mediated changes in respiration and ER-mitochondria tethering. Regardless, our results suggest Ypt7 can regulate MAM formation and mitochondrial respiration.

A question that arises from these results is: why do Ypt7T22N cells grow poorly when respiring on acetate (Figure 4.3B) when they have more MERCs (Figure 4.2A)? Firstly, it is important to note that our electron microscopy experiment was performed in 2% YPD. Thus, our quantifications are not reflective of the status of MCS on acetate, but rather their status during homeostasis on glucose, where WT yeast preferentially perform glycolysis [113]. Yet this point raises another question, why do Ypt7T22N cells have so many more MERCs in YPD if, like WT cells, they should be performing glycolysis rather than OXPHOS? One possibility is that Ypt7T22N promotes MAM formation, as evidenced by our microscopy results (Figure 4.2A), but that an increase in MAMs does not increase respiration in yeast, as evidenced by the growth

defect of this strain on acetate (Figure 4.3B). In other words, it is possible *S. cerevisiae* MAMs are not required for mitochondrial respiration, unlike the mammalian model. However, there is abundant evidence that yeast mitochondria accumulate Ca^{2+} and that their respiration is regulated by Ca^{2+}, as described previously [102,133,138,184]. Therefore, there must be a regulatory mechanism for mitochondrial Ca^{2+} uptake. If this mechanism is not ER-mitochondria tethering as in mammals, it could instead by vacuole-mitochondria tethering. In this model, vacuolar Ca^{2+} uptake would regulate the availability of Ca^{2+} for mitochondria, which would in turn regulate mitochondrial respiration, as hypothesized above. Our microscopy results revealed Ypt7T22N cells had roughly twice the number of vacuole-mitochondria MCS compared to WT cells (Figure 4.2B). Therefore, Ypt7T22N would have lower mitochondrial Ca^{2+}, which is consistent with their impaired growth on acetate (Figure 4.3B). Testing of this model would require extensive organellar Ca^{2+} measurements in this mutant as well as vacuolar Ca^{2+} mutants Δ*pmc1* and Δ*yvc1* and ER Ca^{2+} mutants Δ*pmc1* and Δ*spf1/cod1*.

4.4.4 ER stress regulates mitochondrial respiration in yeast

Mammalian cells can increase mitochondrial respiration during ER stress by promoting MAM tethering [15,185,411]. Whether this also occurs in yeast is not known, but recent studies have shown ER stress can be relieved by promoting mitochondrial respiration [138,184]. Thus, it is possible changes in MAM formation could explain this increase in respiration during yeast ER stress. We therefore incubated cells with the Ire1 inhibitor STF and hypothesized this treatment would decrease growth on acetate. Our results suggest this is the case, since all strains treated with STF had decreased growth on acetate (Figure 4.3C). Thus, we conclude yeast also have ER-stress dependent increases in mitochondrial respiration, suggesting ER stress promotes MAM formation. This hypothesis could be further tested by performing electron microscopy and measuring MERCs with and without STF incubation. If our hypothesis is correct, then cells grown on 2% YPA + STF should have fewer MERCs. Similarly, this experiment could be done in Δ*ire1* and Δ*hac1* strains, though it is possible these cells could develop adaptations to overcome having fewer MERCs. In this case, vCLAMPs should also be quantified.

Interestingly, Ypt7 might directly interact with the ER stress machinery. Specifically, *HAC1* messenger ribonucleic acid (mRNA) has been shown to interact with several Ypt proteins, including Ypt7 [320]. In this study, the authors found Ypt1 binds *HAC1* mRNA during homeostasis

and promotes its decay. This interaction declines upon ER stress, allowing HAC1 to be spliced and participate in the UPR. Although only Ypt1 was tested to demonstrate *HAC1* decay, it is possible Ypt7 also regulates *HAC1* mRNA stability. If Ypt7 does indeed promote *HAC1* mRNA degradation in basal conditions, then acetate, which triggers ER stress [422], likely causes Ypt7-*HAC1* to dissociate, allowing for HAC1 translation. This could explain why Δ*ypt7* cells did not have growth defects in acetate (Figure 4.3), since they would have basal levels of ER stress if *HAC1* is not being bound and degraded. Thus, Δ*ypt7* cells are likely to have adaptations to deal with basal ER stress, which could include increased MAM tethering and respiration. This would give Δ*ypt7* cells a slight growth advantage on acetate. Indeed, Δ*ypt7* cells grew slightly better than WT cells, though this difference was not statistically significant (Figure 4.3B). This hypothesis could be tested by monitoring *HAC1* decay via reverse transcription polymerase chain reaction (RT-PCR) as well as binding to Ypt7 via RNA chromatin immunoprecipitation (RIP-ChIP).

Chapter 5: Cne1 and Eps1 regulation of mitochondrial respiration and ER-mitochondria tethering in *S. cerevisiae*

5.1 Abstract

The mitochondria-associated membrane (MAM) is a dynamic ER subdomain that responds to a multitude of stimuli and pathways, including Ca^{2+} flux, changing metabolic demands, and ER stress. A group of proteins that helps create a coordinated response to these conditions are ER folding assistants. The mammalian MAM houses a large number of these proteins, including TMX1 and Calnexin. At the MAM, TMX1 and Calnexin interact with the SERCA2b Ca^{2+} ATPase pump and regulate its activity through redox modification of its luminal cysteines. In basal conditions, SERCA2b activity is partly maintained by Calnexin, which is thought to promote Nox4- and Ero1α-mediated oxidation of its luminal cysteines. Therefore, loss of Calnexin causes significant decreases in ER Ca^{2+} content, ER-mitochondrial Ca^{2+} flux, and mitochondrial respiration. The reductase TMX1 instead inhibits SERCA2b, increasing ER Ca^{2+} content, ER-mitochondria Ca^{2+} flux and mitochondrial respiration. These effects were also coupled to changes in the number of ER-mitochondria contact sites as well as their tethering. Thus, these folding assistants act as critical regulators of MAM function and structure. We wanted to investigate if *Saccharomyces cerevisiae* folding assistants also regulate ER-mitochondria contact sites, particularly in light of recent evidence demonstrating loss of Glutaredoxin 6 (Grx6) decreased ER Ca^{2+} content. Therefore, we sought to characterize the effects of loss of the Calnexin homolog Cne1 as well as the hypothesized TMX1 homolog, Eps1. Our results reveal both Δ*cne1* and Δ*eps1* cells have growth advantages when cells are forced to respire in non-fermentable acetate. These effects were reversed when Ca^{2+} was chelated with BAPTA-AM, suggesting Ca^{2+} was required for their improved fitness when respiring. This strongly suggests Δ*cne1* and Δ*eps1* cells have higher ER-mitochondria Ca^{2+} transfer, fueling higher and/or more efficient respiration. Δ*cne1* cells also had significantly higher maximal respiration as assayed by respirometry measurements. Δ*cne1* cells also had roughly 40% shorter ER-mitochondria contacts and looser tethering between these membranes. These effects were coupled with an increase in the average number of contact sites per cell. Δ*eps1* instead had no significant changes in oxygen consumption or ER-mitochondria contact site tethering. Therefore, our results demonstrate the Calnexin homolog, Cne1, is a MAM modulator in *S. cerevisiae.*

5.2 Background

5.2.1 Redox regulation of SERCA2b at MAMs

ER Ca^{2+} homeostasis in mammals requires tight regulation of IP_3R and SERCA activity. One way these proteins are post-translationally regulated at the MAM is via redox modification of cysteines [81,258]. These redox reactions are catalyzed by ER oxidoreductases with a conserved TRX motif composed of two cysteines separated by any two amino acids (CxxC) [274]. This motif is quite variable, and many proteins have at least one cysteine replaced with another thiol-containing amino acid such as serine or threonine. Members of the PDI superfamily can catalyze disulfide bond formation or isomerization via oxidation of their TRX-like motif cysteines [149]. Instead, cysteine reduction in the TRX-like motif results in disulfide bond hydrolysis in the client. Disulfide bonds are important not only for a protein's structure but also for its activity [423]. For example, several studies have shown the ATPase activity of SERCA2b, the ubiquitous isoform enriched in MAMs, can be altered via redox regulation of its luminal cysteines and cytosolic cysteines [81,255–257]. These studies have largely focused on a single conserved cytosolic cysteine, cysteine 674 (C674), since modification of the remaining cytosolic cysteines does not significantly alter ATPase activity [256]. These studies suggest overall hyperoxidation of SERCA2b's cysteines inhibits its activity [257,258]. Reversible oxidation of C674 is instead associated with increased ATPase activity [256].

Fewer studies have investigated its two intraluminal cysteines found on the longest loop connecting the 11 transmembrane domains of SERCA2b, loop 4 (L4) [81,257]. Several studies suggest oxidation of L4 cysteines and disulfide bond formation between them inhibits SERCA2b [81,255,25781,255,257]. In one study performed in *Xenopus* oocytes, a system commonly used to study Ca^{2+}, ERp57 overexpression inhibited SERCA2b [257]. This was investigated by measuring SERCA2b-mediated cytosolic Ca^{2+} oscillations, which are created by successive waves of Ca^{2+} release induced by IP_3R and uptake by SERCA2b. The authors also demonstrated ERp57 interacts with SERCA2b by binding L4. This interaction decreased when ER Ca^{2+} fell below 50μM during ER stress, suggesting binding occurs only during homeostasis. Although there was no direct evidence of ERp57 oxidizing the luminal cysteines, the authors also showed the effect on cytosolic Ca^{2+} was lost when ERp57's active site was mutated. Together, these results suggest ERp57 inhibits SERCA2b in basal conditions by catalyzing oxidation of the L4 cysteines.

On the other hand, reduction of the L4 cysteines via hydrolysis of their disulfide bond can activate SERCA2b [255]. For example, the reductase ERdj5 binds SERCA2b during ER stress when ER Ca^{2+} levels drop significantly. Under these conditions, ERdj5 can reduce the L4 cysteines and activate SERCA2b, likely in an effort to restore ER Ca^{2+} homeostasis by increasing Ca^{2+} uptake. Moreover, loss of ERdj5 via siRNA KD increased L4 cysteine oxidation and correlated with lower SERCA2b activity. However, some level of oxidation is required for SERCA2b activity [255,257,258]. Indeed, several studies suggest SERCA2b is most active when its luminal, and likely also cytosolic, cysteines are partially oxidized [81,257,258]. In summary, these studies suggest oxidation activates SERCA2b while partial reduction or extensive oxidation inhibits it.

Two other MAM-localized folding assistant also regulate SERCA2b: Calnexin and TMX1 [259,260,267]. Importantly, studies in Calnexin and TMX1 KOs have shown loss of their SERCA2b regulation has direct effects on MAM functions and structure.

5.2.2 Calnexin and TMX1 oppositely regulate SERCA2b activity

Calnexin interacts with SERCA2b in basal conditions in its palmitoylated form, a post-translational modification that enriches it at the MAM [266,267]. Palmitoylated Calnexin can also interact with the RTC, particularly in the peripheral ER, where it participates in protein folding of newly synthesized glycoproteins [266]. Depalmitoylation causes Calnexin to redistribute throughout the bulk ER, a process that can be triggered by short-term ER stress induced by tunicamycin or reducing agent DTT [267].

Previous results from our laboratory suggest Calnexin is required for SERCA2b activation in a redox-dependent manner [259,267]. This was determined in part by measuring ATPase activity from isolated light membranes [259]. These experiments demonstrated Calnexin KOs had significantly lower ATPase activity derived from SERCA2b compared to their WT counterparts. A BIAM switch assay also revealed Calnexin KOs had significantly more reduced SERCA2b compared to WT cells, suggesting Calnexin is required to maintain SERCA2b oxidation. This suggests Calnexin likely promotes oxidation of the L4 cysteines to maintain SERCA2b in an active state.

Calnexin interacts with several oxidoreductases which are likely to catalyze SERCA2b L4 cysteine oxidation. One of these interactors is the nicotinamide-adenine dinucleotide phosphate

(NADPH) oxidase Nox4, which is known to oxidize and activate SERCA2b [424,425]. When WT and Calnexin KO cells were chemically inhibited for Nox4, WT and KOs behaved similarly. Specifically, SERCA2b oxidation and ATPase activity decreased in WT cells to roughly the same levels as KOs [259]. This effect was also observed when cells were treated with an Ero1α inhibitor. Together, these results demonstrate Calnexin maintains SERCA2b oxidation and activity in basal conditions by promoting Nox4- and Ero1α- mediated SERCA2b oxidation. Therefore, Calnexin KOs have a number of defects, including significantly lower ER Ca^{2+}. Calnexin KOs did not have increased UPR induction though, which has also been reported in other studies [259,267,426]. They also have lower cytosolic and mitochondrial Ca^{2+} levels [259]. Additionally, electron microscopy revealed they have tighter and longer ER-mitochondria contacts and more tethering proteins. Thus, Calnexin KOs have more MAMs overall, likely to compensate for their decreased ER-mitochondria Ca^{2+} flux. Lastly, they had a lower respiration rate and were more reliant on glycolysis.

TMX1 instead inhibits SERCA2b, though the mechanism for this effect is less understood. TMX1-SERCA2b interaction occurs preferentially when cells are undergoing oxidative stress, such as after incubation with the oxidant buthionine sulfoximine (BSO) [260]. These conditions promote TMX1 MAM enrichment, which likely contributes to this increased interaction. In support of the hypothesis that TMX1 inhibits SERCA2b, TMX1 KOs have higher ER Ca^{2+} while cells overexpressing TMX1 have decreased ER Ca^{2+}. Moreover, TMX1 overexpression was coupled with increased mitochondrial Ca^{2+} uptake and oxygen consumption, suggesting mitochondrial respiration was induced. Like Calnexin KOs, TMX1 KOs do not have increased levels of basal ER stress [427]. However, TMX1 loss caused better ER Ca^{2+} uptake and decreased ER Ca^{2+} release [260]. Consistent with these results, TMX1 KOs had a significant decrease in ER-mitochondria contact site length as assayed by electron microscopy. Mitochondrial Ca^{2+} and respiration also decreased in these cells. Additionally, TMX1 KOs had a shift to glycolytic metabolism since they had higher amounts of glycolytic enzymes, possibly to compensate for their lower respiration rate.

However, another study found stable TMX1-silenced cells have higher mitochondrial Ca^{2+} and respiration rate compared to WT cells [427]. This study also found TMX1 KD caused an increase in mitochondrial proximity to the plasma membrane. These cells also had shorter and looser MERCs, suggesting TMX1 silencing reduces ER-mitochondria MCS but promotes plasma

membrane-mitochondria MCS. Importantly, mitochondrial Ca^{2+} levels have been shown to increase upon shorter plasma membrane-mitochondria distances [428]. Therefore, it is likely TMX1 KD cells compensate for their shorter and looser MAMs by increasing plasma membrane-mitochondria proximity, resulting in an overall increased mitochondrial Ca^{2+} and respiration. Although this hypothesis reconciles the TMX1 KO and KD results, taken together, these studies suggest loss of TMX1 results in complex phenotypes with compensatory pathways.

5.2.3 ER Ca^{2+} regulation in *S. cerevisiae*

ER Ca^{2+} in *S. cerevisiae* is largely dependent on the Ca^{2+} ATPase pump Pmr1 [98,101,102]. The Spf1/Cod1 ATPase pump is also thought to transport Ca^{2+} into the ER, although there is still no direct evidence of Ca^{2+} being one of its substrates [102,104,105]. Nevertheless, loss of either ATPase significantly decreases ER Ca^{2+}, which in turn causes defects in protein folding and ERAD [98,101,102]. Spf1/Cod1 is not related to SERCA and instead belongs to a group of poorly understood ER-localized ATPases with no known function [105]. While Pmr1 is found on both the ER and Golgi, Spf1/Cod1 is exclusively ER-localized [98,101,102]. This difference could explain why Δ*spf1/cod1* cells have high basal UPR signaling but Δ*pmr1* cells do not [95,98]. Another factor that could prevent Δ*pmr1* cells from activating the UPR in basal conditions is the fact they have a stimulated high affinity Ca^{2+} system (HACS) at the plasma membrane [95,98]. This results in higher cytosolic Ca^{2+}, activation of the Ca^{2+} cell survival (CCS) pathway, and calcineurin-mediated transcription changes, which improve the cell's survival [95,98]. Pmr1 does not share extensive homology with SERCA either and is more related to mammalian Golgi-localized secretory pathway Ca^{2+} ATPases (SPCAs) instead [101]. Nevertheless, mammalian SERCA rescues Pmr1 loss, which causes decreased ER Ca^{2+} levels and defects in protein folding, sorting, and ERAD [95,98,101,102]. Thus, Pmr1 is thought to act as a SERCA functional homolog [101]. As previously mentioned, no IP_3R homolog has been found in *S. cerevisiae* and the main mechanism by which this species releases ER Ca^{2+} into the cytosol remains unknown [20]. One hypothesis is that it occurs occur via diffusion along the secretory pathway, though this has not been tested [100].

Very little is known regarding Pmr1 and Spf1/Cod1 post-translational regulation. However, a recent study found ER Ca^{2+} levels drop upon loss of an ER folding assistant, an effect that is also observed in Calnexin KOs [108,259]. This study investigated the ER/Golgi Glutaredoxin 6 (Grx6), one of two glutathione-dependent oxidoreductases in *S. cerevisiae* [108]. Glutaredoxins catalyze the

reversible post-translational addition of glutathione, the cell's most abundant antioxidant [429]. Grx6 is predicted to have deglutathionylation activity and therefore likely catalyzes the reversible removal of glutathione via reduction of a client's disulfide bond [108,282]. This study found Δ*grx6* cells had decreased ER Ca^{2+} levels but no significant UPR induction, phenocopying Δ*pmr1* cells [98,108]. Δ*grx6* cells also had more a more oxidizing ER compared to WT cells [108]. Lastly, Grx6 loss increased cytosolic Ca^{2+} via HACS, which resulted in activation of the CCS pathway and calcineurin-mediated transcription changes, once more phenocopying Δ*pmr1* cells [98,108]. In brief, although Pmr1 activity was not directly tested, these results suggest redox regulation by ER folding assistants can influence luminal Ca^{2+} levels in yeast too.

5.2.4 Cne1 and Eps1: MAM regulators?

The yeast homolog of mammalian Calnexin, Cne1, is also an ER membrane chaperone [268]. Although it only shares roughly 23% amino acid identity with Calnexin, Cne1 has similar chaperoning activities [268,269]. Indeed, Cne1 also binds glycoproteins and can prevent their aggregation [268]. Unlike Calnexin though, it does not bind or require Ca^{2+} [268,269]. There is very little known regarding the potential for Cne1 to regulate MAMs or even interact with the MAM proteome. Thus, there is no evidence Cne1 interacts, physically or genetically, with either *S. cerevisiae* ER Ca^{2+} pump. It is also unknown if Cne1 can interact with the ER-localized yeast NADPH oxidase 1 (Yno1), the only NOX enzyme in *S. cerevisiae* [430]. Likewise, a Cne1-Ero1 interaction has not been reported, though there is also no evidence of Calnexin-Ero1α binding in mammals. Nevertheless, Cne1 interacts with and can increase the reductase activity of Mpd1, which catalyzes disulfide bond formation for Cne1-bound glycoproteins [283]. Therefore, like Calnexin, Cne1 interacts with at least one oxidoreductase, which could in turn regulate MAM proteins as in mammals. Though not experimentally tested, Mpd1 is hypothesized to be functionally homologous to ERp57, suggesting Mpd1 could have substrates similar to those of ERp57 [283]. Given ERp57 oxidizes SERCA2b and impairs its activity [257], it is possible Mpd1 acts on the SERCA2b functional homolog Pmr1. This hypothesis is supported by the recent evidence that Grx6 loss oxidizes the ER lumen and decreases ER Ca^{2+} content [108]. This strongly suggests the presence of a redox-dependent mechanism that regulates ER Ca^{2+} uptake in *S. cerevisiae*. If this mechanism is similar to regulation of mammalian SERCA2b, then Pmr1 could be a target of these redox-dependent ER Ca^{2+} changes. In other words, if Pmr1 activity is regulated by its

oxidative state, then Cne1-mediated Mpd1 reductase activity could directly activate or inhibit this Ca^{2+} ATPase. A similar scenario could involve Cne1 altering the ER's redox state via Mpd1 activity rather than Mpd1 directly binding and regulating Pmr1. This would result in a similar redox-dependent change in ER Ca^{2+} levels like that of Δ*grx6* cells. Therefore, we hypothesize Cne1 can also regulate ER Ca^{2+} in a redox-dependent manner, causing changes in MAM tethering and or/function.

Several lines of evidence suggest the closest TMX1 homolog in yeast is Eps1. Firstly, Eps1 is the only transmembrane member of the yeast PDI family [285]. Thus, Eps1 substrates are likely similar to TMX1 substrates. Indeed, both proteins interact exclusively with membrane-bound substrates [272,286]. Secondly, a phylogenetic study of TRX-like proteins across thousands of species from all domains suggests TMX1 and Eps1 are part of the same phylogenetic group based on their active site motif properties [274]. Thirdly, both Eps1 and TMX1 participate in ERAD of membrane-bound proteins [278,286,287]. No oxidative or reductase activity has been demonstrated for Eps1 yet, so it remains unclear how Eps1 participates in this process. Nevertheless, several studies suggest Eps1 can catalyze disulfide bond reactions. For example, Δ*eps1* cells have impaired secretion of proteins containing disulfide bonds [286]. Additionally, crystallography and phylogenetic analysis of its two TRX-like motifs suggests Eps1 has disulfide isomerization activity [289]. Additional studies suggest its first TRX-like motif, CPHC, is active, while its second motif, CDKC, aids the first but is inactive by itself [287,288]. Taken together, these studies demonstrate Eps1 and TMX1 have similar a localization, function, and catalytic activity. As with Cne1, there is no reported physical or genetic interaction of Eps1 with either ER Ca^{2+} pump. Nevertheless, Eps1 loss could alter the ER's oxidizing environment and alter luminal Ca^{2+} levels in a similar manner as Δ*grx6* cells. Therefore, we hypothesize Eps1 will also regulate ER-mitochondria Ca^{2+} flux, mitochondrial metabolism, and/or MAM tethering.

5.3 Results

5.3.1 Eps1 and TMX1 are reciprocal best BLAST hits (RBHs)

To investigate if Eps1 is the most closely related yeast protein to TMX1 we performed a RBH analysis wherein we used the human TMX1 sequence as a query in a protein-protein BLAST search in the *S. cerevisiae* genome. The best match for this search was Eps1 with 33.7%

identity (Figure 5.1A). This hit was followed by the mitochondrial thioredoxin Trx3 at 33.3%, and the cytosolic thioredoxin Trx1 at 30.2% [431] (Figure 5.1A). The remaining 4 yeast PDI family members, Pdi1, Eug1, Mpd1 and Mpd2, all fell below 30% identity (Figure 5.1A), which significantly decreases confidence in a RBH analysis [396]. Together, this suggests Eps1 is the closest TMX1 homolog in *S. cerevisiae.* Next, we performed the reciprocal BLAST search with Eps1 as the query and found TMX1 to be the best match with 33.7% identity, followed by PDI at 32.8% (Figure 5.1B). TMX3 and TMX4 were also closely related, with 30.6% and 29.9% identity, respectively (Figure 5.1B). Lastly, we performed sequence alignment to compare the active sites of TMX1 and Eps1 (Figure 5.1C). As previously mentioned, Eps1's first TRX-like motif binds ERAD substrates and is predicted to have disulfide isomerase activity, while its second motif is likely inactive [287–289]. We observed good conservation between TMX1's CPAC motif and Eps1's first motif, CPHC (Figure 5.1C). Lastly, we found Eps1 as the best match in a BLAST search with the CPAC sequence as query in the *S. cerevisiae* genome (Figure 5.1D). Together, these results demonstrate TMX1 and Eps1 are a RBH pair, strongly suggesting Eps1 is the *S. cerevisiae* homolog of mammalian TMX1.

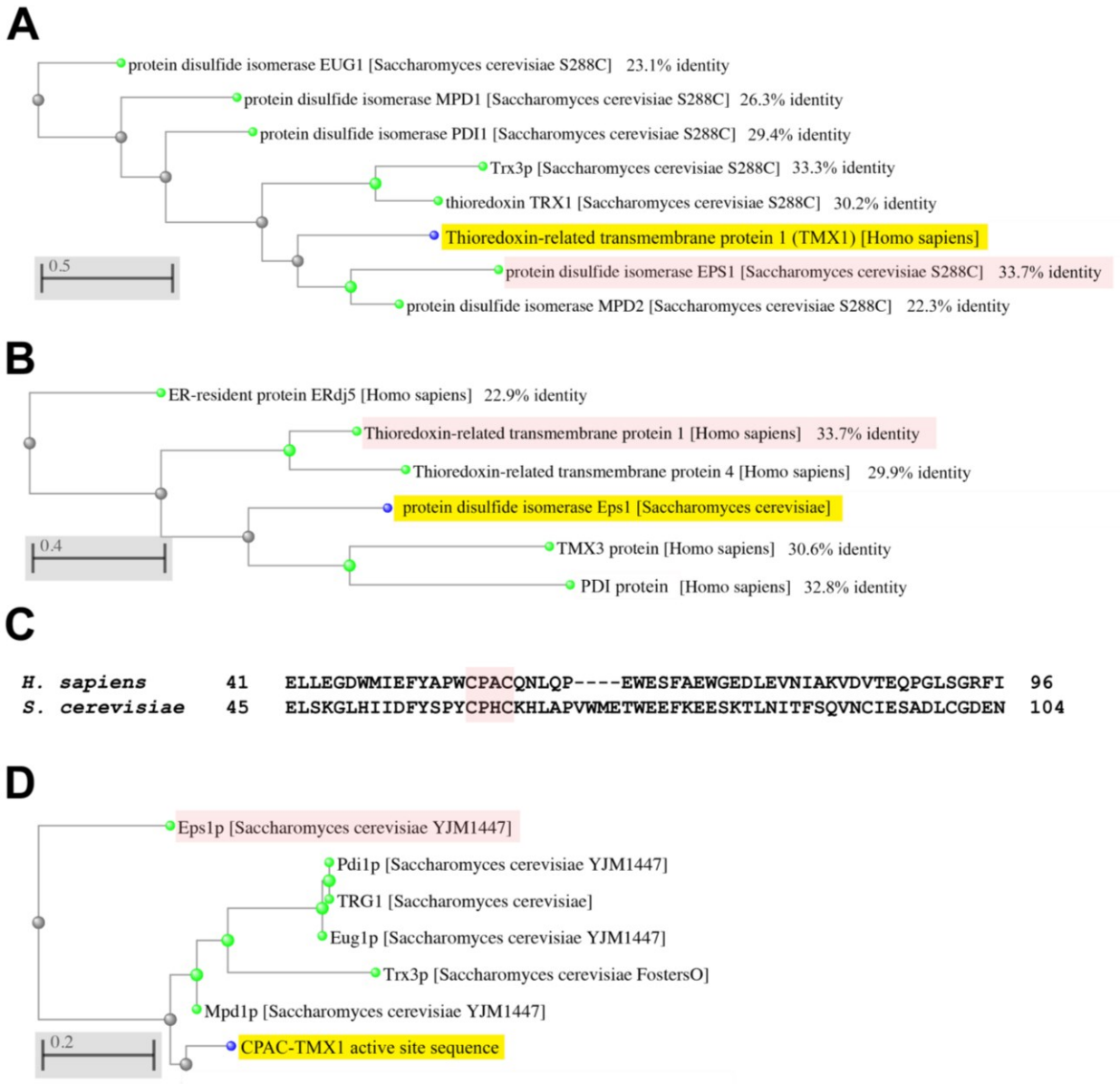

Figure 5.1 Eps1 is the closest TMX1 homolog in *Saccharomyces cerevisiae*
A. Phylogenetic tree generated by NCBI protein-protein BLAST with *Homo sapiens* TMX1 as query in the *Saccharomyces cerevisiae* genome identifies Eps1 as the best match. Query is highlighed in yellow and best match in red. Square brackets indicate genome dataset eg. [S288C] and are followed by percent identity of each pairwise alignment. **B.** Reciprocal BLAST search with best match from A, Eps1, identifies TMX1 in the *Homo sapiens* genome. Query is highlighted in yellow and best match in red. Percent identitiy of each pairwise alignment is also indicated. **C.** Sequence alignment of Eps1 and TMX1 sequences. TMX1 active site highlighted in red shows good conservation with TRX-like motif in Eps1. **D.** Phylogenetic tree as in A with TMX1 active site as query instead identifies Eps1 as the best match. Square brackets indicate genome dataset.

5.3.2 Δ*eps1* and Δ*cne1* have growth advantages on acetate

To investigate the bioenergetics of these strains, we compared growth on glucose (YPD) versus acetate (YPA) in liquid and solid media. As previously mentioned, non-fermentable acetate forces *S. cerevisiae* to respire while glucose allows cells to perform glycolysis, their preferred metabolic pathway [113]. We assayed growth in liquid media by measuring absorbance after 24hrs of growth from an initial OD_{600} of 0.2. At the same time, we plated serial dilutions on agar plates and observed colony growth. We also used cells lacking the ERMES subunits Gem1 and Mdm34 as positive controls for MAM disruption. Due to their disrupted ER-mitochondria tethering, both strains have impaired growth in another non-fermentable carbon, glycerol [35,36,409].

Our results showed Δ*eps1* had a small but statistically significant growth defect of roughly 10% in YPD (Figure 5.2A). This effect was less obvious on solid media, where there was only a minimal decrease in Δ*eps1* growth at 10^{-3} compared to WT (Figure 5.2A). Although Δ*gem1* and Δ*mdm34* have been previously reported to be slightly growth impaired on YPD [36,409], we did not observe statistically significant changes for these strains in liquid or solid YPD (Figure 5.2A). In brief, our results indicate Δ*eps1* had a small growth defect on YPD while Δ*cne1* and ERMES mutants behaved like WT cells.

Next, we investigated growth on YPA, where we observed growth defects for both ERMES mutants on liquid and solid YPA (Figure 5.2B). These results are consistent with their role in the formation of MAMs that favor mitochondrial metabolism. They are also consistent with previously published results on non-fermentable glycerol [35,36]. Δ*cne1* and Δ*eps1* instead grew significantly better than WT, with a roughly 15% higher OD_{600} (Figure 5.2B). This effect was more pronounced in liquid media, while there was only a slight advantage on our plates (Figure 5.2B). These results suggest Cne1 and Eps1 loss improves TCA efficiency and/or promotes mitochondrial respiration. In order to distinguish between these scenarios, we performed respirometry experiments (see below).

We also assessed growth in YPD supplemented with cobalt (II) chloride hexahydrate ($CoCl_2 \cdot 6H_2O$) to simulate hypoxia, which inhibits mitochondrial respiration while allowing for glycolysis to proceed. This experiment revealed no growth changes for Δ*cne1* or Δ*eps1* compared to WT (Figure 5.2C). This was also the case for both ERMES mutants (Figure 5.2C). Overall, these results are very similar to those obtained in YPD plates (Figure 5.2A). Thus, it appears hypoxia does not significantly alter metabolism when cells have access to glucose. In

other words, MAM disruption or loss of the folding assistants Eps1 or Cne1 does not affect growth when cells are performing glycolysis. We also assayed for growth on YPD supplemented with 2-deoxyglucose (2-DG), a glucose analog that inhibits glycolysis. All strains behaved similarly to WT, once again phenocopying growth on the untreated YPD plate (Figure 5.2A,D). Therefore, these results suggest glycolysis inhibition and hypoxia do not significantly affect growth of Δ*eps1*, Δ*cne1,* or ERMES mutants.

5.3.3 Ca^{2+} chelation eliminates growth advantages of Δ*eps1* and Δ*cne1* on acetate

Lastly, we investigated the effect of Ca^{2+} chelation on Δ*cne1* and Δ*eps1* growth when forced to respire on YPA. Ca^{2+} shortage is known to trigger ER stress and decrease growth and cell size in yeast [138]. Interestingly, a recent study suggests Ca^{2+} shortage can also promote mitochondrial metabolism, although this effect was dependent on the type of carbon provided [138]. In media with trace amounts of Ca^{2+}, non-fermentable glycerol induced mitochondrial respiration while glucose did not. This is likely because yeast will only respire when fermentable carbons like glucose are completely exhausted [113]. Thus, Ca^{2+} shortage in glucose did not promote respiration because glycolysis was still strongly favoured over mitochondrial respiration.

We performed our experiments on non-fermentable YPA and chelated Ca^{2+} with 1,2-Bis(2-aminophenoxy)ethane-N,N,N′,N′-tetraacetic acid tetrakis(acetoxymethyl ester) (BAPTA-AM). These experiments revealed both Δ*cne1* and Δ*eps1* had very similar growth to the WT strain under low (0.5mM) and high (5mM) concentrations (Figure 5.2E). These results differed from our untreated YPA conditions, where both Δ*cne1* and Δ*eps1* had growth advantages over WT (Figure 5.2B). Thus, Ca^{2+} chelation appears to remove the growth advantage of Δ*cne1* and Δ*eps1* on YPA, suggesting their increased and/or more efficient respiration is Ca^{2+}-dependent. Specifically, we hypothesize this is due to disrupted ER-mitochondria Ca^{2+} flux. Therefore, we next investigated their mitochondrial metabolism by measuring oxygen consumption.

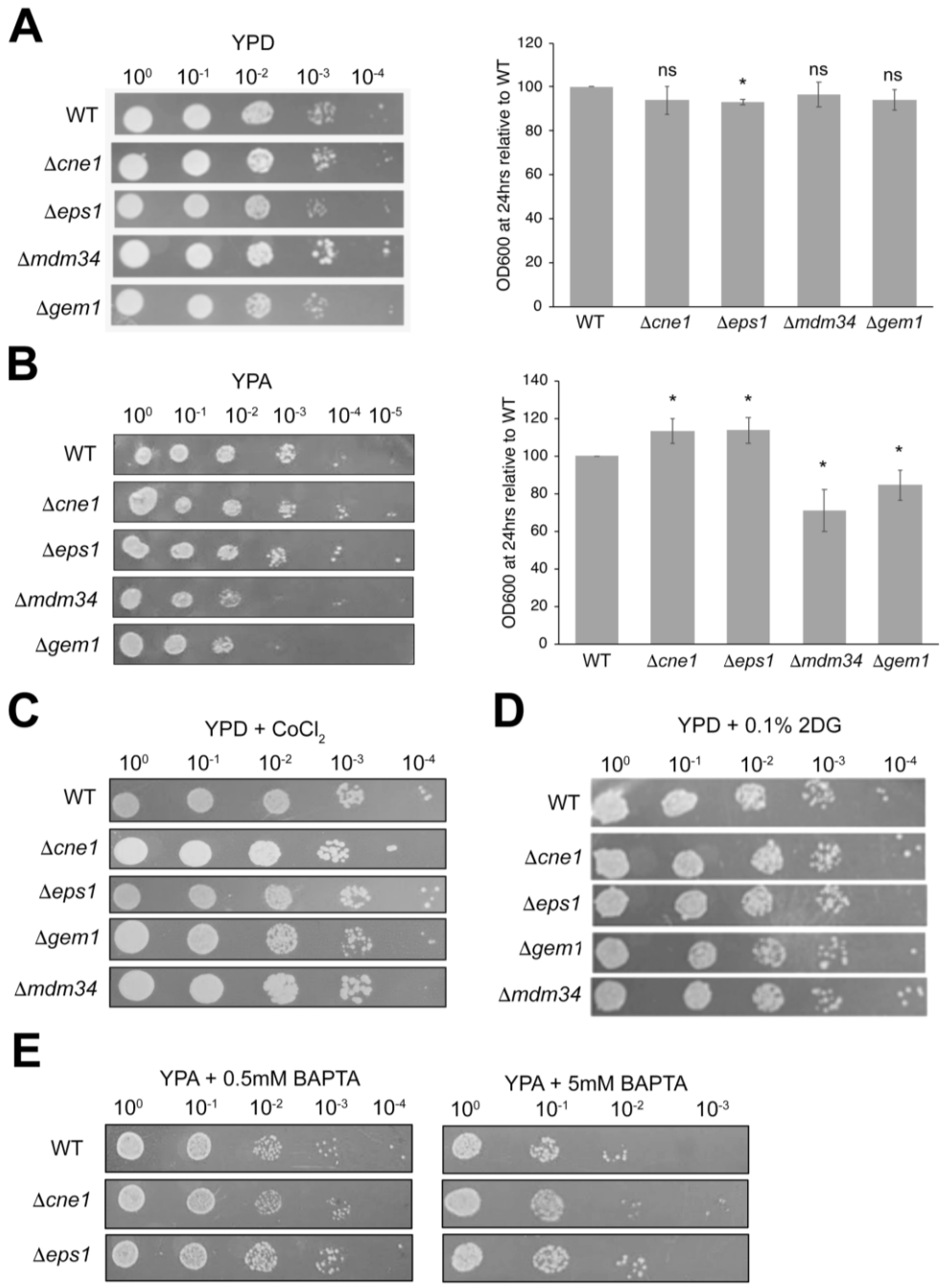

Figure 5.2 Δ*cne1* and Δ*eps1* have growth advantages on non-fermentable acetate
A. Spot assay in 2% YPD shows a small growth defect for Δ*eps1*. Absorbance measurements were taken to obtain optical density (OD_{600}). Strains were grown from an initial OD_{600} of 0.2 and assayed at 24hrs. (n=5). ns=not significant. *p≤0.05. **B.** Spot assay in 2% YPA reveals Δ*cne1* and Δ*eps1* mutants have growth advantages. Absorbance measurements performed as in A in YPA. (n=3). *p≤0.05. **C.** Spot assay in 2% YPD + 1mM $CoCl_2$ has no effect. **D.** Spot assay in 2% YPD + 0.1% 2-deoxyglucose (2DG) has no effect. **E.** Spot assay in 2% YPA + BAPTA-AM (0.5mM and 5mM) indicates Ca^{2+}-dependent effect of growth advantage in Δ*cne1* and Δ*eps1*. Panels C, D and E were performed in conjunction with Alicia Wu.

5.3.4 Δ*cne1* have higher maximal respiration rates

To assess cellular respiration, we measured oxygen concentration changes in an Oroboros respirometer in intact WT, Δ*cne1* and Δ*eps1* cells. All strains were grown overnight in YPA and equal amounts were loaded into the oxygen chambers, where oxygen concentration was measured over time. From these measurements, oxygen flux per milligram (pmol/s*mg) was obtained and graphed (Figure 5.3). Although we observed a small increase in Δ*cne1* basal respiration ('Routine'), and a small decrease for Δ*eps1*, these differences were not statistically significant (Figure 5.3). As a vector control for carbonyl cyanide 4-(trifluoromethoxy) phenylhydrazone (FCCP), ethanol was then added ('Routine-EtOH). As expected, addition of ethanol alone did not cause any significant changes (Figure 5.3). Lastly, we added the uncoupler FCCP by stepwise addition to obtain a maximal response. This allows us to obtain a measure of electron transfer system capacity ('ET') (Figure 5.3). This revealed Δ*cne1* cells had a significantly higher maximal respiration rate compared to that of WT cells (Figure 5.3). Together, these results reveal Cne1 loss significantly improves maximal mitochondrial respiration rate while Eps1 loss does not alter basal or maximal mitochondrial respiration.

These results are consistent with the significant growth advantage of Δ*cne1* in YPA (Figure 5.2B), suggesting these cells have increased and/or more efficient OXPHOS. We could not detect citrate synthase activity in these samples, so at the moment we cannot determine whether this effect is due to a more efficient TCA cycle. Nevertheless, our respirometry results revealed statistically significant changes (Figure 5.3), confirming Δ*cne1* cells have increased OXPHOS when grown on acetate. We also observed the growth advantage on acetate disappear when Δ*cne1* were incubated with BAPTA-AM (Figure 5.2E). Together, these results indicate the growth advantage of Δ*cne1* cells on YPA is Ca^{2+}-dependent, suggesting ER-mitochondria Ca^{2+} flux is involved.

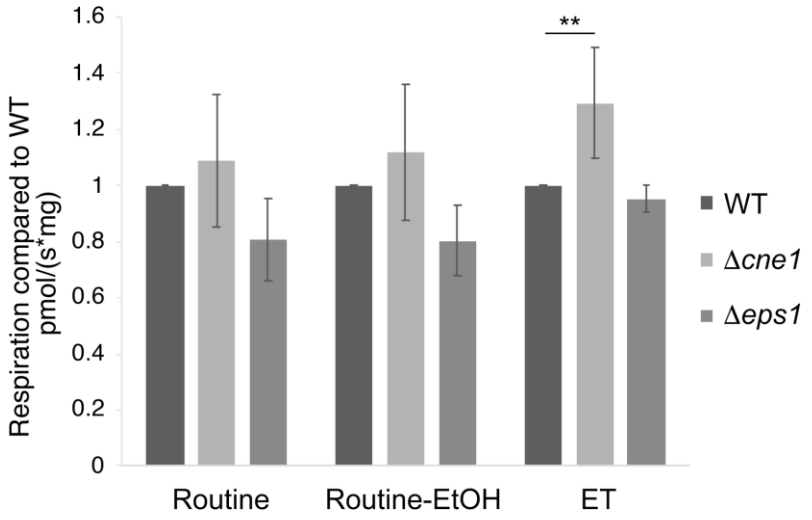

Figure 5.3 Δ*cne1* have higher maximal respiration rates
Respiration rate of intact cells grown in 2% YPA was calculated and normalized to WT. Oxygen concentration was measured in an Oroboros 2k respirometer at 30°C. Equal amounts (0.1mg) of cells were loaded into oxygen chambers. Cells were allowed to stabilize for routine measurement ('Routine'), then 40µL of pure ethanol was added (Routine-EtOH) as a vector control for FCCP. This was followed by stepwise addition of 1mM FCCP to calculate maximal electron transfer (ET) capacity. n=3 **$p \leq 0.01$. Experiments were performed in conjunction with Alicia Wu. Results were analyzed by Dr. Hélène Lemieux.

5.3.5 Δ*cne1* have more ER-mitochondria contact sites per cell

Lastly, we performed electron microscopy to investigate if the growth and respiration effects we observed are associated with changes in MAMs. To do this, we grew WT, Δ*eps1*, and Δ*cne1* cells overnight in YPD and prepared them for electron microscopy analysis the following day. After imaging, we quantified the total number of ER-mitochondria contact sites per cell (Figure 5.4A,B). We also obtained the average distance between the ER and mitochondrial membranes in individual ER-mitochondria contacts (Figure 5.4D). Additionally, we obtained the length of individual ER-mitochondria contact sites by measuring the length of a continuous ER membrane ≤50nm from the membrane of a mitochondrion (Figure 5.4E). We then calculated a MAM coefficient by dividing the length of each contact by the average distance between the membranes (Figure 5.4C). This allows us to obtain a factor proportional to MAM content for each strain.

This experiment revealed Δ*eps1* cells were not statistically different from WT cells in terms of number of MAMs per cell (Figure 5.4B). They also had no significant differences in MAM length (Figure 5.4E), distance (Figure 5.4D), or length/distance (Figure 5.3C). On the other hand, Δ*cne1* cells had a significant increase of almost 20% in the number of MAMs per cell (Figure 5.4B). They also had a small but significant increase in contact site distance, indicating Δ*cne1* cells have looser MAMs (Figure 5.4D). This effect was coupled with ~40% decrease in average MAM length (Figure 5.4E). Together, these measurements resulted in a significantly lower MAM coefficient or length/distance ratio (Figure 5.4C). In summary, these results demonstrate Eps1 loss does not alter the number of MAMs in cells nor their tethering or length. Conversely, Cne1 increases the number of contact sites, but these are shorter and looser contacts, causing in an overall decrease in the MAM coefficient.

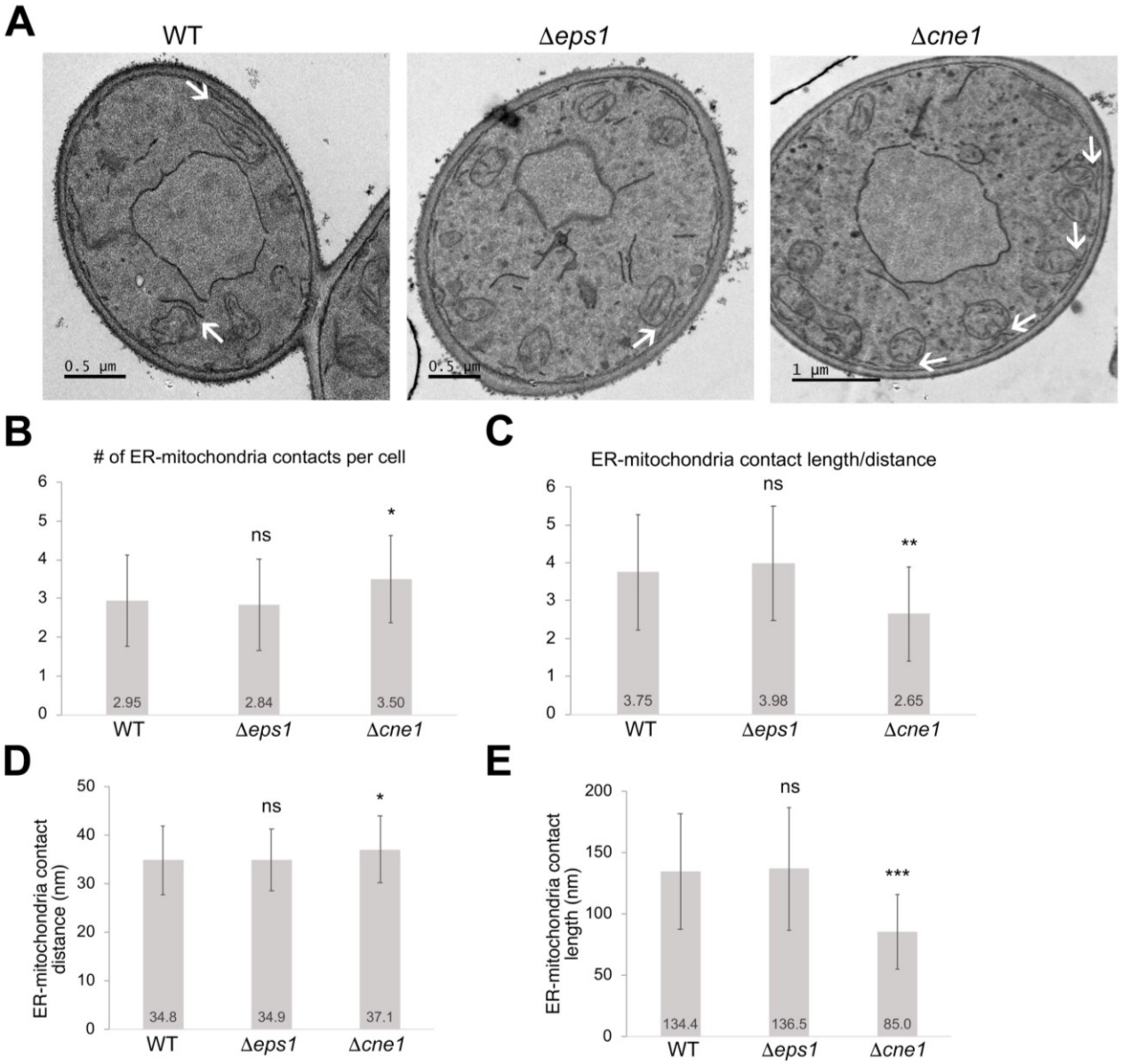

Figure 5.4 Δ*cne1* have more ER-mitochondria contact sites per cell

A. Representative images of electron microscopy for WT, Δ*cne1*, and Δ*eps1* cells. ER-mitochondria MCS are indicated by white arrows. Cells were grown in 2% YPD. **B.** Average number of ER-mitochondria contact sites per cell. Average values indicated at the base of each bar. n=100. ns= not significant. *p≤0.05. **C.** Average ER-mitochondria contact site coefficient calculated by dividing the average length of contacts by the distance between the membranes involved. Distances within 10-50nm between ER and mitochondria membranes were measured at several points along a continous MCS to obtain an average MAM distance value. The length of the continous ER membrane engaged in the MCS was measured to obtain an average MAM length value. Average values indicated at the base of each bar. n=100. ns= not significant. **p≤0.01 **D.** Average ER-mitochondria contact site distance was measured in nm. Average values indicated at the base of each bar. n=100. **E.** Average ER-mitochondria contact site length was measured in nm. Average values indicated at the base of each bar. n=100. ***p≤0.001. Sample preparation and contact site quantification was performed in conjunction with Alicia Wu.

5.4 Discussion

5.4.1 Cne1 is a MAM modulator

ER folding assistants are well represented in the MAM proteome in mammalian cells [170]. Many of these proteins have been shown to influence Ca^{2+} homeostasis via IP_3R or SERCA2b activity regulation. For example, Calnexin binds SERCA2b in basal conditions and promotes its activity by maintaining its oxidation status via Nox4 and Ero1α action [259]. TMX1 instead interacts with SERCA2b following oxidative stress [260]. Under these conditions, TMX1 inhibits SERCA2b through a still unknown mechanism. Loss of TMX1 or Calnexin therefore causes Ca^{2+} dysregulation and changes in MAM tethering [259,260,267]. Hence, loss of Calnexin-mediated SERCA2b activity increases MAM length/distance as well as the number of ER-mitochondria contact sites per cell [259]. In TMX1 KOs, an increase in SERCA2b activity is likely responsible for the reduced MAM length observed in these cells [260]. In brief, these results demonstrate Calnexin and TMX1 are important modulators of MAMs.

Our electron microscopy results revealed Cne1 loss caused a significant increase in the average number of ER-mitochondria contacts per cell (Figure 5.4B). We also observed a significant drop in MAM length/distance of almost 30% compared to WT cells (Figure 5.4C). Thus, although Cne1 loss increased the number of MAMs per cell, it led to an overall decrease in their MAM coefficient (Figure 5.4B, C). Although at first counterintuitive, these results can be explained by the fact the contact sites were looser and almost 40% shorter (Figure 5.4D, E). Together, these results suggest Δ*cne1* cells have more MAMs, though these are shorter and looser contacts that result in an overall lower MAM content.

Although Calnexin loss also caused an increase in the number of MAMs per cell in mammalian cells, it instead caused an overall increase in the MAM coefficient [259]. MCS in these cells were also investigated using the split-green fluorescent protein-based contact site sensor (SPLICS), which allows for *in vivo* quantification of tight/short (8-10nm) versus loose/long (40-50nm) contacts via expression of a $SPLICS_{short}$ or $SPLICS_{long}$ plasmid. This assay revealed Calnexin KOs have significantly more loose contacts while the number of tight contacts remained unchanged. Lastly, their overall contact site length was significantly larger compared to WT cells. Taking all this information together, Calnexin loss increases MAM content by increasing the number of contact sites as well as their overall length, counteracting its

concomitant increase in loose contacts. Our results now show Cne1 loss increases the number of MAMs per cells, much like Calnexin KOs. However, these contacts are shorter and looser, causing an overall reduction in the MAM coefficient, as opposed to Calnexin KOs. Before we speculate as to what these observations suggest, we will first address our respirometry results.

5.4.2 Cne1 dampens mitochondrial respiration

Our results demonstrate Cne1 loss significantly increased maximal respiration (Figure 5.3) while Calnexin KOs had lower basal and maximal respiration [259]. However, the measurements in mammalian cells were normalized to citrate synthase activity, as the reaction catalyzed by this enzyme is the rate-limiting step in the TCA [432]. These measurements revealed Calnexin KOs have significantly higher citrate synthase activity compared to WT cells [259]. Thus, although Calnexin KOs have lower SERCA2b activity and therefore decreased ER-mitochondria Ca^{2+} flux and respiration, their TCA is more active [259]. This could be a compensatory mechanism whereby Calnexin KOs adapt to their lower mitochondrial Ca^{2+} content by increasing the activity or efficiency of TCA enzymes. Since we could not obtain citrate synthase activity measurements for our samples, it is possible Δ*cne1* cells also have decreased respiration when normalized to citrate synthase activity. Therefore, it will be important to obtain these measurements in the future. Nevertheless, Δ*cne1* cells displayed better growth on acetate compared to WT cells (Figure 5.2B), which is further evidence that they respire more, regardless of whether they do so more efficiently or not.

A factor that could also alter our respirometry results is oxygen consumption unrelated to mitochondrial respiration. This includes oxygen required for redox reactions catalyzed by ER oxidoreductases and peroxisomal oxidases, which catalyze fatty acid oxidation [433,434]. Since we are dealing with strains lacking ER folding assistants, changes in oxygen consumption in the ER are likely occurring. Hence, it will be important to assay for oxygen consumption by ER oxidoreductases by blocking mitochondrial oxygen consumption with ATP synthase inhibitor triethyltin. This experiment will be particularly important to perform in Δ*eps1* since they accumulate redox-sensitive proteins and are therefore likely to have high ROS and oxidative stress levels [286,287]. Loss of another ER-localized oxidoreductase, Grx6, results in a more oxidizing ER lumen, suggesting Δ*eps1* could also have this phenotype [108]. Δ*cne1* cells could also have redox imbalances since Cne1 increases the reductase activity of Mpd1 [283]. There is some

evidence yeast PDI family members can compensate for each other [281,283], so it is also possible loss of Eps1 or Cne1, and in turn Mpd1 activity, does not cause significant redox or respiration changes. ROS measurements will allow us to test these hypotheses in the future. This can be done with dihyroethidium (DHE), a quantifiable fluorescent ROS probe.

5.4.3 Cne1 modulates the MAM but in an opposite manner as Calnexin

Growth on non-fermentable carbons has been previously used to investigate mitochondrial metabolism in yeast, including the metabolism of ERMES mutants [35]. Our growth assays on YPA confirm Δ*gem1* and Δ*mdm34* have limited growth on non-fermentable carbons, as previously published [35,36]. This phenotype in ERMES mutants was originally attributed to a decrease in ER-mitochondria Ca^{2+} flux arising from their disrupted MAMs, which would result in lower mitochondrial respiration and hence, inhibited growth on non-fermentable carbons [35,36]. Our results show Δ*cne1* has a small but significant Ca^{2+}-dependent (Figure 5.2E) growth advantage on YPA (Figure 5.2B) as well as a higher maximal respiration rate (Figure 5.3). Thus, their improved growth on YPA is very likely dependent on ER-mitochondria Ca^{2+} flux. Together, these results strongly suggest Cne1 inhibits ER-mitochondria MCS, ER-mitochondria Ca^{2+} flux, and mitochondrial respiration. Interestingly, these results are largely those observed in Calnexin KOs, which have low ER-mitochondria Ca^{2+} flux and low respiration, but a higher MAM coefficient and higher incidence of long ER-mitochondria contacts [259]. Therefore, our results argue Cne1 can modulate the MAM, but has largely the opposite effect of Calnexin.

This is likely due to differences in how Cne1 regulates ER Ca^{2+} as opposed to Calnexin. It could also be due to differences in redox regulation in *S. cerevisiae.* Indeed, it remains unclear if Cne1 regulates ER-mitochondria contacts through the same mechanism as Calnexin: SERCA2b Ca^{2+} pump activation [259]. Since BAPTA-AM was able to eliminate the growth advantage of Δ*cne1* on YPA, this strongly suggests Cne1's absence increases mitochondrial Ca^{2+} uptake. To test if Cne1 mediates this effect similarly to Calnexin, a co-immunoprecipitation for the SERCA functional homolog Pmr1 should be performed. The ER-localized ATPase Spf1/Cod1 and the Ca^{2+}/H^{+} antiporter Gdt1/Grc1 should also be tested. An interaction with any of these candidates suggests Cne1 could regulate their folding or Mpd1-mediated redox regulation. For example, if Cne1 participates in Pmr1 folding, then Cne1 loss could phenocopy Δ*pmr1*, which have low luminal Ca^{2+} [92,98,101,102]. This decrease in ER Ca^{2+} could lead to a decrease in ER-mitochondria

Ca^{2+} flux such as that observed in Calnexin KOs [259]. However, our results suggest Δ*cne1* cells actually have higher ER-mitochondria Ca^{2+} flux, which could be a result of compensation. Thus, if Δ*cne1* cells have less functional Pmr1, they could adapt by having more ER-mitochondria contacts, which we observed (Figure 5.4B). Although redox regulation of Pmr1 or other ER Ca^{2+} regulators has not been demonstrated in yeast, oxidative stress due to loss of oxidoreductase Grx6 caused a decrease in luminal Ca^{2+} [108]. This strongly suggests redox regulation of ER Ca^{2+} pumps occurs in *S. cerevisiae* as well. Hence, Cne1 could regulate Pmr1 through Mpd1 activity, so Pmr1 redox modifications and redox-dependent changes in Pmr1 activity should also be investigated as previously published for known Mpd1 substrates [435]. These experiments should be performed in conjunction with measurements of luminal Ca^{2+} to detect Pmr1 activity as previously published for Δ*pmr1* cells [92].

5.4.4 Eps1 is not a MAM modulator, unlike its homolog TMX1

To investigate if *S. cerevisiae* folding assistants are also MAM modulators, we sought to identify a TMX1 homolog. Our RBH analysis revealed Eps1 and TMX1 are a RBH pair (Figure 5.1). This is consistent with previous studies demonstrating Eps1 is the only membrane-bound PDI family protein in yeast and functions in ERAD of membrane substrates like TMX1 [278,285,286]. Nevertheless, Eps1 has previously only been hypothesized to be homologous to TMX1 [283]. Thus, our results are the first to demonstrate, through RBH analysis, that Eps1 is the closest *S. cerevisiae* homolog to mammalian TMX1.

Our electron microscopy results revealed Eps1 loss did not alter any of the ER-mitochondria contact site aspects we assessed. Specifically, we observed no changes in MAM length, distance, or number (Figure 5.4B-E), demonstrating Eps1 does not modulate MAM structure. As with Δ*cne1* and both ERMES mutants, hypoxia and glycolysis inhibition did not affect their growth on YPD (Figure 5.2C, D), though Ca^{2+} chelation removed their growth advantage on YPA (Figure 5.2E). This suggests ER-mitochondria Ca^{2+} flux was responsible for their improved fitness when forced to respire. However, we did not observe an increase in respiration in Δ*eps1* (Figure 5.3). We also did not observe any changes in MAM abundance or tethering (Figure 5.4B-E). Together, these results suggest Eps1 loss provides a growth advantage on acetate that is not dependent on an increase in MAMs and/or respiration.

One possible explanation for this is that their mitochondria uptake Ca^{2+} from another source that is not the ER. This could theoretically occur at vCLAMPs or at plasma membrane-mitochondria contact sites. Though Ca^{2+} flux at vCLAMPs has not been reported, vacuolar uptake is the main cytosolic Ca^{2+} buffering system in yeast [186], so it is possible the vacuole could regulate mitochondrial Ca^{2+}. Similarly, though plasma membrane-mitochondria contacts in yeast have not been reported to house Ca^{2+} flux, these MCS in mammals are known to regulate mitochondrial Ca^{2+} [427]. As previously mentioned, TMX1 KD cells had shorter plasma membrane-mitochondria distances [427]. This study suggested these MCS led to the increase in respiration observed in TMX1-silenced cells despite their looser MAMs. Since BAPTA-AM removed Δ*eps1*'s acetate growth advantage (Figure 5.2E), Eps1 loss appears to promote mitochondrial metabolism in a Ca^{2+}-dependent manner. Therefore, it is possible Δ*eps1* have shorter plasma membrane-mitochondria contact sites fueling their TCA cycle.

However, our respirometry analysis demonstrated Eps1 loss has no effect on oxygen consumption (Figure 5.3), suggesting that unlike TMX1 KOs [260], Δ*eps1* did not shift metabolism away from mitochondrial respiration. Specifically, TMX1 loss in mammalian cells lowers mitochondrial respiration when normalized to citrate synthase activity [260]. Given we observed no increase in oxygen consumption in Δ*eps1* (Figure 5.3), the most likely explanation for our results is that these cells have a significantly higher citrate synthase activity. This would explain their Ca^{2+}-dependent growth advantage on YPA despite the fact they did not have more MAMs. Although it is possible these cells also have shorter plasma membrane-mitochondria contact sites like TMX1 KD cells [427], we did not observe any significant changes in MAM numbers or tethering (Figure 5.4B-E), unlike the shorter MAMs observed in mammals. Thus, Δ*eps1* would not require compensatory plasma membrane-mitochondria contact sites. We therefore think it is unlikely mitochondria move closer to the plasma membrane in these cells.

Another factor that could contribute to oxygen consumption in these strains is ER stress. In mammals, ER stress is a well-known inducer of mitochondrial respiration and MAMs [185]. A recent study in *S. cerevisiae* found cells undergoing short term ER stress following incubation with tunicamycin or oxidative stressor DTT had a significant increase in oxygen consumption [184]. This suggests ER and oxidative stress induce mitochondrial respiration in yeast. Although *Δcne1* do not have increased ER stress compared to their WT counterpart, previous studies have shown *Δeps1* cells have higher basal UPR signaling [287]. Our results revealed *Δeps1* cells did not

increase their basal or maximal respiration rates (Figure 5.3), suggesting their high basal ER stress does not induce respiration. One possible explanation for this is that only acute, short term ER stress promotes respiration, while long term stress such as that in strains with high basal UPR, does not.

TMX1 KOs also had a shift towards glycolysis, while Δ*eps1* cells did not, since they had decreased growth on YPD (Figure 5.2A). Δ*eps1* also had no growth advantage over WT cells when glycolysis was coupled with hypoxia (Figure 5.2C), further suggesting Eps1 loss does not significantly induce glycolysis. In summary, our results argue Eps1 does not share TMX1's MAM-related functions. Instead, Eps1 is likely restricted to TMX1's role as a folding assistant, including their shared role in ERAD of membrane proteins [278,286,287].

We also incubated cells with $CoCl_2$•$6H_2O$ to simulate hypoxia and inhibit mitochondrial respiration. This eliminated the small growth defects observed in YPD for Δ*eps1* cells (Figure 5.2A, C). In other words, when respiration is inhibited but glucose is available, Eps1 loss no longer causes glycolysis defects. These puzzling results could be due to the effects of hypoxic stress on cells, which causes a strong upregulation of oxidoreductases [436,437]. Without Eps1, these cells are likely to have redox defects, which would trigger hypoxic stress. Indeed, these cells accumulate proteins requiring disulfide bonds, which can cause oxidative and ER stress [286,287]. Δ*eps1* cells also have higher basal UPR induction [287]. This would in turn upregulate other oxidoreductases. This stress alone could contribute to their growth defect observed in YPD (Figure 5.2A). In addition, these cells are likely better equipped to deal with this kind of stress under minimal hypoxia, since they would already have more oxidoreductases than WT cells. This would likely eliminate their growth defects compared to WT cells, as was observed when cells were incubated with $CoCl_2$•$6H_2O$ (Figure 5.2C). High hypoxia levels could therefore sensitize these cells and result in growth defects instead. This hypothesis could be tested by increasing $CoCl_2$•$6H_2O$ concentration above 1mM, which was tested here (Figure 5.2C).

Chapter 6: Discussion

6.1 Rab32 regulates MAM composition, structure, and function

The MAM is a highly regulated structure that serves as a platform for a multitude of processes. Tethering at the MAM is a dynamic process that responds to the cell's bioenergetic demands, stressors, and Ca^{2+} levels, amongst other variables [15,18,19]. MAM abundance can also change drastically so that ~5-20% of all mitochondrial surface at any one time is engaged in a MERC [15,19]. In this work, we sought to develop a better understanding of proteins known to regulate the MAM. One of these proteins is the small GTPase Rab32, which has been previously shown to influence the MAM proteome, ER-mitochondria Ca^{2+} flux, and mitochondrial fission [267,290,305], amongst its many other functions. One of its additional functions is a poorly understood role in autophagy, with several studies reporting defects in this process with loss of Rab32 [310,311]. Other studies have demonstrated cargo recruitment and traffic in melanosome biogenesis requires Rab32 [300,301,303]. Therefore, we hypothesized Rab32 performs cargo recruitment and/or traffic for biogenesis of another LRO in non-melanogenic cells, the autophagosome.

Overwhelming evidence suggests autophagosome biogenesis in response to starvation-induced autophagy begins at the MAM, where Rab32 is enriched [203–206,290]. This process starts at the omegasome, a PI3P-enriched portion of the ER that acts as a platform for biogenesis of the isolation membrane [206,210]. The ULK1 and PI3K III complexes are then recruited to the MAM with the help of Syntaxin-17, which binds the PI3K III complex subunit Atg14L [203]. This binding is preceded by Syntaxin-17-Rab32 binding, which prevents Rab32 from recruiting PKA to the MAM to inhibit Drp1[307]. Therefore, starvation likely allows Rab32 to change binding partners, potentially to an autophagy-related effector.

In Chapter 3, we demonstrate dominant-active Rab32, Rab32Q85L, induced selective autophagy of the MAM (Figures 3.4, 3.5), which we propose to call "MAMphagy". Rab32Q85L altered MAM composition, as several MAM-localized proteins were significantly reduced (Figure 3.5). MAM structure was also altered with Rab32Q85L, which caused an increase in the distance between the ER and mitochondrial membranes and ~50% decrease in their length (Figure 3.7C,D). Rab32Q85L also delayed apoptosis (Figure 3.12A), suggesting Rab32 alters MAM function. We also identified RTN3L as a *bona fide* effector for Rab32 (Figures 3.8, 3.9). Our results suggest RTN3L is required for MAMphagy since its KD impaired degradation of TMX1 (Figure 3.9D), which was otherwise degraded by ~50% with Rab32Q85L (Figure 3.5A).

Our results also indicated Rab32 KD impaired starvation-induced autophagy (Figure 3.3), suggesting Rab32 is involved in this process. Rab32 KD also caused a significant accumulation of TMX1 in untreated cells (Figure 3.6B), suggesting Rab32 is required for basal degradation of this reductase. However, starvation did not induce degradation of TMX1 in control cells (Figure 3.6A), possibly suggesting starvation does not trigger Rab32-mediated MAMphagy, and consequently, TMX1 degradation. Another possible explanation for these results is that longer starvation periods are required to observe significant changes in TMX1, which was particularly abundant in MCF7 cells (Figure 3.5A). Thus, we cannot conclude whether or not starvation induces Rab32- and RTN3L-dependent MAMphagy. However, given Rab32 KD caused a significant decrease in autophagosome formation (Figure 3.3B) and LC3II levels (Figure 3.3D) during starvation, it appears Rab32 contributes to at least one type of starvation-induced autophagy. Therefore, the most likely scenario is that during starvation, Rab32 participates in non-selective starvation-induced autophagy at the MAM, and not in MAMphagy. In support of this hypothesis, a study reported MERCs increase significantly following starvation-induced autophagy [438]. In stark contrast, we observed Rab32Q85L caused a significant decrease in MERCs (Figure 3.7B). This strongly suggests the process of Rab32-mediated MAMphagy we describe in this work is different from starvation-induced autophagy.

If we incorporate this knowledge into the model of starvation-induced isolation membrane formation at the MAM, Rab32 likely participates in this process after Syntaxin-17 releases it to bind Atg14L. Future research will have to investigate the exact mechanistic role of Rab32 in this type of non-selective autophagy. For example, future experiments could investigate if Rab32 has any other autophagy-related effectors, particularly those known to become MAM-enriched following starvation. Although we did not find an interaction with Atg14L (Figure 3.8A), other ULK1 and PI3K III subunits should be tested in the future.

A question that arises from these observations is how Rab32 participates in both non-selective starvation-induced autophagy and MAMphagy. Of the models and hypotheses discussed in Chapter 3, we propose the following unifying model (Figure 6.1). As previously published, Syntaxin-17 binds Rab32 and inhibits its AKAP activity in homeostasis, allowing Drp1 to mediate mitochondrial fission as needed [307]. Starvation triggers Syntaxin-17 binding to Atg14L, releasing Rab32 and allowing it to act as an AKAP [307]. Previous research has shown starvation-induced autophagy blocks mitochondrial fission via PKA-mediated inhibition of

Drp1[439]. Drp1 inactivation under these conditions could be mediated by Rab32T39N, which can increase PKA-mediated inhibitory phosphorylation of Drp1 at the MAM [290]. In a third scenario, a yet unknown condition or stressor would instead promote MAMphagy. Since mitophagy requires fission to proceed [387], it is likely MAMphagy has the same requirement. Rab32Q85L does not alter PKA localization [290], suggesting Drp1 can mediate mitochondrial fission when Rab32 is activated. Therefore, we propose Drp1-mediated fission precedes MAMphagy. It is unclear how RTN3L is recruited and/or activated at the MAM, but one possibility is that it accumulates to promote ER tubulation required for Drp1-mediated mitochondrial fission. This is consistent with its activity as an ER shaping protein [372] and with studies demonstrating ER tubulation at MAMs precedes Drp1-mediated fission [196]. This tubulation could involve RTN3S and RTN3L, but MAMphagy would only be triggered by accumulation and oligomerization of RTN3L.

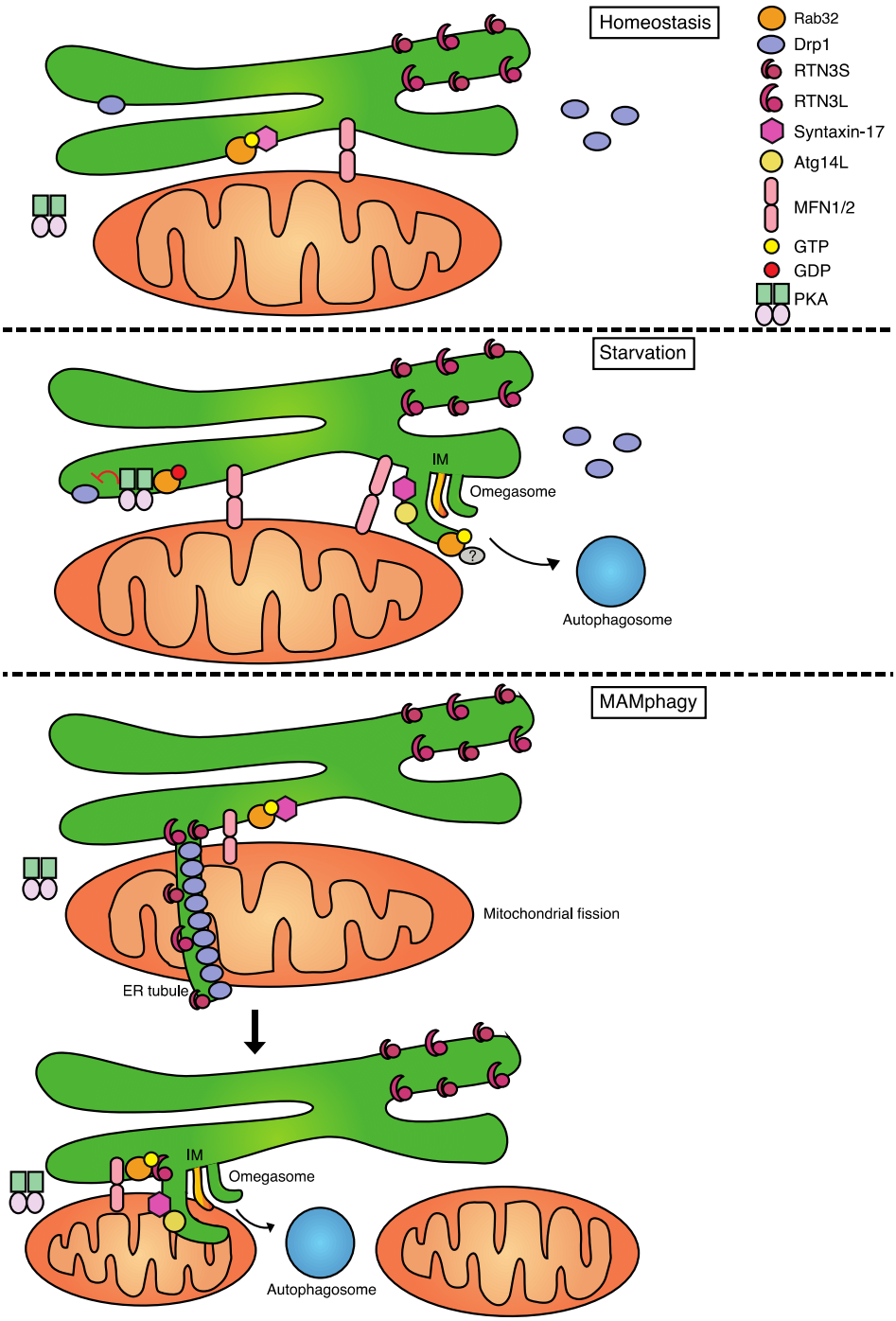

Figure 6.1 Proposed model for Rab32 activities at the MAM
Schematic drawing of the effects of Rab32 on autophagy at the MAM. Starvation triggers bulk autophagy at the MAM, which begins with isolation membrane (IM) biogenesis at the omegasome. Rab32 participates in this process with an unidentified effector. Mitofusin-2 tethering is required for this process as well as MAMphagy. MAMphagy is presumably preceded by Drp1-mediated mitochondrial fission, which occurs when an ER tubule at the MAM extends around a mitochondrion. Given RTN3 maintains ER tubules, we hypothesize both the short and long isoforms of RTN3 will become enriched here. Once fission is complete, MAMphagy can proceed. Here, active Rab32 interacts with RTN3L to promote degradation of the MAM.

6.2 Ypt7 regulation of MAMs in *S. cerevisiae*

Saccharomyces cerevisiae is a model organism that has been extremely useful in the field of MCS. Indeed, studies in *S. cerevisiae* identified the ERMES complex [35] and more recently, vCLAMP, a complex that establishes MCS between the vacuole and mitochondria [347,348]. To deepen our understanding of MAM regulation in *S. cerevisiae,* we sought to identify a functional homolog for the mammalian MAM regulator Rab32. Our phylogenetic analysis identified Ypt7 as the most closely related protein in this organism (Figure 4.1). Although Ypt7 is largely known for its functions in endolysosomal traffic [330,343,344,399,403], more recent research has demonstrated Ypt7 is a component of vCLAMP [347].

Research has shown vCLAMPs and ERMES are regulated by the cell's energetics. Specifically, vCLAMPs were strongly induced when yeast were grown on fermentable carbons compared to non-fermentable carbons [347]. ERMES subunits were instead upregulated on non-fermentable carbons, where yeast are forced to respire. Research in mammalian cells has also identified lysosome-mitochondria MCS [349]. This study reported mitochondrial recruitment of the Rab7 GAP TBCD151 decreased these MCS, suggesting Rab7 activation untethers these organelles.

These studies prompted us to study both ER-mitochondria and vacuole-mitochondria contacts in Ypt7 mutants. Our results on YPD show a mutant strain with dominant-negative Ypt7, Ypt7T22N, had more than double the number of MERCs compared to WT cells (Figure 4.2A). They also had a significantly larger MAM coefficient, suggesting they have more MAM content (Figure 4.2A). We also observed a doubling of vacuole-mitochondria MCS compared to WT cells (Figure 4.2B). Additionally, we investigated growth of this mutant on non-fermentable acetate as a proxy for MAM-dependent activation of respiration. These experiments revealed Ypt7T22N grew significantly worse than WT cells (Figure 4.3A). Together, our results suggest Ypt7 inactivation promotes ERMES and vCLAMP tethering when yeast have access to glucose (Figure 6.2). On acetate, Ypt7 inactivation causes a respiration defect that results in a growth defect.

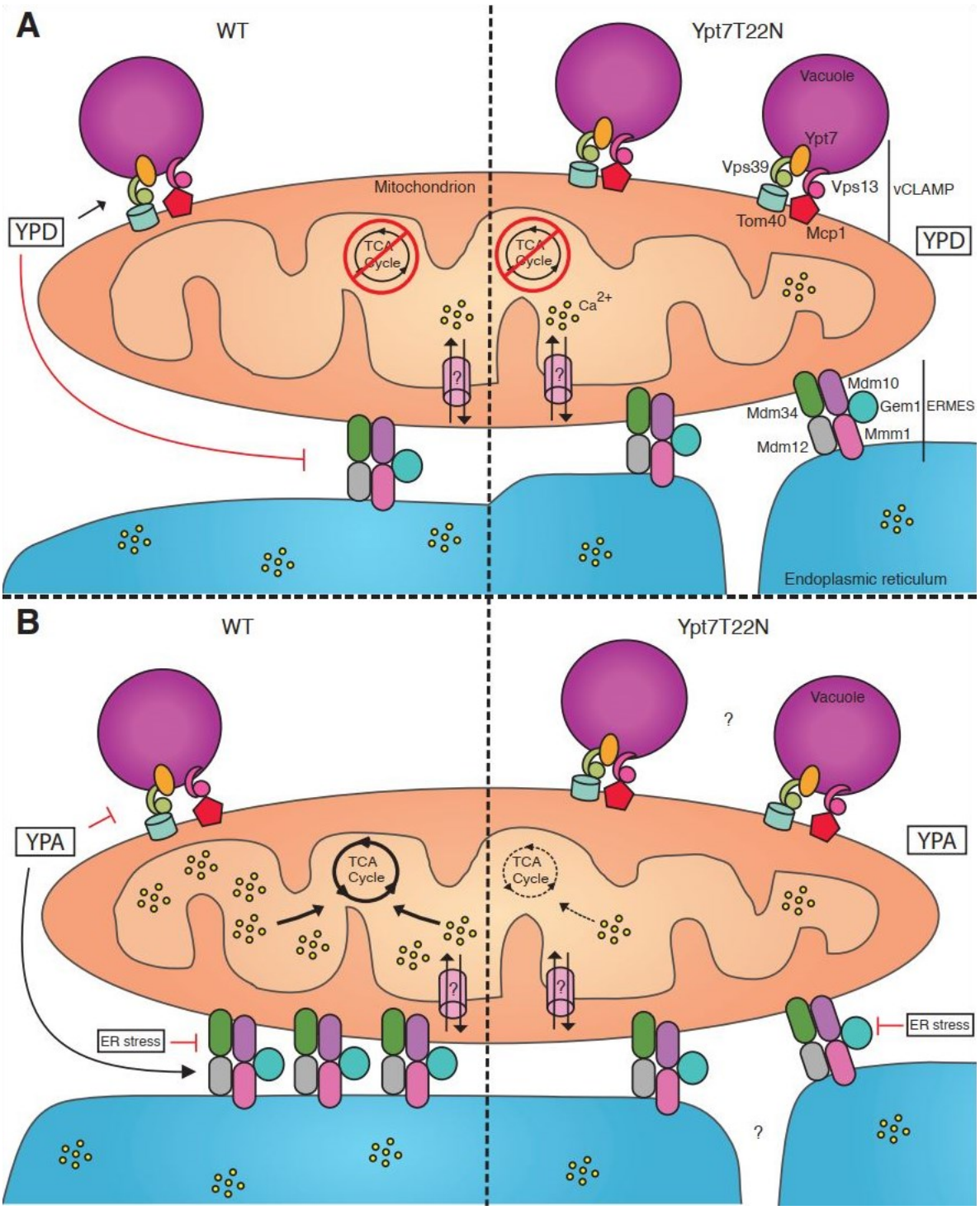

Figure 6.2 Proposed model for dominant-negative Ypt7 effects on MCS in *S. cerevisiae*
A. Schematic for growth in YPD. Ypt7T22N increases MAMs and vCLAMPs. In WT cells YPD increases vCLAMPs and reduces ERMES. Unknown channel mediates mitochondrial Ca^{2+} uptake. **B.** Schematic for growth in YPA. Ypt7T22N have decreased growth, potentially due to lower TCA activity. The status of MCS in YPA in Ypt7T22N remains unknown (?).

These results raise several questions. Firstly, the fact that Ypt7T22N increased MERCs on glucose (Figure 4.2A) but impaired growth when cells were shifted to a respiratory metabolism (Figure 4.3B) was an unexpected result. Ypt7T22N cells have more MERCs than WT cells when grown on glucose (Figure 4.2A), when yeast preferentially perform glycolysis[113] and have been reported to have few ERMES [347]. When yeast were previously shifted to a non-fermentable carbon, ERMES abundance increased [347]. Therefore, the high number of MERCs in Ypt7T22N cells in glucose (Figure 4.2A) should give them an advantage when shifted to acetate (Figure 4.3B). However, these cells grew significantly less than WT cells on acetate (Figure 4.3B), suggesting Ypt7T22N cannot further increase MERCs to the level required for WT growth on acetate. These results could be explained by several scenarios, including: i) Ypt7T22N prevents further MERC upregulation than that observed on glucose ii) Ypt7T22N cells are unable to detect and/or signal a shift towards respiration, or iii) Ypt7T22N cells have inefficient TCA enzymes, so that despite having more MERCs, they have low respiratory capacity.

A number of experiments will be needed to understand this phenotype. Firstly, electron microscopy in YPA should be performed to confirm Ypt7T22N have fewer MERCs than WT cells under these conditions. Secondly, respiration and citrate synthase activity should be measured to confirm this mutant is outperformed by WT on acetate. Ca^{2+} chelation or depletion should also be used to test the effects are dependent on ER-mitochondria Ca^{2+} flux, as we expect.

Another aspect of this work that requires further research is whether Ypt7 mediates these MAM-related effects through the same mechanisms as Rab32. Both Rab32Q85L and Ypt7T22N caused significant changes in MAM length/distance (Figures 3.7B, 4.2A), suggesting MAM content and structure was altered. Interestingly, Ypt7 was required for yeast ERphagy [417], so it is possible Ypt7 also mediates some type of subdomain-specific ERphagy like Rab32. However, it is also possible Ypt7 is required for ERphagy only for its ability to induce autophagosome-vacuole fusion [346,399]. Therefore, it remains unclear if Ypt7 regulates MAM structure via a similar mechanism as Rab32.

In terms of regulation of MAM activity, both Rab32 and Ypt7 appear to regulate ER-mitochondria Ca^{2+} flux, though the mechanisms for these effects remain unknown. Previous research has suggested Rab32Q85L could decrease SERCA2b activity [290]. We hypothesized Ypt7 instead altered MAMs, and in turn ER-mitochondria Ca^{2+} flux, via regulation of vCLAMP formation. As discussed in Chapter 4, several experiments should be performed to confirm this is

the case. Alternatively, Ypt7 could mediate these effects via a mechanism similar to that proposed for Rab32Q85L: regulation of ER Ca^{2+} uptake. This seems unlikely, however, since unlike Rab32, Ypt7 does not localize to the ER and so does not have direct access to ER Ca^{2+} channels and pumps. In brief, the mechanisms for the Ypt7-mediated effects on MAM structure and function we have reported require clarification.

Lastly, another important contribution from our work is evidence that MAMs in yeast are also induced by ER stress. Specifically, Ire inhibition caused a significant growth defect in WT yeast grown on acetate (Figure 4.3C), suggesting respiration, and therefore MAMs, were impaired.

6.3 Cne1 regulation of MAMs in *S. cerevisiae*

Studies in mammals have demonstrated the MAM is particularly enriched in chaperones and oxidoreductases [170]. Additional studies have detailed how many of these proteins regulate the activity of IP_3R and SERCA2b, resulting in changes in ER-mitochondria Ca^{2+} flux. SERCA2b ATPase activity is significantly lower in Calnexin KOs, suggesting this chaperone is required to sustain SERCA2b activity [259]. This study also revealed Calnexin required the activity of Nox4 and Ero1α to activate SERCA2b. Decreased SERCA2b activity in Calnexin KOs resulted in several MAM-associated defects, including: i) lower ER Ca^{2+}, ii) lower ER-mitochondria Ca^{2+} transfer, iii) lower respiration rates, and iv) tighter MERCs.

In Chapter 5 we demonstrate loss of the Calnexin homolog Cne1 also causes MAM-associated defects. Specifically, our results revealed Δ*cne1* cells have i) more MERCs per cell (Figure 5.4B), ii) looser (Figure 5.4D) and shorter (Figure 5.4E) MERCs, and iii) a lower MAM length/distance ratio (Figure 5.4B), suggesting MAM content decreased. Δ*cne1* cells also had: iv) a higher maximal respiration (Figure 5.3) and v) a Ca^{2+}-dependent growth advantage when respiring in YPA (Figure 5.2B, E). In brief, our results do not fully replicate the effects observed in Calnexin KOs. Instead, they suggest Cne1 dampens maximal respiration, which results in a growth defect when cells are forced to respire on acetate. This growth difference on acetate disappeared with Ca^{2+} chelation, suggesting Cne1 dampens Ca^{2+}-dependent activation of TCA enzymes in mitochondria. In turn, this points towards Cne1 decreasing Ca^{2+} release from the ER.

How Cne1 mediates this process will have to be the focus of future studies. Based on our results and previous research, we propose a model (Figure 6.3) whereby Cne1 determines Mdp1-

mediated redox regulation of Pmr1 since this ATPase is the main determinant of ER Ca^{2+} in yeast, though regulation of Spf1/Cod1 could also occur [102,104]. Recent research has shown redox regulation of Ca^{2+} channel activity by oxidoreductases occurs in *S. cerevisiae*, supporting our hypothesis [262]. Cne1 is known to activate Mpd1 reductase activity [283]. Therefore, we hypothesize Δ*cne1* cells have lower Mpd1 activity and higher ER ROS. We also hypothesize Mpd1 reduces Pmr1 and/or Spf1/Cod1 and promotes their ATPase activity. This would cause Δ*cne1* cells to have lower Pmr1 and/or Spf1/Cod1 activity, resulting in low ER Ca^{2+}, higher cytosolic Ca^{2+}, and higher mitochondrial Ca^{2+}. In turn, this likely increases TCA activity, improving growth on acetate (Figure 5.2B) and increasing respiration (Figure 5.3).

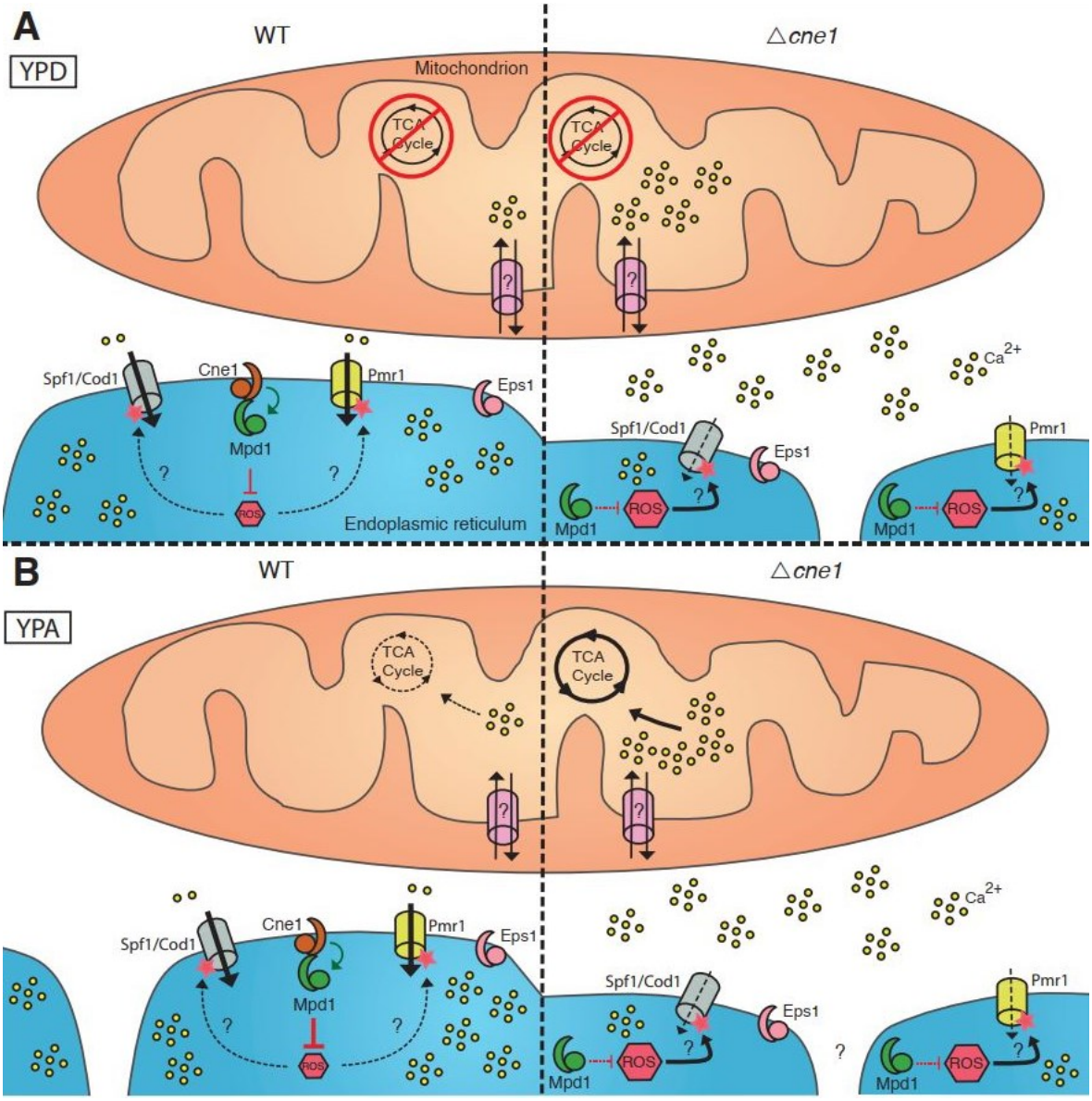

Figure 6.3 Proposed model for Cne1 regulation of *S. cerevisiae* MAMs
A. Schematic of growth on YPD. In WT cells, Cne1 maintains Mpd1 reductase activity, which reduces ROS and presumably activates Pmr1 and/or Spf1/Cod1 in a redox-dependent manner. Redox modification indicated by red star. Δ*cne1* cells have more MAMs, though they are looser and shorter. Loss of Cne1 would result in lower Pmr1 and/or Spf1/Cod1 activity, resulting in higher cytosolic and mitochondria Ca^{2+}. Unknown channel mediates mitochondrial Ca^{2+} uptake. **B.** Schematic of growth on YPA. The status of MAMs in Δ*cne1* cells is unclear (?), though they have a Ca^{2+}-dependent increase in TCA activity.

6.4 Conclusion

In summary, in Chapter 3 we demonstrate Rab32 is capable of a large restructuring of the MAM by promoting its specific degradation when activated. We propose to call this type of selective autophagy that targets ER-mitochondria contacts "MAMphagy". The specificity of this pathway was assayed via immunoblotting of several ER, mitochondrial and MAM proteins, as well as electron microscopy. This process is promoted by activation of the MAM protein Rab32, whose role in autophagy had not been fully explored previously. We also show the long isoform of the ERphagy receptor RTN3, RTN3L, is an effector of GTP-bound Rab32. Together, Rab32 and RTN3L also promote the degradation of Bcl-2 proteins found at the MAM. We also found active Rab32 delayed tunicamycin-induced apoptosis in breast cancer cells. Lastly, patient data showed breast cancer outcomes worsened with high Rab32 and RTN3L mRNA levels, suggesting MAMphagy could be detrimental to the survival of breast cancer patients.

Our work in *S. cerevisiae* revealed two previously unknown regulators of MAM in this organism: Ypt7 and Cne1. Specifically, we show Ypt7 inactivation induces ER-mitochondria MCS formation. When these cells were forced to respire, they grew worse than WT cells. Together, these results suggest Ypt7 inactivation results in lower respiratory capacity, likely due to lower TCA enzyme efficiency, despite their increased MAM content. We also demonstrate Cne1 helps maintain ER-mitochondria MCS. Interestingly, Cne1 appears to simultaneously dampen respiration in a Ca^{2+}-dependent manner, suggesting it regulates ER-mitochondria Ca^{2+} flux.

Together, this work provides new knowledge on how cells regulate MAM tethering, structure, and composition, to adapt to the cell's bioenergetic demands. This knowledge should in turn help scientists better understand this dynamic and complex cellular structure that has been implicated in diseases such as cancer.

References

1. Essner E, Novikoff AB. Cytological studies on two functional hepatomas: Interrelations of endoplasmic reticulurn, golgi apparatus, and lysosomes. *J Cell Biol*. 1962;15(2):289-312. doi:10.1083/jcb.15.2.289
2. Rothman JE, Fine RE. Coated vesicles transport newly synthesized membrane glycoproteins from endoplasmic reticulum to plasma membrane in two successive stages. *Proc Natl Acad Sci U S A*. 1980;77(2 II):780-784. doi:10.1073/pnas.77.2.780
3. Bernhard W, Rouiller C. Close topographical relationship between mitochondria and ergastoplasm of liver cells in a definite phase of cellular activity. *J Biophys Biochem Cytol*. 1956;2(4):73-77.
4. Fawcett DW. Observations on the Cytology and Electron Microscopy of Hepatic Cells. *J Natl Cancer Inst*. 1955;III(Ii):1475-1503.
5. Katz J, Wals PA, Golden S, Raijman L. Mitochondrial-reticular cytostructure in liver cells. *Biochem J*. 1983;214(3):795-813. doi:10.1042/bj2140795
6. Lever JD, Chappell JB. Mitochondria isolated from rat brown adipose tissue and liver. *J Biophys Biochem Cytol*. 1958;4(3):287-290. doi:10.1083/jcb.4.3.287
7. Pickett CB, Rosenstein NR, Jeter RL. The physical association between rat liver mitochondria and rough endoplasmic reticulum. *Exp Cell Res*. 1981;132:225-234.
8. Meier PJ, Spycher MA, Meyer UA. Isolation and characterization of rough endoplasmic reticulum associated with mitochondria from normal rat liver. *BBA - Biomembr*. 1981;646(2):283-297. doi:10.1016/0005-2736(81)90335-7
9. Vance JE. Phospholipid synthesis in a membrane fraction associated with mitochondria. *J Biol Chem*. 1990;265(13):7248-7256. doi:10.1016/s0021-9258(19)39106-9
10. Vance JE. MAM (mitochondria-associated membranes) in mammalian cells: Lipids and beyond. *Biochim Biophys Acta - Mol Cell Biol Lipids*. 2014;1841(4):595-609. doi:10.1016/j.bbalip.2013.11.014
11. Rusiñol AE, Cui Z, Chen MH, Vance JE. A unique mitochondria-associated membrane fraction from rat liver has a high capacity for lipid synthesis and contains pre-Golgi secretory proteins including nascent lipoproteins. *J Biol Chem*. 1994;269(44):27494-27502.
12. Voelker DR. Phosphatidylserine translocation to the mitochondrion is an ATP-dependent process in permeabilized animal cells. *Proc Natl Acad Sci U S A*. 1989;86(24):9921-9925. doi:10.1073/pnas.86.24.9921
13. AhYoung AP, Jiang J, Zhang J, et al. Conserved SMP domains of the ERMES complex bind phospholipids and mediate tether assembly. *Proc Natl Acad Sci U S A*. 2015;112(25):E3179-E3188. doi:10.1073/pnas.1422363112
14. Helle SCJ, Kanfer G, Kolar K, Lang A, Michel AH, Kornmann B. Organization and function of membrane contact sites. *Biochim Biophys Acta - Mol Cell Res*. 2013;1833(11):2526-2541. doi:10.1016/j.bbamcr.2013.01.028
15. Csordás G, Renken C, Várnai P, et al. Structural and functional features and significance of the physical linkage between ER and mitochondria. *J Cell Biol*. 2006;174(7):915-921. doi:10.1083/jcb.200604016
16. De Brito OM, Scorrano L. Mitofusin 2 tethers endoplasmic reticulum to mitochondria. *Nature*. 2008;456(7222):605-610. doi:10.1038/nature07534
17. Giacomello M, Pellegrini L. The coming of age of the mitochondria–ER contact: a matter

of thickness. *Cell Death Differ*. 2016;23(9):1417-1427. doi:10.1038/cdd.2016.52
18. Ilacqua N, Sánchez-álvarez M, Bachmann M, Costiniti V, Del Pozo MA, Giacomello M. Protein localization at mitochondria-ER contact sites in basal and stress conditions. *Front Cell Dev Biol*. 2017;5(DEC):1-14. doi:10.3389/fcell.2017.00107
19. Rizzuto R, Pinton P, Carrington W, et al. Close contacts with the endoplasmic reticulum as determinants of mitochondrial Ca2+ responses. *Science (80-)*. 1998;280(5370):1763-1766. doi:10.1126/science.280.5370.1763
20. Herrera-Cruz MS, Simmen T. Of yeast, mice and men: MAMs come in two flavors. *Biol Direct*. 2017;12(1). doi:10.1186/s13062-017-0174-5
21. Herrera-Cruz MS, Simmen T. Over Six Decades of Discovery and Characterization of the Architecture at Mitochondria-Associated Membranes (MAMs). In: Vol 997. ; 2017:13-31. doi:10.1007/978-981-10-4567-7
22. Ma JH, Shen S, Wang JJ, et al. Comparative proteomic analysis of the mitochondria-associated ER membrane (MAM) in a long-term type 2 diabetic rodent model. *Sci Rep*. 2017;7(1):1-17. doi:10.1038/s41598-017-02213-1
23. Cho I-T, Adelmant G, Lim Y, Marto JA, Cho G, Golden JA. Ascorbate peroxidase proximity labeling coupled with biochemical fractionation identifies promoters of endoplasmic reticulum mitochondrial contacts. *J Biol Chem*. 2017:jbc.M117.795286. doi:10.1074/jbc.M117.795286
24. Hung V, Lam SS, Udeshi ND, et al. Proteomic mapping of cytosol-facing outer mitochondrial and ER membranes in living human cells by proximity biotinylation. 2017:1-39.
25. Kwak C, Shin S, Park JS, et al. Contact-ID, a tool for profiling organelle contact sites, reveals regulatory proteins of mitochondrial-associated membrane formation. *Proc Natl Acad Sci U S A*. 2020;117(22):1-12. doi:10.1073/pnas.1916584117
26. Szabadkai G, Bianchi K, Várnai P, et al. Chaperone-mediated coupling of endoplasmic reticulum and mitochondrial Ca2+ channels. *J Cell Biol*. 2006;175(6):901-911. doi:10.1083/jcb.200608073
27. De vos KJ, Mórotz GM, Stoica R, et al. VAPB interacts with the mitochondrial protein PTPIP51 to regulate calcium homeostasis. *Hum Mol Genet*. 2012;21(6):1299-1311. doi:10.1093/hmg/ddr559
28. Zhao YG, Liu N, Miao G, Chen Y, Zhao H, Zhang H. The ER Contact Proteins VAPA/B Interact with Multiple Autophagy Proteins to Modulate Autophagosome Biogenesis. *Curr Biol*. 2018;28(8):1234-1245.e4. doi:10.1016/j.cub.2018.03.002
29. Iwasawa R, Mahul-Mellier AL, Datler C, Pazarentzos E, Grimm S. Fis1 and Bap31 bridge the mitochondria-ER interface to establish a platform for apoptosis induction. *EMBO J*. 2011;30(3):556-568. doi:10.1038/emboj.2010.346
30. Simmen T, Aslan JE, Blagoveshchenskaya AD, et al. PACS-2 controls endoplasmic reticulum-mitochondria communication and Bid-mediated apoptosis. *EMBO J*. 2005;24(4):717-729. doi:10.1038/sj.emboj.7600559
31. Myhill N, Lynes EM, Nanji JA, et al. The Subcellular Distribution of Calnexin is Mediated by PACS-2. *Mol Biol Cell*. 2008;18(July):3250-3263. doi:10.1091/mbc.E07
32. Filadi R, Greotti E, Turacchio G, Luini A, Pozzan T, Pizzo P. Mitofusin 2 ablation increases endoplasmic reticulum-mitochondria coupling. *Proc Natl Acad Sci U S A*. 2015;112(17):E2174-E2181. doi:10.1073/pnas.1504880112
33. Naon D, Zaninello M, Giacomello M, et al. Critical reappraisal confirms that Mitofusin 2

is an endoplasmic reticulum–mitochondria tether. *Proc Natl Acad Sci*. 2016;113(40):11249-11254. doi:10.1073/pnas.1606786113
34. Herrera-Cruz MS, Simmen T. Cancer: Untethering mitochondria from the endoplasmic reticulum? *Front Oncol*. 2017;7(MAY). doi:10.3389/fonc.2017.00105
35. Kornmann B, Currie E, Collins SR, et al. An ER-Mitochondria Tethering Biology Screen. 2009;325(July):477-482.
36. Kornmann B, Osman C, Walter P. The conserved GTPase Gem1 regulates endoplasmic reticulum-mitochondria connections. *Proc Natl Acad Sci*. 2011;108(34):14151-14156. doi:10.1073/pnas.1111314108
37. Yamano K, Tanaka-Yamano S, Endo T. Mdm10 as a dynamic constituent of the TOB/SAM complex directs coordinated assembly of Tom40. *EMBO Rep*. 2010;11(3):187-193. doi:10.1038/embor.2009.283
38. Hirabayashi Y, Kwon S-K, Paek H, et al. ER-mitochondria tethering by PDZD8 regulates Ca^{2+} dynamics in mammalian neurons. *Science (80-)*. 2017;358(6363):623-630. doi:10.1126/science.aan6009
39. Petrungaro C, Kornmann B. Lipid exchange at ER-mitochondria contact sites: a puzzle falling into place with quite a few pieces missing. *Curr Opin Cell Biol*. 2019;57:71-76. doi:10.1016/j.ceb.2018.11.005
40. Lahiri S, Chao JT, Tavassoli S, et al. A Conserved Endoplasmic Reticulum Membrane Protein Complex (EMC) Facilitates Phospholipid Transfer from the ER to Mitochondria. *PLoS Biol*. 2014;12(10). doi:10.1371/journal.pbio.1001969
41. Wideman JG. The ubiquitous and ancient ER membrane protein complex (EMC): tether or not? *F1000Research*. 2015;4:624. doi:10.12688/f1000research.6944.1
42. Chitwood PJ, Juszkiewicz S, Guna A, Shao S, Hegde RS. EMC Is Required to Initiate Accurate Membrane Protein Topogenesis. *Cell*. 2018;175(6):1507-1519.e16. doi:10.1016/j.cell.2018.10.009
43. Shurtleff MJ, Itzhak DN, Hussmann JA, et al. The ER membrane protein complex interacts cotranslationally to enable biogenesis of multipass membrane proteins. *Elife*. 2018;7:1-23. doi:10.7554/eLife.37018
44. Shiao YJ, Lupo G, Vance JE. Evidence that phosphatidylserine is imported into mitochondria via a mitochondria-associated membrane and that the majority of mitochondrial phosphatidylethanolamine is derived from decarboxylation of phosphatidylserine. *J Biol Chem*. 1995;270(19):11190-11198. doi:10.1074/jbc.270.19.11190
45. Stone SJ, Vance JE. Phosphatidylserine synthase-1 and -2 are localized to mitochondria-associated membranes. *J Biol Chem*. 2000;275(44):34534-34540. doi:10.1074/jbc.M002865200
46. Claypool SM, Oktay Y, Boontheung P, Loo JA, Koehler CM. Cardiolipin defines the interactome of the major ADP/ATP carrier protein of the mitochondrial inner membrane. *J Cell Biol*. 2008;182(5):937-950. doi:10.1083/jcb.200801152
47. Gonzalvez F, Schug ZT, Houtkooper RH, et al. Cardiolipin provides an essential activating platform for caspase-8 on mitochondria. *J Cell Biol*. 2008;183(4):681-696. doi:10.1083/jcb.200803129
48. Galmes R, Houcine A, Vliet AR, Agostinis P, Jackson CL, Giordano F. ORP5/ORP8 localize to endoplasmic reticulum–mitochondria contacts and are involved in mitochondrial function. *EMBO Rep*. 2016;17(6):800-810. doi:10.15252/embr.201541108

49. Lewin TM, Kim JH, Granger DA, Vance JE, Coleman RA. Acyl-CoA Synthetase Isoforms 1, 4, and 5 are Present in Different Subcellular Membranes in Rat Liver and Can Be Inhibited Independently. *J Biol Chem*. 2001;276(27):24674-24679. doi:10.1074/jbc.M102036200
50. Bravo-sagua R, Parra V, Navarro-marquez COM, et al. Caveolin-1 impairs PKA-DRP1-mediated remodelling of ER–mitochondria communication during the early phase of ER stress. *Cell Death Differ*. 2018;1. doi:10.1038/s41418-018-0197-1
51. Elbaz-Alon Y, Eisenberg-Bord M, Shinder V, et al. Lam6 Regulates the Extent of Contacts between Organelles. *Cell Rep*. 2015;12(1):7-14. doi:10.1016/j.celrep.2015.06.022
52. Murley A, Sarsam RD, Toulmay A, Yamada J, Prinz WA, Nunnari J. Ltc1 is an ER-localized sterol transporter and a component of ER-mitochondria and ER-vacuole contacts. *J Cell Biol*. 2015;209(4):539-548. doi:10.1083/jcb.201502033
53. Giordano F. Non-vesicular lipid trafficking at the endoplasmic reticulum–mitochondria interface. *Biochem Soc Trans*. 2018;(March):BST20160185. doi:10.1042/BST20160185
54. Yamashita S, Nikawa J ichi. Phosphatidylserine synthase from yeast. *Biochim Biophys Acta - Lipids Lipid Metab*. 1997;1348(1-2):228-235. doi:10.1016/S0005-2760(97)00102-1
55. Trotter PJ, Voelker DR. Identification of a non-mitochondrial phosphatidylserine decarboxylase activity (PSD2) in the yeast Saccharomyces cerevisiae. *J Biol Chem*. 1995;270(11):6062-6070. doi:10.1074/jbc.270.11.6062
56. Friedman JR, Kannan M, Toulmay A, et al. Lipid Homeostasis Is Maintained by Dual Targeting of the Mitochondrial PE Biosynthesis Enzyme to the ER. *Dev Cell*. 2018;44(2):261-270.e6. doi:10.1016/j.devcel.2017.11.023
57. Patergnani S, Suski JM, Agnoletto C, et al. Calcium signaling around Mitochondria Associated Membranes (MAMs). *Cell Commun Signal*. 2011;9:1-10. doi:10.1186/1478-811X-9-19
58. Rizzuto R, Pozzan T. Microdomains of intracellular Ca2+: Molecular determinants and functional consequences. *Physiol Rev*. 2006;86(1):369-408. doi:10.1152/physrev.00004.2005
59. Rizzuto R, Simpson AW, Brini M, Pozzan T. Rapid changes of mitochondrial Ca2+ revealed by specifically targeted recombinant aequorin. *Nature*. 1992;358:325-327.
60. Kaufman RJ, Malhotra JD. Calcium trafficking integrates endoplasmic reticulum function with mitochondrial bioenergetics. *Biochim Biophys Acta - Mol Cell Res*. 2014;1843(10):2233-2239. doi:10.1016/j.bbamcr.2014.03.022
61. Van Coppenolle F, Vanden Abeele F, Slomianny C, et al. Ribosome-translocon complex mediates calcium leakage from endoplasmic reticulum stores. *J Cell Sci*. 2004;117(18):4135-4142. doi:10.1242/jcs.01274
62. Biden TJ, Wollheim CB, Schlegelq W. Inositol 1,4,5-Trisphosphate and Intracellular Ca homeostasis in Clonal Pituitary cells (GH3). *Jo*. 1986;261(16):7223-7229.
63. Csordás G, Hajnóczky G. Sorting of calcium signals at the junctions of endoplasmic reticulum and mitochondria. *Cell Calcium*. 2001;29(4):249-262. doi:10.1054/ceca.2000.0191
64. Mallilankaraman K, Doonan P, Cárdenas C, et al. MICU1 is an essential gatekeeper for mcu-mediated mitochondrial Ca 2+ uptake that regulates cell survival. *Cell*. 2012;151(3):630-644. doi:10.1016/j.cell.2012.10.011
65. Mendes CCP, Gomes DA, Thompson M, et al. The type III inositol 1,4,5-trisphosphate

receptor preferentially transmits apoptotic Ca2+ signals into mitochondria. *J Biol Chem*. 2005;280(49):40892-40900. doi:10.1074/jbc.M506623200
66. Bartok A, Weaver D, Golenár T, et al. IP3 receptor isoforms differently regulate ER-mitochondrial contacts and local calcium transfer. *Nat Commun*. 2019;10(1):3726. doi:10.1038/s41467-019-11646-3
67. Berridge MJ. Rapid accumulation of inositol trisphosphate reveals that agonists hydrolyse polyphosphoinositides instead of phosphatidylinositol. *Biochem J*. 1983;212(3):849-858. doi:10.1042/bj2120849
68. Bootman MD, Berridge MJ, Taylor CW. All-or-nothing Ca2+ mobilization from the intracellular stores of single histamine-stimulated HeLa cells. *J Physiol*. 1992;450(1):163-178. doi:10.1113/jphysiol.1992.sp019121
69. Bingham Smith J, Smith L, Higgins BL. Temperature and nucleotide dependence of calcium release by myo-inositol 1,4,5-triphosphate in cultured vascular smooth muscle cells. *J Biol Chem*. 1985;260(27):14413-14416. doi:10.1016/S0021-9258(17)38581-2
70. Finch EA, Turner TJ, Goldin SM. Calcium as a coagonist of inositol 1,4,5-trisphosphate-induced calcium release. *Science (80-)*. 1991;252(5004):443-446. doi:10.1126/science.2017683
71. Bezprozvanny I, Watras J, Ehrlich BE. Bell-shaped calcium-response curves of lns(1,4,5)P3- and calcium-gated channels from endoplasmic reticulum of cerebellum. *Nature*. 1991;6329(June 1991):751-754.
72. Tu H, Wang Z, Bezprozvanny I. Modulation of mammalian inositol 1,4,5-trisphosphate receptor isoforms by calcium: A role of calcium sensor region. *Biophys J*. 2005;88(2):1056-1069. doi:10.1529/biophysj.104.049601
73. Betzenhauser MJ, Wagner LE, Iwai M, Michikawa T, Mikoshiba K, Yule DI. ATP modulation of Ca2+ release by type-2 and type-3 inositol (1, 4, 5)-triphosphate receptors: Differing ATP sensitivities and molecular determinants of action. *J Biol Chem*. 2008;283(31):21579-21587. doi:10.1074/jbc.M801680200
74. Pacher P, Csordás G, Schneider TG, Hajnóczky G. Quantification of calcium signal transmission from sarco-endoplasmic reticulum to the mitochondria. *J Physiol*. 2000;529(3):553-564. doi:10.1111/j.1469-7793.2000.00553.x
75. De Stefani D, Raffaello A, Teardo E, Szabo I, Rizzuto R. A 40 kDa protein of the inner membrane is the mitochondrial calcium uniporter. *Nature*. 2014;476(7360):336-340. doi:10.1038/nature10230.A
76. Phillips MJ, Voeltz GK. Structure and function of ER membrane contact sites with other organelles. *Nat Rev Mol Cell Biol*. 2016;17(2):69-82. doi:10.1038/nrm.2015.8
77. Wang HJ, Guay G, Pogan L, Sauvé R, Nabi IR. Calcium regulates the association between mitochondria and a smooth subdomain of the endoplasmic reticulum. *J Cell Biol*. 2000;150(6):1489-1497. doi:10.1083/jcb.150.6.1489
78. Palty R, Silverman WF, Hershfinkel M, et al. NCLX is an essential component of mitochondrial Na+/Ca 2+ exchange. *Proc Natl Acad Sci U S A*. 2010;107(1):436-441. doi:10.1073/pnas.0908099107
79. Baker DL, Dave V, Reed T, Misra S, Periasamy M. A novel E box/AT-rich element is required for muscle-specific expression of the sarcoplasmic reticulum Ca2+-ATPase (SERCA2) gene. *Nucleic Acids Res*. 1998;26(4):1092-1098. doi:10.1093/nar/26.4.1092
80. Roderick HL, Lechleiter JD, Camacho P. Cytosolic phosphorylation of calnexin controls intracellular Ca2+ oscillations via an interaction with SERCA2b. *J Cell Biol*.

2000;149(6):1235-1247. doi:10.1083/jcb.149.6.1235
81. Appenzeller-Herzog C, Simmen T. ER-luminal thiol/selenol-mediated regulation of Ca $^{2+}$ signalling. *Biochem Soc Trans*. 2016;44(2):452-459. doi:10.1042/BST20150233
82. Wu MM, Buchanan JA, Luik RM, Lewis RS. Ca2+ store depletion causes STIM1 to accumulate in ER regions closely associated with the plasma membrane. *J Cell Biol*. 2006;174(6):803-813. doi:10.1083/jcb.200604014
83. Varnai P, Hunyady L, Balla T. STIM and ORAI, the long awaited constituents of store-operated calcium entry. *Bone*. 2008;23(1):1-7. doi:10.1016/j.tips.2008.11.005.STIM
84. Van Vliet AR, Agostinis P. When under pressure, get closer: PERKing up membrane contact sites during ER stress. *Biochem Soc Trans*. 2016;44(2):499-504. doi:10.1042/BST20150272
85. Sampieri A, Santoyo K, Asanov A, Vaca L. Association of the IP3R to STIM1 provides a reduced intraluminal calcium microenvironment, resulting in enhanced store-operated calcium entry. *Sci Rep*. 2018;8(1):1-13. doi:10.1038/s41598-018-31621-0
86. Cui J, Kaandorp JA, Sloot PMA, Lloyd CM, Filatov M V. Calcium homeostasis and signaling in yeast cells and cardiac myocytes. *FEMS Yeast Res*. 2009;9(8):1137-1147. doi:10.1111/j.1567-1364.2009.00552.x
87. Cui J, Kaandorp JA, Ositelu OO, et al. Simulating calcium influx and free calcium concentrations in yeast. *Cell Calcium*. 2009;45(2):123-132. doi:10.1016/j.ceca.2008.07.005
88. Eilam Y, Lavi H, Grossowicz N. Cytoplasmic Ca2+ homeostasis maintained by a vacuolar Ca2+ transport system in the yeast Saccharomyces cerevisiae. *J Gen Microbiol*. 1985;131(3):623-629. doi:10.1099/00221287-131-6-1551
89. D'hooge P, Coun C, Eyck V Van, et al. Ca 2 + homeostasis in the budding yeast Saccharomyces cerevisiae : Impact of ER / Golgi Ca 2 + storage. *Cell Calcium*. 2015;58(2):226-235. doi:10.1016/j.ceca.2015.05.004
90. Denis V, Cyert MS. Internal Ca2+ release in yeast is triggered by hypertonic shock and mediated by a TRP channel homologue. *J Cell Biol*. 2002;156(1):29-34. doi:10.1083/jcb.200111004
91. Cunningham KW. Acidic calcium stores of Saccharomyces cerevisiae. *Cell Calcium*. 2011;50(2):129-138. doi:10.1016/j.ceca.2011.01.010
92. Strayle J, Pozzan T, Rudolph HK. Steady-state free Ca2+ in the yeast endoplasmic reticulum reaches only 10 μM and is mainly controlled by the secretory pathway pump Pmr1. *EMBO J*. 1999;18(17):4733-4743. doi:10.1093/emboj/18.17.4733
93. Muller EM, Mackin NA, Erdman SE, Cunningham KW. Fig1p facilitates Ca2+ influx and cell fusion during mating of Saccharomyces cerevisiae. *J Biol Chem*. 2003;278(40):38461-38469. doi:10.1074/jbc.M304089200
94. Martin DC, Kim H, Mackin NA, et al. New regulators of a high affinity Ca2+ influx system revealed through a genome-wide screen in yeast. *J Biol Chem*. 2011;286(12):10744-10754. doi:10.1074/jbc.M110.177451
95. Locke EG, Bonilla M, Liang L, Takita Y, Cunningham KW. A Homolog of Voltage-Gated Ca2+Channels Stimulated by Depletion of Secretory Ca2+ in Yeast. *Mol Cell Biol*. 2000;20(18):6686-6694. doi:10.1128/mcb.20.18.6686-6694.2000
96. Popa CV, Dumitru I, Ruta LL, Danet AF, Farcasanu IC. Exogenous oxidative stress induces Ca2+ release in the yeast Saccharomyces cerevisiae. *FEBS J*. 2010;277(19):4027-4038. doi:10.1111/j.1742-4658.2010.07794.x

97. Bonilla M, Nastase KK, Cunningham KW. Essential role of calcineurin in response to endoplasmic reticulum stress. *EMBO J*. 2002;21(10):2343-2353. doi:10.1093/emboj/21.10.2343
98. Dürr G, Strayle J, Plemper R, et al. The medial-Golgi ion pump Pmr1 supplies the yeast secretory pathway with Ca2+ and Mn2+ required for glycosylation, sorting, and endoplasmic reticulum-Associated protein degradation. *Mol Biol Cell*. 1998;9(5):1149-1162. doi:10.1091/mbc.9.5.1149
99. Demaegd D, Foulquier F, Colinet AS, et al. Newly characterized Golgi-localized family of proteins is involved in calcium and pH homeostasis in yeast and human cells. *Proc Natl Acad Sci U S A*. 2013;110(17):6859-6864. doi:10.1073/pnas.1219871110
100. Liu W. Control of Calcium in Yeast Cells Yeast. In: *Introduction to Modeling Biological Cellular Control Systems*. ; 2012:95-122. doi:10.1007/978-88-470-2490-8
101. Antebi A, Fink GR. The yeast Ca2+-ATPase homologue, PMR1, is required for normal Golgi function and localizes in a novel Golgi-like distribution. *Mol Biol Cell*. 1992;3(6):633-654. doi:10.1091/mbc.3.6.633
102. Vashist S, Frank CG, Jakob CA, Ng DTW. Two Distinctly localized P-Type ATPases Collaborate to Maintain Organelle Homeostasis Required for Glycoprotein Processing and Quality Control. *Mol Biol Cell*. 2002;13(June):1977-2000. doi:10.1091/mbc.02
103. Cronin SR, Khoury A, Ferry DK, Hampton RY. Regulation of HMG-CoA reductase degradation requires the P-type ATPase Cod1p/Spf1p. *J Cell Biol*. 2000;148(5):915-924. doi:10.1083/jcb.148.5.915
104. Cronin SR, Rao R, Hampton RY. Cod1p/Spf1p is a P-type ATPase involved in ER function and Ca2+ homeostasis. *J Cell Biol*. 2002;157(6):1017-1028. doi:10.1083/jcb.200203052
105. Sørensen DM, Holen HW, Pedersen JT, et al. The P5A ATPase Spf1p is stimulated by phosphatidylinositol 4-phosphate and influences cellular sterol homeostasis. *Mol Biol Cell*. 2019;30(9):1069-1084. doi:10.1091/mbc.E18-06-0365
106. Tanida I, Takita Y, Hasegawa A, Ohya Y, Anraku Y. Yeast Cls2p/Csg2p localized on the endoplasmic reticumul membrane regulates a non-exchangeable intracellular Ca2+ pool cooperatively with calcineurin. 1996;379:38-42.
107. Takita Y, Ohya Y, Anraku Y. The CLS2 gene encodes a protein with multiple membrane-spanning domains that is important Ca2+ tolerance in yeast. *MGG Mol Gen Genet*. 1995;246(3):269-281. doi:10.1007/BF00288599
108. Puigpinós J, Casas C, Herrero E. Altered intracellular calcium homeostasis and endoplasmic reticulum redox state in Saccharomyces cerevisiae cells lacking Grx6 glutaredoxin. *Mol Biol Cell*. 2015;26(1):104-116. doi:10.1091/mbc.E14-06-1137
109. Bradshaw PC, Jung DW, Pfeiffer DR. Free Fatty Acids Activate a Vigorous Ca2+:2H+ Antiport Activity in Yeast Mitochondria. *J Biol Chem*. 2001;276(44):40502-40509. doi:10.1074/jbc.M105062200
110. McCormack JG, Denton RM. The role of Ca2+ ions in the regulation of intramitochondrial metabolism and energy production in rat heart. *J Mol Cell Cardiol*. 1988;20:24. doi:10.1016/0022-2828(88)90256-8
111. Territo PR, Mootha VK, French SA, et al. Ca2+ activation of heart mitochondrial oxidative phosphorylation: role of the F0/F1-ATPase. *Am J Physiol Physiol*. 2000;(2):17-20.
112. Cárdenas C, Miller RA, Smith I, et al. Essential Regulation of Cell Bioenergetics by

Constitutive InsP3 Receptor Ca2+ Transfer to Mitochondria. *Cell*. 2010;142(2):270-283. doi:10.1016/j.cell.2010.06.007
113. Lee YJ, Jang JW, Kim KJ, Maeng PJ. TCA cycle- independent acetate metabolism via the glyoxylate cycle in Saccharomyces cerevisiae. *Yeast*. 2011;1(November 2010):153-166. doi:10.1002/yea
114. Xiberras J, Klein M, Nevoigt E. Glycerol as a substrate for Saccharomyces cerevisiae based bioprocesses – Knowledge gaps regarding the central carbon catabolism of this 'non-fermentable' carbon source. *Biotechnol Adv*. 2019;37(6):107378. doi:10.1016/j.biotechadv.2019.03.017
115. Martins VM, Fernandes TR, Lopes D, et al. Contacts in Death: The Role of the ER–Mitochondria Axis in Acetic Acid-Induced Apoptosis in Yeast. *J Mol Biol*. 2019;431(2):273-288. doi:10.1016/j.jmb.2018.11.002
116. Uribe S, Rangel P, Pardo JP. Interactions of calcium with yeast mitochondria. *Cell Calcium*. 1992;13(4):211-217. doi:10.1016/0143-4160(92)90009-H
117. Tisi R, Rigamonti M, Groppi S, Belotti F. Calcium homeostasis and signaling in fungi and their relevance for pathogenicity of yeasts and filamentous fungi. *AIMS Mol Sci*. 2016;3(September):505-549. doi:10.3934/molsci.2016.4.505
118. Crompton M, Ellinger H, Costi A. Inhibition by cyclosporin A of a Ca2+-dependent pore in heart mitochondria activated by inorganic phosphate and oxidative stress. *Biochem J*. 1988;255(1):357-360.
119. Baffy G, Miyashita T, Williamson JR, Reed JC. Apoptosis induced by withdrawal of interleukin-3 (IL-3) from an IL-3- dependent hematopoietic cell line is associated with repartitioning of intracellular calcium and is blocked by enforced Bcl-2 oncoprotein production. *J Biol Chem*. 1993;268(9):6511-6519. doi:10.1016/s0021-9258(18)53280-4
120. Scorrano L, Oakes SA, Opferman JT, et al. BAX and BAK regulation of endoplasmic reticulum Ca2+: A control point for apoptosis. *Science (80-)*. 2003;300(5616):135-139. doi:10.1126/science.1081208
121. Pinton P, Ferrari D, Rapizzi E, Di Virgilio F, Pozzan T, Rizzuto R. The Ca2+ concentration of the endoplasmic reticulum is a key determinant of ceramide-induced apoptosis: Significance for the molecular mechanism of Bcl-2 action. *EMBO J*. 2001;20(11):2690-2701. doi:10.1093/emboj/20.11.2690
122. Alavian KN, Beutner G, Lazrove E, et al. An uncoupling channel within the c-subunit ring of the F1F O ATP synthase is the mitochondrial permeability transition pore. *Proc Natl Acad Sci U S A*. 2014;111(29):10580-10585. doi:10.1073/pnas.1401591111
123. Baines CP, Kaiser RA, Sheiko T, Craigen WJ, Molkentin JD. Voltage-dependent anion channels are dispensable for mitochondrial-dependent cell death. *Nat Cell Biol*. 2007;9(5):550-555. doi:10.1038/ncb1575
124. Vervliet T, Parys JB, Bultynck G. Bcl-2 proteins and calcium signaling: Complexity beneath the surface. *Oncogene*. 2016;35(39):5079-5092. doi:10.1038/onc.2016.31
125. Cheng EHY, Wei MC, Weiler S, et al. BCL-2, BCL-XL sequester BH3 domain-only molecules preventing BAX- and BAK-mediated mitochondrial apoptosis. *Mol Cell*. 2001;8(3):705-711. doi:10.1016/S1097-2765(01)00320-3
126. Gavathiotis E, Suzuki M, Davis ML, et al. BAX activation is initiated at a novel interaction site. *Nature*. 2008;455(7216):1076-1081. doi:10.1038/nature07396
127. Puthalakath H, Huang DCS, O'Reilly LA, King SM, Strasser A. The proapoptotic activity of the Bcl-2 family member Bim is regulated by interaction with the dynein motor

complex. *Mol Cell*. 1999;3(3):287-296. doi:10.1016/S1097-2765(00)80456-6
128. Monaco G, Beckers M, Ivanova H, et al. Profiling of the Bcl-2/Bcl-XL-binding sites on type 1 IP3 receptor. *Biochem Biophys Res Commun*. 2012;428(1):31-35. doi:10.1016/j.bbrc.2012.10.002
129. Monaco G, Decrock E, Arbel N, et al. The BH4 domain of anti-apoptotic Bcl-XL, but not that of the related Bcl-2, limits the voltage-dependent anion channel 1 (VDAC1)-mediated transfer of pro-apoptotic Ca2+ signals to mitochondria. *J Biol Chem*. 2015;290(14):9150-9161. doi:10.1074/jbc.M114.622514
130. Lewis A, Hayashi T, Betenbaugh MJ. Bcl-2 family in inter-organelle modulation of calcium signaling; roles in bioenergetics and cell survival. *J Bioenerg Biomembr*. 2014;46(1):1-15. doi:10.1007/s10863-013-9527-7.Bcl-2
131. Dremina ES, Sharov VS, Kumar K, Zaidi A, Michaelis EK, Schöneich C. Anti-apoptotic protein Bcl-2 interacts with and destabilizes the sarcoplasmic/endoplasmic reticulum Ca2+-ATPase (SERCA). *Biochem J*. 2004;383(2):361-370. doi:10.1042/BJ20040187
132. Shimizu S, Narita M, Tsujimoto Y. BcL-2 family proteins regulate the release of apoptogenic cytochrome c by the mitochondrial channel VDAC (Nature (1999) 399 (438-487)). *Nature*. 1999;399:483-486. doi:10.1038/35037638
133. Pozniakovsky AI, Knorre DA, Markova O V, Hyman AA, Skulachev VP, Severin FF. Role of mitochondria in the pheromone- and amiodarone-induced programmed death of yeast. *J Cell Biol*. 2005;168(2):257-269. doi:10.1083/jcb.200408145
134. Váchová L, Palková Z. Caspases in yeast apoptosis-like death: Facts and artefacts. *FEMS Yeast Res*. 2007;7(1):12-21. doi:10.1111/j.1567-1364.2006.00137.x
135. Kajiwara K, Muneoka T, Watanabe Y, Karashima T, Kitagaki H, Funato K. Perturbation of sphingolipid metabolism induces endoplasmic reticulum stress-mediated mitochondrial apoptosis in budding yeast. *Mol Microbiol*. 2012;86(5):1246-1261. doi:10.1111/mmi.12056
136. Carmona-Gutierrez D, Bauer MA, Zimmermann A, et al. Guidelines and recommendations on yeast cell death nomenclature. *Microb Cell*. 2018;5(1):4-31. doi:10.15698/mic2018.01.607
137. Váchová L, Palková Z. Physiological regulation of yeast cell death in multicellular colonies is triggered by ammonia. *J Cell Biol*. 2005;169(5):711-717. doi:10.1083/jcb.200410064
138. Busti S, Mapelli V, Tripodi F, et al. Respiratory metabolism and calorie restriction relieve persistent endoplasmic reticulum stress induced by calcium shortage in yeast. *Sci Rep*. 2016;6(June):1-17. doi:10.1038/srep27942
139. Yamada A, Yamamoto T, Yoshimura Y, et al. Ca2+-induced permeability transition can be observed even in yeast mitochondria under optimized experimental conditions. *Biochim Biophys Acta - Bioenerg*. 2009;1787(12):1486-1491. doi:10.1016/j.bbabio.2009.07.001
140. Carraro M, Bernardi P. Calcium and reactive oxygen species in regulation of the mitochondrial permeability transition and of programmed cell death in yeast. *Cell Calcium*. 2016;60(2):102-107. doi:10.1016/j.ceca.2016.03.005
141. van Vliet AR, Agostinis P. Mitochondria-associated membranes and ER stress. In: *Coordinating Organismal Physiology Through the Unfolded Protein Response*. ; 2017:73-102. doi:10.1007/82_2017_2
142. Halperin L, Jung J, Michalak M. The many functions of the endoplasmic reticulum

chaperones and folding enzymes. *IUBMB Life*. 2014;66(5):318-326. doi:10.1002/iub.1272
143. Ruddock LW, Molinari M. N-glycan processing in ER quality control. *J Cell Sci*. 2006;119(21):4373-4380. doi:10.1242/jcs.03225
144. Hebert DN, Foellmer B, Helenius A. Calnexin and calreticulin promote folding, delay oligomerization and suppress degradation of influenza hemagglutinin in microsomes. *EMBO J*. 1996;15(12):2961-2968. doi:10.1002/j.1460-2075.1996.tb00659.x
145. Kozlov G, Gehring K. Calnexin cycle – structural features of the ER chaperone system. *FEBS J*. 2020. doi:10.1111/febs.15330
146. Hammond C, Braakman I, Helenius A. Role of N-linked oligosaccharide recognition, glucose trimming, and calnexin in glycoprotein folding and quality control. *Proc Natl Acad Sci U S A*. 1994;91(3):913-917. doi:10.1073/pnas.91.3.913
147. Miller DJ, Fort PE. Heat shock proteins regulatory role in neurodevelopment. *Front Neurosci*. 2018;12(NOV):1-15. doi:10.3389/fnins.2018.00821
148. Bakunts A, Orsi A, Vitale M, et al. Ratiometric sensing of BiP-client versus BiP levels by the unfolded protein response determines its signaling amplitude. *Elife*. 2017;6:1-21. doi:10.7554/eLife.27518
149. Appenzeller-Herzog C, Ellgaard L. The human PDI family: Versatility packed into a single fold. *Biochim Biophys Acta - Mol Cell Res*. 2008;1783(4):535-548. doi:10.1016/j.bbamcr.2007.11.010
150. Darby NJ, Creighton TE. Functional Properties of the Individual Thioredoxin-like Domains of Protein Disulfide Isomerase. *Biochemistry*. 1995;34(37):11725-11735. doi:10.1021/bi00037a009
151. Holmgren A, Soderberg BO, Eklund H, Branden CI. Three dimensional structure of Escherichia coli thioredoxin S2 to 2.8 Å resolution. *Proc Natl Acad Sci U S A*. 1975;72(6):2305-2309. doi:10.1073/pnas.72.6.2305
152. Hetz C, Zhang K, Kaufman RJ. Mechanisms, regulation and functions of the unfolded protein response. *Nat Rev Mol Cell Biol*. 2020;(Box 1):1-18. doi:10.1038/s41580-020-0250-z
153. Credle JJ, Finer-Moore JS, Papa FR, Stroud RM, Walter P. On the mechanism of sensing unfolded protein in the endoplasmic reticulum. *Proc Natl Acad Sci U S A*. 2005;102(52):18773-18784. doi:10.1073/pnas.0509487102
154. Chuan Yin Liu, Schroder M, Kaufman RJ. Ligand-independent dimerization activates the stress response kinases IRE1 and PERK in the lumen of the endoplasmic reticulum. *J Biol Chem*. 2000;275(32):24881-24885. doi:10.1074/jbc.M004454200
155. Liu CY, Wong HN, Schauerte JA, Kaufman RJ. The protein kinase/endoribonuclease IRE1α that signals the unfolded protein response has a luminal N-terminal ligand-independent dimerization domain. *J Biol Chem*. 2002;277(21):18346-18356. doi:10.1074/jbc.M112454200
156. Bertolotti A, Zhang Y, Hendershot LM, Harding HP, Ron D. Dynamic interaction of BiP and ER stress transducers in the unfolded-protein response. *Nat Cell Biol*. 2000;2(6):326-332. doi:10.1038/35014014
157. Shen J, Chen X, Hendershot L, Prywes R. ER stress regulation of ATF6 localization by dissociation of BiP/GRP78 binding and unmasking of Golgi localization signals. *Dev Cell*. 2002;3(10):99-111.
158. Yoshida H, Matsui T, Yamamoto A, Okada T, Mori K. XBP1 mRNA is induced by ATF6 and spliced by IRE1 in response to ER stress to produce a highly active transcription

factor. *Cell*. 2001;107(7):881-891. doi:10.1016/S0092-8674(01)00611-0
159. Harding HP, Zhang Y, Ron D. Protein translation and folding are coupled by an endoplasmic- reticulum-resident kinase. *Nature*. 1999;397(6716):271-274. doi:10.1038/16729
160. Fawcett TW, Martindale JL, Guyton KZ, Hai T, Holbrook NJ. Complexes containing activating transcription factor (ATF)/cAMP-responsive-element-binding protein (CREB) interact with the CCAAT/enhancer-binding protein (C/EBP)–ATF composite site to regulate Gadd153 expression during the stress response. *Biochem J*. 1999;339:135-141. doi:10.1002/9780470753248.ch9
161. Puthalakath H, O'Reilly LA, Gunn P, et al. ER Stress Triggers Apoptosis by Activating BH3-Only Protein Bim. *Cell*. 2007;129(7):1337-1349. doi:10.1016/j.cell.2007.04.027
162. Ruggiano A, Foresti O, Carvalho P. ER-associated degradation: Protein quality control and beyond. *J Cell Biol*. 2014;204(6):869-879. doi:10.1083/jcb.201312042
163. Molinari M, Calanca V, Galli C, Lucca P, Paganetti P. Role of EDEM in the release of misfolded glycoproteins from the calnexin cycle. *Science (80-)*. 2003;299(5611):1397-1400. doi:10.1126/science.1079474
164. Hosokawa N, Wada I, Nagasawa K, Moriyama T, Okawa K, Nagata K. Human XTP3-B forms an endoplasmic reticulum quality control scaffold with the HRD1-SEL1L ubiquitin ligase complex and BiP. *J Biol Chem*. 2008;283(30):20914-20924. doi:10.1074/jbc.M709336200
165. Ushioda R, Hoseki J, Araki K, Jansen G, Thomas DY, Nagata K. ERdj5 is required as a disulfide reductase for degradation of misfolded proteins in the ER. *Science (80-)*. 2008;321(5888):569-572. doi:10.1126/science.1159293
166. Hershko A, Ganoth D, Sudakin V, et al. Components of a system that ligates cyclin to ubiquitin and their regulation by the protein kinase cdc2. *J Biol Chem*. 1994;269(7):4940-4946. doi:10.1016/s0021-9258(17)37636-6
167. Sommer T, Jentsch S. A protein translocation defect linked to ubiquitin conjugation at the endoplasmic reticulum. *Nature*. 1993;365(6442):176-179. doi:10.1038/365176a0
168. Hoseki J, Ushioda R, Nagata K. Mechanism and components of endoplasmic reticulum-associated degradation. *J Biochem*. 2010;147(1):19-25. doi:10.1093/jb/mvp194
169. Hendershot LM, Wei JY, Gaut JR, Lawson B, Freiden PJ, Murti KG. In vivo expression of mammalian BiP ATPase mutants causes disruption of the endoplasmic reticulum. *Mol Biol Cell*. 1995;6(3):283-296. doi:10.1091/mbc.6.3.283
170. Gutiérrez T, Simmen T. Endoplasmic reticulum chaperones tweak the mitochondrial calcium rheostat to control metabolism and cell death. *Cell Calcium*. 2017. doi:10.1016/j.ceca.2017.05.015
171. Vishnu N, Khan MJ, Karsten F, et al. ATP increases within the lumen of the endoplasmic reticulum upon intracellular Ca2+ release. *Mol Biol Cell*. 2014;25(3):368-379. doi:10.1091/mbc.E13-07-0433
172. Michalak M, Parker JMR, Opas M. Ca2+ signaling and calcium binding chaperones of the endoplasmic reticulum. *Cell Calcium*. 2002;32(5-6):269-278. doi:10.1016/S0143416002001884
173. Wang R, McGrath BC, Kopp RF, et al. Insulin secretion and Ca2+ dynamics in β-cells are regulated by PERK (EIF2AK3) in concert with calcineurin. *J Biol Chem*. 2013;288(47):33824-33836. doi:10.1074/jbc.M113.503664
174. van Vliet AR, Giordano F, Gerlo S, et al. The ER Stress Sensor PERK Coordinates ER-

Plasma Membrane Contact Site Formation through Interaction with Filamin-A and F-Actin Remodeling. *Mol Cell*. 2017;65(5):885-899.e6. doi:10.1016/j.molcel.2017.01.020
175. Wu H, Ng BSH, Thibault G. Endoplasmic reticulum stress response in yeast and humans. *Biosci Rep*. 2014;34(4):321-330. doi:10.1042/BSR20140058
176. Okamura K, Kimata Y, Higashio H, Tsuru A, Kohno K. Dissociation of Kar2p/BiP from an ER sensory molecule, Ire1p, triggers the unfolded protein response in yeast. *Biochem Biophys Res Commun*. 2000;279(2):445-450. doi:10.1006/bbrc.2000.3987
177. Cox JS, Walter P. A novel mechanism for regulating activity of a transcription factor that controls the unfolded protein response. *Cell*. 1996;87:1-14. papers3://publication/uuid/1C5E757F-7771-4F4A-BECB-43A63139AB55.
178. Pilon M, Schekman R, Römisch K. Sec61p mediates export of a misfolded secretory protein from the endoplasmic reticulum to the cytosol for degradation. *EMBO J*. 1997;16(15):4540-4548. doi:10.1093/emboj/16.15.4540
179. Hofer AM, Fasolato C, Pozzan T. Capacitative Ca2+ entry is closely linked to the filling state of internal Ca2+ stores: A study using simultaneous measurements of I(CRAC) and intraluminal [Ca2+]. *J Cell Biol*. 1998;140(2):325-334. doi:10.1083/jcb.140.2.325
180. Farcasanu IC, Popa CV, Ruta LL. Calcium and Cell Response to Heavy Metals: Can Yeast Provide an Answer? In: *Calcium and Signal Transduction*. Vol i. ; 2018:23-41. doi:http://dx.doi.org/10.5772/57353
181. Cyert MS. Calcineurin signaling in Saccharomyces cerevisiae: How yeast go crazy in response to stress. *Biochem Biophys Res Commun*. 2003;311(4):1143-1150. doi:10.1016/S0006-291X(03)01552-3
182. Cunningham KW, Fink GR. Ca2+ transport in Saccharomyces cerevisiae. 1994;166:157-166.
183. Cyert MS. Genetic analysis of calmodulin and its targets in Saccharomyces cerevisiae. *Annu Rev Genet*. 2001;35(2):647-672.
184. Knupp J, Arvan P, Chang A. Increased mitochondrial respiration promotes survival from endoplasmic reticulum stress. *Cell Death Differ*. 2018;26(3):487-501. doi:10.1038/s41418-018-0133-4
185. Bravo R, Vicencio JM, Parra V, et al. Increased ER-mitochondrial coupling promotes mitochondrial respiration and bioenergetics during early phases of ER stress. *J Cell Sci*. 2011;124(Pt 13):2143-2152. doi:10.1242/jcs.080762
186. Cyert MS, Philpott CC. Regulation of cation balance in Saccharomyces cerevisiae. *Genetics*. 2013;193(3):677-713. doi:10.1534/genetics.112.147207
187. Saotome M, Safiulina D, Szabadkai G, et al. Bidirectional Ca2+-dependent control of mitochondrial dynamics by the Miro GTPase. *Proc Natl Acad Sci U S A*. 2008;105(52):20728-20733. doi:10.1073/pnas.0808953105
188. Friedman JR, Webster BM, Mastronarde DN, Verhey KJ, Voeltz GK. ER sliding dynamics and ER-mitochondrial contacts occur on acetylated microtubules. *J Cell Biol*. 2010;190(3):363-375. doi:10.1083/jcb.200911024
189. Wang X, Schwarz TL. The Mechanism of Ca2+-Dependent Regulation of Kinesin-Mediated Mitochondrial Motility. *Cell*. 2009;136(1):163-174. doi:10.1016/j.cell.2008.11.046
190. Ishihara N, Eura Y, Mihara K. Mitofusin 1 and 2 play distinct roles in mitochondrial fusion reactions via GTPase activity. *J Cell Sci*. 2004;117(Pt 26):6535-6546. doi:10.1242/jcs.01565

191. Hermann GJ, Thatcher JW, Mills JP, et al. Mitochondrial fusion in yeast requires the transmembrane GTPase Fzo1p. *J Cell Biol*. 1998;143(2):359-373. doi:10.1083/jcb.143.2.359
192. Giacomello M, Pyakurel A, Glytsou C, Scorrano L. The cell biology of mitochondrial membrane dynamics. *Nat Rev Mol Cell Biol*. 2020. doi:10.1038/s41580-020-0210-7
193. Smirnova E, Griparic L, Shurland D-L, Van Der Bliek AM. Drp1 Is Required for Mitochondrial Division in Mammalian Cells. *Mol Biol Cell*. 2001;12(August):2245-2256. https://www.ncbi.nlm.nih.gov/pmc/articles/PMC58592/pdf/mk0801002245.pdf.
194. Bleazard W, McCaffery JM, King EJ, et al. The dynamin-related GTPase Dnm1 regulates mitochondrial fission in yeast. *Nat Cell Biol*. 1999;1(5):298-304. doi:10.1038/13014
195. Murley A, Lackner LL, Osman C, et al. ER-associated mitochondrial division links the distribution of mitochondria and mitochondrial DNA in yeast. 2013:1-16. doi:10.7554/eLife.00422
196. Friedman JR, Lackner LL, West M, DiBenedetto JR, Nunnari J, Voeltz GK. ER tubules mark sites of mitochondrial division. *Science (80-)*. 2011;334(6054):358-362. doi:10.1126/science.1207385
197. Korobova F, Ramabhadran V, Higgs H. An Actin-Dependent Step in Mitochondrial Fission Mediated by the ER-Associated Formin INF2. 2013;339(January):464-468.
198. Mizushima N, Yoshimori T, Ohsumi Y. The Role of Atg Proteins in Autophagosome Formation. *Annu Rev Cell Dev Biol*. 2011;27(1):107-132. doi:10.1146/annurev-cellbio-092910-154005
199. Narendra D, Tanaka A, Suen DF, Youle RJ. Parkin is recruited selectively to impaired mitochondria and promotes their autophagy. *J Cell Biol*. 2008;183(5):795-803. doi:10.1083/jcb.200809125
200. Grumati P, Morozzi G, Hölper S, et al. Full length RTN3 regulates turnover of tubular endoplasmic reticulum via selective autophagy. *Elife*. 2017;6:1-32. doi:10.7554/eLife.25555
201. Lamb CA, Yoshimori T, Tooze SA. The autophagosome: Origins unknown, biogenesis complex. *Nat Rev Mol Cell Biol*. 2013;14(12):759-774. doi:10.1038/nrm3696
202. Kroemer G, Mariño G, Levine B. Autophagy and the Integrated Stress Response. *Mol Cell*. 2010;40(2):280-293. doi:10.1016/j.molcel.2010.09.023
203. Hamasaki M, Furuta N, Matsuda A, et al. Autophagosomes form at ER-mitochondria contact sites. *Nature*. 2013;495(7441):389-393. doi:10.1038/nature11910
204. Biazik J, Ylä-Anttila P, Vihinen H, Jokitalo E, Eskelinen EL. Ultrastructural relationship of the phagophore with surrounding organelles. *Autophagy*. 2015;11(3):439-451. doi:10.1080/15548627.2015.1017178
205. Hayashi-Nishino M, Fujita N, Noda T, Yamaguchi A, Yoshimori T, Yamamoto A. A subdomain of the endoplasmic reticulum forms a cradle for autophagosome formation. *Nat Cell Biol*. 2009;11(12):1433-1437. doi:10.1038/ncb1991
206. Axe EL, Walker SA, Manifava M, et al. Autophagosome formation from membrane compartments enriched in phosphatidylinositol 3-phosphate and dynamically connected to the endoplasmic reticulum. *J Cell Biol*. 2008;182(4):685-701. doi:10.1083/jcb.200803137
207. Hosokawa N, Hara T, Kaizuka T, et al. Nutrient-dependent mTORC1 association with the ULK1-Atg13-FIP200 complex required for autophagy. *Mol Biol Cell*. 2009;20(m):2673-2683. doi:10.1091/mbc.E08
208. Russell RC, Tian Y, Yuan H, et al. ULK1 induces autophagy by phosphorylating Beclin-1

and activating VPS34 lipid kinase. *Nat Cell Biol*. 2013;15(7):741-750. doi:10.1038/ncb2757
209. Garofalo T, Matarrese P, Manganelli V, et al. Evidence for the involvement of lipid rafts localized at the ER-mitochondria associated membranes in autophagosome formation. *Autophagy*. 2016;12(6):917-935. doi:10.1080/15548627.2016.1160971
210. Matsunaga K, Morita E, Saitoh T, et al. Autophagy requires endoplasmic reticulum targeting of the PI3-kinase complex via Atg14L. *J Cell Biol*. 2010;190(4):511-521. doi:10.1083/jcb.200911141
211. Polson HEJ, De Lartigue J, Rigden DJ, et al. Mammalian Atg18 (WIPI2) localizes to omegasome-anchored phagophores and positively regulates LC3 lipidation. *Autophagy*. 2010;6(4):506-522. doi:10.4161/auto.6.4.11863
212. Ylä-Anttila P, Vihinen H, Jokitalo E, Eskelinen EL. 3D tomography reveals connections between the phagophore and endoplasmic reticulum. *Autophagy*. 2009;5(8):1180-1185. doi:10.4161/auto.5.8.10274
213. Mizushima N. A brief history of autophagy from cell biology to physiology and disease. *Nat Cell Biol*. 2018;20(May):521-527. doi:10.1038/s41556-018-0092-5
214. Itakura E, Mizushima N. Characterization of autophagosome formation site by a hierarchical analysis of mammalian Atg proteins. *Autophagy*. 2010;6(6):764-776. doi:10.4161/auto.6.6.12709
215. Kabeya Y, Mizushima N, Ueno T, et al. LC3, a mammalian homolog of yeast Apg8p, is localized in autophagosome membranes after processing. *EMBO J*. 2000;19(21):5720-5728. doi:10.1093/emboj/cdg454
216. Pankiv S, Clausen TH, Lamark T, et al. p62/SQSTM1 binds directly to Atg8/LC3 to facilitate degradation of ubiquitinated protein aggregates by autophagy*[S]. *J Biol Chem*. 2007;282(33):24131-24145. doi:10.1074/jbc.M702824200
217. Zhao YG, Zhang H. Autophagosome maturation: An epic journey from the ER to lysosomes. *J Cell Biol*. 2019;218(3):757-770. doi:10.1083/jcb.201810099
218. Stenmark H. Rab GTPases as coordinators of vesicle traffic. *Nat Rev Mol Cell Biol*. 2009;10(8):513-525. doi:10.1038/nrm2728
219. Harrison RE, Bucci C, Vieira O V., Schroer TA, Grinstein S. Phagosomes Fuse with Late Endosomes and/or Lysosomes by Extension of Membrane Protrusions along Microtubules: Role of Rab7 and RILP. *Mol Cell Biol*. 2003;23(18):6494-6506. doi:10.1128/mcb.23.18.6494-6506.2003
220. Jäger S, Bucci C, Tanida I, et al. Role for Rab7 in maturation of late autophagic vacuoles. *J Cell Sci*. 2004;117(20):4837-4848. doi:10.1242/jcs.01370
221. Jiang P, Nishimura T, Sakamaki Y, et al. The HOPS complex mediates autophagosome-lysosome fusion through interaction with syntaxin 17. *Mol Biol Cell*. 2014;25(8):1327-1337. doi:10.1091/mbc.E13-08-0447
222. Jahn R, Scheller RH. SNAREs - Engines for membrane fusion. *Nat Rev Mol Cell Biol*. 2006;7(9):631-643. doi:10.1038/nrm2002
223. Nakatogawa H, Suzuki K, Kamada Y, Ohsumi Y. Dynamics and diversity in autophagy mechanisms: Lessons from yeast. *Nat Rev Mol Cell Biol*. 2009;10(7):458-467. doi:10.1038/nrm2708
224. Suzuki K, Kirisako T, Kamada Y, Mizushima N, Noda T, Ohsumi Y. The pre-autophagosomal structure organized by concerted functions of APG genes is essential for autophagosome formation. *EMBO J*. 2001;20(21):5971-5981.

doi:10.1093/emboj/20.21.5971
225. Jahreiss L, Menzies FM, Rubinsztein DC. The itinerary of autophagosomes: From peripheral formation to kiss-and-run fusion with lysosomes. *Traffic*. 2008;9(4):574-587. doi:10.1111/j.1600-0854.2008.00701.x
226. Yamamoto A, Masaki R, Tashiro Y. Characterization of the isolation membranes and the limiting membranes of autophagosomes in rat hepatocytes by lectin cytochemistry. *J Histochem Cytochem*. 1990;38(4):573-580. doi:10.1177/38.4.2319125
227. Ravikumar B, Moreau K, Jahreiss L, Puri C, Rubinsztein DC. Plasma membrane contributes to the formation of pre-autophagosomal structures. *Nat Cell Biol*. 2010;12(8):747-757. doi:10.1038/ncb2078
228. Hailey DW, Rambold AS, Satpute-Krishnan P, et al. Mitochondria Supply Membranes for Autophagosome Biogenesis during Starvation. *Cell*. 2010;141(4):656-667. doi:10.1016/j.cell.2010.04.009
229. Tooze SA, Yoshimori T. The origin of the autophagosomal membrane. *Nat Cell Biol*. 2010;12(9):831-835. doi:10.1038/ncb0910-831
230. Ktistakis NT. ER platforms mediating autophagosome generation. *Biochim Biophys Acta - Mol Cell Biol Lipids*. 2019;(February):1-8. doi:10.1016/j.bbalip.2019.03.005
231. Nakatogawa H. Mechanisms governing autophagosome biogenesis. *Nat Rev Mol Cell Biol*. 2020. doi:10.1038/s41580-020-0241-0
232. Gomez-Suaga P, Paillusson S, Stoica R, Noble W, Hanger DP, Miller CCJ. The ER-Mitochondria Tethering Complex VAPB-PTPIP51 Regulates Autophagy. *Curr Biol*. 2017;27(3):371-385. doi:10.1016/j.cub.2016.12.038
233. Zhao YG, Chen Y, Miao G, et al. The ER-Localized Transmembrane Protein EPG-3/VMP1 Regulates SERCA Activity to Control ER-Isolation Membrane Contacts for Autophagosome Formation. *Mol Cell*. 2017;67(6):974-989.e6. doi:10.1016/j.molcel.2017.08.005
234. Wong A, Grubb DR, Cooley N, Luo J, Woodcock EA. Regulation of autophagy in cardiomyocytes by Ins(1,4,5)P3 and IP3-receptors. *J Mol Cell Cardiol*. 2013;54(1):19-24. doi:10.1016/j.yjmcc.2012.10.014
235. Rabinowitz JD, White E. Autophagy and metabolism. *Metabolism*. 2010;1029(December):1344-1349. doi:10.1002/kjm2.12299
236. Booth DM, Enyedi B, Geiszt M, Várnai P, Hajnóczky G. Redox Nanodomains Are Induced by and Control Calcium Signaling at the ER-Mitochondrial Interface. *Mol Cell*. 2016;63(2):240-248. doi:10.1016/j.molcel.2016.05.040
237. Gilady SY, Bui M, Lynes EM, et al. Ero1α requires oxidizing and normoxic conditions to localize to the mitochondria-associated membrane (MAM). *Cell Stress Chaperones*. 2010;15(5):619-629. doi:10.1007/s12192-010-0174-1
238. Joseph SK, Booth DM, Young MP, Hajnóczky G. Redox regulation of ER and mitochondrial Ca 2+ signaling in cell survival and death. *Cell Calcium*. 2019;79:89-97. doi:10.1016/j.ceca.2019.02.006
239. Dong Z, Shanmughapriya S, Tomar D, et al. Mitochondrial Ca2+ Uniporter Is a Mitochondrial Luminal Redox Sensor that Augments MCU Channel Activity. *Mol Cell*. 2017;65(6):1014-1028.e7. doi:10.1016/j.molcel.2017.01.032
240. Csordás G, Weaver D, Hajnóczky G. Endoplasmic Reticular–Mitochondrial Contactology: Structure and Signaling Functions. *Trends Cell Biol*. 2018;xx:1-18. doi:10.1016/j.tcb.2018.02.009

241. Bouman L, Schlierf A, Lutz AK, et al. Parkin is transcriptionally regulated by ATF4: evidence for an interconnection between mitochondrial stress and ER stress. *Cell Death Differ*. 2011;18(5):769-782. doi:10.1038/cdd.2010.142
242. Sano R, Annunziata I, Patterson A, et al. GM1-Ganglioside Accumulation at the Mitochondria-Associated ER Membranes Links ER Stress to Ca2+-Dependent Mitochondrial Apoptosis. *Mol Cell*. 2009;36(3):500-511. doi:10.1016/j.molcel.2009.10.021
243. Ngoh GA, Papanicolaou KN, Walsh K. Loss of mitofusin 2 promotes endoplasmic reticulum stress. *J Biol Chem*. 2012;287(24):20321-20332. doi:10.1074/jbc.M112.359174
244. Muñoz JP, Ivanova S, Sánchez-Wandelmer J, et al. Mfn2 modulates the UPR and mitochondrial function via repression of PERK. *EMBO J*. 2013;32(17):2348-2361. doi:10.1038/emboj.2013.168
245. Schneeberger M, O Dietrich M, Sebastian D, et al. Mitofusin 2 in POMC Neurons Connects ER Stress with Leptin Resistance and Energy Imbalance. *Cell*. 2013;155(1):1-23. doi:10.1016/j.cell.2013.09.003.Mitofusin
246. Verfaillie T, Rubio N, Garg AD, et al. PERK is required at the ER-mitochondrial contact sites to convey apoptosis after ROS-based ER stress. *Cell Death Differ*. 2012;19(11):1880-1891. doi:10.1038/cdd.2012.74
247. Mori T, Hayashi T, Hayashi E, Su TP. Sigma-1 Receptor Chaperone at the ER-Mitochondrion Interface Mediates the Mitochondrion-ER-Nucleus Signaling for Cellular Survival. *PLoS One*. 2013;8(10). doi:10.1371/journal.pone.0076941
248. Son SM, Byun J, Roh SE, Kim SJ, Mook-Jung I. Reduced IRE1 mediates apoptotic cell death by disrupting calcium homeostasis via the InsP3 receptor. *Cell Death Dis*. 2014;5(4):1-13. doi:10.1038/cddis.2014.129
249. Carreras-Sureda A, Jaña F, Urra H, et al. Non-canonical function of IRE1α determines mitochondria-associated endoplasmic reticulum composition to control calcium transfer and bioenergetics. *Nat Cell Biol*. 2019;21(June). doi:10.1038/s41556-019-0329-y
250. Simmen T, Lynes EM, Gesson K, Thomas G. Oxidative protein folding in the endoplasmic reticulum: Tight links to the mitochondria-associated membrane (MAM). *Biochim Biophys Acta - Biomembr*. 2010;1798(8):1465-1473. doi:10.1016/j.bbamem.2010.04.009
251. Hayashi T, Su TP. Sigma-1 Receptor Chaperones at the ER- Mitochondrion Interface Regulate Ca2+ Signaling and Cell Survival. *Cell*. 2007;131(3):596-610. doi:10.1016/j.cell.2007.08.036
252. Higo T, Hattori M, Nakamura T, Natsume T, Michikawa T, Mikoshiba K. Subtype-specific and ER lumenal environment-dependent regulation of inositol 1,4,5-trisphosphate receptor type 1 by ERp44. *Cell*. 2005;120(1):85-98. doi:10.1016/j.cell.2004.11.048
253. Joseph SK, Young MP, Alzayady K, et al. Redox regulation of type-I inositol trisphosphate receptors in intact mammalian cells. *J Biol Chem*. 2018;293(45):17464-17476. doi:10.1074/jbc.RA118.005624
254. Li G, Mongillo M, Chin KT, et al. Role of ERO1-α-mediated stimulation of inositol 1,4,5-triphosphate receptor activity in endoplasmic reticulum stress-induced apoptosis. *J Cell Biol*. 2009;186(6):783-792. doi:10.1083/jcb.200904060
255. Ushioda R, Miyamoto A, Inoue M, et al. Redox-assisted regulation of Ca2+ homeostasis in the endoplasmic reticulum by disulfide reductase ERdj5. *Proc Natl Acad Sci U S A*. 2016;113(41):E6055-E6063. doi:10.1073/pnas.1605818113

256. Tong XY, Evangelista A, Cohen RA. Targeting the redox regulation of SERCA in vascular physiology and disease. *Curr Opin Pharmacol*. 2010;10(2):133-138. doi:10.1016/j.coph.2009.11.008
257. Li Y, Camacho P. Ca2+-dependent redox modulation of SERCA 2b by ERp57. *J Cell Biol*. 2004;164(1):35-46. doi:10.1083/jcb.200307010
258. Roscoe JM, Sevier CS. Pathways for Sensing and Responding to Hydrogen Peroxide at the Endoplasmic Reticulum. *Cells*. 2020;9(10):1-21. doi:10.3390/cells9102314
259. Gutiérrez T, Qi H, Tahbaz N, et al. The ER Chaperone Calnexin Controls Mitochondrial Positioning and Respiration. *Sci Signal*. 2020;6660(June):1-15.
260. Raturi A, Gutiérrez T, Ortiz-Sandoval C, et al. TMX1 determines cancer cell metabolism as a thiolbased modulator of ER-mitochondria Ca^{2+} flux. *J Cell Biol*. 2016;214(4). doi:10.1083/jcb.201512077
261. Cho I-T, Adelmant G, Lim Y, Marto JA, Cho G, Golden JA. Ascorbate peroxidase proximity labeling coupled with biochemical fractionation identifies promoters of endoplasmic reticulum mitochondrial contacts. *J Biol Chem*. 2017:jbc.M117.795286. doi:10.1074/jbc.M117.795286
262. Chandel A, Das KK, Bachhawat AK. Glutathione depletion activates the yeast vacuolar transient receptor potential channel, Yvc1p, by reversible glutathionylation of specific Cysteines. *Mol Biol Cell*. 2016;27(24):3913-3925. doi:10.1091/mbc.E16-05-0281
263. Chandel A, Bachhawat AK. Redox regulation of the yeast voltage-gated Ca2+ channel homolog Cch1p by glutathionylation of specific cysteine residues. *J Cell Sci*. 2017;132(18). doi:10.1242/jcs.238410
264. Bergeron JJM, Brenner MB, Thomas DY, Williams DB. Calnexin: a membrane-bound chaperone of the endoplasmic reticulum. *Trends Biochem Sci*. 1994;19(3):124-128. doi:10.1016/0968-0004(94)90205-4
265. Ou W, Cameron PH, Thomas DY, Bergeron JJM. Association of folding intermediates of glycoproteins with calnexin during protein maturation. *Nature*. 1993;364:771-776.
266. Lakkaraju AKK, Abrami L, Lemmin T, et al. Palmitoylated calnexin is a key component of the ribosome-translocon complex. *EMBO J*. 2012;31(7):1823-1835. doi:10.1038/emboj.2012.15
267. Lynes EM, Raturi A, Shenkman M, et al. Palmitoylation is the switch that assigns calnexin to quality control or ER Ca2+ signaling. *J Cell Sci*. 2013;126(17):3893-3903. doi:10.1242/jcs.125856
268. Parlati F, Dominguez M, Bergeron JJM, Thomas DY. Saccharomyces cerevisiae CNE1 encodes an endoplasmic reticulum (ER) membrane protein with sequence similarity to calnexin and calreticulin and functions as a constituent of the ER quality control apparatus. *J Biol Chem*. 1995;270(1):244-253. doi:10.1074/jbc.270.1.244
269. Xu X, Azakami H, Kato A. P-domain and lectin site are involved in the chaperone function of Saccharomyces cerevisiae calnexin homologue. *FEBS Lett*. 2004;570(1-3):155-160. doi:10.1016/j.febslet.2004.06.039
270. Meaden P, Hill K, Wagner J, Slipetz D, Sommer SS, Bussey H. The yeast KRE5 gene encodes a probable endoplasmic reticulum protein required for (1----6)-beta-D-glucan synthesis and normal cell growth. *Mol Cell Biol*. 1990;10(6):3013-3019. doi:10.1128/mcb.10.6.3013
271. Song Y, Azakami H, Shamima B, He J, Kato A. Different effects of calnexin deletion in Saccharomyces cerevisiae on the secretion of two glycosylated amyloidogenic lysozymes.

FEBS Lett. 2002;512(1-3):213-217. doi:10.1016/S0014-5793(02)02258-5
272. Matsuo Y, Akiyama N, Nakamura H, Yodoi J, Noda M, Kizaka-Kondoh S. Identification of a Novel Thioredoxin-related Transmembrane Protein. *J Biol Chem*. 2001;276(13):10032-10038. doi:10.1074/jbc.M011037200
273. Guerra C, Molinari M. Thioredoxin-Related Transmembrane Proteins : 2020:1-11.
274. Atkinson HJ, Babbitt PC. An atlas of the thioredoxin fold class reveals the complexity of function-enabling adaptations. *PLoS Comput Biol*. 2009;5(10). doi:10.1371/journal.pcbi.1000541
275. Matsuo Y, Nishinaka Y, Suzuki S, et al. TMX, a human transmembrane oxidoreductase of the thioredoxin family: The possible role in disulfide-linked protein folding in the endoplasmic reticulum. *Arch Biochem Biophys*. 2004;423(1):81-87. doi:10.1016/j.abb.2003.11.003
276. Matsuo Y, Hirota K. Transmembrane thioredoxin-related protein TMX1 is reversibly oxidized in response to protein accumulation in the endoplasmic reticulum. *FEBS Open Bio*. 2017;7(11):1768-1777. doi:10.1002/2211-5463.12319
277. Matsuo Y, Masutani H, Son A, Kizaka-Kondoh S, Yodoi J. Physical and functional interaction of transmembrane thioredoxin-related protein with major histocompatibility complex class I heavy chain: redox-based protein quality control and its potential relevance to immune response. *Mol Biol Cell*. 2009;20:4524-4530. doi:10.1091/mbc.E09
278. Guerra C, Brambilla Pisoni G, Soldà T, Molinari M. The reductase TMX1 contributes to ERAD by preferentially acting on membrane-associated folding-defective polypeptides. *Biochem Biophys Res Commun*. 2018;503(2):938-943. doi:10.1016/j.bbrc.2018.06.099
279. Sevier CS, Kaiser CA. Conservation and diversity of the cellular disulfide bond formation pathways. *Antioxidants Redox Signal*. 2006;8(5-6):797-811. doi:10.1089/ars.2006.8.797
280. Hacioglu E, Esmer I, Fomenko DE, Gladyshev VN, Koc A. The roles of thiol oxidoreductases in yeast replicative aging. *Mech Ageing Dev*. 2010;131(11-12):692-699. doi:10.1016/j.mad.2010.09.006
281. Nørgaard P, Westphal V, Tachibana C, Alsøe L, Holst B, Winther JR. Functional differences in yeast protein disulfide isomerases. *J Cell Biol*. 2001;153(3):553-562. doi:10.1083/jcb.152.3.553
282. Xiao R, Wilkinson B, Solovyov A, et al. The contributions of protein bisulfide isomerase and its homologues to oxidative protein folding in the yeast endoplasmic reticulum. *J Biol Chem*. 2004;279(48):49780-49786. doi:10.1074/jbc.M409210200
283. Kimura T, Hosoda Y, Sato Y, et al. Interactions among yeast protein-disulfide isomerase proteins and endoplasmic reticulum chaperone proteins influence their activities. *J Biol Chem*. 2005;280(36):31438-31441. doi:10.1074/jbc.M503377200
284. Delic M, Valli M, Graf AB, Pfeffer M, Mattanovich D, Gasser B. The secretory pathway: Exploring yeast diversity. *FEMS Microbiol Rev*. 2013;37(6):872-914. doi:10.1111/1574-6976.12020
285. Wang Q, Chang A. Eps1, a novel PDI-related protein involved in ER quality control in yeast. *EMBO J*. 1999;18(21):5972-5982. doi:10.1093/emboj/18.21.5972
286. He J, Sakamoto T, Song Y, et al. Effect of EPS1 gene deletion in Saccharomyces cerevisiae on the secretion of foreign proteins which have disulfide bridges. *FEBS Lett*. 2005;579(11):2277-2283. doi:10.1016/j.febslet.2005.03.019
287. Wang Q, Chang A. Substrate recognition in ER-associated degradation mediated by Eps1, a member of the protein disulfide isomerase family. *EMBO J*. 2003;22(15):3792-3802.

doi:10.1093/emboj/cdg378
288. Vitu E, Kim S, Sevier CS, et al. Oxidative activity of yeast Ero1p on protein disulfide isomerase and related oxidoreductases of the endoplasmic reticulum. *J Biol Chem*. 2010;285(24):18155-18165. doi:10.1074/jbc.M109.064931
289. Biran S, Gat Y, Fass D. The Eps1p protein disulfide isomerase conserves classic thioredoxin superfamily amino acid motifs but not their functional geometries. *PLoS One*. 2014;9(12):1-14. doi:10.1371/journal.pone.0113431
290. Bui M, Gilady SY, Fitzsimmons REB, et al. Rab32 modulates apoptosis onset and Mitochondria-associated Membrane (MAM) properties. *J Biol Chem*. 2010;285(41):31590-31602. doi:10.1074/jbc.M110.101584
291. Chavrier P, Parton RG, Hauri HP, Simons K, Zerial M. Localization of low molecular weight GTP binding proteins to exocytic and endocytic compartments. *Cell*. 1990;62(2):317-329. doi:10.1016/0092-8674(90)90369-P
292. Soldati T, Shapiro AD, Dirac-Svejestrup BA, Pfeffer SR. Membrane targeting of the small GTPase Rab9 is accompanied by nucleotide exchange. *Nature*. 1994;369:76-78.
293. Stenmark H, Parton RG, Steele-Mortimer O, Lütcke A, Gruenberg J, Zerial M. Inhibition of rab5 GTPase activity stimulates membrane fusion in endocytosis. *EMBO J*. 1994;13(6):1287-1296. doi:10.1002/j.1460-2075.1994.tb06381.x
294. Seabra MC, Goldstein JL, Sudhof TC, Brown MS. Rab geranylgeranyl transferase. A multisubunit enzyme that prenylates GTP- binding proteins terminating in Cys-X-Cys or Cys-Cys. *J Biol Chem*. 1992;267(20):14497-14503. doi:10.1016/s0021-9258(19)49740-8
295. Blümer J, Rey J, Dehmelt L, et al. RabGEFs are a major determinant for specific Rab membrane targeting. *J Cell Biol*. 2013;200(3):287-300. doi:10.1083/jcb.201209113
296. Li G, Marlin MC. *Rab Family of GTpases*. Vol 1298.; 2015. doi:10.1007/978-1-4939-2569-8_1
297. Ullrich O, Stenmark H, Alexandrov K, et al. Rab GDP dissociation inhibitor as a general regulator for the membrane association of rab proteins. *J Biol Chem*. 1993;268(24):18143-18150.
298. Soldati T, Riederer MA, Pfeffer SR. Rab GDI: A solubilizing and recycling factor for rab9 protein. *Mol Biol Cell*. 1993;4(4):425-434. doi:10.1091/mbc.4.4.425
299. Zahraoui A, Touchot N, Chardin P, Tavitian A. The human rab genes encode a family of GTP-binding proteins related to yeast YPT1 and SEC4 products involved in secretion. *J Biol Chem*. 1989;264(21):12394-12401. doi:10.1016/s0021-9258(18)63872-4
300. Wasmeier C, Romao M, Plowright L, Bennett DC, Raposo G, Seabra MC. Rab38 and Rab32 control post-Golgi trafficking of melanogenic enzymes. *J Cell Biol*. 2006;175(2):271-281. doi:10.1083/jcb.200606050
301. Bultema JJ, Ambrosio AL, Burek CL, Di Pietro SM. BLOC-2, AP-3, and AP-1 proteins function in concert with Rab38 and Rab32 proteins to mediate protein trafficking to lysosome-related organelles. *J Biol Chem*. 2012;287(23):19550-19563. doi:10.1074/jbc.M112.351908
302. Bowman SL, Bi-Karchin J, Le L, Marks MS. The road to lysosome-related organelles: Insights from Hermansky-Pudlak syndrome and other rare diseases. *Traffic*. 2019;20(6):404-435. doi:10.1111/tra.12646
303. Gerondopoulos A, Langemeyer L, Liang JR, Linford A, Barr FA. BLOC-3 mutated in Hermansky-Pudlak syndrome is a Rab32/38 guanine nucleotide exchange factor. *Curr Biol*. 2012;22(22):2135-2139. doi:10.1016/j.cub.2012.09.020

304. Alto NM, Soderling J, Scott JD. Rab32 is an A-kinase anchoring protein and participates in mitochondrial dynamics. *J Cell Biol*. 2002;158(4):659-668. doi:10.1083/jcb.200204081
305. Ortiz-Sandoval CG, Hughes SC, Dacks JB, Simmen T. Interaction with the effector dynamin-related protein 1 (Drp1) is an ancient function of Rab32 subfamily proteins. *Cell Logist*. 2014;4(4):e986399. doi:10.4161/21592799.2014.986399
306. Itakura E, Kishi-Itakura C, Mizushima N. The hairpin-type tail-anchored SNARE syntaxin 17 targets to autophagosomes for fusion with endosomes/lysosomes. *Cell*. 2012;151(6):1256-1269. doi:10.1016/j.cell.2012.11.001
307. Arasaki K, Shimizu H, Mogari H, et al. A Role for the ancient SNARE syntaxin 17 in regulating mitochondrial division. *Dev Cell*. 2015;32(3):304-317. doi:10.1016/j.devcel.2014.12.011
308. Ravikumar B, Imarisio S, Sarkar S, O'Kane CJ, Rubinsztein DC. Rab5 modulates aggregation and toxicity of mutant huntingtin through macroautophagy in cell and fly models of Huntington disease. *J Cell Sci*. 2008;121(10):1649-1660. doi:10.1242/jcs.025726
309. Pankiv S, Alemu EA, Brech A, et al. FYCO1 is a Rab7 effector that binds to LC3 and PI3P to mediate microtubule plus end - Directed vesicle transport. *J Cell Biol*. 2010;188(2):253-269. doi:10.1083/jcb.200907015
310. Hirota Y, Tanaka Y. A small GTPase, human Rab32, is required for the formation of autophagic vacuoles under basal conditions. *Cell Mol Life Sci*. 2009;66(17):2913-2932. doi:10.1007/s00018-009-0080-9
311. Wang C, Liu Z, Huang X. Rab32 is important for autophagy and lipid storage in drosophila. *PLoS One*. 2012;7(2):1-9. doi:10.1371/journal.pone.0032086
312. Pei Y, Yue L, Zhang W, et al. Improvement in Mouse iPSC Induction by Rab32 Reveals the Importance of Lipid Metabolism during Reprogramming. *Sci Rep*. 2015;5(October):1-12. doi:10.1038/srep16539
313. Yeo JC, Wall AA, Luo L, Stow JL. Sequential recruitment of Rab GTPases during early stages of phagocytosis. *Cell Logist*. 2016;6(1):1-12. doi:10.1080/21592799.2016.1140615
314. Diekmann Y, Seixas E, Gouw M, Tavares-Cadete F, Seabra MC, Pereira-Leal JB. Thousands of Rab GTPases for the cell biologist. *PLoS Comput Biol*. 2011;7(10). doi:10.1371/journal.pcbi.1002217
315. Lipatova Z, Hain AU, Nazarko VY, Segev N. Ypt/Rab GTPases: Principles learned from yeast. *Crit Rev Biochem Mol Biol*. 2015;50(3):203-211. doi:10.3109/10409238.2015.1014023
316. Elias M, Brighouse A, Gabernet-Castello C, Field MC, Dacks JB. Sculpting the endomembrane system in deep time: High resolution phylogenetics of Rab GTPases. *J Cell Sci*. 2012;125(10):2500-2508. doi:10.1242/jcs.101378
317. Brighouse A, Dacks JB, Field MC. Rab protein evolution and the history of the eukaryotic endomembrane system. *Cell Mol Life Sci*. 2010;67(20):3449-3465. doi:10.1007/s00018-010-0436-1
318. Pereira-Leal JB. The Ypt/Rab family and the evolution of trafficking in fungi. *Traffic*. 2008;9(1):27-38. doi:10.1111/j.1600-0854.2007.00667.x
319. Laurent JM, Garge RK, Teufel AI, Wilke CO, Kachroo AH, Marcotte EM. Humanization of yeast genes with multiple human orthologs reveals functional divergence between paralogs. *PLoS Biol*. 2020;18(5):1-25. doi:10.1371/journal.pbio.3000627
320. Tsvetanova NG, Riordan DP, Brown PO. The yeast rab GTPase Ypt1 modulates unfolded

protein response dynamics by regulating the stability of HAC1 RNA. *PLoS Genet*. 2012;8(7). doi:10.1371/journal.pgen.1002862
321. Singer-Krüger B, Stenmark H, Düsterhöft A, et al. Role of three rab5-like GTPases, Ypt51p, Ypt52p, and Ypt53p, in the endocytic and vacuolar protein sorting pathways of yeast. *J Cell Biol*. 1994;125(2):283-298. doi:10.1083/jcb.125.2.283
322. Klöpper TH, Kienle N, Fasshauer D, Munro S. Untangling the evolution of Rab G proteins: implications of a comprehensive genomic analysis. *BMC Biol*. 2012;10. doi:10.1186/1741-7007-10-71
323. Langemeyer L, Borchers AC, Herrmann E, et al. A conserved and regulated mechanism drives endosomal rab transition. *Elife*. 2020;9:1-20. doi:10.7554/eLife.56090
324. Nielsen E, Severin F, Backer JM, Hyman AA, Zerial M. Rab5 regulates motility of early endosomes on microtubules. *Nat Cell Biol*. 1999;1(6):376-382. doi:10.1038/14075
325. Schmidt O, Weyer Y, Fink MJ, et al. Regulation of Rab5 isoforms by transcriptional and post-transcriptional mechanisms in yeast. *FEBS Lett*. 2017;591(18):2803-2815. doi:10.1002/1873-3468.12785
326. Gorvel JP, Chavrier P, Zerial M, Gruenberg J. Rab5 Controls Early Endosome Fusion in Vitro. *Cell*. 1991;64(5):915-925. doi:10.1016/0092-8674(91)90316-Q
327. Nagano M, Toshima JY, Elisabeth Siekhaus D, Toshima J. Rab5-mediated endosome formation is regulated at the trans-Golgi network. *Commun Biol*. 2019;2(1):1-12. doi:10.1038/s42003-019-0670-5
328. Bucci C, Parton RG, Mather IH, et al. The small GTPase rab5 functions as a regulatory factor in the early endocytic pathway. *Cell*. 1992;70(5):715-728. doi:10.1016/0092-8674(92)90306-W
329. Purushothaman LK, Arlt H, Kuhlee A, Raunser S, Ungermann C. Retromer-driven membrane tubulation separates endosomal recycling from Rab7/Ypt7-dependent fusion. *Mol Biol Cell*. 2017;28(6):783-791. doi:10.1091/mbc.e16-08-0582
330. Nordmann M, Cabrera M, Perz A, et al. The Mon1-Ccz1 complex is the GEF of the late endosomal Rab7 homolog Ypt7. *Curr Biol*. 2010;20(18):1654-1659. doi:10.1016/j.cub.2010.08.002
331. Robinson JS, Klionsky DJ, Banta LM, Emr SD. Protein sorting in Saccharomyces cerevisiae: isolation of mutants defective in the delivery and processing of multiple vacuolar hydrolases. *Mol Cell Biol*. 1988;8(11):4936-4948. doi:10.1128/mcb.8.11.4936
332. Rothman JH, Howald I, Stevens TH. Characterization of genes required for protein sorting and vacuolar function in the yeast Saccharomyces cerevisiae. *EMBO J*. 1989;8(7):2057-2065. doi:10.1002/j.1460-2075.1989.tb03614.x
333. Gerrard SR, Bryant NJ, Stevens TH. VPS21 controls entry of endocytosed and biosynthetic proteins into the yeast prevacuolar compartment. *Mol Biol Cell*. 2000;11(2):613-626. doi:10.1091/mbc.11.2.613
334. Lipatova Z, Segev N. Ypt/Rab GTPases and their TRAPP GEFs at the Golgi. *FEBS Lett*. 2019;593(17):2488-2500. doi:10.1002/1873-3468.13574
335. Jedd G, Richardson C, Litt R, Segev N. The Ypt1 GTPase is essential for the first two steps of the yeast secretory pathway. *J Cell Biol*. 1995;131(3):583-590. doi:10.1083/jcb.131.3.583
336. Segev N. Ypt and Rab GTPases: Insight into functions through novel interactions. *Curr Opin Cell Biol*. 2001;13(4):500-511. doi:10.1016/S0955-0674(00)00242-8
337. Lipatova Z, Belogortseva N, Zhang XQ, Kim J, Taussig D, Segev N. Regulation of

selective autophagy onset by a Ypt/Rab GTPase module. *Proc Natl Acad Sci U S A*. 2012;109(18):6981-6986. doi:10.1073/pnas.1121299109
338. Mao K, Wang K, Liu X, Klionsky DJ. The scaffold protein Atg11 recruits fission machinery to drive selective mitochondria degradation by autophagy. *Dev Cell*. 2013;26(1):9-18. doi:10.1016/j.devcel.2013.05.024
339. Zou S, Chen Y, Liu Y, et al. Trs130 participates in autophagy through GTPases Ypt31/32 in Saccharomyces cerevisiae. 2014;14(2):233-246. doi:10.1111/tra.12024.Trs130
340. Goud B, Salminen A, Walworth NC, Novick PJ. A GTP-binding protein required for secretion rapidly associates with secretory vesicles and the plasma membrane in yeast. *Cell*. 1988;53(5):753-768. doi:10.1016/0092-8674(88)90093-1
341. Bultema JJ, Boyle JA, Malenke PB, et al. Myosin Vc interacts with Rab32 and Rab38 proteins and works in the biogenesis and secretion of melanosomes. *J Biol Chem*. 2014;289(48):33513-33528. doi:10.1074/jbc.M114.578948
342. Suda Y, Kurokawa K, Hirata R, Nakano A. Rab GAP cascade regulates dynamics of Ypt6 in the Golgi traffic. *Proc Natl Acad Sci U S A*. 2013;110(47):18976-18981. doi:10.1073/pnas.1308627110
343. Wichmann H, Hengst L, Gallwitz D. Endocytosis in yeast: Evidence for the involvement of a small GTP-binding protein (Ypt7p). *Cell*. 1992;71(7):1131-1142. doi:10.1016/S0092-8674(05)80062-5
344. Haas A, Scheglmann D, Lazar T, Gallwitz D, Wickner W. The GTPase Ypt7p of Saccharomyces cerevisiae is required on both partner vacuoles for the homotypic fusion step of vacuole inheritance. *EMBO J*. 1995;14(21):5258-5270. doi:10.1002/j.1460-2075.1995.tb00210.x
345. Huotari J, Helenius A. Endosome maturation. *EMBO J*. 2011;30(17):3481-3500. doi:10.1038/emboj.2011.286
346. Kirisako T, Baba M, Ishihara N, et al. Formation process of autophagosome is traced with Apg8/Aut7p in yeast. *J Cell Biol*. 1999;147(2):435-446. doi:10.1083/jcb.147.2.435
347. Hönscher C, Mari M, Auffarth K, et al. Cellular metabolism regulates contact sites between vacuoles and mitochondria. *Dev Cell*. 2014;30(1):86-94. doi:10.1016/j.devcel.2014.06.006
348. Elbaz-Alon Y, Rosenfeld-Gur E, Shinder V, Futerman AH, Geiger T, Schuldiner M. A dynamic interface between vacuoles and mitochondria in yeast. *Dev Cell*. 2014;30(1):95-102. doi:10.1016/j.devcel.2014.06.007
349. Wong YC, Ysselstein D, Krainc D. Mitochondria–lysosome contacts regulate mitochondrial fission via RAB7 GTP hydrolysis. *Nat 2018*. 2018. doi:10.1038/nature25486
350. Lewandowska A, MacFarlane J, Shaw JM. Mitochondrial association, protein phosphorylation, and degradation regulate the availability of the active Rab GTPase Ypt11 for mitochondrial inheritance. *Mol Biol Cell*. 2013;24(8):1185-1195. doi:10.1091/mbc.E12-12-0848
351. Itoh T, Watabe A, Toh-e A, Matsui Y. Complex Formation with Ypt11p, a rab-Type Small GTPase, Is Essential To Facilitate the Function of Myo2p, a Class V Myosin, in Mitochondrial Distribution in Saccharomyces cerevisiae. *Mol Cell Biol*. 2002;22(22):7744-7757. doi:10.1128/mcb.22.22.7744-7757.2002
352. Buvelot Frei S, Rahl PB, Nussbaum M, et al. Bioinformatic and Comparative Localization of Rab Proteins Reveals Functional Insights into the Uncharacterized GTPases Ypt10p

and Ypt11p. *Mol Cell Biol*. 2006;26(19):7299-7317. doi:10.1128/mcb.02405-05
353. Lynch-Day MA, Bhandari D, Menon S, et al. Trs85 directs a Ypt1 GEF, TRAPPIII, to the phagophore to promote autophagy. *Proc Natl Acad Sci U S A*. 2010;107(17):7811-7816. doi:10.1073/pnas.1000063107
354. Rybnicek J, Samtleben S, Herrera-Cruz MS, Simmen T. Expression of a T39N mutant Rab32 protein arrests mitochondria movement within neurites of differentiated SH-SY5Y cells. *Small GTPases*. 2020;11(4):289-292. doi:10.1080/21541248.2017.1411312
355. Schneider CA, Rasband WS, Eliceiri KW. NIH Image to ImageJ: 25 years of image analysis. *Nat Methods*. 2012;9(7):671-675. doi:10.1038/nmeth.2089
356. Liu RZ, Graham K, Glubrecht DD, Germain DR, Mackey JR, Godbout R. Association of FABP5 expression with poor survival in triple-negative breast cancer: Implication for retinoic acid therapy. *Am J Pathol*. 2011;178(3):997-1008. doi:10.1016/j.ajpath.2010.11.075
357. Brachmann CB, Davies A, Cost GJ, et al. Designer deletion strains derived from Saccharomyces cerevisiae S288C: A useful set of strains and plasmids for PCR-mediated gene disruption and other applications. *Yeast*. 1998;14(2):115-132. doi:10.1002/(SICI)1097-0061(19980130)14:2<115::AID-YEA204>3.0.CO;2-2
358. Frederick RL, McCaffery JM, Cunningham KW, Okamoto K, Shaw JM. Yeast Miro GTPase, Gem1p, regulates mitochondrial morphology via a novel pathway. *J Cell Biol*. 2004;167(1):87-98. doi:10.1083/jcb.200405100
359. Jones EW, Zubenko GS, Parker RR. PEP4 gene function is required for expression of several vacuolar hydrolases in Saccharomyces cerevisiae. *Genetics*. 1982;102(4):665-677.
360. Eitzen G, Will E, Gallwitz D, Haas A, Wickner W. Sequential action of two GTPases to promote vacuole docking and fusion. *EMBO J*. 2000;19(24):6713-6720. doi:10.1093/emboj/19.24.6713
361. Simonovik B, Gnaiger E. A Mitochondrial Reference Assay for High-Resolution Respirometry Using Freeze- Dried Baker's Yeast . *Mitochondrial Physiol Netw*. 2017;3:1-3.
362. Kirkin V, Rogov V V. A Diversity of Selective Autophagy Receptors Determines the Specificity of the Autophagy Pathway. *Mol Cell*. 2019;76(2):268-285. doi:10.1016/j.molcel.2019.09.005
363. Lazarou M, Sliter DA, Kane LA, et al. The ubiquitin kinase PINK1 recruits autophagy receptors to induce mitophagy. *Nature*. 2015;524(7565):309-314. doi:10.1038/nature14893
364. Dikic I. Open questions: why should we care about ER-phagy and ER remodelling? *BMC Biol*. 2018;16(1):131. doi:10.1186/s12915-018-0603-7
365. Bhaskara RM, Grumati P, Garcia-Pardo J, et al. Curvature induction and membrane remodeling by FAM134B reticulon homology domain assist selective ER-phagy. *Nat Commun*. 2019;10(1). doi:10.1038/s41467-019-10345-3
366. Smith MD, Harley ME, Kemp AJ, et al. CCPG1 Is a Non-canonical Autophagy Cargo Receptor Essential for ER-Phagy and Pancreatic ER Proteostasis. *Dev Cell*. 2018;44(2):217-232.e11. doi:10.1016/j.devcel.2017.11.024
367. Chen Q, Xiao Y, Chai P, Zheng P, Teng J, Chen J. ATL3 Is a Tubular ER-Phagy Receptor for GABARAP-Mediated Selective Autophagy. *Curr Biol*. 2019;29(5):846-855.e6. doi:10.1016/j.cub.2019.01.041
368. Lee C-W, Wilfling F, Jentsch S, Beck M, Pfander B. Selective autophagy degrades

nuclear pore complexes. *Nat Cell Biol*. 2019;accepted f(FebruarY). doi:10.1038/s41556-019-0459-2
369. Ogata M, Hino S, Saito A, et al. Autophagy Is Activated for Cell Survival after Endoplasmic Reticulum Stress. *Mol Cell Biol*. 2006;26(24):9220-9231. doi:10.1128/mcb.01453-06
370. Khaminets A, Heinrich T, Mari M, et al. Regulation of endoplasmic reticulum turnover by selective autophagy. *Nature*. 2015;522(7556):354-358. doi:10.1038/nature14498
371. Rismanchi N, Soderblom C, Stadler J, Zhu PP, Blackstone C. Atlastin GTPases are required for Golgi apparatus and ER morphogenesis. *Hum Mol Genet*. 2008;17(11):1591-1604. doi:10.1093/hmg/ddn046
372. Shemesh T, Klemm RW, Romano FB, et al. A model for the generation and interconversion of ER morphologies. *Proc Natl Acad Sci U S A*. 2014;111(49):E5243-E5251. doi:10.1073/pnas.1419997111
373. Brady JP, Claridge JK, Smith PG, Schnell JR, DeGrado WF. A conserved amphipathic helix is required for membrane tubule formation by Yop1p. *Proc Natl Acad Sci U S A*. 2015;112(7):E639-E648. doi:10.1073/pnas.1415882112
374. Fumagalli F, Noack J, Bergmann TJ, et al. Translocon component Sec62 acts in endoplasmic reticulum turnover during stress recovery. *Nat Cell Biol*. 2016;18(11):1173-1184. doi:10.1038/ncb3423
375. Haqq C, Nosrati M, Sudilovsky D, et al. The gene expression signatures of melanoma progression. *Proc Natl Acad Sci U S A*. 2005;102(17):6092-6097. doi:10.1073/pnas.0501564102
376. Cerami E, Gao J, Dogrusoz U, et al. The cBio Cancer Genomics Portal: An open platform for exploring multidimensional cancer genomics data. *Cancer Discov*. 2012;2(5):401-404. doi:10.1158/2159-8290.CD-12-0095
377. Gao J, Aksoy BA, Dogrusoz U, et al. Integrative analysis of complex cancer genomics and clinical profiles using the cBioPortal. *Sci Signal*. 2013;6(269):1-20. doi:10.1126/scisignal.2004088
378. Popgeorgiev N, Jabbour L, Gillet G. Subcellular localization and dynamics of the Bcl-2 family of proteins. *Front Cell Dev Biol*. 2018;6(FEB):1-11. doi:10.3389/fcell.2018.00013
379. Wu W, Lin C, Wu K, et al. FUNDC1 regulates mitochondrial dynamics at the ER–mitochondrial contact site under hypoxic conditions. *EMBO J*. 2016;35(13):1368-1384. doi:10.15252/embj.201593102
380. Zhou Y, Sun K, Ma Y, et al. Autophagy inhibits chemotherapy-induced apoptosis through downregulating Bad and Bim in hepatocellular carcinoma cells. *Sci Rep*. 2014;4:1-9. doi:10.1038/srep05382
381. Cook KL, Soto-Pantoja DR, Abu-Asab M, Clarke PAG, Roberts DD, Clarke R. Mitochondria directly donate their membrane to form autophagosomes during a novel mechanism of parkin-associated mitophagy. *Cell Biosci*. 2014;4(1):1-9. doi:10.1186/2045-3701-4-16
382. Mizushima N, Yoshimori T, Levine B. Methods in Mammalian Autophagy Research. *Cell*. 2010;140(3):313-326. doi:10.1016/j.cell.2010.01.028
383. Forrester A, De Leonibus C, Grumati P, et al. A selective ER-phagy exerts procollagen quality control via a Calnexin-FAM134B complex. *EMBO J*. 2019;38(2):e99847. doi:10.15252/embj.201899847
384. Narendra DP, Kane LA, Hauser DN, Fearnley IM, Youle RJ. p62/SQSTM1 is required for

Parkin-induced mitochondrial clustering but not mitophagy; VDAC1 is dispensable for both. *Autophagy*. 2010;6(8):1090-1106. doi:10.4161/auto.6.8.13426
385. Oertle T, Schwab ME. Nogo and its paRTNers. *Trends Cell Biol*. 2003;13(4):187-194. doi:10.1016/S0962-8924(03)00035-7
386. Zhang H, Hu J. Shaping the Endoplasmic Reticulum into a Social Network. *Trends Cell Biol*. 2016;26(12):934-943. doi:10.1016/j.tcb.2016.06.002
387. Twig G, Elorza A, Molina AJA, et al. Fission and selective fusion govern mitochondrial segregation and elimination by autophagy. *EMBO J*. 2008;27(2):433-446. doi:10.1038/sj.emboj.7601963
388. Chonghaile TN, Sarosiek KA, Vo TT, et al. Pretreatment mitochondrial priming correlates with clinical response to cytotoxic chemotherapy. *Science (80-)*. 2011;334(6059):1129-1133. doi:10.1126/science.1206727
389. Singh R, Letai A, Sarosiek K. Regulation of apoptosis in health and disease: the balancing act of BCL-2 family proteins. *Nat Rev Mol Cell Biol*. 2019;20(3):175-193. doi:10.1038/s41580-018-0089-8
390. Haile Y, Deng X, Ortiz-Sandoval C, et al. Rab32 connects ER stress to mitochondrial defects in multiple sclerosis. *J Neuroinflammation*. 2017;14(1):1-13. doi:10.1186/s12974-016-0788-z
391. Bosc C, Broin N, Fanjul M, et al. Autophagy regulates fatty acid availability for oxidative phosphorylation through mitochondria-endoplasmic reticulum contact sites. *Nat Commun 2020 111*. 2020;11(1):1-14. doi:10.1038/s41467-020-17882-2
392. Decuypere JP, Monaco G, Bultynck G, Missiaen L, De Smedt H, Parys JB. The IP3 receptor-mitochondria connection in apoptosis and autophagy. *Biochim Biophys Acta - Mol Cell Res*. 2011;1813(5):1003-1013. doi:10.1016/j.bbamcr.2010.11.023
393. Hu Y, Chen H, Zhang L, et al. The AMPK-MFN2 axis regulates MAM dynamics and autophagy induced by energy stresses. *Autophagy*. 2020;00(00):1-15. doi:10.1080/15548627.2020.1749490
394. Schneiter R. Genetics , Molecular and Cell Biology of Yeast. 2004;(January).
395. Segev N, Mulholland J, Botstein D. The yeast GTP-binding YPT1 protein and a mammalian counterpart are associated with the secretion machinery. *Cell*. 1988;52(6):915-924. doi:10.1016/0092-8674(88)90433-3
396. Canizares DG, del Rio Garcia S, Herrera F, Gallardo EA, Antunes A, Aquero-Chapin G. Big Data Supervised Pairwise Ortholog Detection in Yeasts. In: *Yeast-Industrial Applications*. ; 2017:41-63. doi:10.1016/j.colsurfa.2011.12.014
397. Ulrich AKC, Wahl MC. Human MFAP1 is a cryptic ortholog of the Saccharomyces cerevisiae Spp381 splicing factor. *BMC Evol Biol*. 2017;17(1):91. doi:10.1186/s12862-017-0923-1
398. Wurmser AE, Sato TK, Emr SD. New component of the vacuolar class C-Vps complex couples nucleotide exchange on the Ypt7 GTPase to SNARE-dependent docking and fusion. *J Cell Biol*. 2000;151(3):551-562. doi:10.1083/jcb.151.3.551
399. Balderhaar HJK, Arlt H, Ostrowicz C, et al. The Rab GTPase Ypt7 is linked to retromer-mediated receptor recycling and fusion at the yeast late endosome. *J Cell Sci*. 2010;123(23):4085-4094. doi:10.1242/jcs.071977
400. Seals DF, Eitzen G, Margolis N, Wickner WT, Price A. A Ypt/Rab effector complex containing the Sec1 homolog Vps33p is required for homotypic vacuole fusion. *Proc Natl Acad Sci U S A*. 2000;97(17):9402-9407. doi:10.1073/pnas.97.17.9402

401. Ostrowicz CW, Bröcker C, Ahnert F, et al. Defined Subunit Arrangement and Rab Interactions Are Required for Functionality of the HOPS Tethering Complex. *Traffic*. 2010;11(10):1334-1346. doi:10.1111/j.1600-0854.2010.01097.x
402. Peplowska K, Markgraf DF, Ostrowicz CW, Bange G, Ungermann C. The CORVET Tethering Complex Interacts with the Yeast Rab5 Homolog Vps21 and Is Involved in Endo-Lysosomal Biogenesis. *Dev Cell*. 2007;12(5):739-750. doi:10.1016/j.devcel.2007.03.006
403. Ostrowicz CW, Bröcker C, Ahnert F, et al. Defined Subunit Arrangement and Rab Interactions Are Required for Functionality of the HOPS Tethering Complex. *Traffic*. 2010;11(10):1334-1346. doi:10.1111/j.1600-0854.2010.01097.x
404. Peplowska K, Markgraf DF, Ostrowicz CW, Bange G, Ungermann C. The CORVET Tethering Complex Interacts with the Yeast Rab5 Homolog Vps21 and Is Involved in Endo-Lysosomal Biogenesis. *Dev Cell*. 2007;12(5):739-750. doi:10.1016/j.devcel.2007.03.006
405. Kiontke S, Langemeyer L, Kuhlee A, et al. Architecture and mechanism of the late endosomal Rab7-like Ypt7 guanine nucleotide exchange factor complex Mon1-Ccz1. *Nat Commun*. 2017;8:1-10. doi:10.1038/ncomms14034
406. Boriack-Sjodin PA, Margarit SM, Bar-Sagi D, Kuriyan J. The structural basis of the activation of Ras by Sos. *Nature*. 1998;394(6691):337-343. doi:10.1038/28548
407. Kucharczyk R, Kierzek AM, Slonimski PP, Rytka J. The Ccz1 protein interacts with Ypt7 GTPase during fusion of multiple transport intermediates with the vacuole in S. cerevisiae. *J Cell Sci*. 2001;114(17):3137-3145.
408. González Montoro A, Auffarth K, Hönscher C, et al. Vps39 Interacts with Tom40 to Establish One of Two Functionally Distinct Vacuole-Mitochondria Contact Sites. *Dev Cell*. 2018;45(5):621-636.e7. doi:10.1016/j.devcel.2018.05.011
409. English A, Kornmann B, Shaw J, Hughes A. ER-Mitochondria Contacts Promote Mitochondrial-Derived Compartment Biogenesis. 2020;219(12). doi:10.1101/2020.03.13.991133
410. Kumar N, Leonzino M, Hancock-Cerutti W, et al. VPS13A and VPS13C are lipid transport proteins differentially localized at ER contact sites. *J Cell Biol*. 2018;217(10):3625-3639. doi:10.1083/JCB.201807019
411. Hajnóczky G, Hager R, Thomas AP. Mitochondria suppress local feedback activation of inositol 1,4,5- trisphosphate receptors by Ca2+. *J Biol Chem*. 1999;274(20):14157-14162. doi:10.1074/jbc.274.20.14157
412. Milburn M V., Tong L, DeVos AM, et al. Molecular switch for signal transduction: Structural differences between active and inactive forms of protooncogenic ras proteins. *Science (80-)*. 1990;247(4945):939-945. doi:10.1126/science.2406906
413. Coppola U, Ristoratore F, Albalat R, D'Aniello S. The evolutionary landscape of the Rab family in chordates. *Cell Mol Life Sci*. 2019;(0123456789). doi:10.1007/s00018-019-03103-7
414. Diekmann Y, Pereira-Leal JB. Bioinformatic approaches to identifying and classifying rab proteins. *Methods Mol Biol*. 2015;1298:17-28. doi:10.1007/978-1-4939-2569-8_2
415. Remm M, Storm CEV, Sonnhammer ELL. Automatic clustering of orthologs and in-paralogs from pairwise species comparisons. *J Mol Biol*. 2001;314(5):1041-1052. doi:10.1006/jmbi.2000.5197
416. Peter ATJ, Herrmann B, Antunes D, Rapaport D, Dimmer KS, Kornmann B. Vps13-Mcp1

interact at vacuole – mitochondria interfaces and bypass ER – mitochondria contact sites. *J Cell Biol*. 2017. doi:10.1083/jcb.201610055
417. Mochida K, Oikawa Y, Kimura Y, et al. Receptor-mediated selective autophagy degrades the endoplasmic reticulum and the nucleus. *Nature*. 2015;522(7556):359-362. doi:10.1038/nature14506
418. Yamano K, Fogel AI, Wang C, van der Bliek AM, Youle RJ. Mitochondrial Rab GAPs govern autophagosome biogenesis during mitophagy. *Elife*. 2014;3:1-24. doi:10.7554/elife.01612
419. Jansen G, Wu C, Schade B, Thomas DY, Whiteway M. Drag&Drop cloning in yeast. *Gene*. 2005;344:43-51. doi:10.1016/j.gene.2004.10.016
420. Cieri D, Vicario M, Giacomello M, et al. SPLICS: A split green fluorescent protein-based contact site sensor for narrow and wide heterotypic organelle juxtaposition. *Cell Death Differ*. 2018;25(6):1131-1145. doi:10.1038/s41418-017-0033-z
421. Bone DH, Fowden L. Tramsamination and the oxidation of some amino-acids by mung bean mitochondria. *J Exp Bot*. 1960;11(1):104-115. doi:10.1093/jxb/11.1.104
422. Kawazoe N, Kimata Y, Izawa S. Acetic acid causes endoplasmic reticulum stress and induces the unfolded protein response in Saccharomyces cerevisiae. *Front Microbiol*. 2017;8(JUN):1-10. doi:10.3389/fmicb.2017.01192
423. Tu BP, Weissman JS. Oxidative protein folding in eukaryotes: Mechanisms and consequences. *J Cell Biol*. 2004;164(3):341-346. doi:10.1083/jcb.200311055
424. Prior KK, Wittig I, Leisegang MS, et al. The endoplasmic reticulum chaperone calnexin is a NADPH oxidase NOX4 interacting protein. *J Biol Chem*. 2016;291(13):7045-7059. doi:10.1074/jbc.M115.710772
425. Chernorudskiy AL, Zito E. Regulation of Calcium Homeostasis by ER Redox: A Close-Up of the ER/Mitochondria Connection. *J Mol Biol*. 2017;429(5):620-632. doi:10.1016/j.jmb.2017.01.017
426. Coe H, Bedard K, Groenendyk J, Jung J, Michalak M. Endoplasmic reticulum stress in the absence of calnexin. *Cell Stress Chaperones*. 2008;13(4):497-507. doi:10.1007/s12192-008-0049-x
427. Zhang X, Gibhardt CS, Will T, et al. Redox signals at the ER –mitochondria interface control melanoma progression. *EMBO J*. 2019;38(15):1-22. doi:10.15252/embj.2018100871
428. Pivovarova NB, Hongpaisan J, Andrews SB, Friel DD. Depolarization-induced mitochondrial Ca accumulation in sympathetic neurons: Spatial and temporal characteristics. *J Neurosci*. 1999;19(15):6372-6384. doi:10.1523/jneurosci.19-15-06372.1999
429. Zhang H, Forman HJ. Glutathione synthesis and its role in redox signaling. *Semin Cell Dev Biol*. 2012;23(1):1-7. doi:10.1016/j.semcdb.2012.03.017.Glutathione
430. Rinnerthaler M, Büttner S, Laun P, et al. Yno1p/Aim14p, a NADPH-oxidase ortholog, controls extramitochondrial reactive oxygen species generation, apoptosis, and actin cable formation in yeast. *Proc Natl Acad Sci U S A*. 2012;109(22):8658-8663. doi:10.1073/pnas.1201629109
431. Zadrag-Tecza R, Ma R, Bednarska S, Kwolek-mirek M. *Stress Response Mechanisms in Fungi*.; 2018. doi:10.1007/978-3-030-00683-9
432. Lanza IR, Nair KS. Chapter 20: Functional Assessment of Isolated Mitochondria In Vitro. In: *Methods in Enzymology*. Vol 457. ; 2009:349-372. doi:10.1016/S0076-6879(09)05020-

4
433. Kowaltowski AJ, Vercesi AE, Rhee SG, Netto LES. Catalases and thioredoxin peroxidase protect Saccharomyces cerevisiae against Ca2+-induced mitochondrial membrane permeabilization and cell death. *FEBS Lett*. 2000;473(2):177-182. doi:10.1016/S0014-5793(00)01526-X
434. Abdel-Rahman EA, Mahmoud AM, Aaliya A, et al. Resolving Contributions of Oxygen-Consuming and ROS-Generating Enzymes at the Synapse. *Oxid Med Cell Longev*. 2016;2016. doi:10.1155/2016/1089364
435. Vitu E, Gross E, Greenblatt HM, Sevier CS, Kaiser CA, Fass D. Yeast Mpd1p Reveals the Structural Diversity of the Protein Disulfide Isomerase Family. *J Mol Biol*. 2008;384(3):631-640. doi:10.1016/j.jmb.2008.09.052
436. Tanaka S, Uehara T, Nomura Y. Up-regulation of protein-disulfide isomerase in response to hypoxia/brain ischemia and its protective effect against apoptotic cell death. *J Biol Chem*. 2000;275(14):10388-10393. doi:10.1074/jbc.275.14.10388
437. Gess B, Hofbauer KH, Wenger RH, Lohaus C, Meyer HE, Kurtz A. The cellular oxygen tension regulates expression of the endoplasmic oxidoreductase ERO1-Lα. *Eur J Biochem*. 2003;270(10):2228-2235. doi:10.1046/j.1432-1033.2003.03590.x
438. Yang Z, Zhao X, Xu J, Shang W, Tong C. A novel fluorescent reporter detects plastic remodeling of mitochondria-ER contact sites. *J Cell Sci*. 2018;131(1):jcs208686. doi:10.1242/jcs.208686
439. Gomes LC, Benedetto G Di, Scorrano L. During autophagy mitochondria elongate, are spared from degradation and sustain cell viability. *Nat Cell Biol*. 2011;13(5):589-598. doi:10.1038/ncb2220